# Enhancing energy flexibility: resources integration in smart grids. A transversal approach for the ASM Terni power network

*Ph.D. Course in Engineering and Applied Science for Energy and Industry*

*XXXVI cycle*


Tutors:
**Prof. Alberto Geri**
**Ing. Massimo Cresta**

Candidate:
**Marco Antonio Bucarelli**


A.A. 2022-2023

SAPIENZA
UNIVERSITÀ DI ROMA

**Enhancing energy flexibility: resources integration in smart grids. A transversal approach for the ASM Terni power network**

Sapienza University of Rome


Author's email: marcoantonio.bucarelli@uniroma1.it

# Table of Contents

## List of Abbreviations

| Acronym | Definition |
|---|---|
| AI | Artificial Intelligence |
| DER | Distributed Energy Resources |
| DN | Distribution Network |
| DR | Demand Response |
| DSO | Distribution System Operator |
| DT | Digital Twin |
| EESS | Electrical Energy Storage System |
| EV | Electric Vehicle |
| EVCS | Electric Vehicle Charging Station |
| Heq | Equivalent Hours |
| HV | High Voltage |
| HVAC | Heating, Ventilation and Air Conditioning |
| IoT | Internet of Things |
| LV | Low Voltage |
| MAE | Mean Absolute Error |
| ML | Machine Learning |
| MSE | Mean Squared Error |
| MV | Medium Voltage |
| NRMSE | Normalized Root Mean Squared Error |
| PMU | Phasor Measurement Unit |
| PV | Photovoltaic |
| REC | Renewable Energy Community |
| RES | Renewable Energy Sources |
| RMSE | Root Mean Squared Error |
| RPF | Reverse Power flow |
| SCADA | Supervisory Control And Data Acquisition |
| SCR | Self Consumption Rate |
| SG | Smart Grid |
| SOC | State Of Charge |
| SSR | Self Sufficiency Rate |

# Abstract

The ongoing transition towards a more sustainable and resilient electrical system has initiated profound changes within electricity distribution networks. The substantial increase in renewable energy installations, electric vehicle adoption, and energy consumption, underscoring the urgent need for a comprehensive grid reinforcement strategy.

This PhD thesis advocates a holistic perspective to facilitate the transition of distribution networks towards the smart grids. Central to this approach is the effective utilisation of network management tools, which harness the full potential of existing flexibility resources. Implementing intelligent strategies begins with the pivotal digitalisation step, incorporating real-time SCADA systems, Internet of Things devices, and distributed sensors. The thesis delves into innovative algorithms within this framework, including machine learning-based optimisation and forecasting models, transformer's ageing prediction and energy district management, validating the tools within real case studies.

The thesis further explores three key application areas, illustrating how flexibility services can integrate into distribution grids in the context of electric mobility, hydrogen infrastructure, and energy communities.

The transition towards network modernisation is complex, necessitating a collaborative effort from various stakeholders, including distribution system operators, aggregators, energy retailers, end-users, energy communities, researchers, and legislators. A transversal approach and incremental steps are essential to overcome the existing barriers and provide environmentally friendly services. Ultimately, these efforts aim to foster a sustainable energy future, where distribution networks are the cornerstone of a resilient and eco-conscious electrical system.

# 1 Introduction

## 1.1 Motivation and context

The spread of renewable energy sources and the need for a resilient energy system are leading to significant changes in the electricity distribution network.
According to the most recent European legislation the end user is no longer a passive participant in the system, he can consume electricity, produce it, participate in demand response mechanisms, form energy communities, recharge electric vehicles and has the right to know the dynamics of the electricity system with transparency. The distribution network, being in direct contact with the end user, must adapt quickly to the change.
The distribution network already feels some of the effects of the change in consumption and distributed generation, partly due to the high average age of installations. The spread of photovoltaic installations means that the loading of lines and transformers is higher and there are frequent episodes of reverse flow, which can lead to various technical problems. In addition, fast charging stations for electric vehicles are rapidly occupying the hosting capacity in the grids.
Future forecasts predict a 32 % increase in PVs by 2025, a 452 % increase in electric vehicle penetration and a further 2.05 % increase in consumption. The impact on the grid will then be very significant and a reinforcement of the grid is necessary.
The strategies to be implemented in this case are twofold: i) the construction of new, better-performing infrastructures; ii) the use of tools to manage the network effectively and make optimal use of the flexibility resources already present.
In the course of this thesis, various active strategies are analysed, considering that none alone can solve all network problems: an integrated approach is necessary.
The first step in the implementation of intelligent strategies is digitisation: using real-time SCADA, IoT devices and distributed sensors makes it possible to acquire fundamental data to better manage the network. In this context, the thesis shows an original, simple and inexpensive measurement device based on Raspberry Pi, which communicates with SCADA via MQTT.
Among the various tools serving the network, optimisation and forecasting models are shown, based on machine learning, such as the prediction of the ageing of transformers located in secondary substations of the Terni network, based on the power and noise emitted; a forecasting model of the consumption and generation of an energy district based on Reinforcement Learning; a digital twin that integrates state estimation through a genetic algorithm and the optimisation of an energy community in order to maximise self-consumption. Finally, in the area of digitisation, the role of cybersecurity cannot be overlooked.
In this thesis, three application areas are presented where flexibility services can be provided for the electricity distribution grid: electric mobility, hydrogen infrastructure and energy communities.
Studies are presented on electric mobility, which is managed as a grid flexibility tool, capable of absorbing power at peak generation times, while respecting the needs of end users. The approach of building a new grid, parallel to the existing grid, exclusively dedicated to powering electric mobility, is investigated, thus not burdening the current grid, but rather increasing its resilience.
Energy scenarios predict significant growth in hydrogen production, with 40 GW in 2030. The use of hydrogen is particularly interesting in the hard-to-abate sectors; in the thesis it

is mainly seen in relation to the electricity grid, i.e. as a highly flexible load, which interfaces to the grid via electrolysers and constitutes an important flexibility resource.
The active participation of citizens can turn the concept of the distribution network upside down: the emergence of energy communities, interconnected to the electricity grid, but transitioning energy internally, makes it possible to limit costs for end users, delegating to the grid only a supporting role.

## 1.2 Objectives

The primary objective of this thesis is to demonstrate that facilitating the energy transition within distribution networks necessitates a holistic perspective. Rather than confining the focus to a singular technology or a specific domain, it is imperative to adopt an integrated approach. Such an approach must encompass a wide spectrum of elements, ranging from generation facilities and end consumers to grid reinforcement, considering both passive and active strategies.
The integration of emerging information technology solutions into the grid infrastructure holds the key to unlocking the tremendous potential of data amassed through the Internet of Things devices. Leveraging this data resource empowers us to discern and implement cost-effective, sustainable, and readily deployable remedies for enhancing the grid's resilience and efficiency.
The path towards network modernisation is extremely complex, and its implementation requires time, resources and expertise, but with a multi-transversal approach, involving Distribution System Operators, aggregators, energy retailers, end-users, energy communities, technology providers, researchers and legislators, it is possible to proceed in incremental steps towards overcoming barriers and implementing increasingly environment and user-friendly services.

## 1.3 Structure of the thesis

The thesis is organised as follows: after this introductory chapter, Chapter 2 shows the current state of the distribution network in Italy, highlighting the challenges it faces in the near future with a focus on the need for flexibility resources. Three analyses of the current situation of distribution networks are shown: the first concerns a study of barriers to innovation in the smart grid, providing a quantitative analysis of each barrier, the second shows the variation over time of the behavioural habits of end users of the Terni network and the third is a preliminary analysis of the resilience of a portion of the Terni distribution network. Finally, the characteristics of Terni's distribution network, managed by ASM Terni, are shown, and some of the innovations carried out within the research projects of the continental Horizon 2020 and Horizon Europe programmes are shown.
In Chapter 3, it is shown how advanced information technologies and the deployment of IoT devices bring high added value to electricity grid services. The grid's Digital Twin is shown as the essential platform on which to establish all innovations in the field of electrical analysis. Analytics such as energy forecasting, grid optimisation and predictive maintenance are studied in detail and brought into real applications. Special attention is paid to cybersecurity, showing how vulnerable the grid is to the injection of false data that could potentially cause irreparable damage.
In the following chapters, analysis are shown among the consumer sectors that are expected to develop significantly in the years to come: electric mobility, the hydrogen

chain and energy communities. These sectors are analysed by showing how they can be integrated into the electricity grid and what the added value in terms of flexibility is.
In Chapter 4, the role of mobility as a service provider for the electric grid is shown, analysing both the impact of a complete mobility conversion for the city of Terni, in particular a 500 kW recharging system, and the role of electric company fleets and the different management methods.
Chapter 5 investigated how the hydrogen sector can provide flexibility services to the electric distribution network and in particular evaluated the application in the conversion of a company fleet from diesel to fuel cell electric vehicles.
Chapter 6 analysed how Renewable Energy Communities can bring benefits to the electricity grid and in particular the impact of the deployment of energy communities in the Terni grid by 2030, evaluating user behaviour that is more or less willing to change their habits to provide services to the grid.
Finally, in Chapter 7 the conclusions and main results are reported.
Published materials and references are listed at the end of the thesis.

# 2 Electrical distribution network: state of the art and challenges

## 2.1 Considerations on the state of the art, challenges and evolution of the distribution network in Italy

The electric Distribution Network (DN) is a fundamental infrastructure in the energy system, and has the task of distributing electricity to end users in a safe, sustainable and continuous way. The DN needs to adapt to the ongoing energy transition, with the development of Renewable Energy Sources (RES) and the need to increase the resilience of the grid. The Smart Grid (SG) adapts to the transition of the generation system from centralized to distributed, with a large percentage of RES. SGs are becoming more and more common. These use advanced communication and control technologies to improve the efficiency and resilience of the electricity system. This includes smart metering, active demand management, automated distribution, and real-time monitoring.

Today, electricity distribution networks are invested with the crucial task of creating the conditions, through their renewal and technological upgrading, for the evolution of the electricity system in the direction of energy-environmental objectives. In Italy there are 128 operators who manage the more than 36 million withdrawal points throughout the country for a distributed energy of almost 270 thousand GWh. The DN sector has been subject to major regulatory transformations in recent years and, for the service offered, DSOs are recognized by the Regulatory Authority for costs that amount to over 5 billion euros. From the point of view of the domestic customer, the distribution and metering service accounts for 15.5% of the final electricity expenditure. On the basis of the estimates made, it is possible to predict a total regulatory value of the DNs of about 25 billion euros. Equally important is to maintain a high quality of service, which is increasingly stressed by the presence of Distributed Energy Resources (DERs), Electrical Energy Storage Systems (EESSs) and inverter-connected loads.

The need to adapt to the rapid technological evolution and digitalization processes, which are considered as essential to achieve the stated objectives and make the network flexible and resilient, is an additional cost factor. To this end, a coordinated and long-term vision for the energy sector is needed that is able to manage its transformations without delays or errors. The state of electricity DNs is constantly evolving, with an increasing focus on efficiency, safety, sustainability and the integration of RES. The main challenges facing DNs are:

- Leakage Management: DNs are investing in advanced technologies to reduce energy losses during transmission and distribution. This includes the use of smart sensors to detect leaks and defects in networks.
- Integration of DER, with a total number currently around 970,000, for a capacity of at least 37 GW in the Italian context.
- Cybersecurity: Cybersecurity has become a critical aspect of DNs, as the increasing automation and interconnectedness of networks makes them vulnerable to cyberattacks. Protecting critical infrastructure is a priority.
- Energy efficiency: Optimising energy efficiency is a key objective. This includes adopting energy-efficient technologies, promoting more efficient buildings and industrial processes, and managing demand intelligently.

- The integration of Electric Vehicles (EVs): The adoption of EVs is increasing, which poses additional challenges and opportunities for DNs. EV charging requires efficient charging infrastructure and managing peak demand.
- Storage usage: EESSs are becoming increasingly important for balancing electricity supply and demand. These systems help to ensure a constant supply of energy, especially from RES.
- Regulation: Regulation plays an important role in the development of distribution networks. Regulators are often trying to promote innovation and sustainability through incentives and appropriate policies.
- Monitoring and preventive maintenance: The maintenance of electrical infrastructure is critical to the safety and reliability of the system. The use of advanced technologies, such as data analytics, is becoming increasingly common to prevent breakdowns and optimize maintenance.

## 2.2 The need for flexible resources

The flexibility resources of the electricity grid are varied and it is necessary to exploit all available technologies to guarantee RES integration, power flow balancing and voltage and frequency regulation services. Below are the main technologies used as flexibility resources for the DN.

### 2.2.1 Storage systems

EESS play a crucial role in the modern energy landscape by serving as one of the main flexibility resources. These systems store electricity and release it when needed, which helps balance supply and demand on the electrical grid. EESS function as flexibility resources in serveral ways, for example for load leveling and to reduce the peaks. EESSs facilitate the integration of RES, injecting power when is mainly needed and not when the non programmable RES produce. EESSs can provide ancillary services to the DN, as voltage and frequency regulation, increasing the stability of the grid.
The EESS are optimal to be included in Demand Response (DR) mechanisms allowing customers to reduce their energy consumption during peak periods and, in turn, receive incentives or lower electricity rates.

### 2.2.2 Electric mobility

EVs can serve as flexibility resources for the DN, offering a range of benefits to both grid operators and EV owners. EVs can participate in DR programmes, where they charge during off-peak hours and reduce or delay charging during peak periods. Grid operators can send signals to EVs to adjust their charging patterns, helping to balance electricity supply and demand. If properly configured, Electric Vehicle Charging Station (EVCSs) can also inject power to the grid, allowing the Vehicle-to-Grid technology, that enables bidirectional power flow between the EV and the grid. EVs can discharge stored electricity back to the grid during peak demand periods or in response to grid signals. This can help alleviate stress on the grid and reduce the need for additional generation capacity.
The flexible energy available from electric mobility can be used by the DN to provide innovative services, i.e. frequency regulation, RES integration, and grid voltage balancing. However, it's important to note that the widespread adoption of EVs as flexibility resources for the DN requires supportive policies, standards, and the development of

vehicle-to-grid infrastructure. Additionally, it must consider the impact on the battery life of EVs, as frequent discharging and charging can affect the longevity of the battery. As technology advances and grid operators and regulators adapt to accommodate vehicle-to-grid, EVs have the potential to play a significant role in enhancing the flexibility and reliability of DN while supporting the integration of RES.

### 2.2.3 Demand response mechanisms

DR is a valuable flexibility resource for the DN, helping grid operators manage electricity supply and demand more effectively. DR is the active participation of end users in order to shift the energy consumption from peaks to time interval in which is better for the DN. In this operation way is possible to allow load shifting, peak reduction and valley filling. The active contribution of end users can also allow to variate the power flow in the grid, allowing to balance the grid, reduce the overvoltages and undervoltages and limiting the loading of the power cables. The DR mechanisms can facilitate the management of voltage and frequency stability issues.

To effectively utilize DR as a flexibility resource for the DN, it requires advanced technologies, smart meters, communication systems, and supportive policies. Grid operators and utilities must also work closely with participants to ensure the success of DR programs. As the grid becomes more modern and digitized, DR will play an increasingly important role in optimizing grid operations, supporting RES integration, and ensuring grid reliability.

### 2.2.4 Power to gas process

Power-to-gas technology, which converts electricity into hydrogen or other synthetic gases, can serve as a flexibility resource for the DN. Hydrogen, produced through power-to-gas or other methods, can play a significant role in enhancing grid flexibility and reliability. Hydrogen can be used as flexibility resources for the DN as an energy storage, since it allows excess electricity, particularly from RES like wind and solar, to be converted into hydrogen. This hydrogen can be stored for later use. During times of high electricity demand or when RES generation is low, the stored hydrogen can be converted back into electricity through fuel cells or gas turbines, providing a valuable energy storage solution for grid operators. Hydrogen storage, unlike EESSs, allows for seasonal accumulation, in which the difference in renewable production between summer and winter is exploited.

While power-to-gas and hydrogen offer numerous benefits for grid flexibility and decarbonization, challenges include the cost of electrolysis, hydrogen storage, and infrastructure development. Additionally, hydrogen transportation and distribution infrastructure must be expanded to realize the full potential of hydrogen as a flexibility resource for the DN. Nonetheless, ongoing research and development are addressing these challenges and paving the way for hydrogen to play a crucial role in the future of grid flexibility and sustainability.

## 2.3 Analysis of the barriers to the Smart Grid

The SG technology has the potential to modernise the electricity system, offering several advantages in terms of grid resilience, environmental impact, and management efficiency. However, the progress faces economic, technological, regulatory, organisational, and human obstacles. An original study has been carried out [VIII] providing a comprehensive examination of these barriers, focusing on their manifestations in five European countries, drawing on data collected from the BRIGHT European project [52]. This study involved establishing a standardised metric survey and convening five round table discussions, engaging 26 stakeholders from various European nations. Numerous literature articles have addressed SG barriers, including Luthra et al. [293], which identified 12 such barriers through an extensive literature review and employed interpretive structural modelling to elucidate their interrelationships. Building on this classification of 12 barriers, [VIII] aims to contribute to the existing literature by addressing the need for more quantitative data on these barriers. This study thoroughly analyses the current status of each SG barrier, gathering insights from academic papers and expert viewpoints. Subsequently, it presents an exploratory quantitative assessment of these barriers, utilising data acquired from a metrics survey administered to electricity grid operators and other relevant stakeholders.

### 2.3.1 Literature review and methodological approach for the quantitative assessment

The methodology of the study is described in Figure 1. An extensive literature review has been conducted to investigate each barrier comprehensively, and the findings have been enriched with insights from BRIGHT project partners' experiences. Our approach involved a detailed examination of each barrier. Regarding the exploratory quantitative analysis, initially a metric based on the Likert Scale [233] has been devised. For each barrier, five options are available, where a rating of 1 indicated that the barrier posed a significant limitation, potentially jeopardising the implementation of SGs. Conversely, a rating of 5 signified that the sector was highly advanced in the country and required no further development.

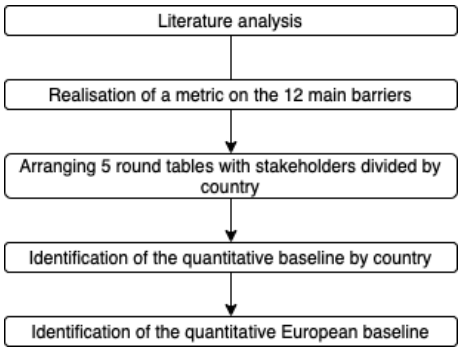


*Figure 1: Work plan schema*

Each barrier evaluation was formulated based on the findings of our literature analysis. Task partners from different countries convened round table discussions with SG stakeholders between April and June 2022. These stakeholders included experts falling into the following categories: i) Distribution System Operators, ii) Universities and research centres, iii) power grid technology providers, iv) BRIGHT Project partners, and v) others. The BRIGHT Project partners are either power systems owners or providers of technology and services in the field. During the round table discussions, the barriers to SG

implementation were debated, and a collective assessment was made to determine the level of development in each nation concerning these barriers. In total, 26 stakeholders participated, with 17 representing entities outside the BRIGHT Project. To collect quantitative data on the state of SG barriers in five European countries—Italy, Romania, Netherlands, Greece, and Slovenia—round tables have been organised to establish the most suitable criteria for evaluating each barrier, using the metric as a reference point.
Each partner's contribution in its country formed a preliminary national baseline. The overall European situation was assessed by considering the findings from these national baselines. Figure 2 illustrates the breakdown of stakeholders by type in a pie chart.

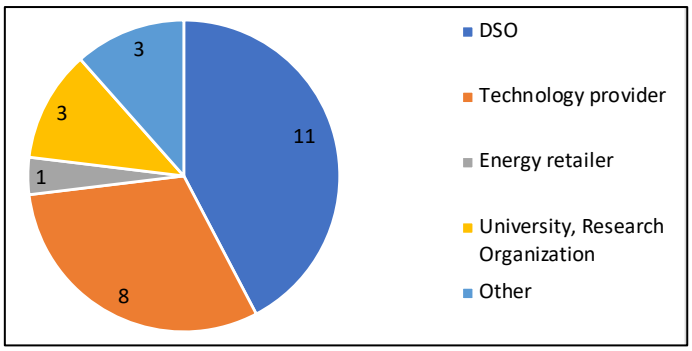


*Figure 2: Distribution of the stakeholders engaged in the quantitative analysis.*

The results of each national round table were analysed and commented on in light of the situation of the electricity system in each country [80],[85],[313].

### 2.3.2 Barriers to smart grid, an in-depth analysis

The ever-evolving energy system demands rapid adaptation from the grid to deliver high-quality and dependable services to users. However, various obstacles hinder and complicate the progress of grid development. The literature lacks a single unified classification for these barriers. In [230], a hierarchical categorisation is proposed, consisting of three primary barriers: economic, technological, and social, along with secondary barriers encompassing political/regulatory, physical, comprehension, and market structure obstacles. Twelve barriers have been identified through a systematic review of barriers to implementing SG technologies, as outlined in Table 1. Luthra [293] was selected as the reference source due to its comprehensive coverage of these barriers.

*Table 1: Barriers to SG technologies*

| N. | Barriers to the smart grid |
|---|---|
| 1 | Financial impact of the investment |
| 2 | Market uncertainty |
| 3 | Lack of regulatory framework |
| 4 | Low public awareness and engagement |
| 5 | Low innovation in the industry |
| 6 | Inadequate infrastructure |
| 7 | Technology immaturity |
| 8 | Workers expertise |
| 9 | RES integration |
| 10 | Inefficient communication system |
| 11 | Availability of open standards |
| 12 | Cyber security and data privacy constraints |

In the following subsections, each of the twelve barriers is described and expanded on based on the identified literature and discussions with the relevant stakeholders.

#### 2.3.2.1 Financial impact of the investments

Implementing SGs requires extra funding for essential infrastructure, communication systems, the recruitment of skilled professionals, and research activities. Due to the substantial initial investment, the payback period is relatively extended [110]. From the end-users' perspective, purchasing Internet of Things (IoT) devices or participating in DR programs can also entail economic uncertainties. To alleviate the hesitancy of vendors and manufacturers, it is essential to establish a secure return on investment through government-backed incentives.

#### 2.3.2.2 Market uncertainty

The tools and components of the SG face vulnerabilities within an evolving market characterised by ambiguities in institutional functions, services, and exchange mechanisms, potentially leading to market obstacles or failures [230]. The direction in which the SG landscape progresses depends on the decisions made by national regulators in supporting investments [60]. Market barriers impede the development of a robust market, resulting in insufficient competition, difficulties in accessing funds, uncertainty, imperfect information, and hidden costs. Furthermore, the required capital costs can discourage investment in SG services, as illustrated by the example of the flexibility market, which can hinder the establishment of a DR market [111] where a comprehensive list of market barriers and failure types is provided. To generate revenue, it is crucial to define SG standards and business models through regulatory frameworks [120].

#### 2.3.2.3 Lack of regulatory framework

A well-structured regulatory framework is essential to foster the development of SGs. Many electrical systems operate under outdated and non-harmonized regulatory structures [272], which can deter investments in innovation. Currently, the regulatory aspects of SGs remain unclear [101]. In [214], it's possible to find an analysis of the regulatory frameworks in each European country. It is imperative to establish clear data measurement and management standards, determine fair compensation for distribution system operators [230], address retail energy market issues, define transparent billing structures, and enhance customer protection. Standardising smart meters and other components would provide greater clarity regarding the services they can offer [1]. A market liberalisation process is underway in European countries, allowing free market users and those under a regulated regime to coexist. The presence of the protected regime can hinder operators' creativity [236].

#### 2.3.2.4 Low public awareness and engagement

The involvement of the public is crucial for the development of the SG. It is essential to raise awareness and provide information about innovative technologies to encourage consumer engagement [244]. Barriers stemming from human factors, particularly related to awareness and trust, hinder participation in DR programs [230]. Enhancing consumer awareness should motivate individuals to adopt new energy consumption patterns [11].

Currently, there is a low level of public awareness and engagement in SG projects, necessitating initiatives to address this issue [41]. Participants with access to additional information tend to be more engaged and persistent in DR programs. Consumer engagement is estimated to increase by 2.5% with additional information and by 1% by incorporating automation technology.

#### 2.3.2.5 Low innovation in the industry

Organisational barriers impede companies' capacity for innovation, stemming from institutional, strategic, and operational factors. At the institutional level, development projects are often perceived as high-risk activities with extended payback periods, frequently hindering their execution [88]. Strategic barriers arise from the company's long-term vision, where individual departments maintain their strategies, and a lack of communication hampers cross-functional innovation. Operational barriers result from the company's operational practices, where activities are governed by stringent standardised procedures, making the quest for new integrated solutions complex. Collaborative interactions between highly innovative small organisations and large companies or institutions with ample resources and established organisational structures facilitate the development of inventive solutions [232].

#### 2.3.2.6 Inadequate infrastructure

Establishing a SG platform involves the integration of both technical infrastructure and a market layer that can effectively coordinate operators [36]. To bring SGs to fruition, it is imperative to have an infrastructure that enables the seamless real-time flow of energy and data, along with robust protection and measurement mechanisms. This requires incorporating various components, including automated control systems, converters, communication networks, meters, and energy management tools [101]. Smooth data transmission between edge devices and cloud-based computers, particularly for control purposes, is of utmost importance. The absence of a standardised set of criteria defining the necessary attributes for smart meters and other devices adds complexity to network communication.

#### 2.3.2.7 Technology immaturity

A technological hurdle arises when the requisite technology is lacking to deliver a stable, dependable, and safe service. This limitation primarily stems from the underdeveloped state of technology and the incomplete widespread dissemination of efficient technologies [56]. Owing to technological immaturity, auxiliary systems struggle to meet the requirements of SGs. While technological knowledge is accessible, it remains unevenly distributed, and the adoption of smart appliances within the grid remains limited. Immature technology results in substantial investment, maintenance expenses, and security concerns. The meaning of technological immaturity is emphasised in [230], and empirical evidence from [319] demonstrates that a deficiency in standardisation, often indicative of technological immaturity, can impede adoption.

#### 2.3.2.8 Workers' expertise

Upon the culmination of the technology transfer process and the integration of technology, there arises a requirement for a fresh cohort of well-trained engineers and managers who can bridge the gap and acquire new proficiencies in analytics, data

management, and decision support [272]. Organisations may delay innovations due to a deficiency in essential technical expertise [56]. As per [344], the fundamental roles of most employees, including line workers, technicians, and electricians, will remain unaltered. The knowledge transfer process predominantly pertains to programmable logic controllers, electronic components and circuits, and digital electronics [82].

#### 2.3.2.9 Renewable Energy Sources integration

Integrating both centralised and DER is a fundamental aspect of SGs, necessitating effective coordination across various energy sectors [180]. RESs play a pivotal role within SGs by offering ancillary services such as frequency regulation, voltage control, and static inertia. To facilitate this, it's crucial to establish interconnected networks among distribution system operators, power plants, and energy consumers [43]. This connectivity can be achieved by providing real-time information on the availability of RES to both energy providers and consumers. Consequently, this allows for large-scale integration through demand-side management, often involving dynamic pricing mechanisms. Utilities are also inclined to share information regarding the energy sources they utilise with their customers, enabling consumers to make informed decisions regarding real-time pricing and their environmental footprint [56].

#### 2.3.2.10 Inefficient communication system

Facilitating the SG is contingent on the seamless bidirectional transmission of both energy and data, as the management of this intricate system relies heavily on the real-time sharing of information and signals [315]. The development of an effective SG is impeded by the absence of coordination between electric energy and telecommunications agencies [277]. To support this, the communication system must consistently and bidirectionally transmit vast amounts of data, necessitating standardised procedures [23]. Management and applications such as DR and automation require minimal latency and maximum reliability to ensure smooth grid operation. Numerous standards have been established to address these requirements, covering various aspects of standardised communication within the SG domain. Notably, standards like SAREF, SGAM, and EEBUS define ontologies and protocols for data exchange in the SG, while others like OpenADR, EFI, and CEN/CENELEC S2 specify DR and flexible interfaces to the SG [84]. Blockchain and Distributed Ledger Technology are potential options for facilitating Peer-to-peer activities in this context.

#### 2.3.2.11 Availability of open standards

The absence of clearly defined standards and guidelines across the grid aimed at promoting system interoperability, significantly impedes the advancement of SGs [357]. Interoperability standards established for energy distribution networks, power sources, and energy consumers may lag behind the progress of SG implementations. It is essential to transition from many proprietary standards to open standards, fostering greater stakeholder involvement and encouraging market entry. This, in turn, promotes innovation among multiple suppliers, driving the development of new technologies while fostering competition in features and performance [102]. The European Union has mandated organisations such as CEN, CENELEC, and ETSI [52] to standardise the functionalities of smart meters and their communication interfaces for application in the

electricity, gas, heat, and water sectors. A more in-depth evaluation of the current standards landscape is available in [318].

#### 2.3.2.12 Cybersecurity and data privacy constraints

Implementing a SG introduces complexity, particularly concerning privacy and cybersecurity considerations [344]. In cybersecurity, establishing a secure SG confronts four distinct challenges: i) The power system necessitates communication requirements that must remain relevant over time without becoming prematurely outdated. ii) Many devices employed in power automation systems are tailored for specific functions, often lacking the computational capabilities required to address security issues. iii) Networking within the power grid encompasses a variety of heterogeneous technologies and protocols, such as ModBus, ModBus+, ProfiBus, ICCP, and DNP3. iv) Power systems are typically proprietary optimised for specific performance and functionality rather than prioritising security measures [317].

Furthermore, frequent data collection and analysis from smart meters can enhance energy efficiency and inform future policies, but it may come at the expense of user privacy concerns [43].

### 2.3.3 Quantitative assessment of barriers in European countries

The literature analysis performed by the authors shows a lack of quantification of the barriers to the SG, limiting approaches to qualitative analyses only. The results of round tables conducted in Italy, Romania, the Netherlands, Slovenia, and Greece are presented below. Finally, a comparison and an indication at the European level, obtained by averaging the values of these states, are shown. The list of stakeholders engaged per country and type is shown in Table 2.

*Table 2: Stakeholders engaged per country and typology*

| | ITA | ROM | NET | SLO | GRE |
|---|---|---|---|---|---|
| DSO | 1 | 4 | 2 | 3 | 1 |
| Tech. provider | 1 | 1 | | 5 | 1 |
| Research Cen. | 1 | 1 | 1 | | |
| Retailers | | | | | 1 |
| Others | 1 | 2 | | | |
| **TOTAL** | **4** | **8** | **3** | **8** | **3** |

#### 2.3.3.1 Barriers in Italy

In 2020, Italy recorded an electricity consumption of 295 TWh, marking a significant growth of 25.6% compared to the levels seen in 1990. RES contributed to 38.8% of this consumption. To meet the targets set by the EU's Fit for 55 package, Italy needs to substantially expand its renewable capacity and introduce additional energy storage systems to ensure grid stability. Italy's storage capacity, primarily consisting of pumped hydro facilities, stands at 7.5 GW. To align with the requirements, this capacity needs to be doubled. At the distribution level, the regulatory authority has established a remuneration system for distribution system operators, which is based on their operational efficiency. This system imposes specific standards for quality indicators such as SAIDI and SAIFI, while also incorporating a penalty and reward system. The deployment of smart meters across the country is overseen by distribution system

operators, resulting in the installation of more than 32 million smart meters. In recent years, Italy has made substantial progress in liberalising its energy market and enhancing infrastructure. While the wholesale market has become competitive, reforms are still necessary in the retail market. It's worth noting that Italy has the highest electricity costs in Europe for industrial consumers and ranks third highest for domestic consumers, with taxes accounting for 40% of these costs. Regarding outage duration, Italy ranks 13th among EU countries. In terms of market dynamics, a single company operates over 30% of the production plants and supplies more than 85% of the distribution network. Despite progress in the wholesale market, there is a notable absence of an independent market observer. Figure 3 illustrates the assessment of the 12 barriers, with critical areas highlighted in red, those close to the average in yellow, and the most developed sectors in green.

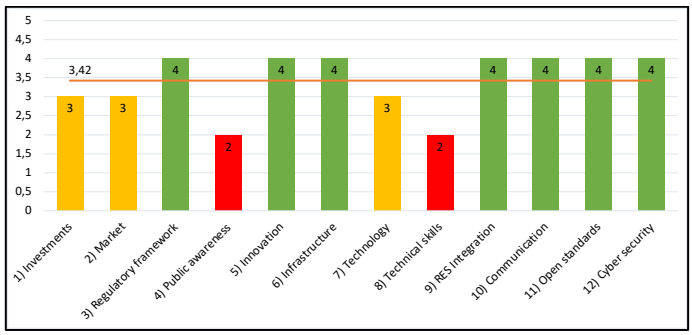


*Figure 3: Quantitative evaluation of SG barriers in Italy*

According to expert assessments, Italy exhibits partial readiness for the adoption of SGs, with favourable ratings in multiple domains. However, the areas where substantial limitations are observed include public awareness and engagement, as well as the expertise of the workforce. Experts have highlighted the need for significant efforts to shift consumer interest in sustainability from a passive stance to widespread active involvement. Moreover, there is a noted challenge in acquiring appropriately qualified personnel for innovative and cross-functional roles.

#### 2.3.3.2 Barriers in Romania

In 2020, Romania's annual electricity consumption amounted to 52 TWh, marking a notable reduction of 22.59% compared to levels recorded in 1990. Impressively, RES contributed to 47.4% of the total electricity generation. The industrial sector emerged as the largest consumer, accounting for 45.9% of electricity usage. Notably, the primary generation companies are state-owned entities. Romania's energy market consists of both regulated and unregulated segments. Significant changes had transpired in the wholesale market structure since 2012 when market transitions necessitated the shift to a centralised market operator with transparent public bidding. Looking ahead to 2030, Romania has ambitious plans, including the phasing out of thermal power plants, a twofold increase in nuclear capacity (currently at 19%), a surge in renewables to 30.75%, and a reduction in energy dependence on foreign sources to 17.8%. The electricity market has undergone liberalisation, although a substantial portion of the population remains in the protected market category. Concerning the development of the SG, Romania has initiated a digitisation process, with the installation of smart meters underway, albeit at relatively

low percentages. Figure 4 offers an assessment of the 12 barriers identified during the Romania round table discussions.

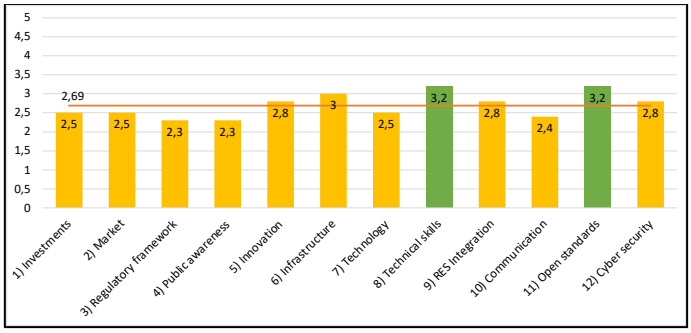


*Figure 4: Quantitative evaluation of SG barriers in Romania*

As per expert evaluations, the state of SG development in Romania can be characterised as moderate, with no particular areas standing out as either notably strong or critically weak. The system requires certain innovations and adjustments to align itself with the integration of SGs. Public awareness and engagement, although not exceptionally high, surpass levels observed in some other countries. However, when compared to other European nations, Romania exhibits lower performance in addressing the bi-directional communication and integration with RES barrier.

#### 2.3.3.3 Barriers in the Netherlands

In 2020, the Netherlands recorded an annual electricity consumption of 116 TWh, marking a substantial increase of 49.8% compared to 1990. However, the portion of energy derived from RES stood at 18.5%, one of the lowest figures in Europe. Nevertheless, this figure is projected to surge to 70% by 2030, primarily attributable to the installation of offshore wind farms. The service sector emerged as the most substantial consumer, accounting for 41% of electricity usage. The Netherlands is undergoing a profound transformation in its energy policy, encompassing changes in the generation fleet and efficient grid operation to enhance the flexibility of the electricity system. Support schemes, including renewables financing through auctions, will drive this energy transition. Furthermore, the country's only nuclear power plant is set for decommissioning. Distribution system operators are tasked with managing smart meters and encouraging data accessibility, with 54% of residential users equipped with smart meters as of 2018. Remarkably, the Netherlands boasts over 50,000 semi-public charging points, representing one of the highest concentrations globally. While the retail market is open and competitive, there is still a significant concentration of market share among energy suppliers. Retail electricity prices are not subject to regulation and are marginally lower than the median of IEA member countries, despite a relatively high tax component of 24%. Dutch stakeholders' perspectives on SGs are illustrated in Figure 5. Their assessments indicate that the Netherlands exhibits cutting-edge aspects in certain areas of SGs, such as innovation within the industry, technical expertise among personnel, and the integration of RES and two-way communication networks. However, the regulatory framework is regarded as the most critical obstacle, necessitating substantial updates to foster SG development. Additionally, enhancing public awareness and engagement represents another noteworthy challenge.

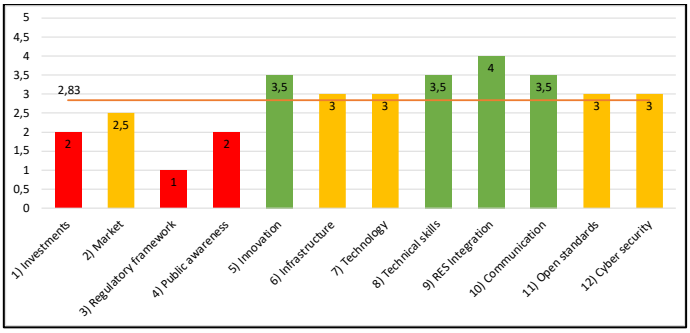


*Figure 5: Quantitative evaluation of SG barriers in the Netherlands*

### 2.3.3.4 Barriers in Slovenia

In 2020, Slovenia's annual electricity consumption amounted to 14 TWh, representing a notable increase of 34.5% since 1990. RES accounted for 32.7% of the total electricity generation, primarily attributed to hydroelectric power, which ranks as the second most utilized energy source in Slovenia, following nuclear energy. Notably, the industrial sector emerged as the largest consumer, accounting for 46.1% of energy usage. Slovenia's approved energy transition plan for 2020 outlines initiatives focused on RES development and investments in energy efficiency. To meet these objectives, the Slovenian production system must evolve to become more efficient, digitalised, optimised, and offer innovative services. The majority of the electricity sector in Slovenia is state-owned. Since 2001, the retail market has been characterised by competition. Electricity costs for consumers and businesses in Slovenia are among the lowest in neighbouring countries, largely attributed to existing tax exemptions. Regarding smart meters, widespread deployment is anticipated by 2025.

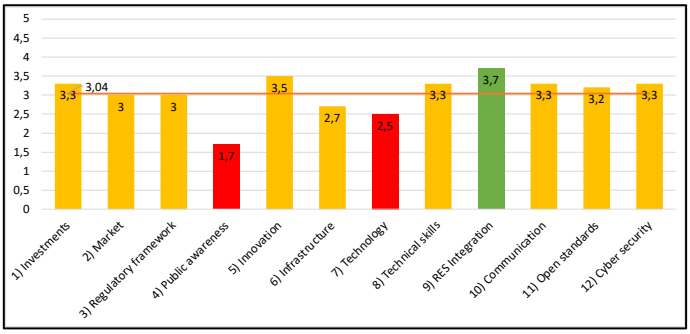


*Figure 6: Quantitative evaluation of SG barriers in Slovenia*

According to expert opinions, Slovenia is moderately prepared for the development of SGs. Certain areas, such as innovation in the industry and the integration of renewables, hold the potential for excellent performance. Conversely, in other domains like public involvement, technology readiness, and existing infrastructure, steps need to be taken to advance towards SGs. When compared to other analysed states, Slovenia neither excels nor falls significantly short in any of the evaluated categories.

### 2.3.3.5 Barriers in Greece

In 2021, Greece's annual electricity consumption stood at 51 TWh, marking a significant increase of 58% compared to the levels recorded in 1990. As of 2021, RES contributed to 41.2% of Greece's electricity production. In recent years, Greece has taken numerous

measures aimed at enhancing competition by liberalising both the wholesale and retail energy markets, aligning with the transition towards the European market structure. The share of RES is anticipated to expand further as the electricity grid extends to reach the previously unconnected large islands. Among the various sectors, the commercial sector emerges as the largest consumer, accounting for 40% of the energy demand. Greece holds a prominent position in Europe as both a producer and consumer of lignite, although this contribution is gradually diminishing. Efforts are underway to redistribute shares in the wholesale and retail markets, with the goal of bolstering market competitiveness. The energy pricing structure underwent liberalisation in 2013, with a tax component of 32% for residential consumers and 19% for industrial consumers. There is room for greater flexibility in the market, as only 3.3 GW of hydropower plants are currently utilised for this purpose. Greece aims to establish a stable regulatory framework by implementing measures that facilitate the development of DR mechanisms and capacity payment systems. BRIGHT Project assessed the present status of SGs across various barriers, as depicted in Figure 7.

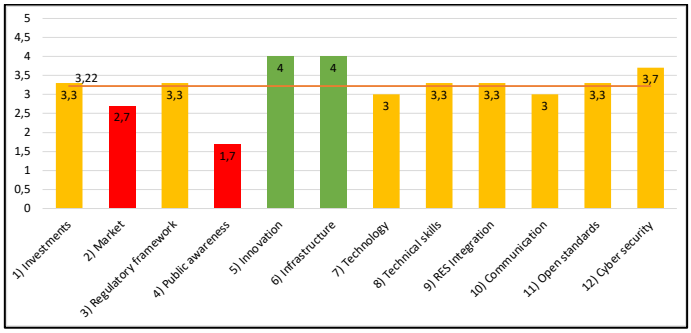


*Figure 7: Quantitative evaluation of SGs barriers in Greece*

SG experts assessed that overall, the situation is favourable and partially ready for the transition to SGs. Some areas, such as industry innovation, existing infrastructure, and cybersecurity, are at the forefront, although could be better. In contrast, public involvement and awareness are the most critical areas.

#### 2.3.3.6 Overall evaluation of barriers in Europe

The analysis reveals variations at the national level, influenced by the unique characteristics of each country, but it also highlights common trends. Figure 8 presents an aggregated analysis of the European landscape. The European electricity grid system is on the cusp of becoming a SG; however, exist barriers that could significantly impede its progress. Notably, the sectors leading the way are cybersecurity and data privacy, where Europe has already established modern standards. The data also show efficient two-way communication, supported by a well-developed infrastructure. Integration with RES is in good shape and Europe has an industry sector that is relatively receptive to innovation.

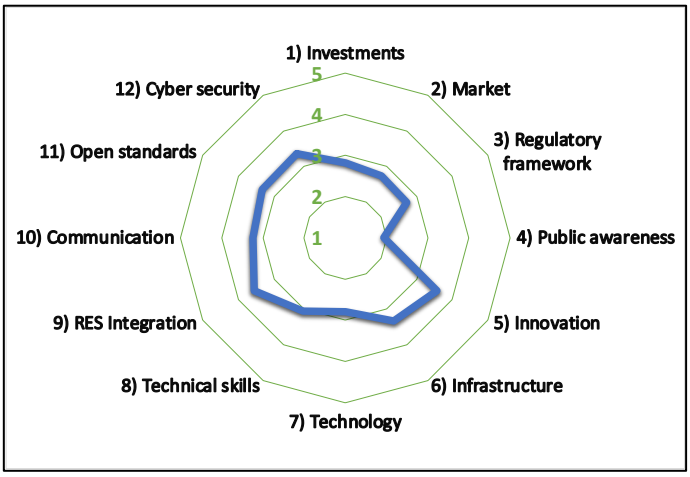


*Figure 8: Quantitative evaluation of SGs barriers in the European Union*

Conversely, the most critical area is users' engagement in active participation in energy management mechanisms. This is a deficiency also due to a need for more awareness of end users in their energy impact.

## 2.4 Analysis of the behaviour of end users

The active participation of the public is crucial for the development of SGs. It is essential that the masses are aware of their impact on energy consumption and the environment. In addition to their choices of sustainable operators and energy-saving activities, consumers can actively contribute to the energy transaction by installing PV plants placed above homes or businesses. In Italy, at the end of 2019, 880,090 PV plants were installed, with a power capacity of 20.9 GW and a yearly generation of 23.7 TWh [121]. More than 92 % of the plants had an installed PV power lower than 20 kW. For prosumers, the operational management of PV plants, possibly connected to EESSs, is generally aimed at high Self Cunsumption Rate (SCR) and Self Sufficiency Rate (SSR) values. The increase of SCR and SSR provides economic profits for the prosumers while reducing congestion and limiting grid losses. The study of prosumers' habits and their impact as aggregate systems plays a significant role in electrical system research, paving the way for the spread of Renewable Energy Communities (RECs), virtual power plants and DR mechanisms.

In Italy, starting from late February 2020, the COVID-19 pandemic introduced dramatic changes in society, changing consumer behaviour due to the national lockdown from March to May 2020 and the following closures and restrictions. Remote working and social distancing became widespread, reducing transport and industrial energy demand and increasing household consumption.

In this context, the study [VII] presents a statistical analysis of producers in the city of Terni during the period 2015-2020. The main goal of this work is to highlight the current trends in prosumers' behaviour, focusing on SCR, SSR and capability of the PV plants. Moreover, it addresses the effects of the national lockdown, taking into account differences between domestic and non-domestic customers.

### 2.4.1 Data collection and handling

After 2011, Terni has witnessed a significant increase in the adoption of DER, mainly PV plants. This emerging trend brings environmental advantages and poses challenges and opportunities for the electrical grid. This research presents findings derived from ASM's smart meters data collected between 2015 and 2020. The information gathered by these smart meters was aggregated and analysed to portray the behaviour of prosumers over the years. The analysis involved using conventional energy metrics, including equivalent hours of plant operation (Heq), SCR, SSR, and the ratio of PV installed capacity to load power (PR). The definitions and formulas for these indicators are presented below.

Heq is the amount of energy produced (Ep) over the installed power (PPV) of the PV plan, as expressed in Equation 1.

*Equation 1:PV plant equivalent hours definition*

$$H_{eq} = \frac{E_p}{P_{PV}}$$

SCR is the ratio of the portion of the PV production consumed by the loads over the produced energy (Ep) of the PV plant. It ranges between 0 % and 100 %, and its expression as a function of energy injected (Ei) is reported in Equation 2.

*Equation 2:Self Consumption Rate definition*

$$SCR = 1 - \frac{E_i}{E_p}$$

SSR is the portion of energy produced that has been consumed, out of the total energy consumed by the utility, i.e., the absorbed energy (Ea) and the self-consumed energy. It ranges between 0 % and 100 %.

*Equation 3:Self Sufficiency Rate definition*

$$SSR = \frac{(E_p - E_i)}{(E_a + E_p - E_i)}$$

PR is defined in Equation 4 as the ratio between the installed PV power (PPV) and the load connection power (PL)

*Equation 4:PV plant power ratio definition*

$$PR = \frac{P_{PV}}{P_L}$$

Regarding data collection, ASM's infrastructure measures monthly energy consumption, production, and injection into the grid. The Distribution System Operator (DSO) gathers static information for each user, including the nominal power of their PV plant, contractual power for their load, address, and energy usage classification (e.g., residential or non-residential). To effectively organise this data, three distinct clusters were identified and analysed. Firstly, the authors examined a group of users who had installed their PV systems prior to 2015, ensuring the availability of consistent monthly data for meaningful comparisons of evolving capabilities. Additionally, the authors applied filters to exclude inconsistent measurements and focused the analysis on prosumers, excluding users with minimal SCR. Thus, for this cluster, the following filters were applied to the data:

- data available for all 12 months each year from 2015 to 2020
- the PV plant in operation for each month
- the yearly SCR ≥ 5%
- the PR between 0.2 and 3
- PPV lower than 20 kW

In so doing, 413 prosumers were selected and analysed. Moreover, two additional clusters were identified, i.e., domestic and non-domestic prosumers. The group of domestic prosumers, with data available for 12 months, was selected with PR lower than 3 and annual Heq greater than 100 kWh/kW. The group of non-domestic prosumers comprises small and medium-sized factories and large commercial activities, identified applying as filters the data available for 12 months, SCR greater than 20 %, a PR between 0.2 and 3, PPV between 10 and 300 kW and annual Heq greater than 100 kWh/kW. Table 3 shows the number of PV arrays in operation from 2015 to 2020 for domestic and non-domestic clusters.

*Table 3:Number of PV plants installed each year*

| Year | Domestic | Non-domestic |
|---|---|---|
| 2015 | 709 | 50 |
| 2016 | 758 | 68 |
| 2017 | 836 | 69 |
| 2018 | 881 | 79 |
| 2019 | 936 | 86 |
| 2020 | 1004 | 82 |

### 2.4.2 Prosumers' behaviour trends

Initially, a pool of 413 prosumers, domestic and non-domestic, were selected, and their SCR and SSR were analysed from 2015 to 2020, aiming to observe the overall trend over time.

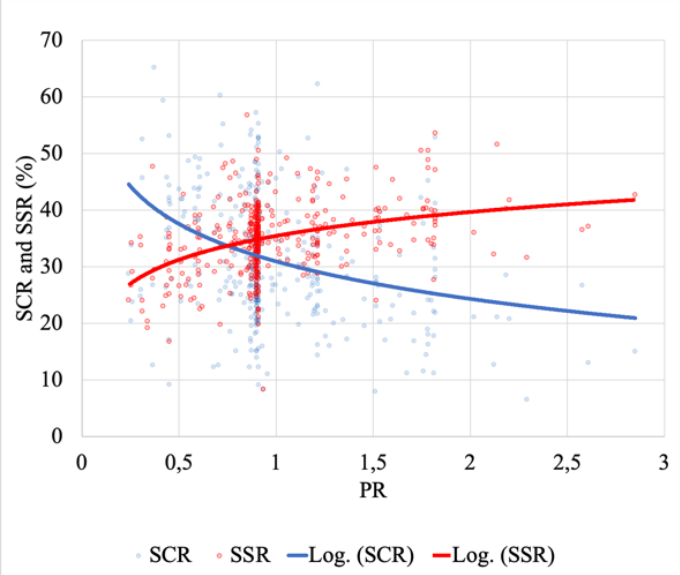


*Figure 9: Distribution of prosumers' SCR and SSR related to the PR*

Figure 9 shows the distribution of SCR and SSR related to PR, confirming that prosumers aim to maximise SCR and SSR to obtain more significant financial savings for PV plants. As shown in Figure 9 and reported in [57], these parameters are almost complementary; an increase in PR results in an increase in SCR and a decrease in SSR, and vice versa.

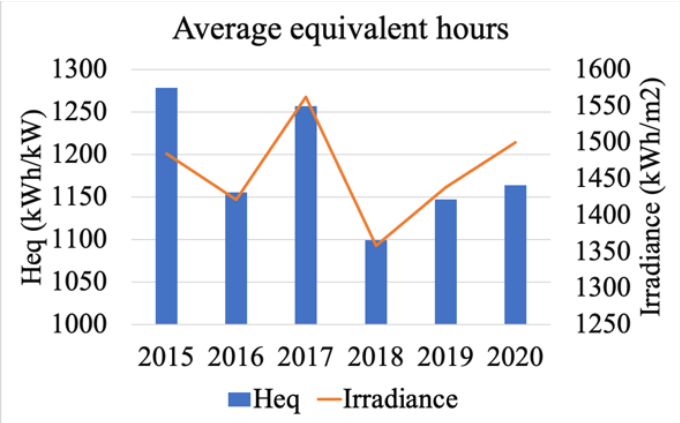


*Figure 10: Relation of $H_{eq}$ for each year with the annual irradiance in Terni*

To assess the trend in the productivity of PV arrays over time, a comparative analysis of Heq and solar irradiance was conducted using data between 2015 to 2020. This analysis is presented in Figure 10. The yearly fluctuations in Heq align with the annual irradiance patterns observed in the Italian region, with average irradiation data for Italy being publicly accessible, as referenced in [121] and [320]. Furthermore, the maximum PV production and the peak solar irradiance occurred in 2017. These data also indicate that the degradation rate of PV panels is approximately 1.7% per year. A review of the literature on degradation rate, as conducted in [4], reveals that it typically falls within the range of 0.8% to 2.03% per year.

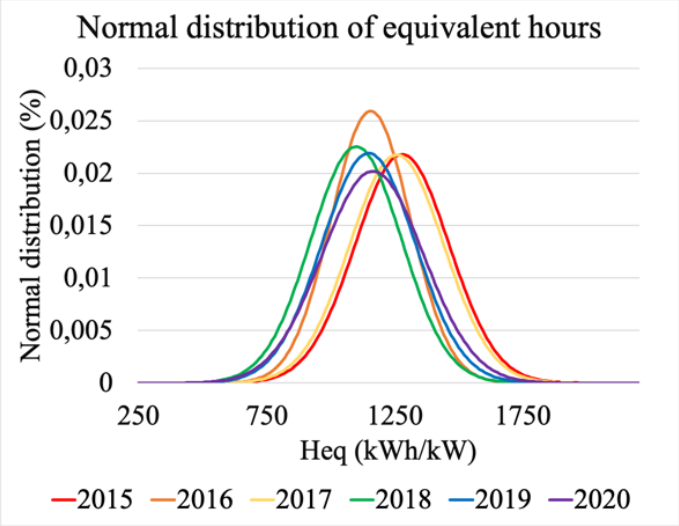


*Figure 11: Normal distribution of $H_{eq}$ from 2015 to 2020*

Regarding the producibility of PV plants, Heq emerges as a pivotal parameter. It underscores the number of plants operating under ideal conditions, encompassing optimised tilt, sun exposure, and panel efficiency. Figure 11 illustrates the normal distribution of equivalent solar hours per year in this context. Consistent with Figure 10, the curves for 2015 and 2017 exhibit a slight rightward shift attributed to the heightened power generation resulting from increased solar irradiance. Mean values and standard deviations are detailed in Table 4. Notably, in the Terni area, the Global Solar Atlas anticipates a potential PV production of about 1,430 Heq, as referenced in [118]. However, the actual PV production in Terni averaged 25% lower in 2018, with the minimum gap being approximately 14% in 2015. This differential should be considered when planning network reinforcement and assessing the impact of RES.

*Table 4: Yearly average equivalent hours and standard deviation for prosumers' PV plants*

| Year | Average $H_{eq}$ (kWh/kW) | Standard deviation |
|---|---|---|
| 2015 | 1237.11 | 210.10 |
| 2016 | 1118.85 | 171.13 |
| 2017 | 1215.27 | 198.31 |
| 2018 | 1058.06 | 181.44 |
| 2019 | 1101.30 | 201.18 |
| 2020 | 1163.67 | 197.66 |

The monthly trends of production, SCR, SSR and energy produced, injected and withdrawn were evaluated, calculating an average value for the 6 years analysed. Figure 12 and Figure 13 show that SSR follows the curve of production, because while the monthly consumption of the identified group varies slightly (by 22.5 %) the production of solar energy changes significantly (by 70.8 %). On the other hand, SCR is higher when production drops, i.e., in the period between November and February, also reaching average values above 45 %.

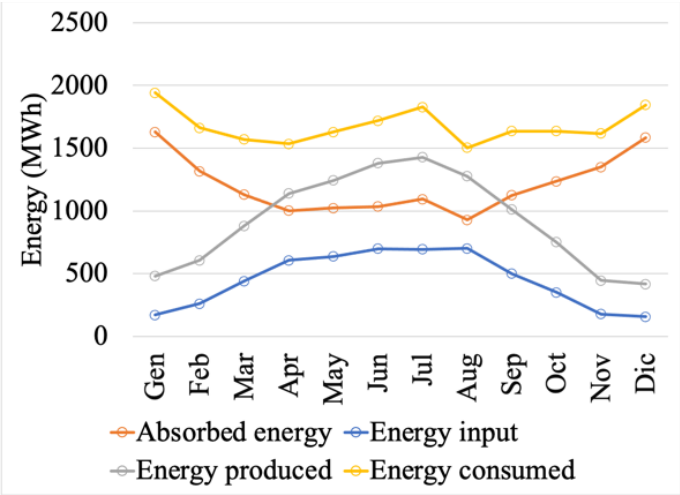


*Figure 12: Monthly energy trends, averaged over the period 2015-2020, for prosumers*

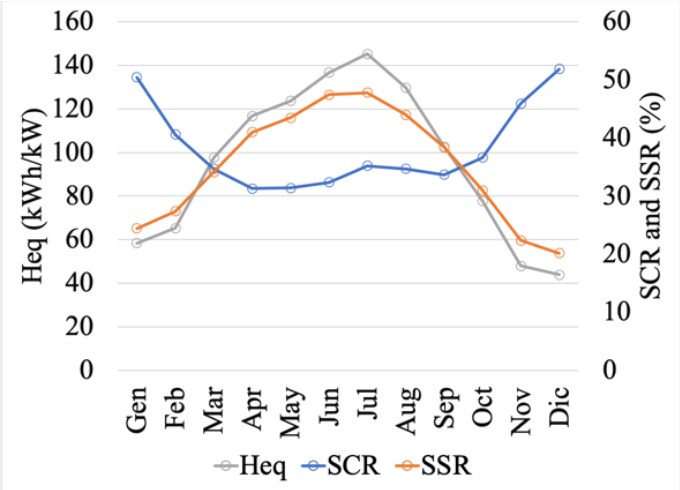


*Figure 13: Monthly $H_{eq}$, SCR and SSR values, averaged over the period 2015-2020, for prosumers.*

As for the energy exchanged with the grid this is closely linked with the production and consumption curves of the prosumer, and in any case, it depends on the seasons that impact both. To sum up, the analyses of six-year data period of a pool of 413 domestic and non-domestic prosumers led to the average values reported in Table 5.

*Table 5: Prosumers' annual average values (2015-2020)*

| Parameter | Average value |
|---|---|
| $P_{PV}$ (kW) | 4.60 |
| PR | 0.98 |
| $H_{eq}$ (kWh/kW) | 1,183 |
| SCR (%) | 29.7 |
| SSR (%) | 35.2 |

### 2.4.2.1 Domestic prosumers

The analysis of different parameters related to 6-year data of domestic prosumers led to the evaluation of some average parameter values, as shown in Table 6.

*Table 6: Annual average values of domestic prosumers (2015-2020)*

| Parameter | Average value |
|---|---|

| | |
|---|---|
| Number of plant annual variation (%) | + 8.3 |
| SCR (%) | 31.1 |
| SSR (%) | 31.3 |
| $H_{eq}$ (kWh/kW) | 1,114 |
| PR | 0.94 |
| $P_{PV}$ (kW) | 3.90 |

Data analysis shows that domestic PV plants have an average installed power of 3.9 kW, almost constant over the last 6 years, with mode values of 3 kW (35% of households) for installed power and a PR of 0.9 (46%). Average SCR and SSR are stable over 30%, as shown in Table 6 and Figure 14, revealing that domestic users have not changed their behaviour or that current consumption patterns do not allow a smooth increase in these parameters. In 2020 only 2.6 % of domestic users were able to perform an SCR greater than 70 %, and 3.1 % were able to have an SSR greater than 50%. To sum up, it is unlikely that householders are able to perfectly overlap consumption and PV production. With the exception of 2015, in Figure 15, it's notable that SCR grows monotonically over time, while the SSR is strongly dependent on the irradiance and, therefore, roughly follows its trend.

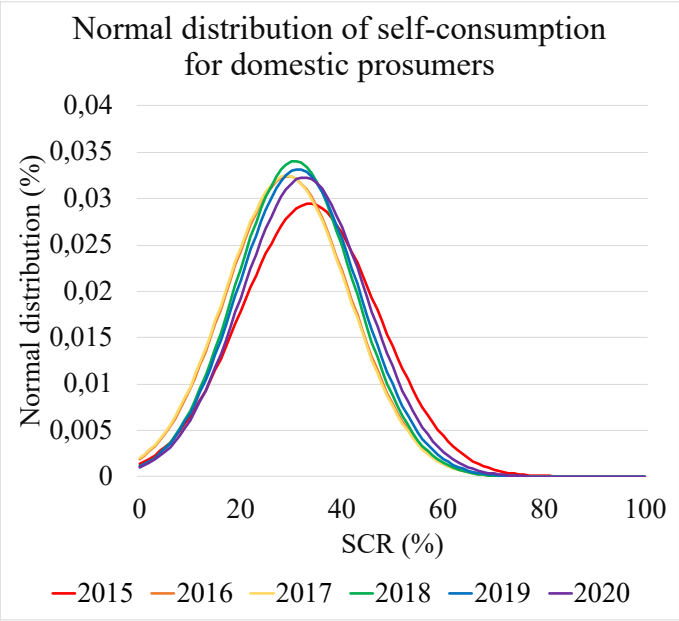


*Figure 14: Distribution curve of domestic prosumers' SCR*

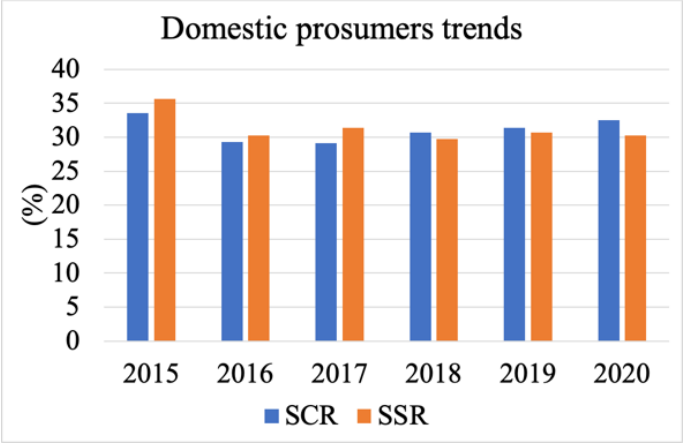


*Figure 15: SCR and SSR trends for domestic prosumers*

### 2.4.2.2 Non-domestic prosumers

The other cluster of prosumers analysed is made up of non-domestic PV plants, which contains small and medium-sized factories and other commercial activities. This group has an average installed power of 40.4 kW and total production greater than 3 GWh each year as shown in Table 7, with a significant increase in the number of installations between 2015 and 2016.

*Table 7: Annual average values of non-domestic prosumers (2015-2020)*

| Parameter | Value |
|---|---|
| Number of plant annual variation (%) | + 12.8 |
| SCR (%) | 49.6 |
| SSR (%) | 34.2 |
| $H_{eq}$ (kWh/kW) | 943 |
| PR | 1.07 |
| $P_{PV}$ (kW) | 40.4 |

Non-domestic installations have sizes that vary over a wide range, with the mode at about 20 kW (12.2% of plants). For non-domestic prosumers, as shown in Figure 16 and Figure 17, there are average SCR values close to 50 %, i.e. 18.3 % higher than for domestic prosumers. Thus, it can be seen that non-domestic prosumers have consumption that takes place more contemporaneously with PV generation than domestic prosumers. The trend of SCR is almost linearly increasing in the period of analysis with an annual increment of 2.3 % (Figure 17).

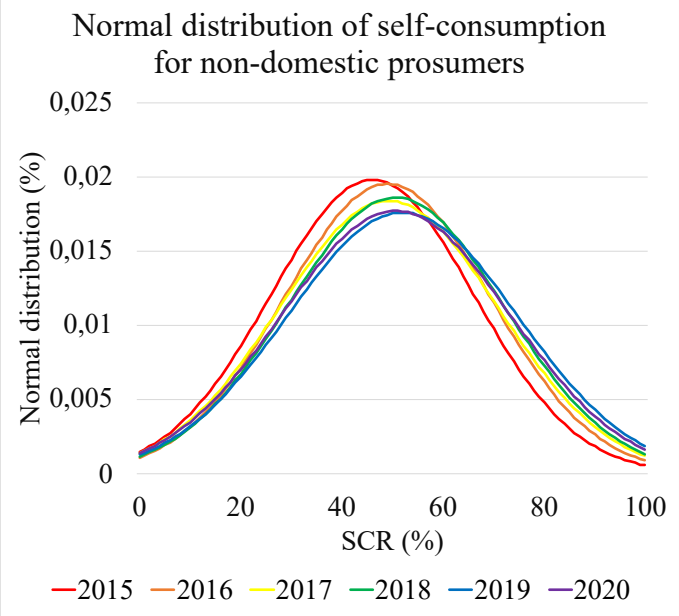


*Figure 16: Distribution curve of non-domestic prosumers' SCR*

Moreover, apart from 2015, SSR is about 5% above domestic customers, perhaps due to availability of plants optimised for the characteristics of the business (Figure 17). It can be noted that in 2020 the 9.7% of plants were able to perform a SCR greater than 90% and the 10.9 % of plants were able to have a SSR greater than 50%, values extremely higher than those expressed in the cluster of domestic prosumers.

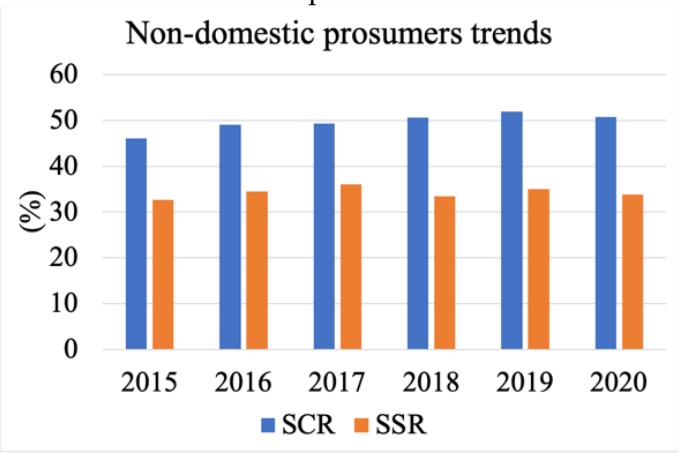


*Figure 17: SCR and SSR trends for non-domestic prosumers*

It's noteworthy to emphasise that this particular group exhibits superior performance in terms of SCR and SSR when compared to the domestic group. This distinction may be attributed to their higher energy consumption during sunny hours, when PV production is at its peak, as opposed to during the evening and early morning hours when domestic energy demand is highest but PV production is minimal. In regard to Heq, this group reports values lower than the previous group, indicating that their average production is 35% lower than the potential production as projected in [118].

### 2.4.3 Covid-19 pandemic effects on prosumers behaviour

Recent studies, as cited in [92] and [77], which examined the emergency pandemic period, have reported a significant reduction in energy consumption across industrial,

commercial, and transportation sectors following the implementation of the initial national lockdown measures. Simultaneously, there was an increase in domestic consumption. Hence, an assessment of the SCR for both domestic and non-domestic clusters was conducted. Table 8 reveals a noticeable rise in the average annual SCR during 2020 compared to the previous year's average. This increase can be attributed primarily to the impact of COVID-19 and a slight upward trend in SCR from year to year. On the other hand, SSR experienced a slight decline in 2020, albeit its value is significantly influenced by annual irradiation levels.

*Table 8: Self-consumption and Self-sufficiency rate effect of Covid-19*

| Year | Parameter | Domestic | Non-domestic |
|---|---|---|---|
| 2015-2019 | SCR (%) | 30.8 | 49.4 |
| 2020 | | 32.5 | 50.7 |
| 2015-2019 | SSR (%) | 31.5 | 34.3 |
| 2020 | | 30.2 | 33.8 |

Figure 18 and Figure 19 show how SCR changed monthly for the domestic and non-domestic prosumers. They clearly show that SCR for domestic prosumers increased significantly when the lockdown started (end of February), in comparison with the previous years; the difference among trends is about 8 %. The increase in SCR during this period is due to the increased presence of people in their homes allowed for an increased focus on more self-consumption-prone behaviour.

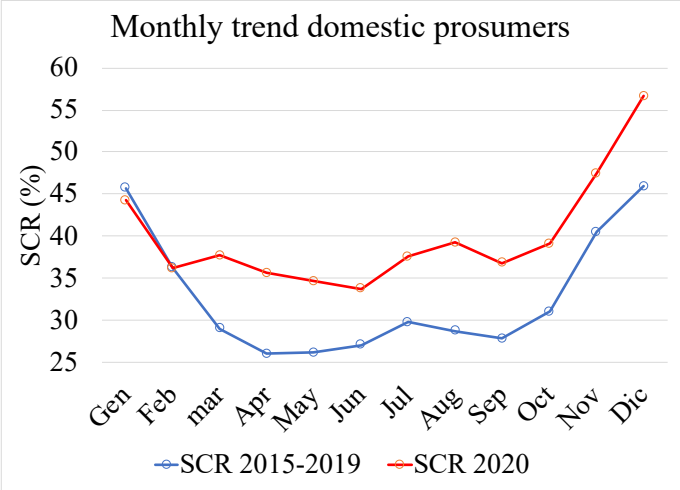


*Figure 18: Domestic SCR in 2020 with respect to average 2015-2019 values*

As to the non-domestic cluster (Figure 19), SCR did not change during the full national lockdown (March-May 2020), but it subsequently increased, likely due to the different restrictions on businesses and venues; more specifically, the increasing in SCR was basically due to the duration of the productive activities, which merely covered the daily hours, matching the energy generation of the PV panels.

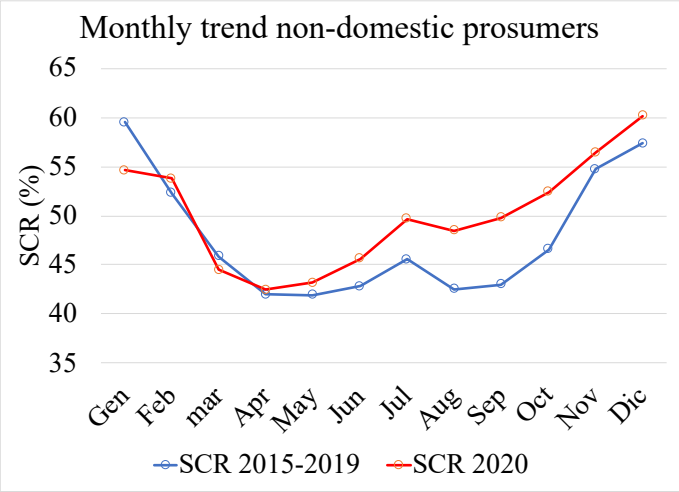


*Figure 19: Non-domestic SCR in 2020 with respect to average 2015-2019 values*

## 2.5 Grid Resilience

In recent years, a transformation in the electricity grid has been underway, due on the one hand to the major environmental issues and on the other to the need to provide electricity of ever better quality and from RES. Due to climate change, extreme natural phenomena such as floods, snowfalls, hurricanes, fires have significantly increased, and the effects on infrastructure are significant, and attacks on the electricity grid also come from humans, both voluntarily and involuntarily. In particular, the DN is most prone to these incidents, in fact it is estimated that 90% of outages have their roots in this layer of the network [358].
In recent years, the concept of resilience has been introduced in the electrical sector, to expand and strengthen the concepts of reliability, continuity and robustness of the grid. There is no unequivocal definition of resilience [58], but for this thesis it was decided to adopt the one present in the 2017 National Energy Strategy [334]: "Resilience is defined as the ability of a system not only to withstand stresses that have exceeded the limits of the system itself, but also the ability to quickly return to its normal operating state. The effectiveness of a resilient system depends on its ability to anticipate, absorb, adapt and/or quickly recover from an extreme event".
In a resilient system, the components are designed to withstand threats and have a maintenance that avoids failure, if a failure occurs the system as a whole continues to function properly thanks to the sufficient redundancies present. In the case of simultaneous degradation of several components, the system progressively degrades in a controlled and adaptive manner thanks to defense systems and by sending communications. Finally, in the event of a fault, the reset is carried out quickly.

### 2.5.1 Resilience assessment

Assessing resilience is performed via two different approaches: a qualitative and a quantitative one, which have different purposes and indicators of results.
Qualitative methods serve for long-term policy and provide a picture of the state of the system. These include that of Carlson et al. [156] and that of McManus et al. [295], which provide results at regional level using interviews and questionnaires with citizens, businesses and institutions to see the overall state of the system's resilience. There are also hierarchical analytical methods, which detect subjective opinions on comparable quantities, which are easier to evaluate in order to be able to make decisions.
Quantitative methods are based on the transposition of system performance into numbers, and are particularly suitable for comparison between multiple systems. There are mainly three categories of quantitative methods: simulation, analytical, and statistical.
The most widespread are simulation methods because they allow a combination of accident scenarios and consequence scenarios, examples are J. Watson et al. [160], M. Shinozuka et al. *[213],* and S. Chanda and A. K. Srivastava [289].
Analytical methods provide the probability that the system will fail in some particular situation, for example the method of J.C.Whitson and J.E.Ramirez-Marquez [27].
Statistical methods, on the other hand, are suitable for systems that have suffered a different number of natural disasters and have a large archive of restorative systems used, the best known being the methods of P. J. Maliszewski and C. Perrings [239], D. A. Reed, K. C. Kapur, and R. D. Christie [69].

In the literature, there are also other advanced methods to calculate resilience, which can be seen as an inverse function of risk or each of the phases in the resilience curve can be analyzed individually over time [248].
Generally, the results are shown through indicators that allow to quickly highlight the resilience of a distribution network, which is mainly assessed through data on the interruption to users. The main indicators are the following:

- System Average Interruption Frequency Index (SAIDI), which is the average number of interruptions per user. With λ which represents the power failure frequency in area i, $N_i$ represents the number of users in area i, and $N_T$ represents the total number of users replenished.

*Equation 5: System Average Interruption Frequency Index*

$$SAIFI = \frac{\sum \lambda_i N_i}{N_T}$$

- System Average Interruption Duration Index, which is the average duration of interruptions per user. With Ui representing the duration of the outages.

*Equation 6: System Average Interruption Duration Index*

$$SAIDI = \frac{\sum U_i N_i}{N_T}$$

- Customer Average Interruption Duration Index, which is the average duration per interruption, set as:

*Equation 7: Customer Average Interruption Duration Index*

$$CAIDI = \frac{SAIDI}{SAIFI}$$

- Average System Availability Index, which is the percentage of time a user receives power:

*Equation 8: Average System Availability Index*

$$ASAI = \frac{t_{supplied}}{t_{total}} \cdot 100\ \%$$

### 2.5.2 Interventions to improve resilience

There are two types of strategies that can be adopted to increase resilience:

- Passive approaches: defined as the physical modification of utility infrastructures to make them less susceptible to extreme events through the growth of the system's toughness. Examples of interventions are: burying conductors, using more robust materials, relocating utilities, introducing redundancy, using protective barriers, carrying out maintenance of the surrounding areas (vegetation), using anti-

rotational devices for overhead cables... Interventions of this type are usually expensive and are only effective for certain types of accidents.

- Active approaches: Use of SG technologies to improve the overall efficiency of the power system, threat prediction, scheduling control actions, rapid responses against outages. Possible interventions are the installation of emergency generators and distributed generators, EESSs, demand management, construction of microgrids, advanced protection and control, use of circuit breakers and remote-controlled disconnectors. These systems can alert in real-time in the event of failures so is possible to act quickly.

Optimal design encompasses both approaches. The active approach is certainly full of benefits, but it can be very expensive, so it is only suitable for critical areas. While the SG approach is systemic, i.e. it predicts failures or recognizes them early and sends communications for immediate recovery.
The study of the resilience of the network was partly carried out in the publication [XII], which shows the analysis of the impact of faults in the Terni distribution network.

### 2.5.3 Short-circuit faults in different neutral configurations: case study of Terni distribution grid

A Medium Voltage (MV) power DN is paramount for efficiently delivering electrical energy to industrial, commercial, and residential areas. Nevertheless, these networks face various faults that pose a substantial risk to their reliability and stability. Understanding the root causes of short-circuit faults and their associated consequences is imperative to devise effective mitigation strategies and enhance system performance. The network resilience topic has been extensively explored in the literature, encompassing conditions like natural disasters [226], [81] and strengthening infrastructure through active [305], [284] or passive interventions [194], [189].
Short-circuit faults present significant challenges to power distribution systems' dependable and secure operation. These faults can lead to high current flows, voltage disturbances, and potential damage to equipment, thereby jeopardizing the stability and continuity of electrical supply. Grasping the behavior and repercussions of short-circuit faults in diverse neutral configurations is pivotal for the efficient design, protection, and operation of power grids [165], [311], [144] and [279].
In MV and High Voltage (HV) power systems, the neutral state is critical in maintaining balanced voltages and currents. Each neutral configuration exhibits distinct responses to short-circuit faults, necessitating a comprehensive exploration of their behavior [224].
This study in [XII] seeks to thoroughly examine the effects of short-circuit faults on current and voltage within various neutral configurations in the power grid of Terni. The analysis centers on fault current magnitude and overvoltages in different neutral states. Understanding these parameters is essential for assessing fault severity, determining equipment resilience, and developing suitable protection schemes. Through this investigation, potential risks can be identified, and mitigation strategies can be proposed to bolster system resilience.
Furthermore, the paper [XII] delves into the role and impact of shielding, only partilly analysed in literature [29], [96], [16].

#### 2.5.3.1 Grid analysis and model tools

To investigate how the network behaves in the presence of faults and the impact on shielding, OpenDSS was utilised. OpenDSS allows for the simulation of each phase and facilitates the analysis of short-circuit faults by introducing a specific component called the "Fault Object." Properly positioned, this object enables the emulation of various fault types. While OpenDSS can simulate shields using the "Tape Shield" object, it doesn't treat them as distinct conductors, preventing the direct tracking of current and voltage. Therefore, it became necessary to model the three-phase conductors with shields as a six-conductor line, where three conductors represent the phases, and the other three represent the shields, each grounded at both ends. To obtain the admittance matrix for this line, we employed modeling and schematic drawing of the conductors using ATPdraw [40].

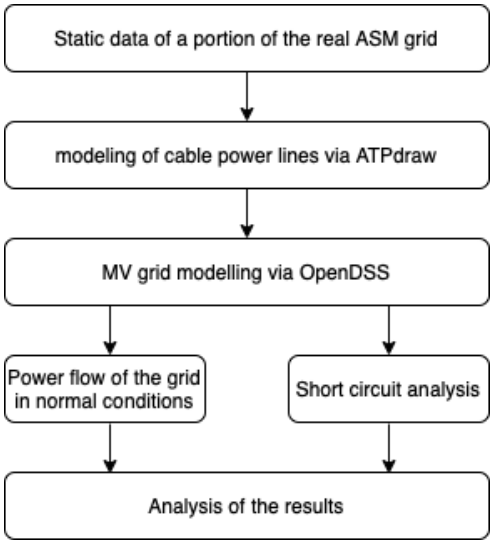


*Figure 20: The methodology applied to the study*

The model was used to evaluate voltages and currents in the network in the event of i) Single-phase earth fault; ii) Double single-phase earth fault, ii) double single-phase earth fault, iii) Single-phase triple fault, iv) Screen fault, v) phase-to-phase fault; vi) Three-phase fault.

The following neutral configurations have been considered:

1. Neutral isolated from earth
2. Neutral connected directly to earth
3. Neutral to earth via resistor
4. Neutral to earth via Petersen Coil
5. Neutral to earth via Petersen Coil in parallel with resistor

Tables displaying the most significant simulation results have been presented for each scenario. The obtained current values can also be valuable input for designing circuit breakers and other protections. Furthermore, network operators can leverage the constructed model to evaluate the feasibility of expanding and reconfiguring their networks. To simulate the network's behavior, OpenDSS was selected because, unlike other open-source softwares, it can calculate electrical characteristics separately for each phase, permits the simulation of screens, and enables the examination of short-circuit events. OpenDSS was not used for modeling conductor screens because it automatically performs Kron reduction, making it impossible to assess the current flow within them.

Consequently, the three-phase conductor with screens was represented as a 6-phase conductor, with only three phases actively powered; this configuration was modeled using a 6 x 6 matrix. The matrix parameters were calculated with the assistance of the open-source tool ATPdraw.

### 2.5.3.2 Short circuit current in various grid configurations

The developed model was tested on a portion of the electricity grid in Terni depicted in Figure 21.

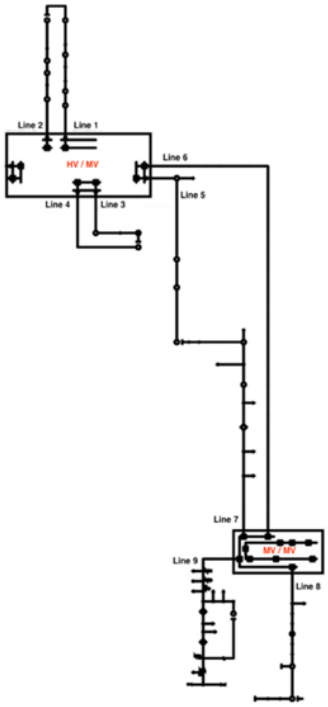


*Figure 21: Grid topology*

Table 9 shows the number of lines in the grid portion and their length for overhead, cable, and underground lines.

*Table 9:Grid features*

| | | | | |
|---|---|---|---|---|
| **Overhead lines (m)** | | | | |
| | **160 mm² Al** | **16 mm² Cu** | **25 mm² Cu** | **35 mm² Cu** |
| Line 6 | 2392 | | | |
| Line 7 | | 1403 | 304 | 1794 |
| Line 8 | | 28 | | 809 |
| Line 9 | | 5964 | 1269 | 2616 |
| **Insulate overhead lines (m)** | | | | |
| | | | | **35 mm² Al** |
| Line 7 | | | | 782 |
| Line 9 | | | | 202 |
| **Underground conductors (m)** | | | | |
| | **150 mm² Al** | **185 mm² Al** | **50 mm² Cu** | **95 mm² Cu** | **185 mm² Cu** |
| Line 1 | 1471 | 291 | | 310 | |
| Line 2 | 1187 | 894 | | 179 | |
| Line 3 | | | | 494 | |
| Line 4 | | | | 473 | |

| | | | | | |
|---|---|---|---|---|---|
| Line 5 | | | 985 | 1415 | |
| Line 6 | | | | | 789 |
| Line 7 | | 501 | | 1061 | |
| Line 8 | | 184 | | 4395 | |
| Line 9 | | 962 | 238 | 1191 | |

The grid is a combination of 16.96 kilometers of overhead lines, 0.98 kilometers of isolated overhead lines, and 17.29 kilometers of underground lines. In those sections where shields are present, they possess a cross-sectional area of 16 mm² and are grounded at both terminals. The primary substation transformer has a capacity of 25 MVA, a rated voltage of 120/20.8 kV, operating at a frequency of 50 Hz, and possessing a short-circuit impedance of 14.11% p.u. Various potential configurations were explored for phase connections and neutral management. Since precise power consumption data is unavailable, and the study's focus is on conducting short-circuit analyses, a constant load of 50 kW is assumed for pole-mounted transformers, and 90 kW is assumed for masonry secondary substations in both cases, maintaining a power factor of 0.95. Given these assumptions, the total demand for the grid is 4.57 MW and 1.12 MVAR. The network does not have any power production.
For configuration III, a resistance of 38.49 ohms was selected, aligning with one of the standard values commonly used in Italy. Considering the network's capacitance in configuration IV, the Petersen coil's reactance is 324.02 ohms. Configuration V, on the other hand, employs a 400-ohm resistor in parallel with a reactance that can offset 95% of the homopolar grid capacitance, which equates to a reactance of 307.84 ohms.

#### 2.5.3.2.1 Permanent electric regime

Across all configurations there are no issues concerning voltage distribution, consistently maintaining between 0.98 and 0.99 p.u. As Table 10 outlines, the current consistently remains below the conductor's ampacity, and line loading never overcomes 20.7%, while the highest recorded current is 72.00 A. Power losses account for 2.49% of the total demand. The column related to shield currents exclusively pertains to insulated conductors, whether overhead or underground. Under steady-state conditions, the current flowing through the shields exhibits variations among the three phases, falling within a range of 2.7% to 8.5% relative to the current in the conductor, with an average value of 5.1%.

*Table 10: Permanent regime power flow*

| Line | $I_{max\ phase}$ (A) | $I_{max\ shield}$ (A) |
|---|---|---|
| L1 | 18.91 | 1.33 |
| L2 | 16.13 | 1.16 |
| L3 | 8.18 | 0.66 |
| L4 | 2.68 | 0.36 |
| L5 | 13.52 | 1.27 |
| L6 | 72.00 | 6.04 |
| L7 | 19.60 | 1.69 |
| L8 | 25.63 | 2.44 |
| L9 | 27.04 | 2.51 |

#### 2.5.3.2.2 Phase to ground faults

Single-phase earth faults were simulated at the termination point of each of the lines, with each fault set to its maximum potential. Table 11 illustrates the highest recorded current values for each configuration and specifies the line in which they occurred. Across the same configuration, there are generally minimal discrepancies in the currents among the lines, except for configuration II. In this configuration, where the neutral is directly connected to the ground, fault currents in lines L7, L8, and L9 are significantly lower, by 60%, than the other lines. In the screens of the faulty phase, a consistent current ranging between 23.8% and 30.7% is observed, while in the screens of the unaffected phases, the current is slightly lower, ranging from 17.2% to 27.8%.

Configuration II exhibits current values that could be considered unacceptable. However, it has a minimal impact on voltage, with the fault phase voltage dropping to 0.72 p.u. In the case of configuration III, neutral management would be feasible with the current values observed. Still, if protection against single-phase earth faults relies on current-operated relays, careful attention must be paid to their correct configuration. In configuration V, the current remains consistently below 30 A, ensuring that full dielectric strength can be restored during self-recovering faults.

*Table 11: Phase to ground faults*

| Configuration | $I_{fault}$ (A) | $V_{max}$ (p.u.) | $I_{shields\ max}$ (A) |
|---|---|---|---|
| I | 35.76 (L9) | 1.75 | 10.65 |
| II | 4530.2 (L3) | 1,20 | 1356.50 |
| III | 302.70 (L3) | 1,68 | 90.79 |
| IV | 0.07 (L2) | 1,72 | 0,02 |
| V | 29.96 (L2) | 1,71 | 7.39 |

A specific type of single-phase fault arises between the conductor and the screen, which can occur if the insulation between the conductor and its screen deteriorates. This fault type resembles the previous one, but it introduces an additional fault impedance from the screen to the ground. Consequently, the fault currents obtained are notably reduced, falling within the range of 5.76 A to 7.33 A across all configurations.

#### 2.5.3.2.3 Double and triple phase-to-ground faults

Within power grids, a scenario can arise where two faults happen concurrently. Following the initial occurrence of a single-phase earth fault, a temporary overvoltage can lead to a second fault in one of the still healthy phases, especially if the insulation in that phase is weakened. These dual single-phase earth faults are more common in medium voltage (MV) networks that employ an isolated neutral. Table 12 presents the current values for situations where these two faults occur either in the same phase or different phases. For the sake of simplicity, our analysis assumes that one fault takes place at the end of L1, while any potential second faults can occur in any of the other lines.

*Table 12: Double phase to ground faults*

| Config. | $I_{fault}$ (A) same phase | $I_{fault}$ (A) diff. phase | $V_{max}$ (p.u.) | $I_{shields\ max}$ (A) same phase | $I_{shields\ max}$ (A) diff. phase |
|---|---|---|---|---|---|
| I | 26.95 (L1-7) | 3990 (L1-3) | 1,73 | 6.44 | 973.22 |

| | | | | | |
|---|---|---|---|---|---|
| II | 4539.50 (L1-8) | 4575 (L1-5) | 1,75 | 1106.80 | 1114.50 |
| III | 325.04 (L1-8) | 4066 (L1-5) | 1,75 | 79.35 | 991.52 |
| IV | 36.71 (L1-8) | 4066 (L1-4) | 1,72 | 10.93 | 991.58 |
| V | 61.11 (L1-8) | 3998 (L1-5) | 1,72 | 15.02 | 974.84 |

If multiple faults occur on the same phase, the current limitations come into play in configuration I, while in configuration II, the current values become unmanageable. In configuration V, it's noticeable that the fault current can double compared to what's observed in the case of a single-phase earth fault. In the isolated neutral configuration for a double single-phase earth fault on the same phase, the current value is lower than that observed with a single phase-to-ground fault, except for all other configurations where the short-circuit current value increases. Notably, in configuration IV, which includes the Petersen coil, the current no longer approaches zero in the case of a double phase-to-ground fault. The current flowing through the shields can reach values as high as 29% of the current on the conductor in the event of such a fault. The voltage consistently remains at about 1.74 p.u., even in configuration II, where it has significantly lower values for a single-phase fault. The results indicate that short-circuit currents for double phase-to-ground faults closely resemble those for phase-to-phase faults. The values obtained are considerably higher when the faults occur on different phases. It's worth noting that these simulations assume no fault resistance, so in actual situations, these values would be lower. The current flowing in the shields can reach up to 24.4% of the current on the conductor. As expected, the voltage of the healthy phase drops in such cases compared to when faults occur on the same line. Specifically, the voltage of the healty phase generally doesn't reach the phase-to-phase voltage level but remains around 1.5 p.u. It increases with the length of the line in which the fault occurs. For a double single-phase fault on different phases between lines L1 (phase 1) and L9 (phase 2), considering the distance between the fault points, the voltage of phase 2 in line L1 does not drop to zero, and the same holds true for line L9 relative to phase 1. Additionally, the overload voltage of the healthy phase increases up to 1.89 p.u. Overvoltages increase as the line length increases, especially if one of the lines is overhead.
In case of a triple phase-to-ground fault, with one fault per phase in different lines, very high current values are obtained, regardless of how the neutral is managed. The maximum fault current value reaches 4608 A, with 1380 A circulating in the shield. These values closely resemble those of three-phase faults, overvoltages are not recorded.

#### 2.5.3.2.4 Phase-to-phase faults

Regarding phase-to-phase faults, there are no variations depending on the type of neutral management. Table 13 shows each line's current value and the screens' maximum current.

*Table 13: Phase-to-phase faults*

| Line. | $I_{fault}$ (A) | $I_{shields\ max}$ (A) |
|---|---|---|
| L1 | 3991.40 | 184.08 |
| L2 | 3991.22 | 184.05 |
| L3 | 3991.72 | 203.96 |

| | | |
|---|---|---|
| L4 | 3991.72 | 204.05 |
| L5 | 3991.40 | 212.69 |
| L6 | 3058.25 | 175.07 |
| L7 | 2207.03 | 120.68 |
| L8 | 3052.04 | 161.05 |
| L9 | 2200.37 | 120.09 |

The current flowing in the shields is, on average equal to 5.18% of the current flowing in the conductor, similar to the stationary regime, but in this case, values higher than the allowable capacity of the shields are reached. Regarding the voltage, the sound phase remains at a value close to the nominal voltage, while the faulty phases reach approximately half the nominal voltage.

#### 2.5.3.2.5 Three-phases faults

The three-phase short-circuit fault remains unaffected by the chosen neutral management configuration, consistently reaching its maximum value at the initial point of the line. Consequently, for lines originating from the primary substation, peak values of 4609.30 A are attained. In contrast, for the three lines originating from the MV/MV substation, namely L7, L8, and L9, the highest recorded current is 4051.20 A. Notably, within the insulated conductor in L6, a current of 313.74 A flows within the shield, surpassing its thermal capacity.

## 2.6 Terni distribution network: an innovation hub

ASM Terni S.p.A. is the entity that manages the electricity DN for the municipality of Terni and the surrounding area. It has been operating in the electricity sector in the municipality of Terni since 1960 and is also responsible for other municipal services such as waste collection, public lighting, public hygiene service, drinking water distribution, wastewater purification, and the operation of the natural gas network.

ASM manages the entire HV, MV and Low Voltage (LV) network in Terni and has fifty employees, divided between workers and specialised technicians, who are responsible for the design, construction and maintenance of the electrical infrastructure. ASM's grid is connected to the national transmission grid through two primary substations, the first delivers 50 MVA in HV and the second delivers 80 MVA in MV. The following table shows the internal characteristics of Terni's grid:

*Table 14: Transformers and substations in Terni distribution network*

| **Transformers and substations** | |
|---|---|
| Primary substations HV/MV | 1 |
| Secondary substations MV/MV | 6 |
| Secondary substations MV/LV | 588 |
| Total transformation power | 115 MVA |

The transformers in the secondary substations are of various sizes, ranging from 40 kVA and 630 kVA with a predominance of 100, 250 and 400 kVA units. About 100 secondary substations are remotely controlled from the operations centre.

*Table 15: Terni distribution network power lines*

| **Power lines** | |
|---|---|
| MV overhead lines (10/20) kV | 395 km |
| MV lines underground cable (10/20) kV | 242 km |
| LV overhead lines with bare conductors | 335 km |
| LV overhead lines with insulated conductors | 495 km |
| LV underground lines | 626 km |

*Table 16: End users of Terni distribution network*

| **End-users** | |
|---|---|
| Number of LV end-users | 65 000 |
| Power installed of LV end-users | 312 MW |
| Average daily consumption of LV users | 890 MWh / day |
| Average yearly consumption of LV users | 218 GWh / year |
| Number of MV end-users | 190 |
| Average daily consumption of MV users | 290 MWh / day |

| | |
|---|---|
| Average yearly consumption of MV users | 167 GWh /year |

*Table 17: Power generators available in Terni distribution grid*

| **Power plants** | |
|---|---|
| Total power installed | 63,4 MVA |
| DER in LV | 13 GWh |
| Number of PV plants in LV | 1276 |
| Power installed in LV | 7,9 MVA |
| DER in MV | 167 GWh |
| Number of generation plants in MV | 53 |
| Power installed in MV | 55,5 MVA |

The plants connected to MV are hydroelectric (4 %), PV (36 %) and thermal (60 %). Overall, DER has produced about 140 GWh/year in recent years, accounting for 40 % of annual energy demand. Among the various plants is the Alviano 2 hydroelectric power plant, which has been in operation since 2002 and uses water from the Tiber river to produce electricity; it has a maximum flow rate of 160 $m^3/s$ and an average flow rate of 72 $m^3/s$, its head is 4.1 m and it produces a nominal power of 2 904 kW [38].

*Figure 22: Hydro-electric power plant Alviano 2*

*Table 18: Public lighting data in the Terni network*

| **Pubblic lighting** | |
|---|---|
| Light points distributed throughout the city | 22,000 |

The ASM headquarter is an energy district that covers an area of about 3 hectares in the suburbs of Terni, with a three-storey building with offices, three warehouses for electrical, gas, and water supplies, used by the multi-utility, and two parking areas covered by PV panels. The microgrid is connected to the external grid via two secondary substations, which have oil-filled electrical transformers with a nominal power of 250 and 400 kVA. Electricity consumption in the building and warehouses, which is approximately 650 MWh per year, is mainly for lighting and powering electrical devices (e.g. computers and servers). The PV generation system comprises 1,100 monocrystalline silicon panels of 150 W at 12 V with dimensions of 98.5 x 98.5 cm. The PV plant is located in the parking area

and interfaces with the microgrid via a 200 kVA inverter. The loads and PV generators are equipped with real-time monitoring sensors using power quality analysers, which allow the voltage, current, active and reactive power values of the various devices to be tracked and stored in a database with a granularity of 1 second. In the parking area there are 3 EVCS, each equipped with two charging points up to 22 kW AC and 32 A, single-phase or three-phase. The EVCSs have a user interface to start and regulate charging, a real-time smart meter, and the option to modulate the charging power remotely.
ASM Terni is responsible for the local door-to-door waste collection in the city of Terni, covering an area of 211 $km^2$ and serving 110,000 citizens on average. The waste collection in the city is carried out by a devoted company fleet which consists of 143 endothermic engine vehicles, that are normally refuelled at the ASM headquarters. Vehicle mileage ranges from 190 km and 46,362 km every year, average, median and standard deviation values are respectively of 10,596 km, 9,843 km and 7,148 km. Light vehicles are those that travel the shortest distance per year (8,901 km), while heavy vehicles are the most used (10,896 km); medium-weight vehicles are at a similar value (10,379 km). The waste management fleet has, to date, annual consumption of about 508 $m^3$ of diesel fuel.

### 2.6.1 Trial site for European projects

ASM is a pioneering and innovative DSO in some areas, which participates and has participated in numerous European projects, within the European Horizon 2020 Programme [134] and Horizon Europe [135]. A brief description of the main projects in which it has made a contribution is given below.

- **BD4NRG: Big Data for Next Generation Energy**. This project [47] envisions to confront big data management challenges for the energy sector, giving a competitive edge to the European stakeholders to improve decision making and at the same time to open new market opportunities. BD4NRG aims to enable an incremental decentralized energy data-driven ecosystem and a collaborative data sovereignty driven ecosystem. The goal is to exploit the economic potential of big data and give to energy sector stakeholders the opportunity to improve their business operational performance. To achieve this and to address the emerging challenges in big data management, BD4NRG partners developed, adapted, and deployed a distributed big data energy analytics framework, consisting of several distributed intelligent collaborative federated nodes, a graphically enriched open modular big data analytics energy toolbox, a scalable big-data energy analytics environment. BD4NRG combined edge processing technologies with federated Machine Learning (ML) and AI, to operate the data-driven energy ecosystem. Also, the project made extensive adoption of open sources technology components, tools and APIs.
- **I-NERGY: Artificial Intelligence for Next Generation Energy**. The deployment of Artificial Intelligence (AI) in the energy sector will radically reshape the energy value chain in the coming years, improving the performance of business processes while increasing environmental sustainability. However, some barriers slow down the introduction of these innovative models within the energy system. I-NERGY [145] aims to validate new energy use cases and technology building blocks, as well as to develop new AI-based energy services, strengthening the competitiveness of SMEs in the energy AI sector. In addition to the AI sector, the

project also deals with the integration of IoT devices and the topics of semantics, federated learning and analytical tools. I-NERGY evolves, scales and demonstrates innovative AI-as-a-Service energy analytics applications and Digital Twin (DT) services that are validated through 9 pilots.

- **IoT-NGIN: Next Generation IoT as part of Next Generation Internet**. IoT is one of the next big concepts to support societal changes and economic growth, being one of the fastest growing information technology segments. A specific challenge is to leverage existing technology strengths to develop solutions that sustain the European industry and values. IoT-NGIN [148] introduces novel research and innovation concepts, which will fuel the next generation of IoT as a part of the European next generation internet. IoT-NGIN uncovers a patterns based meta-architecture that encompasses evolving, legacy, and future IoT architectures. The project also optimizes machine to machine and 5G communications, including using secure-by-design micro-services to extend the edge cloud paradigm. Moreover, it enables IoT systems to be autonomous through privacy-preserving federated ML and with augmented reality support for humans.

# 3 Digital Transition as a flexibility enabler for the energy transition

The deployment of measurement tools and the integration of advanced technologies and services into the electricity grid are pivotal for optimizing grid operations, enhancing resilience, and supporting the transition to a more sustainable and efficient energy system. The development of advanced information technology tools is stricly related with the availability of monitornig devices and metering infrastructures. Placing sensors and IoT devices across the grid's territory enables real-time monitoring of key parameters like voltage, current, and cables temperature. Advanced metering infrastructure including smart meters and sensors, offers a comprehensive view of energy consumption and grid performance at the customer level, and finally geographic information systems and geospatial tools assist in mapping the grid infrastructure, helping utilities identify vulnerabilities and plan for grid upgrades strategically. Smart devices can have edge and cloud computing, to increase the data management and applicability: edge computing devices, situated closer to grid components, provide real-time data processing, reducing latency and enhancing local decision-making, while cloud computing enables scalable data storage, analysis, and remote access to grid information.
The potential for integrating advanced information technology tools is high, depending on the datasets present and the needs of the DSO. Some of the technologies that will be integrated in the coming years are:

- 5G Networks: 5G networks provide low-latency, high-bandwidth communication, enabling real-time data exchange between grid components. This facilitates remote monitoring, control, and response, improving grid reliability and management.
- AI: such algorithms can analyze massive datasets generated by the grid's measurement tools and can identify patterns, predict failures, optimize grid operations, and enhance fault detection and resolution.
- Machine Learning: ML models are adept at forecasting energy demand, identifying anomalies, and optimizing grid operations. They can support predictive maintenance and energy efficiency initiatives.
- Grid Management Platforms: incorporate various technologies, in particular the DT of the grid and receive data from many sensors and IoT devices, offering a unified view of the grid. They enable utilities to monitor, control, and optimize grid performance in real-time.

The integration of these technologies and services into the electricity grid empowers utilities to make informed decisions, enhance grid reliability, reduce losses, and support the integration of RES. Moreover, it fosters a more resilient and efficient grid, meeting the evolving demands of a modern energy landscape.

## 3.1 Digital Twin of the power grid

The proliferation of DER and the growing need to enhance the resilience of DN are prompting DSOs to raise awareness of the real-time status of the networks and actively manage flexible energy resources to enhance system performance. In this context, DT technology plays a crucial role in establishing an affordable distributed framework that supports the management of DNs. The application of DT in the power system draws inspiration from implementations in other sectors, such as manufacturing and building

automation. The research in [XVI] presents a practical case study of developing and integrating a DT with an existing DN. The architecture of the DT adheres to recent standards, and its core components were initially designed to facilitate near-real-time functions like data collection, state estimation, and flexibility calculation. The individual tools integrated into the system and the reliability of the DT were rigorously tested and validated during one-month of operation. The system demonstrated consistent service continuity and accuracy. Results obtained from the flexibility calculator illustrate the effectiveness of the proposed strategies, which have the potential to enhance the energy efficiency of the DN by increasing the local SCR of RES production.

In last years, the adoption of DTs in many industrial fields has allowed performing advanced data analytics and the integration of IoT devices. According to [360], DT is defined as "a living model of the physical asset or system, which continually adapts to operational changes based on the collected online data and information, and can forecast the future of the corresponding physical counterpart". Since the 1990s, DT has been implemented in various industries [8] for applications including real-time monitoring, production control, performance prediction, human-robot interaction, optimization, asset management, and production planning. Among DN applications, the main services are predictive maintenance, fault detection and diagnosis, state monitoring, performance prediction, virtual testing, diagnosis and adaptive degradation analysis of rotating machines [159], prognostics, and health management [95]. Concerning the power system domain, the DT concept is not widely adopted, as reported in [227], which reviews the most recent trends of DT in microgrids. In particular, the few papers that address DT in power systems do not exploit the existing standard requirements or the already defined reference architectures for developing a new DT. Indeed, the exploitation of existing standards can be frequently found in other fields while, in the power system domain, common approaches are missing. It is expected that DT can be an enabling technology for increasing flexibility exploitation as well as market participation, [163], [54]; moreover, it could increase operator awareness and system resilience.

However, some examples of DT for individual components of a power system can be found in [351], where a DT is used for monitoring power converters; in [322], which describes DT for automated fault detection with an analytical rotodynamic model, and [186], which implements DT for fault diagnosis and maintenance of power grid equipment and transmission lines. DT was also exploited to increase awareness about SG status to increase resilience against cyber-attacks, as in [301] and [18]. Few works fully exploit the DT concept on an electrical power system; notably, reference [261] presents the outcomes of a project where a state estimation was developed for simulation and on-field evaluation by controlling one PV plant for optimized voltage regulation; reference [154] reports a DT of DER tested in a hardware-in-the-loop environment; finally, in [125] DT is exploited for optimally scheduling an EESS.

The research in [XVI] aims at deploying the DT concept in the electric DNs for low-cost applications. At first, the authors surveyed the existing architectures that can be used as a reference, mainly exploiting recent reviews on this topic [78]. Once the reference architecture was identified, the DT modules were developed. The authors developed three separated modules: a data collection module, a state estimator algorithm, and a flexibility calculator. Such modules allow the integration of multiple data sources, the calculation of the power flows (also in case of lack of measurements), and the estimation of the flexibility from EESS, EVCS and electrical loads. The modules were developed to be integrated in

the DT framework and to ensure near real-time operation, assuming that field sensors can provide near real-time measurements. For these services, the frequencies of the updates (e.g., the status is updated every 3 s) are suitable to consider the analysis in near real-time. The whole DT was finally integrated with a real DN to validate the modules and evaluate the near real-time performances. Indeed, after the integration, the system continuously worked for a month, then its outcomes were analyzed to finally asses the validation on a real case study. The paper [XVI] reports a real-life integration of the DT and the performance evaluation of the developed modules (i.e., data sharing speed, the execution time of the modules and assessment of the impact on SCR thought the flexibility calculator).

### 3.1.1 Digital Twin architecture and modules

#### *3.1.1.1 System Architecture*

A crucial element in the development of a DT is the establishment of a reference architecture. Numerous papers have presented DT implementations and their associated reference architectures in the literature [260]. An interesting classification provided by [163] distinguishes these architectures into the following categories:

a. Unit architecture: This pertains to a monolithic software architecture designed for systems with low complexity.
b. System architecture: This type suits systems with multiple interactions, albeit with less complex constituent parts.
c. System of Systems: This architecture is geared towards systems with a high number of dependencies in a multi-technology domain.

Several architecture models have been proposed and discussed in the literature. For instance, in [171], the authors introduce a DT architecture reference model for cloud-based Cyber-Physical Systems, which helps identify various degrees of basic and hybrid computation-interaction modes. Reference [353] outlines an application framework consisting of three main layers (Physical space, Information Processing Layer, and Virtual Layer), with DT applied to the physical production line of an equipment factory. However, in the context of power systems, a comprehensive and robust set of architecture models is not readily available. For example, a review focusing on DT for microgrids does not provide any architecture models [227]. Similarly, a review of DT architectures does not mention works related to power systems [151]. Some papers refer to DT architecture in the power system domain. In [353], a DT architecture in the power system extends the functionalities of Supervisory Control And Data Acquisition (SCADA), including state estimation and additional analyses. In [18], DT architecture's power system comprises three layers: the physical layer, the edge control system, and the virtual space, housing different modules.

This study [XVI] draws inspiration from the recent ISO standard for DTs in manufacturing [151]. Figure 23 illustrates the implemented architecture, which consists of two main spaces: the physical entity encompassing power system equipment (such as cables, transformers, loads, and generators), sensors, and actuators, and the DT framework comprising the data collection entity, the core entity, and the user entity.

- The data collection entity is responsible for gathering all state changes from observable elements and transmitting control commands to those elements when adjustments are required. This entity encompasses sensor adapters, data storage, and data pre-processing.

- The core entity contains the models of the DT, reads the data collected by the data collection entity, and utilizes this information to update its models. The core entity includes both services and models. As per [151], the core entity should be subdivided into the operation and management sub-entity and the application and services sub-entity. In this study, the authors have developed a state estimation module that uses a limited set of available measurements to enhance awareness of the network's status. This module comprises a network model and topology and leverages historical data to forecast load profiles. In terms of services, a flexibility calculator has been developed to estimate orders sent to pre-identified flexibility sources.
- Lastly, the user entity houses the user interface for the services, allowing visualization of module outcomes and the configuration of set points for flexibility orders.

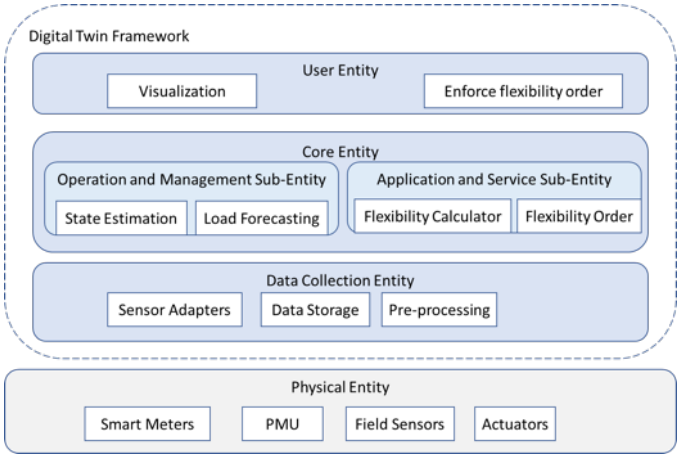


*Figure 23: DT system architecture based on [151].*

### 3.1.1.2 Data Collection

The Data Collection entity plays a pivotal role within the DT architecture, facilitating near real-time operation and continuous interaction with the physical entity. Its function in the DT architecture is illustrated in Figure 23, and further elaboration can be found in Figure 24. This entity encompasses sensor adapters, data storage, and a pre-processing function. Notably, its design does not impose limitations on the integration of sensors; it readily accommodates different open protocols and open data formats by developing the relevant adapters. Adapters are responsible for extracting pertinent information from sensor outputs and aggregating them. The development of adapters is a customized process, which is always necessary due to the diverse array of sensors installed in power systems. Figure 24 offers insights into the adapters created for the real-case study. In particular, the data collection entity leverages existing open protocols and uses edge devices already deployed. These edge devices can provide measurements, even if measurement is not their primary function. Examples of such edge devices include smart meters, power quality analyzers, programmable logic controllers, and intelligent switch breakers. The central adapter that has been developed adds value through the adoption of a reference data structure that is both open and flexible, allowing it to be implemented by the manager of the metering infrastructure.

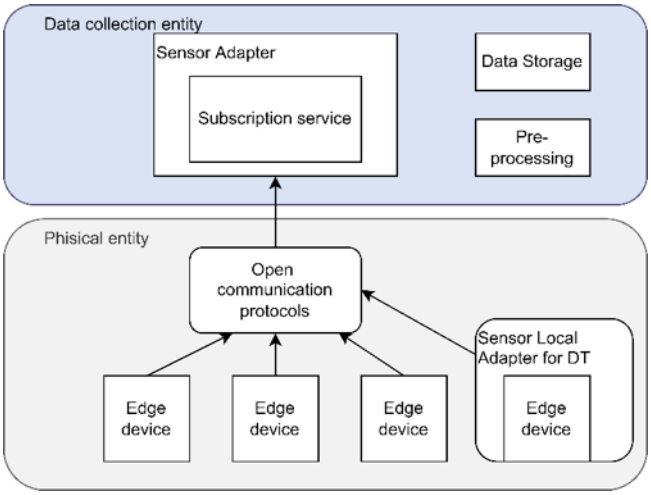


*Figure 24: Data collection entity developed for the case study*

### 3.1.1.3 State estimation

The inclusion of the state estimation module in the architecture serves two primary purposes: to enhance the observability of the DN by utilizing collected measurements and to provide a digital representation of the DN that other modules can further utilize. This module takes actual measurements from the electrical infrastructure as input, specifically voltages, and powers at network nodes equipped with smart meters. These measurements compute power flows along the lines by solving the load flow problem. This computation uses OpenDSS, which is integrated into the Python environment through the Component Object Model interface. The related library is accessible online [182]. OpenDSS was chosen as the power flow solver due to its open-source nature and suitability for analyzing DN issues, including its ability to analyze unbalanced networks. Additionally, it offers compatibility with various additional libraries by interfacing the solver with the Python environment. In particular, OpenDSS calculates node voltages by solving the following system of nonlinear equations:

*Equation 9:*

$$\begin{cases} P_n = \sum_{i=0}^{N_N} V_n V_i Y_{ni} cos\,(\theta_n - \theta_i - \gamma_{ni}) \\ Q_n = \sum_{i=0}^{N_N} V_n V_i Y_{ni} sin\,(\theta_n - \theta_i - \gamma_{ni}) \\ V_{slak} = V_0 \end{cases}$$

In Equation 9, $P_n$ and $Q_n$ are active and reactive power at the node $n$, $V_n$ and $\theta_n$ are the node voltage and its phase angle. $V_j$ and $\theta_j$ are the voltage and angle of the i-th node; $N_N$ is the number of nodes of the network; $Y_{nj}$ is the branch admittance and $\gamma_{nj}$ its related angle. The system, which is summarized in Equation 9, has ($2*N_N - 1$) equations (i.e., 2 equations for each node); the remaining node is the slack bus ($V_{slak}$) for which the reference voltage $V_0$ is set.

The power flow calculation in OpenDSS necessitates input data including the active and reactive power values for all nodes and the voltage at the slack bus. If the number of monitored buses is insufficient to solve the power flow problem, it becomes necessary to estimate the missing active and reactive power values. Voltage measurements are

employed to assess the acceptability of the proposed estimation, using a predefined tolerance as a reference.

A genetic algorithm is employed to estimate these missing power values. This algorithm determines the combination of active and reactive power for the unmonitored buses while minimizing the error between the measured and calculated voltages. While state estimation problems can typically be addressed using well-established techniques [67], using a genetic algorithm becomes beneficial when observability requirements are not met. Consequently, this choice enhances the module's flexibility when integrated into the DT and applied to various networks.

Among the available genetic algorithm versions, a micro genetic algorithm, as detailed in [177], is utilized in the DT. Compared to other genetic algorithms, the micro genetic algorithm starts with a smaller initial random population and converges in just a few generations. Implementation is accomplished using an existing Python library called PyGAD [28], with options for single-point crossover, steady-state parent selection, and random mutation.

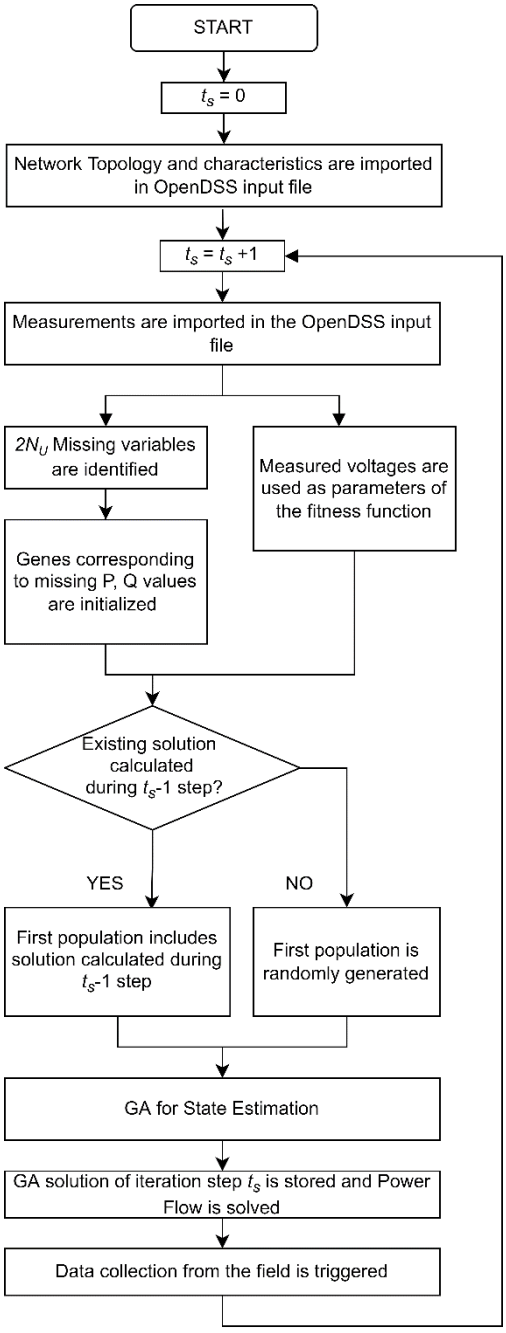


*Figure 25: State estimation module in the DT*

The flowchart in Figure 25 shows the details and functionalities of the state estimation module. After collecting network parameters and topology, these are imported into the OpenDSS input file, which requires to know the value of $2N_N - 1$ electrical variables in order to perform the power flow analysis. When the state estimation starts (i.e., $t_s > 0$), the module considers the measurements that have been just collected and stored. Among these, measured active and reactive power, as well as the voltage of the slack bus are included as input variables in the OpenDSS input file. $N_U$ nodes are the unmonitored nodes, whilst $2N_U$ (i.e., active and reactive power values) are the resulting missing variables that genetic algorithm has to calculate.

The genetic algorithm is initialized and parametrized considering actual missing variables, each of them corresponding to a gene (i.e., each individual has $2N_U$ genes). Each gene can vary in a discrete range defined according to historical data. As an example, the structure of the whole chromosome is reported in Table 19; in that case, defining $P_i^H$ historical active power of the i-th node (kW), the range is between $0.8P_i^H$ and $1.2P_i^H$. In Table 19, $P_i^H$ is a value that can reasonably approximate the actual value to be estimated by the genetic algorithm for node $i$ (e.g., the historical measurement of that specific hour and weekday that is under evaluation). This is a limitation of the DT since a power value highly different from the historical data is not allowed, but this seems to the authors a good compromise between DT accuracy and execution time.

After the initialization, the sequence of generations starts, as it is reported by the flowchart in Figure 26. For each generation $g$, genetic algorithm defines the parameters of all $N_K$ individuals. Then, the fitness of each $k$ individual generated by the genetic algorithm is calculated by using the genes of the individual to complement the input file to the OpenDSS power flow. In this manner, the estimated values of active and reactive power are included in the power flow calculation. After updating the file, OpenDSS, which is coupled with the genetic algorithm, calculates power flow and provides a set of voltages that are compared with the measured values. The actual fitness assigned to each $k$ individual is finally calculated according to the following equation:

*Equation 10:*

$$F_k = \frac{N_M}{\sum_{i=1}^{N_M} |V_i^m - V_i^c|}$$

In Equation 10, $N_M$ is the number of monitored nodes for which voltage values are measured, $V_i^m$ and $V_i^c$ are the measured and calculated voltage of the $i$-th node, respectively. Equation 10 requires in input the measured voltages that are collected in the previous step, according to the flowchart. The best individual is the one with the maximum fitness.

As shown in Figure 26, two stopping criteria are considered: the tolerance on voltages and the maximum number of generations $N_G$ (i.e., $g$=$N_G$). As soon as one stopping criterion is achieved, the best individual is stored as the solution of the genetic algorithm based state estimation. The solution obtained by the genetic algorithm complements the OpenDSS input file, and thus the power flow of the network is calculated. The new power flow solution is used by the other modules that perform additional calculations, such as flexibility estimation as explained in the following subsection.

In the first time step $t_s$= 1 the population is randomly initiated, but when $t_s$ > 1 the best individual of time step $t_s$ – 1 is incorporated in the individuals of the first population. Indeed, as shown in Figure 25, the genetic algorithm is continuously invoked by the state estimation tool and if the time interval between two consecutive steps $t_s$ and $t_s$+ 1 is small, it makes sense to initialize the state estimation solver with the solution calculated in the previous time stamp. This approach allows to reduce the genetic algorithm execution time and quickly fulfills the assigned tolerance, making the DT able to operate in near real-time and therefore to be invoked many times per minute. When the solution in the time step $t_s$ – 1 is the starting point of step $t_s$, the genetic algorithm starts from a solution that already has high fitness and in a few generations, can fulfill the algorithm tolerance. Therefore, even if each genetic algorithm elaboration can be quite limited, a cycling update of the initial population can easily lead to a solution that fulfills the assigned tolerance.

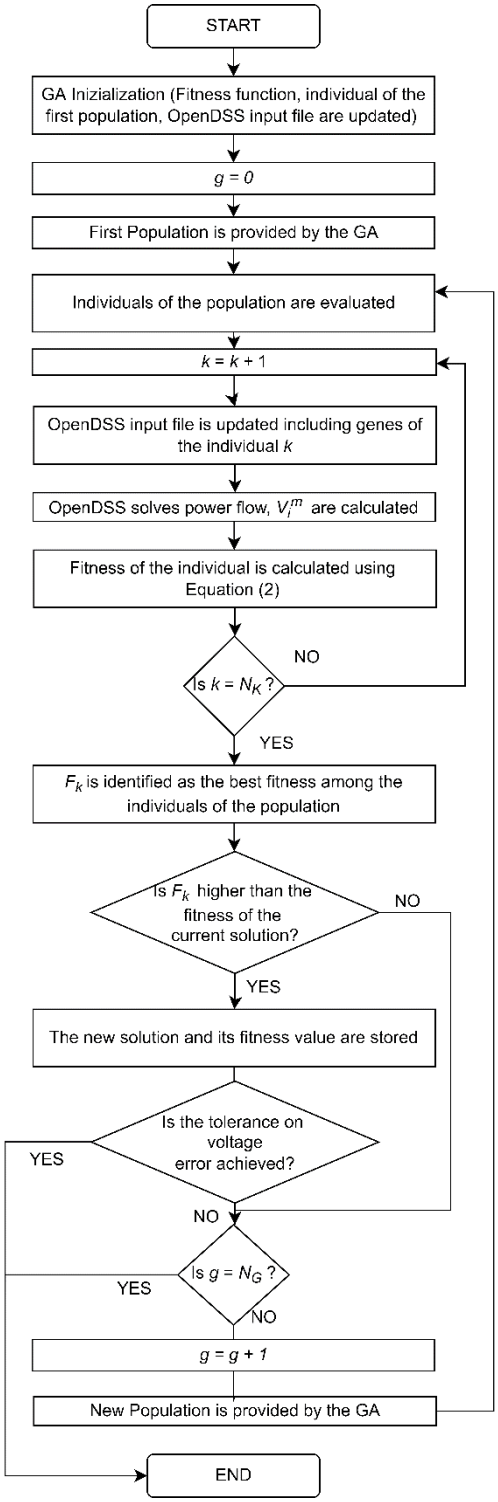


*Figure 26: Genetic algorithm for state estimation*

*Table 19: Structure of the chromosome in genetic algorithm for state estimation*

| **Chromosome Gene** | | | | | |
|---|---|---|---|---|---|
| 1 | … | $N_u$ | $N_u + 1$ | … | $2N_u$ |
| $[0.8P_{1,}^H, 1.2P_1^H]$ | … | $[0.8P_{N_u}^H, 1.2P_{N_u}^H]$ | $[0.8Q_{1,}^H, 1.2Q_1^H]$ | … | $[0.8Q_{N_u}^H, 1.2Q_{N_u}^H]$ |

The complete set of genetic algorithm parameters used in the case study is included in Table 20.

*Table 20: genetic algorithm parameters for the case study*

| | |
|---|---|
| Population | 5 |
| Maximum number of generations | 50 |
| Absolute tolerance on average error | 0.25 V |
| Percentage of genes to mutate | 10 % |
| Number of parents to keep in the population | 1 |
| Number of solutions to be selected as parents | 4 |
| Type of crossover | Single-point |
| Parent selection type | Steady- state selection |
| Type of the mutation operation | Random |

#### 3.1.1.4 Flexibility calculator

The flexibility calculator is an integral component of the DT, designed for the purpose of overseeing the management of distributed flexibility resources that are interconnected with the DN. As defined in [215], flexibility, in this context, refers to a component's capacity to adjust or modify its regular operation temporarily, responding to external service requests without causing unplanned disruptions. This module is primarily responsible for peak load reduction and load shifting, with the ultimate goal of enhancing the SCR of local RES and reducing the average and peak load on transformers and power lines. The decision to prioritize SCR as the main objective of flexibility management stems from its significance in the specific case study for which the DT is tailored and tested. In this particular study, the network under examination experiences Reverse Power Flow (RPF) events. However, it's worth noting that in the future, additional objectives could also be taken into consideration. SCR is described in Equation 2.

To perform this task, OpenDSS is interfaced with a Python module, exploiting a control strategy of flexibility resources based on the power flow value at the connection with the external network (e.g., the power line or the transformer). Flexibility resources include network elements such as:

- EESS;
- Flexible loads, i.e. Heating, Ventilation and Air Conditioning (HVAC), water pumps, and other time-dependent loads (dishwasher, refrigerator, washing machine) for which a DR mechanism is applied;
- EVCS.

The flexibility resources exhibit a range of distinct characteristics, including their capacity for one-way or two-way power exchange with the grid, nominal power ratings, overall capacity, and operational durations. To illustrate, certain devices are capable of activation solely for short-term services, whereas others have the capacity to operate for extended periods throughout the day. Below, we provide a description of each flexibility resource model.

#### 3.1.1.5 Electrical Energy Storage System

Within OpenDSS, the EESS object is represented as a power conversion element. During the charging phase, it is modeled as a constant power load, and during the discharging phase, it acts as a generator. An EESS is inherently subject to limitations imposed by its rated power capacity and stored energy capacity. Illustrated in Figure 27, this model

comprises a storage component that adjusts its State Of Charge (SoC) throughout its operation. Additionally, it incorporates an inverter, which enables the dispatch of the desired amount of reactive power while adhering to a selected power factor. Table 21 outlines the primary characteristics of the storage object.

*Table 21: Storage Object main features*

| state | Storage state: 1) Idling, 2) charging, 3) discharging |
|---|---|
| % Discharge | Discharge rate in percent of the nominal power (%) |
| % Charge | Charging rate in percent of the nominal power (%) |
| $\eta_{ch}$ | Charging efficiency (%) |
| $\eta_{dch}$ | Discharging efficiency (%) |
| $E(t)$ | Available energy at time *t* (kWh) |
| $P_{eff}^{ch}$(t) | Power charging the storage at time *t* (kW) |
| $P_{eff}^{dch}$(t) | Power discharging the storage at time *t* (kW) |
| $P_{in}(t)$ | Power injected in the storage by the grid at time *t* (kW) |
| $P_{out}(t)$ | Power injected in the grid by the storage at time *t* (kW) |
| $P_{idl}$ | Idling power losses (kW) |

When charging, the following balance equation applies:

*Equation 11:*

$$E(t + \Delta t) = E(t) + P_{eff}^{ch}(t) \cdot \Delta t$$

where:

*Equation 12:*

$$P_{eff}^{ch}(t) = (P_{in}(t) \cdot \eta_{inv}(t) - P_{idl}) \cdot \eta_{ch}$$

When discharging, the balance equation is:

*Equation 13:*

$$E(t + \Delta t) = E(t) - P_{eff}^{dch}(t) \cdot \Delta t$$

where:

*Equation 14:*

$$P_{eff}^{dch}(t) = \frac{P_{out}(t)}{\eta_{inv}(t) \cdot \eta_{dch}} + \frac{P_{idl}(t)}{\eta_{dch}}$$

Furthermore, constraints pertaining to the upper and lower limits of the SoC, as well as limits on injected/absorbed power and voltage, are enforced. During periods when the storage component is in an idle state, the losses incurred during idling, along with the corresponding inverter losses, are sourced from the grid. This ensures that the SoC of the storage remains constant during these idle periods.

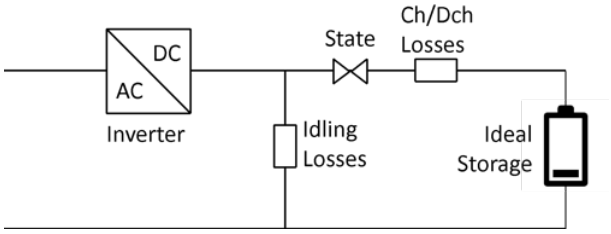


*Figure 27: Storage model*

#### 3.1.1.5.1 Electric vehicle charging station

Recent developments in SG technologies have opened up opportunities for EVs to engage with the grid actively and passively, both on an individual and collective basis. EVCSs can now manage power flow, enabling them to harness their complete capabilities within the electricity DN, all while contributing ancillary services. In this study, as also observed in literature sources [296], EVCSs are simulated with a behavior similar to that of storage systems, limiting the mode of operation to charging only. Table 22 reports the main features of an EVCS as modeled in [XVI].

*Table 22: EVCS model main features*

| | |
|---|---|
| state | 1) No charging, 2) charging |
| % Charge | Charging rate in percent on the nominal power (%) |
| $\eta_{ch}$ | Charging efficiency (%) |
| $SOC_{EV}(t)$ | SoC of the EV connected to the EVCS at time *t* (%) |
| $En_{EV}(t)$ | Nominal capacity of the battery of the EV (kWh) |
| $P_{eff}^{ch}$(t) | Power charging the EV at time *t* (kW) |
| $P_{in}(t)$ | Power injected in the EV by the grid at time *t* (kW) |

We exclusively focused on the grid-to-vehicle charging mode, where the power supply is adjusted in accordance with the grid's requirements, permitting operation solely during vehicle charging sessions. In this scenario, the EVCS is activated as a flexibility source only when, based on the state estimation results, it is determined that a vehicle is actively charging. The amount of power that can be shifted in time spans a range from 25% to 100% of the EVCS's rated power capacity. There are no specific user engagement criteria taken into account in this approach. However, it's worth noting that the EVCS may not be activated for flexibility if the user requires charging at the maximum power level, without concurrently providing any auxiliary services to the grid. When charging, the following balance equation applies:

*Equation 15:*

$$SOC_{EV}(t+\Delta t) = SOC_{EV}(t) + 100 \cdot \frac{P_{eff}^{ch}(t) \cdot \Delta t}{En_{EV}(t)}$$

being

*Equation 16:*

$$P_{eff}^{ch}(t) = (P_{in}(t) \cdot \eta_{inv}(t)) \cdot \eta_{ch}$$

In addition, constraints related to the maximum SoC, absorbed power, and voltage are applied. When there are no EVs connected to the EVCS or the EV is fully charged, power losses are nil.

Figure 28 reports the simplified model of the EVCSs.

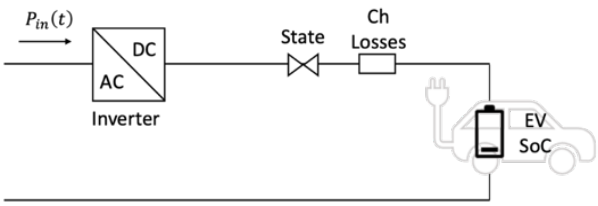


*Figure 28: EVCS model*

#### 3.1.1.5.2 Flexible load for DR

DR encompasses the fluctuations in electricity consumption patterns among end-users in reaction to alterations in electricity prices or incentive schemes designed to encourage reduced electricity consumption during periods of elevated wholesale market prices or when there's a threat to the power system's reliability. DR can be activated through two methods: self-dispatch participation, where consumers engage in load shifting to economize in response to price signals, and incentive-based DR, where consumers are rewarded, often financially, for achieving a specified load reduction or increase within a designated timeframe, aligning with the electricity grid's requirements. Numerous models for DR can be found in the existing body of literature, varying in complexity and considering factors such as the internal characteristics of equipment, technological aspects, societal influences, and environmental considerations. In this study, the authors have opted for a simplified aggregate model of DR, which achieves load shifting [296], [209], [267] and [229]. Load shifting stands out as the most prevalent form of DR, typically involving thermal loads (e.g., air conditioning, heating, cooling), deferrable loads (e.g., washing machines, ventilation, water pumps), or physical storage systems (e.g., hydrogen production). Nonetheless, load shifting encounters various constraints, including technical limitations (e.g., lack of automation in electrical devices or the inability to shed loads), user behavior constraints, process requirements (e.g., certain processes cannot be interrupted or modified once initiated), and the availability of appliances, as mentioned in [42].

The load shifting model employed in the DT closely resembles those used for storage and EVCSs. Essentially, it allows the flexible load to "generate" power by abstaining from consumption during specific periods while being able to "consume" power during other times by increasing or decreasing the expected demand curve. In the model, a DR with load shifting is utilized, incorporating saturation without relying on a base demand profile [113]. When in the charging phase, the following equilibrium equations come into play:

*Equation 17:*

$$P_{DR}(t) = P_{act}(t) + \phi(t) \quad \forall\, t$$

*Equation 18:*

$$\sum_{t=1}^{T} \phi(t) = 0$$

*Equation 19:*

$$P_{min} \leq \phi(t) + P_{act}(t) \leq P_{max} \quad \forall\, t$$

*Equation 20:*

$$P_{DR}(t) \geq 0 \quad \forall\, t$$

*Equation 21:*

$$E(t) = E(t - \Delta t) + \phi(t) \cdot \Delta t \quad \forall\, t$$

*Equation 22:*

$$E_{min} \leq E(t) \leq E_{max} \quad \forall\, t$$

*Equation 23:*

$$E(t = T) = E(t = 0)$$

Equation 17 - Equation 20 are the constraints of an ideal shifting of power without a base demand value, where $\phi(t)$ is the power variation due to the DR mechanism in a certain time period. $P_{min}$ and $P_{max}$ depend directly on the type of load in which the DR mechanism is to be realized. To not change the overall consumption, Equation 18 imposes that increments and reductions are balanced over the time span T. $P_{act}(t)$ is the actual power demand at time t in kW. Equation 21 - Equation 23 involve the free variable E(t) which represents the energy displaced over time by the mechanism, i.e., the capability to anticipate or postpone the consumption, in analogy to EVCS and EESS. In particular, Equation 22 models the load saturation effect by imposing a minimum ($E_{min}$) and maximum ($E_{max}$) level of storage capacity: in this way, unlimited load overconsumption (over-curtailment) during many consecutive periods is not allowed, because the storage will reach its maximum (minimum) level. Equation 23 ensures that the storage level returns to its initial value at the end of the time span T, thus guaranteeing that load demand can be shifted, but the total overall energy consumption will remain the same.

#### 3.1.1.5.3 Flexibility resources management

In order to regulate the behavior of adaptable resources effectively, it is essential to establish an operational criterion. This criterion can either be an inherent attribute of the flexibility resource itself or, more commonly, it can involve the utilization of a controller object. While OpenDSS provides predefined controller modes, which are based on power flow or time scheduling, the authors of this study opted to create a custom controller using Python and the py-dss-interface module. This custom controller enables the adjustment of the operational state and the amount of power consumed or injected by the adaptable resource. It's worth noting that each resource may have its own distinct controller, or a single controller can oversee multiple devices, as exemplified in the DT framework introduced in this paper and illustrated in Figure 29.

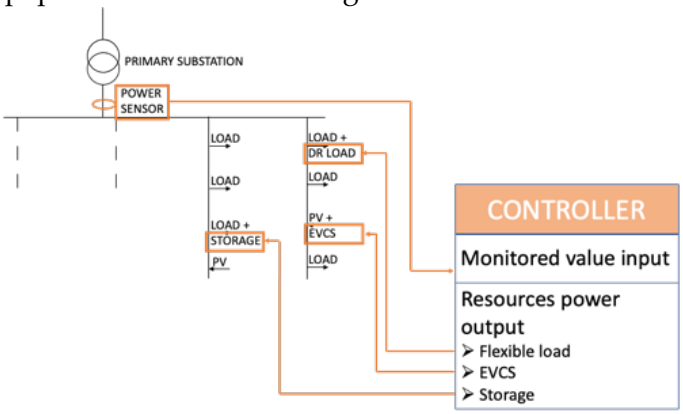


*Figure 29: Storage controller mechanism*

The authors devised a controller model using Python, which interfaces with OpenDSS through the COM Interface. This controller relies on the measurement of a specific parameter in the network's connection element that links it to the remainder of the network. It functions by evaluating the power value in comparison to predefined threshold values and, based on this assessment, instructs the resource to adopt different behaviors, thereby adjusting its operational state and modifying the quantity of power it

either injects into or absorbs from the system. The control system operates by monitoring the power flow within the main feeder, and in the subsequent timestamp, it triggers either power withdrawal or injection by the adaptable resources, as detailed in Table 23. When substantial power levels are observed in the main feeder, the storage resource injects power, while other adaptable resources refrain from power withdrawal. Conversely, when power levels in the main feeder are low, the storage resource charges, and other adaptable resources increase their power consumption. As written by the authors, this operation mode is the result of a simplification and is not without flaws, e.g. swinging phenomena, although rare, can occur.

*Table 23: Storage Controller criteria*

| Threshold | Flexibility resource status | % charging | % discharge |
|---|---|---|---|
| $P \leq P_{th}^{1}$ | Charging | 100 % | - |
| $P_{th}^{1} < P \leq P_{th}^{2}$ | Charging | 75 % | - |
| $P_{th}^{2} < P \leq P_{th}^{3}$ | Charging | 50 % | - |
| $P_{th}^{3} < P \leq P_{th}^{4}$ | Charging | 25 % | - |
| $P_{th}^{4} < P \leq P_{th}^{5}$ | Idling | - | - |
| $P_{th}^{5} < P \leq P_{th}^{6}$ | Discharging | - | 25 % |
| $P_{th}^{6} < P \leq P_{th}^{7}$ | Discharging | - | 50 % |
| $P_{th}^{7} < P \leq P_{th}^{8}$ | Discharging | - | 75 % |
| $P > P_{th}^{8}$ | Discharging | - | 100 % |

To enhance the SCR of the network, we established thresholds employing a genetic algorithm. The process entails utilizing historical data derived from the state estimator, encompassing power demand and generation, and applying the genetic algorithm to retrospectively analyze the past period. This analysis identifies the optimal threshold values that would have yielded the highest self-consumption. These threshold values are then employed for all subsequent iterations until the analysis is terminated. The optimization procedure utilizing genetic algorithm was developed using the Python-based open-access library, PyGAD [28]. This task involves generating 5 solutions within a population for 100 generations, with each solution comprising 8 genes. When executed over one month of data sampled every 20 seconds, the algorithm takes approximately 46 minutes to complete. It's important to note that this execution time, while not negligible, has no impact on the DT since it runs only once, while the DT itself operates in near real-time.

In summary, the management of flexibility resources encompasses the following steps:

1. Identify suitable resources that can be used (e.g., EVCSs are included only if an EV is charging, some resources can be out of service for maintenance activities, etc.);
2. Management of the flexibility resource depending on the power flow in the main feeder (or the connection with the external network compared to threshold values);
3. The power flow of the network with the device thus configured is solved;
4. The energy stored in each device is updated by Equation 11, Equation 13, Equation 15, and Equation 21;
5. Voltage, current, power, and SoC values obtained by the use of flexible resources are exported.

Execution time for the above-described five steps is about 0.01 s, ensuring near real-time operation. The operations performed by the flexibility mechanism in each iteration are shown in Figure 30.

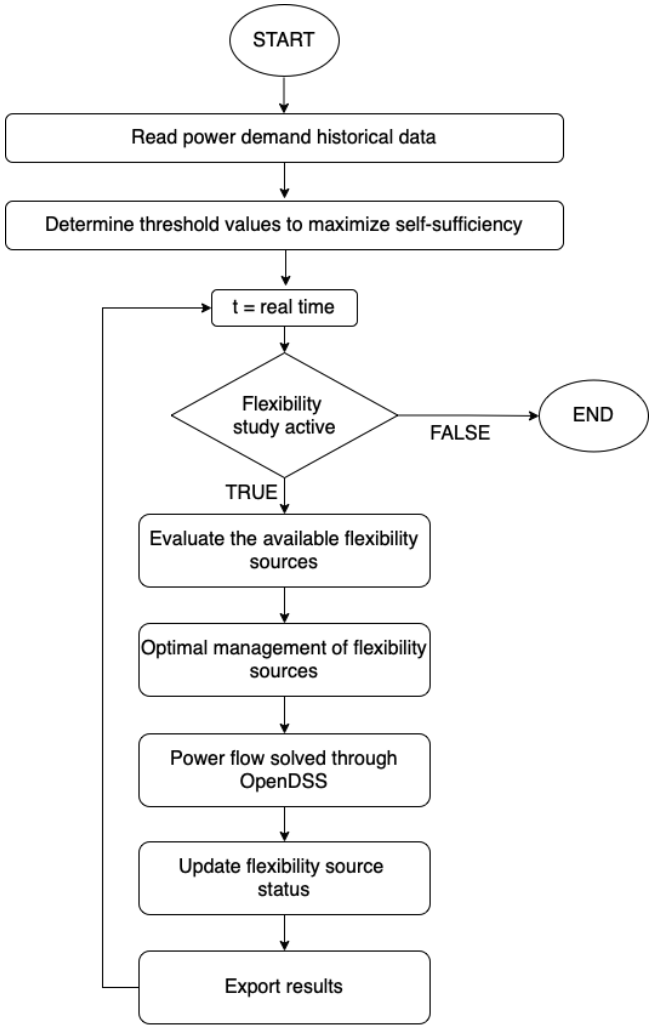


*Figure 30: Flowchart of the flexibility resources management implemented in the DT*

### 3.1.2 Digital Twin of the grid for real time analysis and control in Terni distribution grid

The case study is conducted in a portion of the medium voltage DN of Terni. The network section selected for the case study well represents the set of recently installed technologies enabling the DT implementation. The section is an MV feeder that supplies 5 secondary substations, as shown in Figure 31. Two secondary substations supply the DSO's headquarters. Summing up, it comprises 2 PV arrays (185 kWp and 60 kWp rated power, respectively); an EESS equipped with 72 kWh 2$^{nd}$ life Li-ion battery; two buildings (6,800 m$^2$) and a 1,300 m$^2$ warehouse. The base load is between 50 and 90 kW, whereas the peak load is between 120 and 170 kW. The HVAC of the building is equipped with a Building Energy Management System; 2 private EVCSs and one public EVCS are installed. Figure 32 shows some equipment installed in the case study. Moreover, other users are also supplied by the MV feeder, i.e. 1 MV customer and 35 LV customers with an average 400 kWh daily load demand. Some recorded load profiles are plotted in Figure 33 as an example.

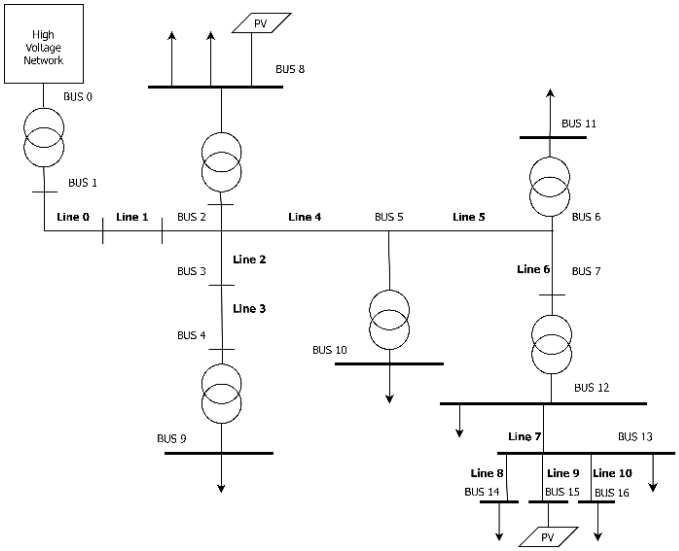


*Figure 31: Single-line diagram of the case study*

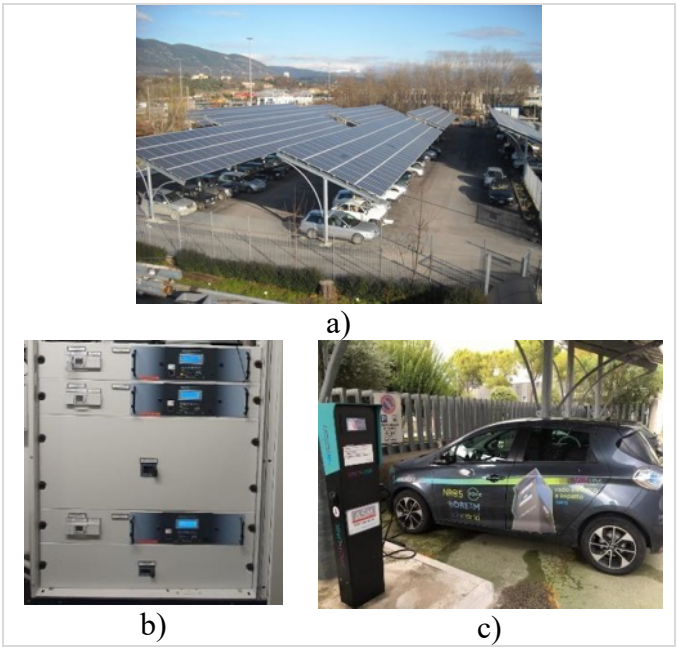


*Figure 32: Some of the equipment installed in the case study: a) PV plant; b) metering devices; c) EVCS.*

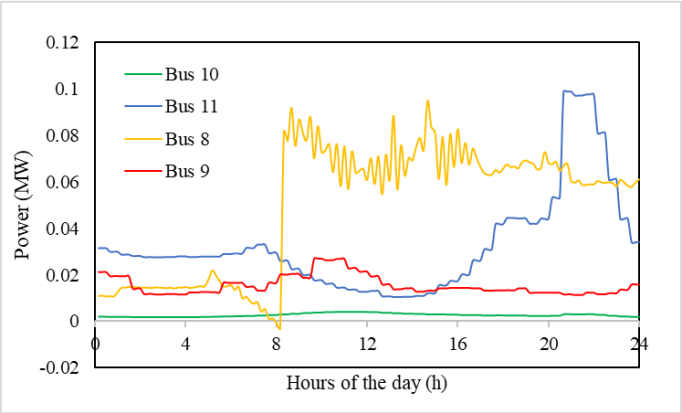


*Figure 33: Example load profiles at some buses of the case study, measured in June 2022.*

The Terni DN is partially equipped with a near real-time metering infrastructure. This infrastructure includes physical sensors such as power quality analyzers embedded within the network and smart meters that communicate with a local extension, typically a Raspberry Pi or a similar single-board computer. These extensions enable the transmission of data in near real-time. Data from these sensors are made available to the modules through the utilization of MQTT protocol. Smart meter extensions and power quality analyzers are configured to publish data every second. To gather these measurements and integrate the data from smart meters, adapters were developed. These adapters subscribe to the relevant topics published by the meters connected within the DN described earlier. It's worth noting that while, in the case study, only power quality analyzers are currently connected to the DN, the adapters developed are adaptable for use with smart meters as well, as the data format remains consistent.

The whole DT of the MV network section was implemented in a remote Workstation with an Intel Core i7-7820X 3.6 GHz CPU and a 64-GB RAM. Various sources of flexibility are installed in the case study, such as EESS, EVCSs, and flexible loads (through DR). These components main features are reported in Table 24.

*Table 24: Flexibility Parameters for the case study*

| Node | Flexibility resources | $P_n$ (kW) | $E_n$ (kWh) |
|---|---|---|---|
| Bus8 | DR for HVAC | 10 | 30 |
| Bus 11 | DR for flexible load | 10 | 10 |
| Bus10 | DR for flexible load | 5 | 5 |
| Bus9 | EESS | 16 | 16 |
| Bus14 | EESS | 72 | 66 |
| Bus8 | EVCS | 22 | 70 |
| Bus16 | EVCS | 50 | 70 |

For electrical loads serving heat consumers like HVAC, it's assumed that 15% of the average power can be rescheduled over a span of 3 hours. As for other flexible electrical loads, it is assumed that the entire rated power of the load can be shifted within a duration of 1 hour.

All storage systems in this analysis are presumed to have a power factor of 1. The efficiency curve of the inverter linked to the storage system, dependent on the utilization factor, is derived from [323] and illustrated in Figure 34.

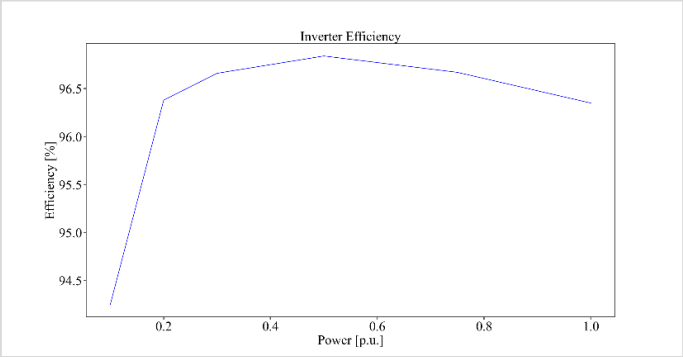


*Figure 34: Inverter efficiency curve implemented in the module*

As depicted in Figure 29, resource management relies on a single controller responsible for monitoring power flow within the primary feeder. This controller can either supply or absorb power with the aim of maximizing the SCR of the specific grid section. When the positive flow of power (i.e., from the HV network) exceeds a predefined threshold, the control system prompts flexibility resources to discharge power. This action helps reduce upstream power flows and associated network losses. Conversely, when the power flow falls below a certain threshold, the flexibility resources are instructed to charge power to mitigate or eliminate RPF. It's worth noting that the threshold values used by the controller are updated each time the simulation is initiated. As an example, Table 25 displays the threshold values following one month of simulation, with a time resolution of 20 seconds. As previously explained in the preceding section, this calculation doesn't impact near real-time operations since it is conducted offline.

*Table 25: Example of the threshold values*

| **Threshold of the power in the main feeder and example** | | **Flexibility resource status** | **% charging / discharging** |
|---|---|---|---|
| $P \leq P_{th}^1$ | $P_{th}^1 = -12\ kW$ | Charging | 100 % |
| $P_{th}^1 < P \leq P_{th}^2$ | $P_{th}^2 = 13\ kW$ | Charging | 75 % |
| $P_{th}^2 < P \leq P_{th}^3$ | $P_{th}^3 = 41\ kW$ | Charging | 50 % |
| $P_{th}^3 < P \leq P_{th}^4$ | $P_{th}^4 = 53\ kW$ | Charging | 25 % |
| $P_{th}^4 < P \leq P_{th}^5$ | $P_{th}^5 = 120\ kW$ | Idling | - |
| $P_{th}^5 < P \leq P_{th}^6$ | $P_{th}^6 = 164\ kW$ | Discharging | 25 % |
| $P_{th}^6 < P \leq P_{th}^7$ | $P_{th}^7 = 172\ kW$ | Discharging | 50 % |
| $P_{th}^7 < P \leq P_{th}^8$ | $P_{th}^8 = 265\ kW$ | Discharging | 75 % |
| $P > P_{th}^8$ | | Discharging | 100 % |

Due to the small number of flexibility resources available in the case study in comparison with the load, some resources are saturated quickly and the shift of the power flow curve is limited.

### 3.1.3 Test network

To evaluate the state estimation module's performance on a larger DN, additional simulations were conducted, implementing state estimation in a test network over the

course of one day. These tests were conducted on the 33-node IEEE test network [199], where 32 nodes represent secondary substations with passive loads, and the final node serves as the primary substation. To simulate daily load profiles, the base power for each secondary substation was considered and employed a standard profile from reference [2]. This profile is expressed as a percentage of the peak load and is sampled hourly. To achieve load profiles sampled every 20 seconds, spline interpolation was applied, and random noise was introduced to differentiate profiles for each substation.
Figure 35 illustrates the maximum and minimum variations imposed every 20 seconds. It's noteworthy that the absolute variation does not exceed 20% of the reference profile. The network's base voltage is set at 11 kV.

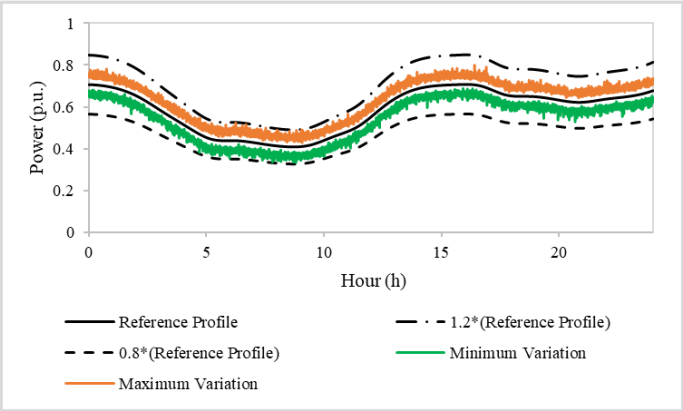


*Figure 35: Reference power profiles and extreme variations evaluated for all timestamps*

The tests primarily center on the state estimation module. The goal is to ensure that state estimation functions correctly even when dealing with a larger network, which involves managing a higher number of variables. In this context, it's important to assess whether the state estimation process remains accurate and efficient despite the slightly increased complexity in power flow calculations when compared to the smaller real-case study presented earlier. As for the flexibility calculator, additional tests were not conducted. This decision stems from the fact that the threshold values are not updated during system operation. In other words, the time it takes to calculate these thresholds does not impact the system's real-time operation.

### 3.1.4 Results of the Digital Twin deployment

#### *3.1.4.1 State estimation*

Over approximately one month, from 05/08/2022 to 09/09/2022, the state estimation module was executed nearly 150,000 times, equivalent to about 3 times per minute. The average execution time for these operations was 0.155 seconds. Instances of unusually long execution times, defined here as exceeding 4 seconds, were rare, occurring only 0.1% of the time.
In terms of accuracy, the average difference between measured and calculated bus voltages was generally acceptable, falling within the ranges of 0.024 V, 0.063 V, and 0.140 V for the 1st, 2nd, and 3rd quartiles, respectively. Cases of average errors surpassing the tolerance established by the genetic algorithm, which is 0.25 V as per Table 26, occurred only 6% of the time.
A more detailed assessment of the state estimation module's performance is provided in Figure 36. This figure illustrates the average absolute error between the state estimation

results and measurements (depicted by the orange line), as well as the execution times (indicated by the blue line) during a 75-minute operation. The state estimation process was executed 235 times within this selected time interval.
Regarding voltage errors during these 75 minutes of DT operation, the average error value was 0.2 V, with a median value of 0.11 V. The median execution time for the genetic algorithm to reach stopping criteria was 0.087 seconds, while the average execution time was 0.46 seconds. Figure 36 reveals several peaks in execution time, leading to a higher average value. These variations in execution time are attributed to the algorithm's tendency to require fewer iterations to meet the specified tolerance in some cases.
Based on these results, it can be concluded that the implemented DT can perform state estimation in near real-time. The developed adapters, which provide a continuous and uninterrupted data flow, also contributed to the system's overall good performance.

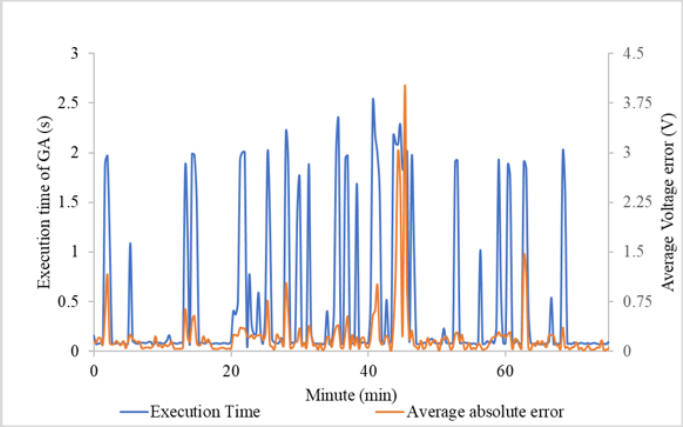


*Figure 36: Execution time of the GA-based state estimation (blue line) and average absolute error between state estimation results and measurements (orange line) during 75 min of operation*

Furthermore, Figure 37 a) and b) offer detailed insights into the calculations performed on 01/09/2022 and 02/09/2022, respectively. These figures present a comparison between the voltage profiles measured and those calculated, explicitly referring to Bus 2, as shown in Figure 31. Figure 37 b) showcases an intriguing aspect of the state estimation algorithm: its ability to track a sudden voltage drop of 8% that occurred around 13:00. In contrast, during the other timestamps depicted in Figure 37 a) and b), the state estimation algorithm exhibited its typical behavior, maintaining a solid agreement between the measured and calculated values.

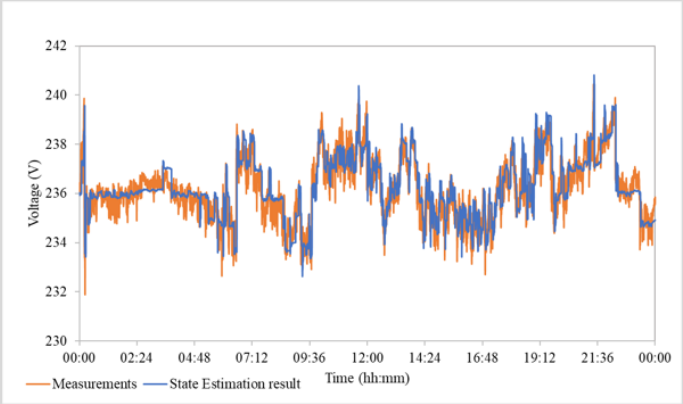


a)

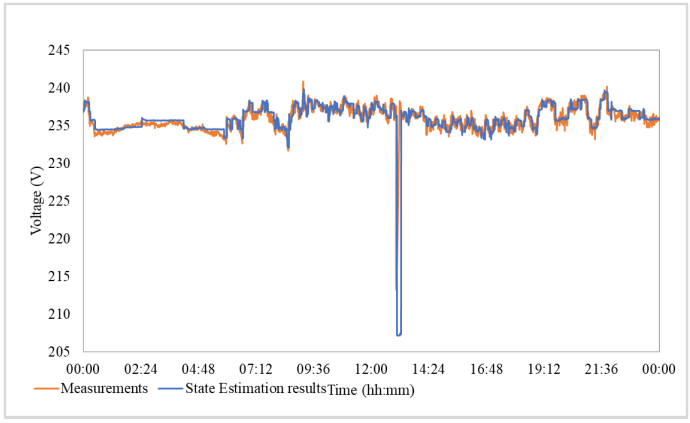


b)

*Figure 37: Measured and calculated voltage profiles at Bus 2 on a) 01/09/2022 and b) 02/09/2022*

Finally, Figure 38 and Figure 39 are selected among the timestamps to show the difference between the two stopping criteria, i.e. minimum tolerance in absolute value on the average error (Figure 38) and the maximum number of generations (Figure 39).

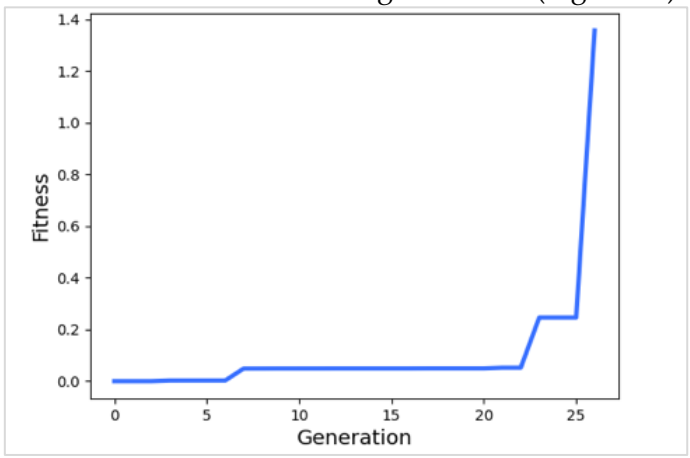


*Figure 38: Fitness evolution when genetic algorithm in state estimation stops since minimum tolerance in absolute value on the average error is achieved*

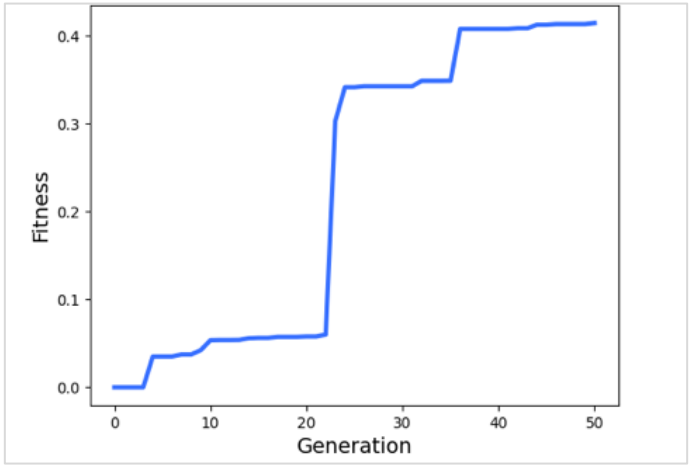


*Figure 39: Fitness evolution when genetic algorithm in state estimation stops since the maximum number of generations is reached*

Finally, some results on the IEEE 33-nodes test case are reported, based on 4 sets of 50 simulations. For each set of simulations, NM is fixed. However, the group of monitored nodes is randomly defined for each simulation (i.e., 50 different configurations are evaluated). It is worth mentioning that power profiles are the same for all the simulations and were carried out assuming that the exact status of the network is known at the first timestamp (i.e., the state estimation overcame the start-up transient). Results of the 200 simulations are averaged and reported in Table 26, which shows that the state estimation can still provide good performances on accuracy and execution time.

*Table 26: Results of the state estimation applied on the test network*

| $N_M$ | **Average time (s)** | **Average error (V)** | **Median time (s)** | **Median error (V)** |
|---|---|---|---|---|
| 25 | 0.0200 | 0.1612 | 0.0239 | 0.0223 |
| 20 | 0.0186 | 0.0736 | 0.0220 | 0.0235 |
| 15 | 0.0176 | 0.0688 | 0.0209 | 0.0276 |
| 10 | 0.0165 | 0.0561 | 0.0190 | 0.0307 |

#### 3.1.4.2 Flexibility calculator

In this section, we delve into the primary performance metrics of the flexibility calculator during the near real-time operation of the DT. Figure 39 a) provides an overview of the active power flow in the main feeder (line 1 in Figure 31) over the course of a week in September 2022, considering actual consumption and generation data that has been post-processed by the state estimation. For a more detailed examination, Figure 39 b) and c) zoom in on specific time windows extracted from the power flow data presented in Figure 39 a), representing one day and one hour, respectively. A consistent pattern emerges from these visuals: flexibility resources are recharged between 9 a.m. and 12 p.m., coinciding with the increase in PV production and relatively low load demand. These resources are then discharged during the pre-evening hours to mitigate peak power consumption. Examining Figure 39 c) closely reveals that the flexibility management system effectively attenuates some peaks by bringing them closer to the average, although its impact varies. This variance occurs because the system operates with thresholds that elicit a non-linear response, and once flexibility resources are saturated, they cannot provide services until they become available again.


*Figure 40: Active power flow in the main feeder during a) one week in September; b) one day (22 of September); c) one hour. Blue line: measurements; red line: power flow using flexibility resources*

Figure 40 provides a depiction of the available energy from the flexibility resources, which include three flexible loads linked to buses 8, 10, and 11, as well as two EESS connected to buses 9 and 14. These data span three days in the latter half of September 2022. It's notable that the utilization pattern of flexible resources exhibits a similar trend across all storage objects. This consistency arises from the presence of a single storage controller overseeing all resources, albeit with varying power and energy constraints. As illustrated in Figure 40, resources are replenished during the midday hours when PV production is at its peak, and the power flow in the main feeder is minimal or negative. Conversely, these resources are discharged from late afternoon until morning.

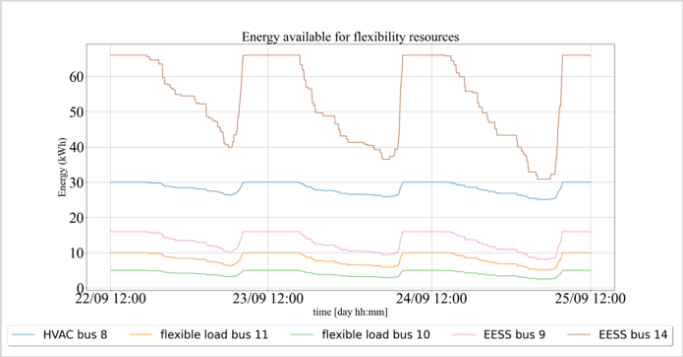


*Figure 41: Available energy from flexibility resources installed in the case study during three days in September*

The utilization of flexibility resources has a negligible impact on bus voltage profiles. This is primarily because the implemented algorithm doesn't optimize bus voltages per se; instead, its objective is to enhance the SCR of the network segment. As a result, when comparing average bus voltage values with and without flexibility, there is minimal difference, measuring 236.124 V and 236.137 V, respectively. The standard deviation is also quite similar, standing at 1.502 V with flexibility and 1.516 V without. This aspect is further clarified by Figure 41 a) and Figure 40 b), which clearly illustrate that only minor voltage variations occur within the network when flexibility resources are employed.

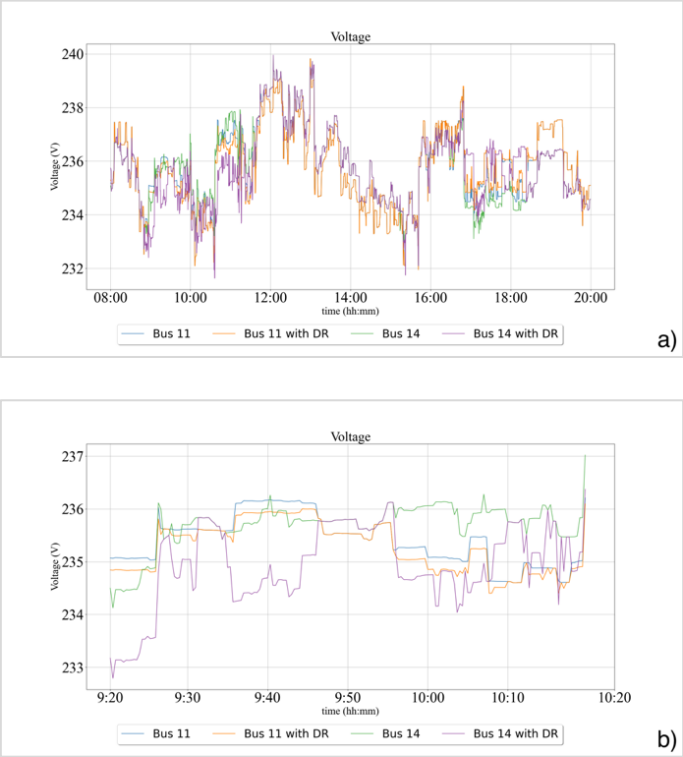


*Figure 42: Voltage profile of two buses on the 22 of September in a) a 12-hours time window and in b) a one-hour time window with and without the use of flexibility services.*

As expected, the impact of flexibility resources on currents is larger than what happens for voltage. The reduction of the average current values on each line is about 4.57%, with a reduction in the standard deviation of 11.48%. Figure 42 a) and b) highlight this effect, allowing in this way the reduction of network losses and, for more stressful power lines, the reduction of thermal risks.

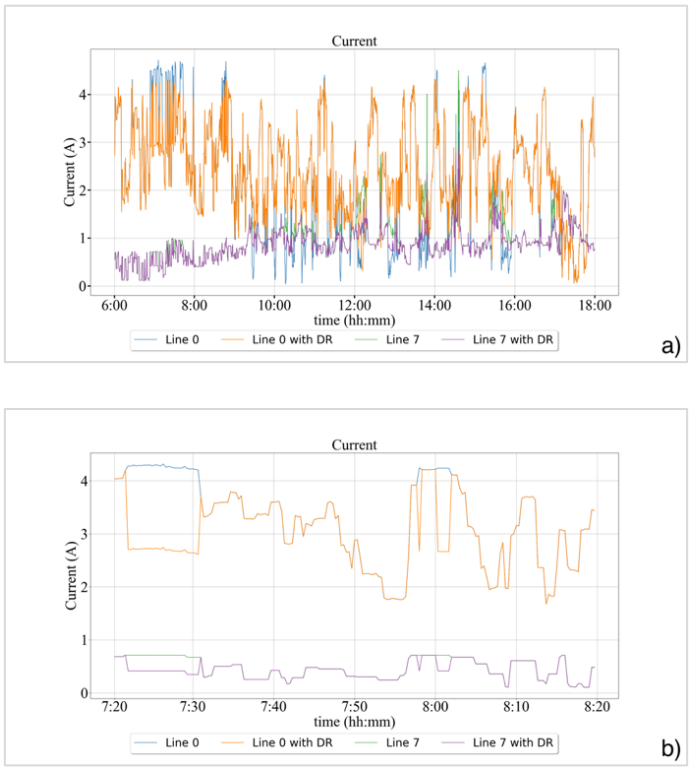


*Figure 43: Current profile of two lines on the 22 of September in a) 12-hours time-window and b) a one-hour time-window with and without the use of flexibility services*

Lastly, Table 27 reports some aggregate results obtained after one month of DT operation. The SCR is increased from 88.42% up to 91.99% and RPF along the main feeder are reduced by 33.01%, with benefits for both LV users and DSO. The peak of the power drawn from the DN is reduced by 23.7%, while the peak from the DN to the external network is reduced by 27.4% in the analyzed month.

*Table 27: Effect of DT operation on global indicators*

| Parameter | Without digital twin | With digital twin |
|---|---|---|
| SCR (%) | 88.42 | 91.99 |
| Reverse energy flows (kWh/month) | 2,999 | 2,022 |
| Max power in main feeder (kW) | 345 | 263 |
| Min power in main feeder (kW) | -204 | -148 |

## 3.2 Internet of Things devices and sensors

The IoT has been identified as one of the next big concepts to support societal changes and economic growth, and one of the fastest growing information and computer technology segments. A whole new range of applications that leverage data and metadata from connected devices provide novel services in various areas such as the SGs. An "thing" in the IoT landscape is any kind of sensor, actuator, wearable device, smart phone or autonomous system, such as autonomous guided vehicles, robots or drones with networking capabilities. In the next generation IoT era, the biggest challenges are to research towards federated on-device intelligence, so that the devices react as self-aware, and when applicable user-aware, semi-autonomous entities, even when their resources are constrained or network connectivity is not reliable; to enforce interoperability and data sovereignty, overcoming scalability and fragmentation of vertically-oriented, closed systems; and to ensure trust, cybersecurity and privacy.

The most important functions needed by an IoT device are flexibility, reliability and performance, along with the security and privacy limitations. Above all, it is the need for a commonly agreed semantic representation of any kind of "things", which will bind existing and future implementations.

The electricity distribution sector is experiencing a transition period in order to achieve the targets set for the fight against climate change and the reduction of climate-altering emissions. The IoT sector offers many prospects and opportunities in the field of SGs. The implementation of IoT in SGs can improve the efficiency, reliability and sustainability of the overall energy system and foster integration with electric mobility.

IoT can enable real-time monitoring of energy consumption and intelligent energy management in SGs. Smart meters collect data on users' energy consumption and transmit it to a central system. This data can be used to optimize energy distribution, manage energy demand more efficiently and prevent any overload problems or power outages, facilitate the integration of non-programmable RES.

IoT can enable advanced automation and control of electrical DN. IoT devices can be used to intelligently monitor and control grid components, such as transformers, switches or EESS devices. This allows more efficient management of energy flow, automatic recovery in case of interruptions and better optimization of network operations.

Using predictive maintenance tools, based on distributed sensors, it is possible to detect in advance the emergence of any failures or malfunctions of the network components. Using IoT sensors, data can be collected on the health and performance of components, applying data analysis algorithms to identify signs of deterioration or anomalies. This enables timely and targeted maintenance, reducing costs and optimizing resource utilization.

A further application is that of IoT devices integrated into the electric mobility sector, favoring efficient charging processes, optimizing the use of RES and offering a better experience to users. Smart charging infrastructure for EVs can be created. IoT sensors can be integrated into EVCSs to monitor charging conditions, outlet availability and wait times. This information can be passed on to e-mobility operators and users, allowing for better planning of charging operations and reducing waiting times. By inserting on board devices into vehicles, the status of EVs' batteries and the optimization of charging are monitored. IoT sensors can collect data on the SOC, temperature, and other key information of batteries. Using data analysis algorithms, charging can be optimized based

on battery needs, extending battery life, reducing charging time, and improving overall energy efficiency. IoT sensors can be installed on vehicles in a corporate or car-sharing fleet to monitor their usage, location, performance and conditions. This information can be used to optimize fleet operations, such as route planning, preventive maintenance and energy consumption monitoring. This enables more efficient and sustainable management of EV fleets. The application of optimization tools makes it possible to exploit EVs as a source of flexibility for the DN, increasing their supply with energy from RES. EVs can act as energy flexibility resources and provide DR services to power grids. The prospects in the IoT sector for SGs are very promising. The use of IoT devices, real-time monitoring, automation, data analysis and integration of RES and EVs contribute to improving energy efficiency, resource management, sustainability and reliability of power grids.

The integration and development of IoT devices in the power grid is one of the scopes of IoT-NGIN project [148]. In literature several information about the applications of the IoT devices in the field of network monitoring have been reported. Many utilities have already started different smart metering practices for consumer billing [162], but few practices of smart metering have focused on the grid infrastructure. The applications focus on MV/LV transformers [292], [167] for their central role in the DN. In [292], the authors proposed a novel IoT infrastructure for asset monitoring with a particular focus on the health of the distribution transformers; their work emphasises the necessity of a low-cost sensor network based on an easily accessible communication network. A minimalistic approach is proposed in [287], where the authors use a computer vision system to take advantage of the possible measurement devices installed in the electrical system but not connected to a TLC infrastructure.

The capillary monitoring infrastructure is exploited in literature to create services for the DSO and the consumers/prosumers, such as detecting energy flexibility sources on the territory and implementing DSR or other decision-making mechanisms [348], [262]. Some studies focus on the devices' capability to work with many electrical/energy measurements and grid status [173], [266], [174], [300] and [153]. In [167], smart meters provide grid operators more visibility into the health and operation of their assets (e.g., transformers lines). In [203], the authors present an original data acquisition and transmission system designed and optimised for online temperature monitoring systems in electric power transformers. In [265], a real-time anomaly detection framework is developed by exploiting data collected at the consumers' premises. In this way, the authors present a system able to detect anomalous events and abnormal conditions. A new method to carry out the load flow analysis in MV networks is presented in [5], based on LV load power measurements applied on an innovative backward/forward algorithm for the power flow resolution. The power quality of public electricity networks is evaluated in [205] through a signal analysis framework based on the data acquisition and transmission of the monitoring devices. Many studies highlight the possibility of building up DR campaigns to exploit the flexibility derived by the customers [235], [327], [286], [341], and [210]. In [204], the DR allows the customers, autonomously or in RECs, to estimate the baseline price in real-time. Based on the estimated price signal, the customers schedule their energy consumption using a cost-sharing strategy to minimise their incommodity level. The authors of [188] suggest an energy management system that runs a simple DR campaign, considering peak and off-peak rates. Most existing studies mainly focus on the theoretical design of DR schemes and do not verify the proposed schemes through implementation, as underlined in [342].

### 3.2.1 State of the art of Internet of Things devices in the distribution grid

One of the significant issues in the future that DNs will face is the high integration of DER such as PV systems, wind turbines and EESSs. This comprehensive integration brings unreliability and unbalancing in the operation of the power system. Thus, the operators of the control centres require an integrated and coordinated system that guarantees the certainty of network operation. Due to the technical and financial restrictions, the monitoring and controlling of power systems at MV and LV sides has not been implemented entirely. In most countries, the monitoring and controlling procedure is done only on primary substations, and the LV or even the MV DNs lack appropriate measurement devices. Consequently, the control centres' operators cannot be exact aware of system conditions on these sides. The dissemination of smart measurement devices in power systems would resolve these problems and bring several proven benefits. An implemented SG scheme would simultaneously tackle the problems of conventional electrical grids (voltage limits, overloads, fault detection, etc.) and allow a variety of beneficial effects. A smart meter infrastructure would bring contemporary social, environmental, and economic advantages. This is possible thanks to the fast response and bi-directional communication infrastructure, collecting and saving of information, displaying and billing function and the ability for loads programming [111]. Regarding the social effects of the spread of smart metering devices, they increase energy efficiency through monitoring information on electricity usage. Nataliya Mogles et al. [231] found that the application of smart meters leads customers to better knowledge about their energy habits. This augmented engagement paves the way for individual energy saving and consequently will diminish the energy sector's environmental impact. Also, on the environmental level, the SG infrastructure would allow a higher penetration of RES on the LV side of the electrical network [172]. G. Dileep [111] stated that the requirement for monitoring DERs is the widespread implementation of smart meters which make the infrastructure of real-time monitoring of power systems. From an economic point of view, realising a reliable power network brings the possibility to control and monitor the components of the electrical network continuously; this brings several benefits, such as fast communication to the operator of any significant or minor failure in systems components. For example, power transformers are at risk of failure for several reasons: any degradation of internal insulation or fluid leak would determine severe internal damage to the transformer, causing an unwanted power outage in the utility grid. Hence, the advantages of settling intelligent monitoring on the power grid include a decrease in the rate of outrage and even maintenance costs. Meanwhile, the periodical overhaul of monitoring and control devices must be done to avoid the failure of monitoring devices such as meters and sensors since it causes the operator to take false action and has no access to reliable data for normalising the system in critical conditions.

All these effects are possible thanks to the variety of applications of smart meters and their fast communications. The developed DN benefits from different equipment that constitute SGs' infrastructure, such as smart device interfaces, transmission subsystem components, intelligent grid distribution components, storage components and demand-side management components. Figure 44 shows the modern technologies which can match itself with smart meters.

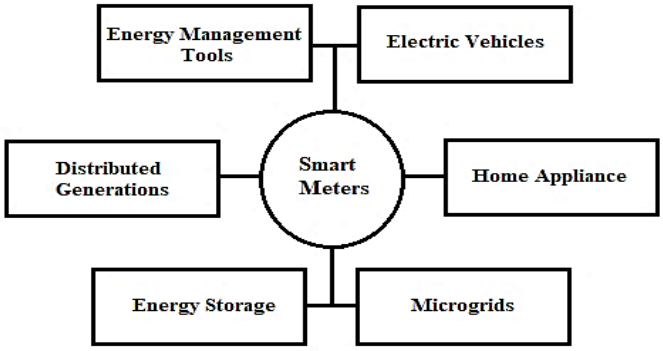


*Figure 44: Smart meters' interface components*

These new potentialities brought by the data exchange of smart meters in both directions have been made possible by the advancement in the information and communication technologies (ICT) sector. It can be seen that the companies which are active in this domain introduced various technologies and protocols for communicating data [212]. Zheng et al. [162] stated that smart meters can be regarded as practical devices for measuring the energy consumption of end users and transferring the obtained data via two current communication technologies, namely Radio Frequency and Power Line Communication, in case of the widespread use of smart metering in the DN (LV side), a robust and reliable bandwidth communication channel for exchanging data among vast numbers of smart meters and controlling units. Meanwhile, the unification of communication protocols with the control centre is vital to avoid discordances in data refining. The exploitation of smart devices depends on the DN's topology, the location's climate, and financial and technical parameters. The monitoring of SGs can be characterised by different metering technologies such as advanced metering infrastructure [9], intelligent electronic devices [99], comprehensive area measurement systems [162], Phasor Measurement Units (PMUs) [12] and different scales: home access network [216], local area network [168], vast area network [15], neighbourhood area network [98]. Another division can be made on the communication network, such as the cloud architecture [206], and the different schemes are chosen according to their task and performance characteristics. Moreover, it can be stated that smart meter devices are applied to various structures.

### 3.2.2 Deplyment of a cost-effective and simple Internet of Things monitoring device in Terni network

The evolution of the DN towards the SG paradigm requires implementing a telecommunication network overlayed to the DN. To achieve this target, a new generation of reliable, cheap, and easily deployable smart meters must be developed. Papers [I] and [II] present a smart meter that fits in a series of possible implementations, from household metering to DER monitoring. The Raspberry Pi ecosystem is chosen for this purpose due to low cost and highly reliable technology to develop an easy-deployable smart meter to collect the principal magnitudes of interest of the monitored side and make them accessible from a Laptop or mobile phone. The designed device is realised and deployed in a secondary substation to monitor a PV power plant in the Terni DN.

#### *3.2.2.1 Device description*

An investigation is conducted in these papers to design and implement smart metering and a monitoring system due to ease of modelling, cost-effectiveness, setup up and use.

The Raspberry Pi single-board computer, an analogue to digital converter, amplification circuit and sensors are the main components of the device, as depicted in Figure 45.

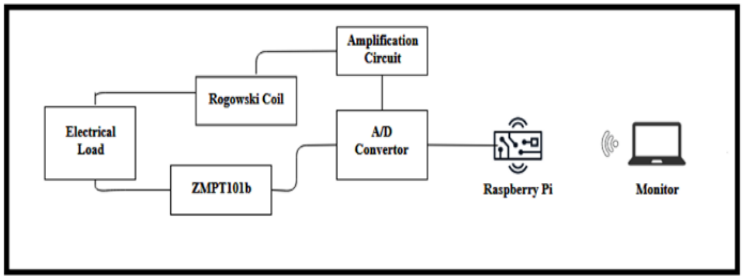


*Figure 45: The functional diagram of the proposed system*

The Raspberry Pi is a single-board computer used in various fields like improving programming skills and implementing electronic projects, and also is applicable both in home automation and industry projects [274]. The third version of Raspberry Pi has been used in this case study. This version is supported by a 1.2 GHz quad-core CPU, 1GB RAM, full-size HDMI, micro USB power source, BCM43438 wireless LAN and Bluetooth Low Energy on board. The lower price of this board is one of the notable properties, which is about $60. Raspberry Pi is based on Linux, which promotes Python and scratch as the primary programming language. This device provides a set of General-Purpose Input/Output pins for communicating with other electronic components for physical computing and exploring the IoT applications.

A Rogowski coil is used for measuring the wide range of current. This kind of sensor is used when it's needed to measure more than tens of amperes up to a thousand amperes and is considered an electrical transducer for measuring AC current's high-speed transients. Rogowski coil can be found in the market in a rigid toroidal core form or flexible belt-like (as that one used in the use case). Quickly wrapping around the conductor, reacting to the fast-changing current due to the low inductance, owing linear characteristics, being highly safe in opening secondary winding, and having a low construction cost are the main advantages of the preferred sensor. The output signal of the Rogowski coil is in analogue.

A sensor module, namely ZMPT101B, has been implemented in the designed system to measure voltage. It measures voltage in the range of 0-250V. This module provides a multi-trim potentiometer to adjust the analogic output. The sensor is efficient and precise, providing galvanic isolation and good consistency for voltage and power measurement. The output of this sensor is analogue and it must be converted into digital form before connecting to the Raspberry Pi. By altering the input signal, the output signal is changed. If there is no load on the primary side, the output signal will equal Vcc/2.

As mentioned above, the sensor's output signal is in analogue form. Thus, it must be converted in digital form to be readable in Raspberry Pi. Therefore, the AD converter, namely ADS1115, is used as an interface between sensors and Raspberry Pi. This converter applies in high-precision instrumentation, automation and in any case where it is needed to obtain a high-precision data collection. The primary function of ADS1115 is amplifying and improving the signal and then converting it to digital form. Moreover, it supports 4 analogue inputs with a 2 - 5.5 V power supply. The data is transferred through the I2C serial interface. This converter is equipped with a programmable gain amplifier, which can amplify the low amplitude signals with high resolution. It can do conversion

operations at 860 samples per second. Four single-channel inputs or two differential inputs allow getting data from more channels simultaneously.
The selected sensor, Rogowski coil, has an output signal of 100 mV / 1 kA. It is evident that when measuring a current under 100 A (which corresponds to 70 kW in a 400V LV distribution system), the generated signal will be shallow (10 mV), which is not in the range of operation of the ADS1115 converter. Looking from the other side, the signal outputs of most sensors are very low and must be amplified. To address this issue, the inverting amplifier circuit can be an exciting scheme for amplifying the output signal. An operational amplifier, namely LM358P, is used in designing this circuit for this aim. LM358P possesses two independent high-gain and frequency-compensated operational amplifiers.
Operational amplifiers are active elements, and signal amplification will not occur unless negative and positive power sources are connected to the appropriate pins. An operational amplifier amplifies the voltage difference between two pins with an extremely high gain. There is an unwanted phenomenon in the operational amplifier, which is called offset. For more explanation, the output value is non-zero in case of having no value in the input. Thus, the voltage should be applied at the input to make zero on the output side. There are two kinds of offset in operational amplifiers: i) input offset voltage ii) input offset current. The input offset voltage for LM358P is lower than 7 mV. The voltage gain of operational amplifiers is exceptionally high (more than 100,000); in practice, applying a negative feedback scheme, a voltage amplifier with stable gain will be designed. To ensure the stability of circuit operation, it is ideal to set the gain voltage between 10 and 10,000. To reach this goal, an amplification circuit uses one amplifier and some resistance. After the amplification, an offset stage is added to send a signal between 0 and 5 V at the ADC.

#### *3.2.2.2 TLC Infrastructure*

The Raspberry Pi 4 is a server that receives the measurement data in the form of strings and stores them for future use. Two Python codes were made in the Thonny IDE environment to provide the software required. The “client” code installed in Raspberry Pi 3 reads the measurement data incoming from the sensors, stores the data for future use, connects to a given host IP address and transfers the data in the form of strings via a socket communication. The “server” code establishes a socket communication, binds it to a port number, and listens to incoming communication. The server receives and stores the measurement data in the Raspberry Pi 4 storage SD card.

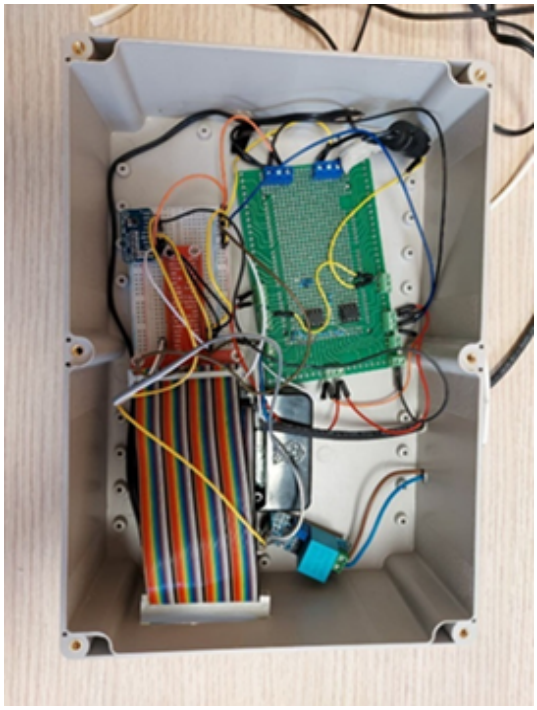

*Figure 46: The prototype system set-up in the outdoor box*

The Raspberry Pi operating system Raspbian GNU/Linux 9 was adopted. The main benefit of the Raspberry Pi consists of the communication interfaces, such as the Secure Shell protocol and Virtual Network Computing utilising the Remote Frame Buffer protocol. These may enable both remote wireless access to the PC and wired access to the PC without the need of connection to a local network with the device to communicate with. In this study, Python programming has been used for measuring temperature and humidity. Socket programming was used to connect two network nodes so that they can interact with one another. One socket listens on a specific port at an IP address, while the other seeks to connect. The most common socket application type is a client-server application, where one side acts as the server and waits for client connections. The server creates the listener socket while the client connects to the server. The communication system based on TCP/IP socket communication consists of two sides: server and client. The client side is responsible for connecting to the server and transmitting the measured data to the server. The server side is responsible for establishing a socket connection and binding it to a port, receiving measurement data from the client, and storing it in the memory of the single-board computer.
The details of the coding of both sides are as follows:

- The client-side Python code is made as follows: i) defines all necessary libraries and variables, including host (server IP address) and port; ii) defines functions responsible for reading the sensor measurements and for the communication with the server; iii) defines a function that writes the measurements into a log file, where each string combines measured variables, date and time of measurement. iv) Then, another function encodes the string containing the measurement variables and sends them via socket communication established before. v) The measuring, logging, combining, encoding, and transmitting functions are put inside an infinite loop to ensure continuity. The measurement granularity is set at every 3 seconds.

- The server code consists of a series of functions that finally log the information received from the client. i) the socket communication is created; ii) it is bound with a pre-defined port number; iii) the server starts listening to potential client requests; when the signal code is received, the server starts a loop. This loop continuously receives the information, decodes it with UTF-8 (by default), and iv) logs it into a file opened previously. This file has no specific format, but the information received is CSV.

#### 3.2.2.3 Deployment of the smart meter in the Terni distribution grid

The designed device is installed in a secondary transformer substation of ASM on the LV line coming from a PV plant with 60 kW peak power capacity. A unified diagram of the secondary cabin of ASM, with reference also to the location of the measurement device, can be found in Figure 47.

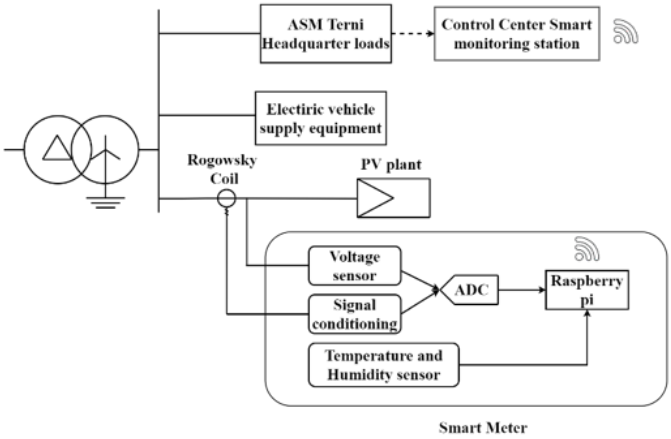


*Figure 47: The schematic diagram of the measurement device in the Terni electricity grid.*


*Figure 48: Location of the measurement device in Terni electricity grid*

The designed system uses a wireless sensor network for the aim of monitoring electrical quantities described in previous sections. The collected data are sent to the A/D converter for changing the form of signal output of sensors from analogue to digital. The obtained parameters can be monitored without any interruption through the graphical interface between Raspberry Pi and a computer. Meanwhile, the whole process of reading the

magnitudes of interest (voltage, current, temperature and humidity), storing the data, and the communication protocol has been done by programming in Python. The voltage and current sensors are connected to the load of the PV plant in a secondary substation for measuring the electrical quantities. The PV power plant located at ASM S.p.A. energy district headquarters has been monitored for a week, proving the reliability of the designed device. By running the system, the operator can be aware of these parameters in the form of remote mode. Also, operators would be capable of stopping or running the measuring process by accessing to the measuring program. In contrast, the access to the measuring environment in Raspberry Pi can be made only by an expert operator due to the operative safety risk against non-specialist persons. The obtained data can be saved in the form of an external file for printing or other evaluations and assessments them. The designed system can be expanded with more sensors by operator and customer's interest. An example of the acquired data in real-time at the secondary substation of the ASM district is illustrated in Figure 49.

data_15_10_2021

```
2021-09-23 10:21:12,29,37,239.51403656505585,40.1972824953052
2021-09-23 10:21:26,29,37,239.82274390654243,38.93296867192161
2021-09-23 10:22:33,29,37,240.3474700576363,42.21117569569517
2021-09-23 10:22:47,29,37,239.00793418050074,40.23104098145572
2021-09-23 10:23:02,29,38,238.31501135365946,39.15485411979299
2021-09-23 10:23:16,29,37,239.48577039056943,39.93262340006662
2021-09-23 10:23:31,29,37,238.49442938463707,38.603692179645854
2021-09-23 10:23:45,29,37,238.90276432628542,37.22508349559887
2021-09-23 10:24:00,29,37,238.19811748901233,37.3552128854603
2021-09-23 10:24:14,29,37,238.54942985573766,38.37223022482295
2021-09-23 10:24:29,29,37,238.0155156038472,46.1199100040364
2021-09-23 10:24:43,29,37,239.37166755968886,38.06815265017782
2021-09-23 10:24:58,29,37,239.07219335979914,46.56811708847692
2021-09-23 10:25:13,29,37,239.51138850358586,49.727492489575106
2021-09-23 10:25:27,29,37,240.10053954860751,45.692576342388165
2021-09-23 10:25:41,29,37,240.20968429110036,38.30766390979444
2021-09-23 10:25:56,29,37,239.76275567087094,38.26686635963246
2021-09-23 10:26:10,29,37,239.11751438038112,46.9255979546912
```

*Figure 49: Data sample*

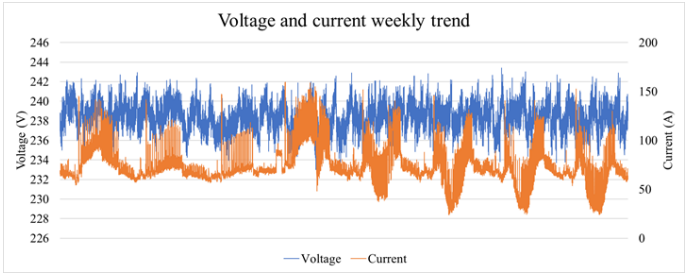


*Figure 50: Voltage and current measured at the ASM secondary station by the proposed monitoring device in the week of 24/09/2021 – 01/10/2021*

Measured data concern secondary substation temperature in °C, secondary substation humidity in %, RMS value of voltage, expressed in Volt, at LV level for ASM district load and RMS value of current, expressed in Ampere, at LV level for ASM district load.
As shown in Figure 50, during the period under consideration, the voltage is always between 242 and 231 V, i.e., in pu between 1.050 and 1.004. Conversely, the current varies more, ranging from around 30 A to almost 150 A. The acquired data concern the electrical quantities of the line connecting ASM's headquarters with the secondary substation; therefore, the trend of the curves is very jagged due to variegate types of loads and the power generation from the PV system. The granularity of the data is 15 seconds, which is feasible for the DSR campaign implementation.

## 3.3 Artificial Intelligence and Machine learnig for the grid

AI is poised to revolutionize the energy sector, reshaping the entire energy value chain and fundamentally altering how the REC conducts its business. The adoption of AI is widely recognized as paramount for energy utilities to enhance the efficiency of their operations and for power network operators to bolster the stability of their grid systems, especially within the context of the emerging decentralized paradigm driven by RES. The transformation of AI in the energy industry will have direct implications on global energy stability and economic prosperity.

Simultaneously, the widespread use of AI in the energy sector holds the promise of significant environmental and social impacts. This extends to aspects such as environmental sustainability, fostering stronger social bonds within local communities, and contributing to the alleviation of energy poverty. Energy fingerprinting, for instance, can be harnessed to provide a variety of consumer-centric AI-driven services that bring substantial social value to individuals and local communities.

In this evolving landscape, the escalating adoption of AI, ML, deep learning, and reinforcement learning presents an unprecedented opportunity for the energy system. It aims to achieve greater grid flexibility, optimized maintenance, and operational efficiency, all while delivering socially-focused, consumer-centric services that encompass energy efficiency, personalized comfort, green energy procurement, the synergy of energy with mobility, and energy fingerprinting-driven social services, such as personal safety, security, and care management.

A significant portion of energy stakeholders anticipates that AI will have a substantial impact on their businesses. However, despite recognizing the potential, many are yet to fully integrate AI into their core operations. This is primarily attributed to the fact that energy utilities, despite their technical expertise in power systems, often lack the information technology background necessary to fully harness the potential of AI applications and services within their processes.

Furthermore, a multitude of innovative small and medium-sized enterprises are emerging, offering a wide array of intelligent services and technologies to stakeholders within the energy value chain. Yet, the unclear and often ambiguous regulations surrounding data access have hindered the development of sustainable business models and return on investment for SMEs, ultimately delaying the widespread adoption of AI throughout the energy value chain.

Moreover, there are several challenges that must be addressed to fully exploit the vast potential that AI offers to the energy sector.

In the following sections, several types of AI-based tools are presented.

### 3.3.1 Energy forecasting services

Forecasting tools within the electricity grid are essential for managing the supply and demand of electricity efficiently. These tools use various data sources and modeling techniques to make predictions about future electricity usage, generation, and other grid-related parameters. Some application of the forecasting tools are: load forecasting, RES generation forecasting, flexibility forecasting... These forecasting tools rely on various data sources, including historical data, weather information, real-time monitoring, and predictive algorithms. They play a critical role in ensuring the efficient operation of the electricity grid, optimizing resource allocation, and accommodating the integration of RES

and evolving grid technologies. Below two forecasting models are presented, developed in studies [III] and [XI] respectively, the first through the multi-layer perceptron model, while the second with a recurrent neural network.

#### 3.3.1.1 Energy forecasting through a Multi-Layer Perceptron model

In [III] a framework was generated in order to obtain day-ahead forecasts for the load and the RES production of the microgrid including 2 PV plants. The energy forecasting tool is based on the weather forecasting. Concerning PV production, accurate forecasting is essential for managing operations in an energy district [290]. Energy production is stochastic and depends on many factors, such as weather, solar radiation, season, hour of the day, and the PV panel's orientation [258]. In literature, several papers deal with analysing forecasting tools for energy production, which are classified as physical models, statistical models, and hybrid models [338], [242], [191], [202], [170], [238] and [201]. The use of ML improves the model accuracy and reduces training time [354], [196].
Concerning load consumption forecasting, it strongly depends on the typology of load, i.e. a commercial activity, a factory, or a residential building. The statistics forecasting model for energy consumption and PV production are similar, but there are differences due to the influence on weather, which in the loads is minor, and to the impact of inhabitants' behaviour, which can vary according to the day or the season [130]. There are several algorithms to provide load forecasting based on statistical models or ML [361].
In [III] two modules have been developed, the first for the PV production and the second for the load forecast. The models were based on Convolutional Neural Network – Long Short-Term Memory Networks since, from previous research, it appears as the most accurate [175], [3]. The model was composed of two stages: in the first, the Convolutional Neural Network layer extracted the spatial characteristics of the features, and then the results were processed by the Long Short-Term Memory Networks layer with the noise partially removed and the identification of the irregular time information using the transmitted spatial features. The model architecture is shown in Figure 51:

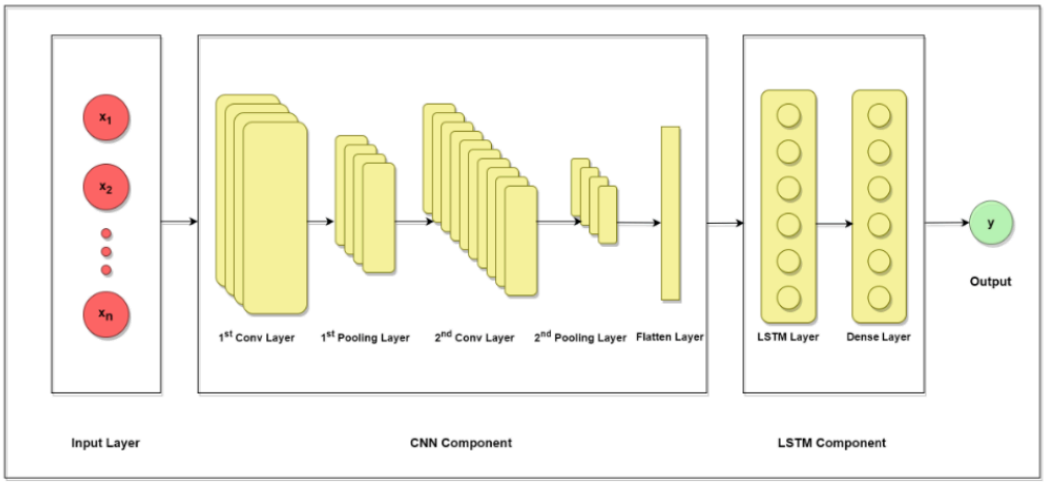


*Figure 51: Architecture of the CNN-LSTM forecasting model*

The features used by the model of the PV production are:

- Environmental temperature
- Environmental relative humidity
- Global radiation
- hour of the day

- month of the year

The features used by the electricity consumption model are:

- 24 hours lag
- 48 hours lag
- 168 hours lag
- hour of the day
- day of the week
- month of the year

Both models were trained using the Keras library, Tensorflow-GPU backend, Cuda Toolkit, and CuDNN.

In the following, a detailed explanation of the forecasting tools is provided. The proposed model was a Multi-Layer Perceptron, a feedforward Artificial Neural Network consisting of a system of interconnected neurons, generally called nodes. These nodes were connected by weights, and a simple non-linear activation function activated them. Since the activation function is non-linear, the Multi-Layer Perceptron was able to provide solutions to non-linear problems. The architecture of the Multi-Layer Perceptron included an input layer, an output layer, and one or more hidden layers. Each node of the Multi-Layer Perceptron was connected to every node in the next layer and the previous layer; thus, it can be considered a fully connected network [115]. An example of an Multi-Layer Perceptron network with two hidden layers is presented in Figure 52. Generally, the output of each hidden and output node was determined by the sum of all the weighted values of the preceding layer's nodes. Afterwards, the result passed through the activation function [51]. The training of the Multi-Layer Perceptron determined the values for each weight and resolved the network's modelling. It was based on an algorithm called backpropagation, which computed the gradient of the cost function concerning the weights of the nodes, aiming to minimise the cost function by adjusting the network's weights and biases [285].

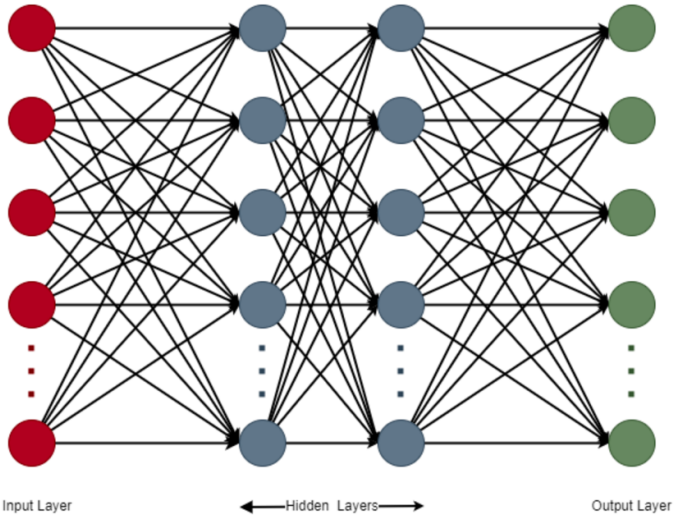


*Figure 52: The architecture of the MLP, a fully connected network that includes an input layer, two hidden layers, and an output layer.*

The main Multi-Layer Perceptron goal was to find a function f that associates the input nodes in X to the output vector sinY (Y= f(X)). In that case, X=[n×k], Y=[n×j], n was the

number of training patterns, k was the number of input nodes/variables, and j was the number of output nodes/variables. During the process of training the model, the function f was optimised. The optimisation came by achieving the lowest possible margin in the output, given the input vectors in X to the target values in Y. The function f was based on the adjustable weights of the network's nodes, and the matrices X and Y represented the training data. The ideas behind the method used for the approximation and prediction are very much alike. The Multi-Layer Perceptron only had one output node, and the dimensions of matrices X and Y in the generic application were n × k and n × 1, respectively, since one variable is modelled from the input data. The prediction required training the model to output the future value of a variable given an input vector containing earlier values [115]. By selecting a suitable set of connecting weights and transfer functions, an Multi-Layer Perceptron can estimate all the perceptible functions within the input and output nodes after choosing the appropriate activation/transfer functions and weights. By training the Multi-Layer Perceptron, the network learned the current training data set, formulateed the input and related output nodes. During this process of training, the Multi-Layer Perceptron was constantly introduced to the training data; by adjusting the weights, the optimal input–output mapping occurred. The training/learning process of an Multi-Layer Perceptron was performed in a supervised approach. When the desired output was not met during a particular input vector, an error signal was identified as the difference between the desired and actual output. During the training process, this error signal was used to establish the adjustable weights to reduce the error signal. As a result, the Multi-Layer Perceptron could extrapolate to unknown but related input data when trained with the appropriate training data [115]. Most traditional ML and deepl learning methods use offline learning, meaning they ingest training data simultaneously to construct a static model. Incremental learning, or online learning, is a branch of ML that involves continuously and in real-time processing incoming data from a data stream. Thus, a model can be trained multiple times and can be iteratively readjusted to new data while still considering older data as well. Training the model incrementally offers multiple advantages and solves many problems of the traditional training methods. Incremental learning algorithms can be used to solve the problem of shortages in computation power. By providing the data in the form of batches, the model is able to fit data quickly and efficiently without the need for a computationally powerful machine. Additionally, on several occasions, the training data size may be unknown or of huge volume, thus making storage impossible. Exploiting incremental learning, a substantial solution is provided by offering the ability to ingest data in batches and retrain the model. As a result, the whole dataset does not need to be stored and can be gradually stockpiled and used. This method is also beneficial when dealing with streaming data or data provided in small chunks and not in one unified pile.

Furthermore, incremental learning helps to implement a system that gradually improves in terms of accuracy whenever new examples emerge, offering an appealing approach to real-life problems and actual scenarios, where changes in the data distribution are continuous and real-time monitoring of environments is essential [48] However, incremental learning brings some difficulties: in the traning/learning process one of the main challenges is catastrophic forgetting, which is the tendency of an artificial neural network to entirely and abruptly forget previously learned information upon learning new information [275]. For that reason, the behaviour of the newly obtained values should be monitored closely. Some simple solutions include rehearsal and pseudo-rehearsal

methods, i.e., retraining the model on the part of old data when new data is introduced [282]. Another obstacle to online learning is concept drift: the properties of the target variable, which the model is trying to predict, change over time in unforeseen ways. This causes problems because the predictions become less accurate as time passes. Concept drift can be avoided by tracking solutions and updating the set using data features in old classes [131].

The proposed methodological framework satisfied the need for incrementally training the proposed ML models and the methods used to implement them. Firstly, the framework included a continuous connection to an MQTT broker for collecting data streams in real-time, as well as the operations of data pre-processing, cleaning, and analysis. The collected data was aggregated into an hourly format and stored in a database. Thus, data could be loaded from the database once daily to periodically retrain the models. The retraining process required only the most recent data and not the whole dataset, thus offering scalability and reduced training time. The updated models were then stored and could be used directly to produce hourly day-ahead forecasts.

First, a real-time connection to a continuous data stream is required, which, was provided via an MQTT broker. All collected data were aggregated hourly and pre-processed to detect unusual details. The pre-processing operations focused on missing data and outliers. Missing values were filled using a special linear interpolation averaging past days' data during the same hour. Some wrong data was detected due to error in the measurement. To handle these outliers, a check was performed, replacing negative or unjustifiably high values. This pre-processing routine resulted in a uniform dataset that could be fed to the models.

Consequently, data were stored in a time-series database for easy and direct querying. In this specific use case, a PostgreSQL database was used to store and retrieve the hourly aggregated information. Thus, data could be loaded daily to re-train ML models. Regarding ML models, the Multi-Layer Perceptron Regressor model of the sklearn.neural_network library was used [53]. The proposed framework involved fitting the model to a chunk of already collected data (one year) and creating a solid baseline model that has learned the patterns of a calendar year. After that period, the baseline model was periodically retrained once daily using the continuous flow of data previously stored in the time-series database. Stored data was given to the model daily in mini-batches of 24 values. Consequently, the model was retrained with the most recent data at the end of the day. As a result of this process, the model kept adjusting to new data every day and could cope with changes in the data distribution in near real-time. At the same time, the stored model generated day-ahead forecasts using the database's most recent records. Moving to the core of the incremental learning process, it is noteworthy that to perform the training process incrementally, the function partial_fit() was used instead of the traditional fit() method. The traditional fit method clears the model and provides a different initialisation of the weights each time. On the contrary, the partial_fit method does not completely clarify and re-initialize the model but updates it concerning the data provided [250]. The small portion of data (usually a data stream) provided as input to the partial_fit method is called a mini-batch. Thus, the ability to learn incrementally from a mini-batch of instances is critical to out-of-core learning, as it guarantees that at any given time, there will be only a small amount of instances in the main memory [309]. As mentioned above, the algorithm used for evaluating incremental learning was the Multi-Layer Perceptron regressor of Scikit-Learn. The Multi-Layer Perceptron regressor was

selected because of its ability to support online learning in mini-batches, as compared to several other ML models. A crucial step of the learning process was the selection of optimal model hyper-parameters, as this offers a significant boost to the accuracy of the ML models. The selected hyper-parameters for the case of PV production and electricity consumption are presented in Table 28.

*Table 28: The hyper-parameters for the PV production and the electricity consumption forecasting models.*

| Measure | PV Production | Electricity Consumption |
|---|---|---|
| Number of hidden Layers | 4 | 3 |
| Neurons per Layer | 641, 286, 432 | 6, 412, 832 |
| Learning Rate | 0.001 | 0.001 |
| Solver | adam | adam |

#### 3.3.1.2 Energy forecasting through MLP model: results

The incremental learning framework was evaluated on ASM infrastructure. A portion of Terni's low-voltage electricity grid was used to test the proposed models, including two secondary substations: ASM's headquarters and a PV production plant of 185 kW. The annual building consumption is about 650 MWh, mainly due to lighting, HVAC, and powering computers and data servers. The data-sharing infrastructure consisted of a SCADA system ans data are transmitted from the sensors via the MQTT and Modbus protocol to the ASM headquarters MQTT broker. The sensors communicate in near real-time with a time resolution of 1 second. Data are then transmitted, to an AVEVA Historian database, accessed through Microsoft SQL Server interface. Two different datasets are used: the first is a PV production time series accompanied by weather data, while the second includes the consumption of the ASM building. Appropriate aggregations were applied, transforming the data resolution to an hourly level. All the data used were hourly and lasted about 2 years and nine months (23,616 hours). A visualisation of the PV production and building consumption time series is presented in Figure 53 and Figure 54:

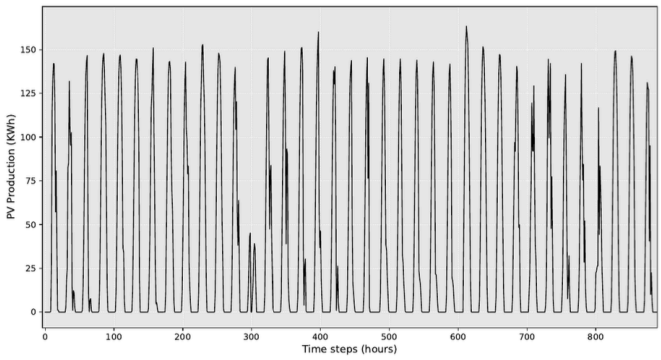


*Figure 53: PV production historical data.*

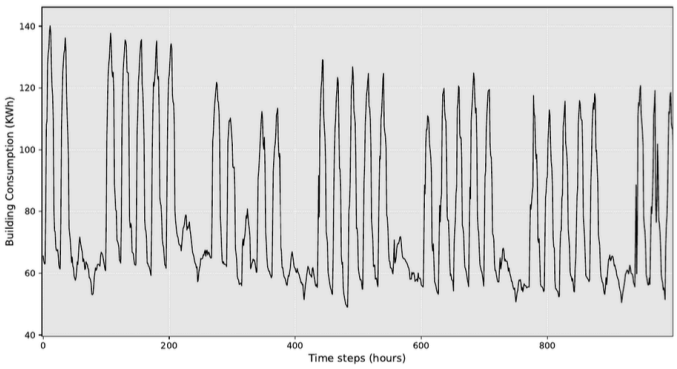


*Figure 54: ASM headquarters consumption historical data.*

PV production has both daily and yearly patterns due to its dependence on solar radiation. Thus, the position of the sun during the day directly affects the output of the PV system, and at the same time, seasonal weather differences affect the production at a yearly level, resulting in much more energy production during the summer period compared to winter. The building consumption time series is more irregular in general, being affected by human factors. An indicative example is the difference observed between weekdays and weekends due to the difference in occupancy levels. The same applies to holiday periods. In general, PV production is stochastic and mainly influenced by weather conditions. Consequently, the main features driving the performance of the PV forecasting model are seasonal features, such as the hour of the day and the month of the year, as well as weather features, mainly solar radiation. The correlation plots between the PV production and the weather feature time series are presented in Figure 55. These plots confirm that PV production is strongly related to solar radiation. While air temperature, cloud coverage, and relative humidity, are much weaker related. Considering all these factors and after experimenting with several combinations of input features, the selected input features for the PV production forecasting model are the following: (a) air temperature, (b) relative humidity, (c) global radiation, (d) month of the year, and (e) hour of the day.

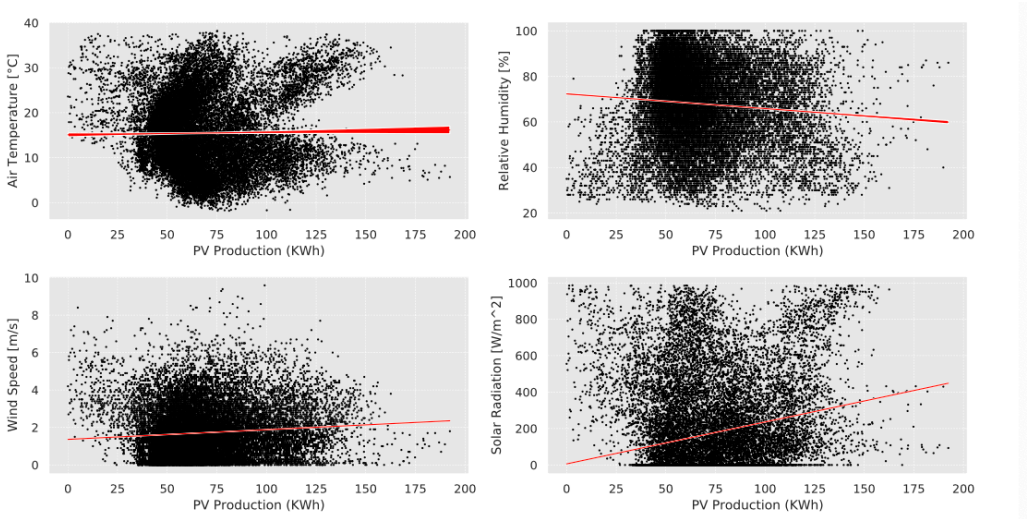


*Figure 55: PV production compared with solar radiation (W/m$^2$), air temperature (°C), relative humidity (%) and wind speed (m/s).*

The consumption of the building is not strongly affected by weather conditions. It is influenced mainly by human behavior and building use patterns. Nevertheless, electricity

consumption demonstrates strong seasonality patterns. Figure 56 presents the auto-correlation function of the electricity consumption time series across a week. The most interesting finding is that the consumption patterns tend to repeat for the same hour on different days. This has led to the use of past electricity consumption data as input features in the consumption forecasting model. Another useful observation is that similar patterns are detected during weekends and weekdays, indicating that the day of the week is another useful feature. With respect to the above findings, the selected input features for the electricity consumption forecast model are the following: (a) hour of the day, (b) day of the week, and (c) month of the year. (d) electricity consumption at the same hour in the last two days, and (e) electricity consumption at the same hour and day in the last week.

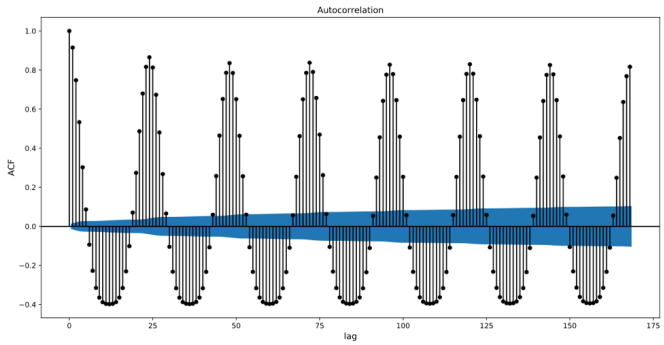


*Figure 56: Auto correlation function of the building consumption across a week (168 h lag).*

The performance of the Multi Layer Perceptron models for both PV production and building consumption was evaluated with the following procedure. The dataset was split into a training dataset and an evaluation dataset using a 63–37% split to allow the models to learn the patterns of more than a year (since the month of the year is given as input) and to be evaluated under a whole year as well. Thus, the first 63% of the dataset (619 days) was used for the training process and the remaining 37% (365 days) was used for testing the models. The accuracy of the models was evaluated by computing the RMSE and the MAE of the respective forecasts across the evaluation period considered. The mathematical formula for these two metrics is presented as follows:

*Equation 24: Root Mean Squared Error*

$$RMSE = \sqrt{\frac{1}{n}\sum_{t=1}^{n}(y_t - \hat{y}_t)^2}$$

*Equation 25: Mean Absolute Error*

$$MAE = \frac{1}{n}\sum_{t=1}^{n}|\, y_t - \hat{y}_t|$$

where $y_t$ is the real value of the PV production or the building consumption time series at hourly intervals t of the evaluation period and $\hat{y}_t$ is the produced forecast of the respective model. Along with these two evaluation metrics, the NRMSE was considered. NRMSE is a metric for comparing models of different scales, relating the RMSE value to the observed range of the variable. It was calculated as follows:

*Equation 26: Normalized Root Mean Squared Error*

$$NRMSE = \frac{RMSE}{\bar{y}}$$

where $\bar{y}$ is the average of the real values.
In the following, results are presented separately for the case of PV production forecasting and the case of the building's electricity consumption forecasting. A comparative plot of the predictions of the two forecasting models for PV production is presented in Figure 57. The model that was periodically re-trained during the evaluation period was more accurate than the traditionally trained one. This can be attributed to the ability of the former model to better adapt to changes in the data distribution or possible trends. For example, if the performance of a PV system changes significantly due to anomalies such as PV cell internal damages or cracks in panels a traditional model cannot adapt to these changes. In contrast, an incrementally trained model is capable of detecting such patterns in the PV production time series, adapt and thus accurately forecast even in these difficult cases.

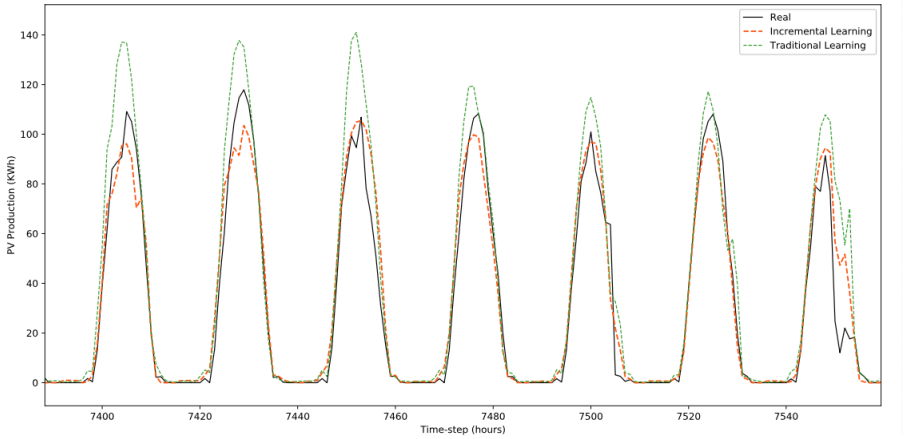


*Figure 57: Comparison between the traditional and the online learning framework for the PV production forecasting task.*

In the case of PV production forecasting, the incrementally trained model demonstrated an MAE index equal to 6.697 kWh, an RMSE index equal to 13.260 kWh, and an NRMSE index equal to 0.527. In contrast, the traditional ML model demonstrated an MAE index equal to 7.273 kWh, an RMSE index equal to 13.340 kWh, and an NRMSE index equal to 0.570, as presented in Table 29. Thus, the incrementally trained model outperforms the traditional one by 8.6% in terms of MAE and 8.1% in terms of RMSE, further highlighting the importance of periodical re-training in the predictive task of PV forecasting.

*Table 29: Error metrics for the PV production forecasting models in the cases of traditional and incremental learning.*

| Measure | Incremental Learning (kWh) | Traditional Learning (kWh) |
|---|---|---|
| MAE | 6.697 | 7.273 |
| RMSE | 13.260 | 14.340 |
| NRMSE | 0.527 | 0.570 |

Considering the case of electricity forecasting in buildings, the impact of re-training the models is even higher. This could be attributed to the fact that electricity consumption is more stochastic compared to the mainly weather-driven PV production forecasting task.

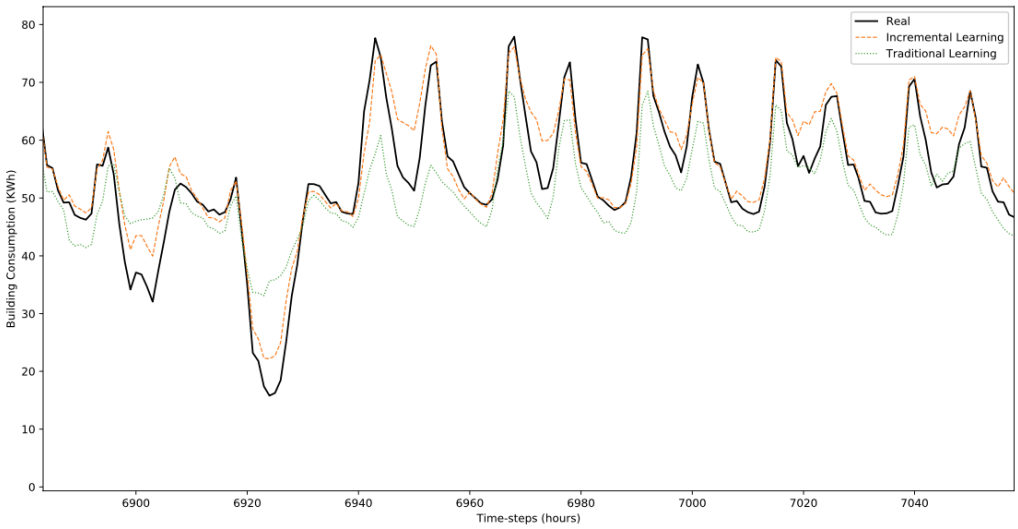


*Figure 58: Comparison between the traditional and the online learning framework for the electricity consumption forecasting task.*

In terms of accuracy metrics, the incrementally trained model outperforms the traditional Multi Layer Perceptron, considering both the MAE error index (8.082 KWh for the incremental model versus 9.048 KWh for the traditional model) and the RMSE index (12.391 KWh for the incremental model versus 13.429 KWh for the traditional model), as presented in Table 30. The respective percentage improvements are 11.9% for MAE and 8.4% for RMSE.

*Table 30: Error metrics for the building consumption forecasting models in the cases of traditional and incremental learning.*

| Measure | Incremental Learning (kWh) | Traditional Learning (kWh) |
|---|---|---|
| MAE | 8.082 | 9.048 |
| RMSE | 12.391 | 13.429 |
| NRMSE | 0.214 | 0.232 |

It can be observed that the impact of incremental learning is higher on the building electricity consumption task compared to the PV production forecasting. As expected, this can be attributed to the more stochastic nature of the electricity consumption time series, which is highly influenced by human behavior. Regarding the benefits in terms of complexity, the incremental learning approach requires over 600 times less memory than the standard learning process in the examined case study. This can be attributed to the incremental learning architecture, which consumes only a single batch of data each time. In terms of time complexity, the incremental models were trained in significantly less time than the traditional ones, although the difference in training time depends on the computational system used. Consequently, using standard training methods makes storage and manipulation more difficult and time-consuming. In contrast, training a model incrementally offers the option to use batches of data. Thus, the required space is reduced, being equal to the size of a single batch. In terms of time complexity, incremental training is more efficient and quicker, since the training time required when using a single batch is significantly lower than the corresponding time when using the entire data set in standard methods.

#### 3.3.1.3 Energy forecasting service through a Recurrent Neural Network

The forecasting model presented in [XI] is based on online learning: the training of models is done continuously when new data is available. This paradigm acquires great importance in the context of IoT due to the large number of sensors or devices that can be present in everyday scenarios and the large amount of information captured by them dynamically. The online learning service supports both Application Programming Interface REST requests and streaming data since most IoT devices generate real-time communication flows. Forecasting the power generated by the grid over a future time frame, based on the historical data collected from grid sensors, consists of predicting the following power values from the last past measured ones. For example, given the last measured 36 h of generated power, predict the next 24 h. Forecasting is computed by a trained ML model that inferences the prediction based on a given input tensor of measured values. This is an example of a univariate time series prediction problem addressed by ML modelling techniques. Before the ML model is ready for computing predictions, it must be trained with historically generated power data. As the sensor continuously pushes the data via MQTT, learning is conducted by an online learning service [50] that collects online data from the topic and trains the model after applying the following data pre-processing procedure: i) power is computed from sensor data, ii) data is resampled by averaging it over each hour, iii) data is scaled in the range [0, 1] as required by ML algorithms applied during training, iv) data is windowed across collected power data, to create a dataset with the shape required by the ML training algorithms. The ML model designed for forecasting the generated power of the grid is a DL model with layers based on recurrent neural networks [70]. Recurrent neural networks have been demonstrated to work well in predicting the future behaviour of time series, although they present some disadvantages, such as the vanishing gradient problem [249]. To overcome this problem, alternative architectures for ML models, evolving from recurrent neural networks, have been proposed, including Long Short-Term Memory and Gated Recurrent Units [263]. The Gated Recurrent Units has been adopted for the power forecasting problem since it solves the vanishing gradient problem suffered by the original Recurrent neural networks and converges faster than other types of Recurrent neural networks (e.g., Long Short-Term Memory). After the recurrent layers, fully connected layers are added for applying linear transformations to the outputs of the Gated Recurrent Units layer. Figure 59 depicts the layers of the implemented architecture.

This proposed model has been trained to minimise the MSE between the fundamental values and the predictions. To understand the performance of the forecasting model, the lower the MSE is, the better the effectiveness is. The MSE has been evaluated as in Equation 27:

*Equation 27: Mean Squared Error*

$$MSE = \frac{1}{n}\sum_{t=1}^{n}(x_t - \hat{x}_t)^2$$

Where $x_t$ is the actual value of the PV production or the building consumption time series at hourly intervals t of the evaluation period and $\hat{x}_t$ is the produced forecast of the respective model.

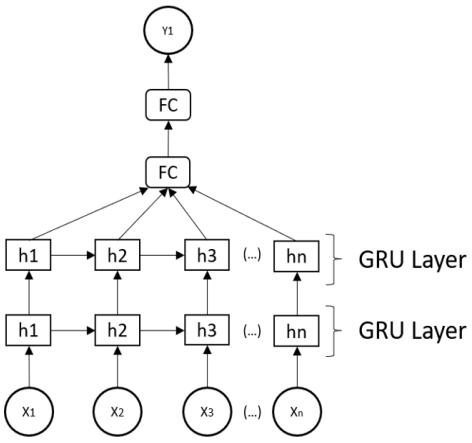


*Figure 59: DL architectures for power forecasting*

A module has been implemented for eXplainable AI that attempts to explain the predictions made to answer the question: Why has the model made this prediction? EXplainable AI is a set of methods and processes that help to comprehend and trust the prediction driven by the ML model. Moreover, it helps to characterise the model performance by providing the impact of the input data for a given prediction, adding transparency to the prediction and capacity for model bias detection. The online learning service is deployed using Kserve [183] through Kubeflow [184]. Kserve allows to deploy 3 types of components: predictor, transformer, and explainer. Each of these components exposes a REST API as an HTTP service. The monitoring service consists of an HTTP endpoint deployed using the FastAPI framework [105], a Prometheus engine [254], and a Grafana web tool [119].

#### 3.3.1.3.1 Energy forecasting service through a Recurrent Neural Network: Results

To verify that the proposed ML architectures are valid, it has been tested to predict the voltage trend and the active and reactive power of the PMU, a smart meter, and two power quality analysers. Forecasting was carried out using a dataset collected for 18 months. It was chosen to have predicted data with a time horizon of 24 hours and a resolution of one hour, whose forecasting is based on the last 36 hours of data averaged every hour. Proposed models have been trained with hyper-parameters shown in Table 31. The optimiser, called Adam, is an algorithm for first-order gradient-based optimisation of stochastic objective functions based on adaptive estimates of lower-order moments [72].

*Table 31: Hyper-parameters for power forecasting models*

| Hyper-parameters | Value |
|---|---|
| Epochs | 50 |
| Learning Rate | 0.005 |
| Optimizer | Adam |
| Loss Function | Mean Squared Error |
| Batch size | 128 |

After training the model, inferences for forecasting the generated power have been computed, comparing predictions with actual measure power. Figure 60 shows the actual power data (orange line), inferences performed by the ML model (blue points), and the

forecasting intervals with a 90% confidence (blue area). The forecasting intervals can be computed when the errors between the actual data and the model predictions present a distribution that can be considered Gaussian. To assume errors that come from the Gaussian distribution, they have been subjected to normality tests: Shapiro-Wilk [297], Anderson-Darling [328], and D'Agostino-Pearson [259]. These tests consist of statistical hypothesis tests that check whether the data contains specific properties. Thus, 2 hypotheses are defined: the null and alternative hypotheses. The null hypothesis supports that the data probably comes from a normal distribution, while the alternative hypothesis argues that the data present a different distribution. The statistical test returns a probability known as the p-value. Suppose this result presents a value lower than the defined significance level (0,05 in this case); the null hypothesis must be rejected so that the data distribution can be assumed normal. Table 32 shows the p-values obtained.

*Table 32: Normality test results (p-values) for power forecasting models*

| Normality test | Value |
|---|---|
| Shapiro-Wilk | 0.47 |
| Anderson-Darling | 0.76 |
| Agostino-Pearson | 0.10 |

Within the confidence intervals, the model learns quite well the seasonal variations of the generated power, as depicted in Figure 60, obtaining an MSE of 0.009 during the training. As shown in Figure 60, there is a good matching between observed and predicted values within the confidence interval, which captures both the trend and seasonality of the future series behaviour.

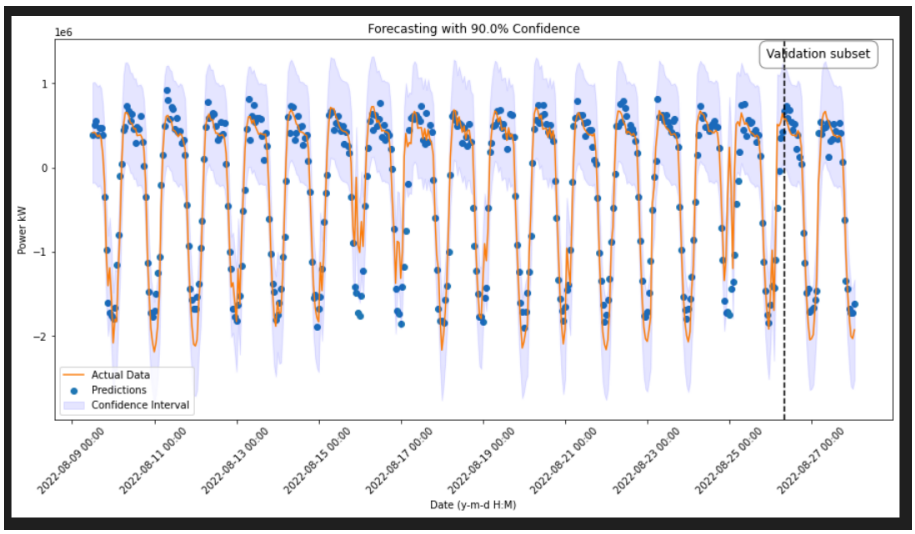


*Figure 60: Training results for generated power forecasting for 20 days of analysis in August 2022*

### 3.3.2 Grid optimization services

Grid optimization services for the electricity DN involve a range of strategies and technologies aimed at improving the efficiency, reliability, and sustainability of the electrical grid. These services are essential for meeting the growing demand for electricity, integrating RES, reducing energy losses, and ensuring the grid's resilience. Some of the applications of the grid optimization include the DR management, the DER integration, the storage integration, the tools for grid analysis and predictiva maintenance, and the analysis to increase grid resilience and environmental impact. Overall, grid optimization services are crucial for modernizing the electricity DN, ensuring its reliability, and facilitating the transition to a more sustainable and resilient energy system. They require a combination of technology, policy, and operational improvements to meet the evolving needs of the electricity grid and the consumers it serves. In the following two grid optimization tools are shown: the first address the management of a microgrid, with various demands and generation sources, while the second, presented in [XI], analyse the DR in a portion of MV grid via Reinforcement Learning

#### *3.3.2.1 Power Scheduling Optimisation between EV Charging Station, Storage System and PV Panels*

In the following study the framework addressed the problem of managing the DER of a microgrid with a specific focus on mitigating issues related to RPF and on increasing the SCR of the local RES. In order to optimize the behaviour of the grid flexible resources were used, i.e. loads that can be shifted in time without varying the quality of the service. Examples of flexible loads are EESS, EVs, washing machines, and thermal loads. The management of flexible loads is crucial in an energy district since it allows to reduction of the impact of the district to the DN leveraging on the local RES [127]. The load shifting, which aims to reduce the energy peaks and fill the energy valley, can be obtained through DR programs: end users receive economic and non-economic benefits for the change of their electrical behaviour. The role of EESS in energy districts is notable and particularly useful, since they can shift the energy absorption in time and inject power when needed, with the constraints of their size and capacity [355]. A heuristic model was developed to find an optimal solution for EV and EESS scheduling. The heuristic load shifting algorithm model received the day-ahead forecasts of the load consumption, the PV production, and the EV demand as input and determined the optimal hours for the charging sessions of the EVs and for the management of the EESS. Each day the algorithm assessed the expected hourly values of the production and the consumption of the microgrid and it aimed to minimise the RPF. Finally, the rule-based control method aspired to simulate the use of the EESS in a microgrid. This optimized algorithm reduced net load during peak hours and increased load when there was excess RES production. The optimization function of the model was the minimization of the dependences from the external grid, and, in other words, the increase of the SCR of the energy district.

The input of the heuristic model for the EV charging sessions scheduling are:

- The number of EVs to be used on a certain day.
- The electricity required by each vehicle in the day and the SoC of the vehicles.
- The hourly predicted net electricity load of the energy district.

The algorithm was iterated over all EVs. For the storage optimal management, the equations that led the process are:

*Equation 28:*

$$P_{PV}(t) + P_{ESS}(t) = P_{EV}(t) + P_{LOAD}(t) + P_{GRID}(t)$$

Explaining the power exchanged with the grid as an exclusive absorption component $P_{DfG}(t)$ and a feed-in component $P_{RPF}(t)$ results in:

*Equation 29:*

$$P_{PV}(t) + P_{ESS}(t) + P_{DfG}(t) = P_{EV}(t) + P_{LOAD}(t) + P_{RPF}(t)$$

With the constrain:

*Equation 30:*

$$P_{ESS_{min}}(t) \leq P_{ESS}(t) \leq P_{ESS_{max}}(t)$$

where Equation 28 and Equation 29 represent the power balance in the energy district. Equation 30 defines the constraints of the power flow from the EESS.

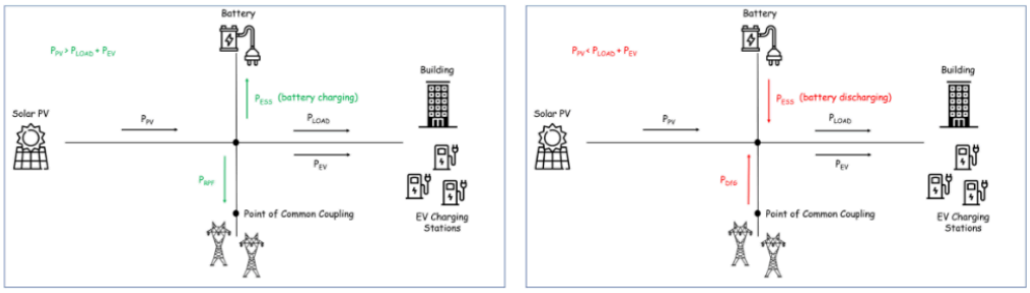


(a) PV-based power generation is greater than the sum of building and EV energy demand.

(b) PV-based power generation is lesser than the sum of building and EV energy demand.

*Figure 61: An overview of the microgrid system topology considered in this study, illustrating the direction of power flows.*

#### 3.3.2.1.1 Power Scheduling Optimisation between electric vehicle charging station, storage system and PV Panels: Results

To better illustrate how the service works in practice and evaluate its potential benefits, four key performance indicators have been identified. These include:

- annual RPF, i.e., the energy that flows from the DN to the transmission grid.
- annual Demand from Grid (DfG),
- energy autonomy (number of days within a year that DfG is zero),
- peak shaving (average daily range of DfG)

Figure 79 provides an illustrative example of how the proposed optimisation framework affects the timing of the EV charging sessions, netload, battery SoC, DfG, and RPF on a randomly selected period date.

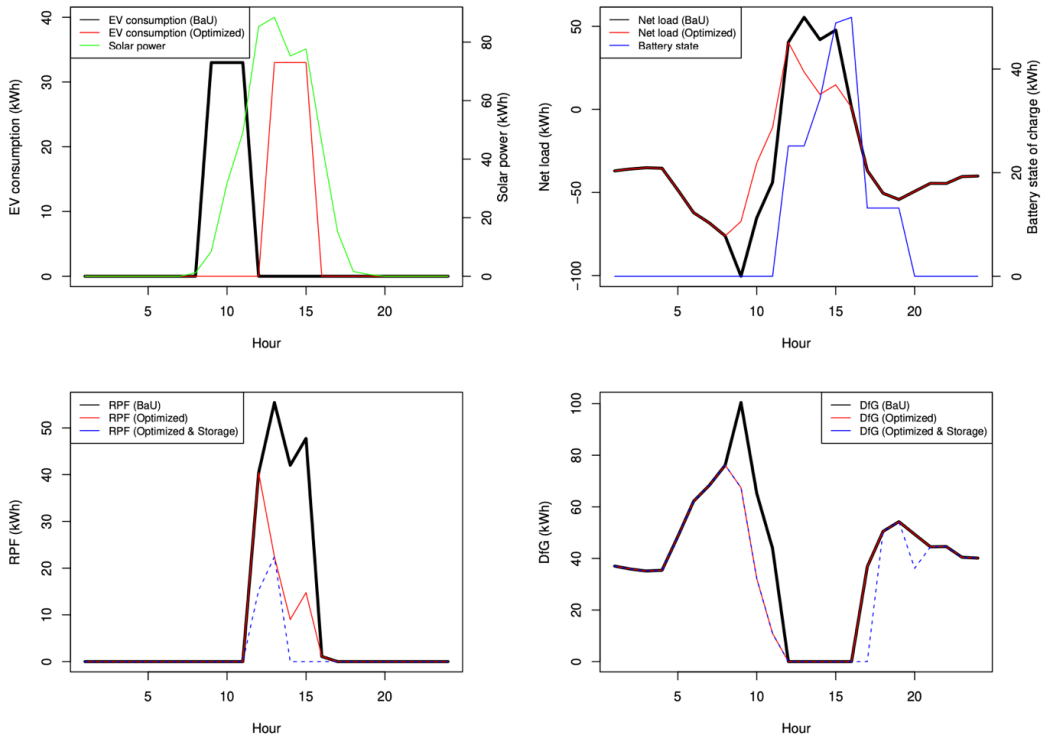


*Figure 62: Example (randomly selected date) illustrating how the proposed optimisation framework affects the timing of the EV charging sessions (top left), net load and battery SoC (top right), DfG (bottom left), and RPF (bottom right). A 50 kWh battery is used, and 5 EVs are considered.*

In the case study, the microgrid was connected to the external grid via two secondary substations, with a nominal power of 250 and 400 kVA. Electricity consumption in the building is approximately 650 MWh per year, mainly for lighting and powering electrical devices. The PV generation system comprises 1,100 monocrystalline silicon panels of 150 W at 12 V with 98.5 x 98.5 cm dimensions. The PV plant is in the parking area and interfaces with the microgrid via a 200 kVA inverter. The loads and PV generators are equipped with real-time monitoring sensors using power quality analysers, which allow the various devices' voltage, current, active, and reactive power values to be tracked and stored in a database with a granularity of 1 second. The parking area has 5 EV charging stations, each equipped with two charging points up to 22 kW AC and 32 A, single-phase or three-phase. The charging stations have a user interface to start and regulate charging, a real-time smart meter, and the option to modulate the charging power remotely. The EV fleet using the charging facilities currently consists of 10 cars. Given that the batteries of the fleet's EVs have an average capacity of about 40 kWh, and assuming that the drivers are willing to charge their cars when the battery level of charge drops to around 20%, each charging session is expected to consume about 33 kWh and last three hours on average. These estimates are consistent with the actual data available on the duration and electricity consumed per charging session. Nevertheless, since the chargers currently available surplus the demand, as expected, it is typical for many users to plug their cars into the chargers when they arrive at the building (around 08:00) and disconnect them when they leave work (around 17:00). To assess the impact that various sizes of EV fleets might have in the future on the examined KPIs, the daily inflow of $N \in \{5, 10, \ldots, 35, 40\}$ EVs for one year (365 days) was simulated. To do so, N numbers were first randomly selected from a

uniform distribution U (0.1, 0.9) ∗ 100%, indicating the initial battery level of charge for each EV. Then, by assuming that all drivers whose car is charged below 20% will be willing to charge their vehicle, the EV inflow on the first day of the simulation period is determined. To estimate the EV inflow for the following days, it was assumed that each car would cover an average distance of 20 km per day, thus appropriately reducing their previous charge level. Similar to the first day of the simulation, whenever the battery level of charge of an EV dropped below 20%, it was assumed to be fully charged the following day. To ensure fair and direct comparisons between different simulations, the EVs SoC initialised was performed just once. To facilitate comparisons and evaluate the potential effect of the proposed framework under various conditions of use, the following three scenarios were considered:

- Business as usual: In this scenario, all drivers interested in charging their EVs connect their cars to the chargers when arriving at work (08:00). Also, no battery was available.
- Optimal scheduling of EV charging sessions: In this scenario, the drivers interested in charging their EVs connect their cars to the chargers at the time the heuristic algorithm for optimally scheduling the charging sessions of EVs suggested. No battery was available.
- Optimal scheduling of EV charging sessions and EESS automation: like the previous scenario, the drivers interested in charging their EVs connect their cars to the chargers according to the suggestions of the proposed algorithm. Moreover, having determined the time the EVs will start charging, a battery was used to automatically store the electricity produced by the PV plant when appropriate. It used it, when necessary, as defined by the rule-based algorithm for controlling the EESS.

To assess the impact that batteries of various capacities may have on the examined indicators, separate simulations were conducted for batteries of capacities C ∈ {5, 10, 15, . . ., 90, 95, 100} kWh. The data used for implementing each scenario and its variants were hourly and lasted about 2 years and 11 months (25536 hours), ranging from 6 September 2019 to 3 August 2022. The period from 4 August 2021 to 3 August 2022 was used for evaluation purposes, while the rest of the data was for training the models to be used for forecasting the electricity consumption in the building and the PV power for the following day (24 hours). As such, the original data set included the total electricity consumed by the building and the electricity produced by the PV plant. However, it was supplemented by the simulated data, indicating the electricity consumed by the EVs. These variables were effectively the input of the proposed optimisation algorithms. Figure 63 summarises the impact of the scheduling algorithm when no battery is available for storing the energy produced by the PV system over the BaU scenario. As expected, the greater the size of the EV fleet becomes, the more energy is consumed from the grid. Nevertheless, the optimisation can still lead to energy savings that range from 1.5% (5 EVs) to 7.2% (40 EVs). In terms of RPF, it was observed that optimal scheduling can indeed be beneficial, reducing its magnitude from 7.2% (5 EVs) to 44.3% (40 EVs). This time, the improvements were consistently greater for larger EV fleets, which is expected given that more EV charging sessions imply less surplus solar power. The scheduling algorithm also significantly impacted peak shaving, reducing the average daily range of the demand from the grid from 3.7% (5 EVs) to 34% (5 EVs). On the contrary, the energy autonomy of

the microgrid remained practically the same for relatively small sizes of EV fleets, being slightly deteriorated for larger ones.

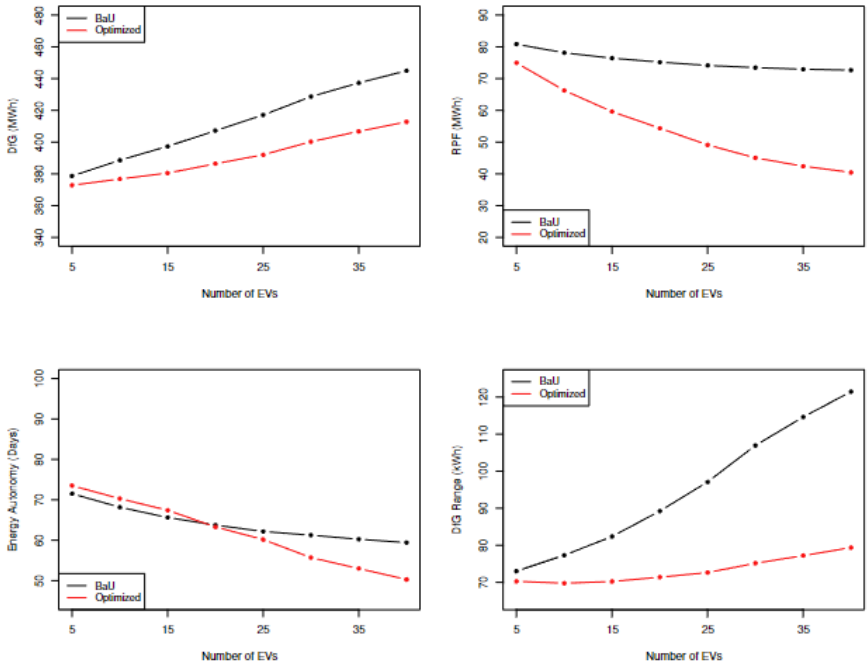


*Figure 63: Impact (full year) of optimally scheduling the EV charging sessions when no battery is available for storing the energy produced by the PV system. Performance is measured both for the BaU and optimised scenario assuming different numbers of EVs.*

Figure 64 provides similar comparisons, but this time focuses on the EESS's impact on the optimised EV charging scheduling. It is observed that batteries of greater capacity can result in less demand from the grid and RPF. The maximum percentage improvements (using no battery versus using a battery of 100 kWh capacity) in terms of demand from the grid remained relatively constant when a certain number of EVs was assumed, ranging from 5% (40 EVs) to 7% (5 EVs). The same was true for peak shaving, which reduced the demand from the grid range by up to 2%. On the contrary, the respective RPF improvements were significantly affected by the number of EVs, ranging from 35% (5 EVs) to 52% (40 EVs). In terms of energy autonomy, the results were similarly encouraging, suggesting that for a given size of EV fleet, instances of zero energy demand could be increased from 33% (5 EVs) to 45% (40 EVs). Thus, electricity storage can complement the scheduling algorithm and further boost its performance regarding reduced RPF and enhanced energy autonomy.

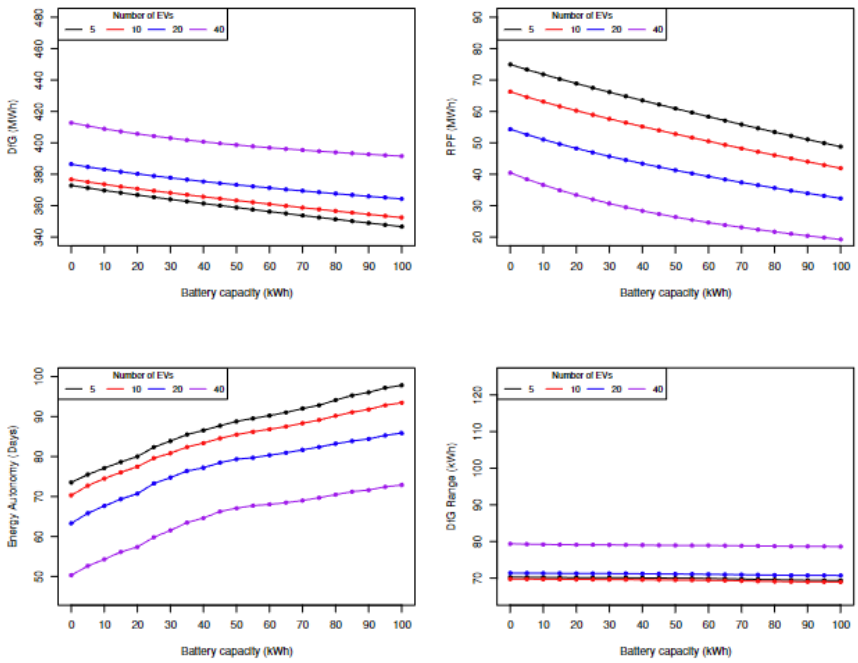


*Figure 64: Impact (full year) of the ESS on the optimal scheduling of the EV charging sessions. Performance is measured assuming various numbers of EVs and battery capacities.*

#### 3.3.2.2 Grid Optimisation leveraging Demand Respons mechnism via Reinforcement Learning

The grid optimisation model reported in [XI], aiming to maximise its SCR and SSR, is designed as an reinforcement learning based optimisation model [321]. Reinforcement learning is a ML discipline centred on learning optimal behavioural policies for the decision-making of a group of agents interacting in a common environment, leading to a maximisation of a cumulative reward (i.e., expert-defined performance metric). In the context of control systems, the learned policy allows for deploying deterministic or stochastic control logic/instructions for agents interacting with the end system, such as, e.g. maximising the grid SCR and SSR ratios. Some of the main concepts of reinforcement learning involve the environment, agents, states, actions, rewards, observations, and policies are reported below:

- The environment refers to the physical or simulated space which the agents interact with.
- Agents are the entities affected by and are in a position to interact with the environment by taking actions.
- Agents take a state (e.g., vector) that represents their status at every point. States are defined as a discrete or a continuous, closed set.
- A set of actions is defined for the agents to take. This group is defined as a discrete or a continuous, closed set.
- Rewards are given by the environment after the undertaking of actions by the autonomous agents.
- Observations are pre-processed snapshots collected after each transition that gather relevant variables of the environment, as well as the previous state and the actions taken, resulting in the state and the observed reward.
- Policies, in broad terms, are the learned (deterministic or stochastic) mapping between the set of states and the set of actions.

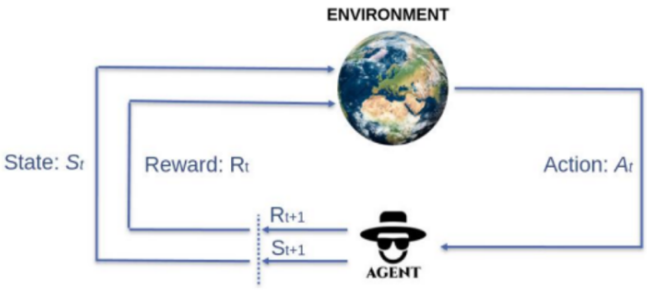


*Figure 65: RL concept*

Depending on the problem to be tackled, experience is gathered through interactions in either a simulated or a real (digital or physical) environment. Based on the knowledge of the environment, it is possible to distinguish between model-free and model-based approaches [321]. For the reinforcement algorithm to learn/approximate an optimal policy, it must buffer enough experience from the environment. The experience collected by the model comprises transitions (steps within episodes), which are made up of observations, including relevant variables from the environment, the previous agent status, the action taken, the following states, and the observed reward. The following describes the reinforcement learning elements for the grid optimization model. The

reinforcement learning service has been deployed with KServe via the Tensorforce framework [332].

#### 3.3.2.2.1 Environment

A grid simulator has been implemented based on the pandapower framework [246]. This framework uses the Pypower solver [256] to create a calculation network program to automate and optimise power systems. As a result, the simulator describes the same environment state as the real grid when connected with the same sources of power generation and consumption. The operation of the simulator is as follows: once the electrical network is specified in pandapower, the simulator reads the power loads demanded by all the consumer groups connected to the grid and the power generated along a day. The data has a resolution of 15 minutes, so there are 96 values per day of domestic and industrial consumers' power demand. Next, the simulator introduces the loads on the grid and performs a simulation. Then, the simulator outputs the grid state, consisting of the parameters to be optimised: network losses, SCR, SSR, and RPF.

#### 3.3.2.2.2 States

The optimiser acts on the customers' energy demand: it modulates the distribution of energy demand throughout the day, so it is necessary to know the state of energy demand or, equivalently, the distribution of current energy demand. Two types of customers can be distinguished: domestic and industrial. There are 13 loads (client groups) of each. A pre-analysis of a dataset collected over a year has been carried out, Figure 66 and Figure 67 show the average distribution of each domestic and industrial load for one day. The available data, provided by the grid owner, provide an averaged curve relating to the industrial cluster and one relating to the domestic cluster, as well as the PV production curve. Furthermore, the capacities of each load and each PV system are known. The user curves are proportional to each other according to installed power. To simplify the optimisation model, it will only act on higher loads, those having a stronger influence on the grid (the top 8 loads, combining 4 domestic and 4 industrial ones, have been selected since they cover, respectively, 70% and 77% of the total cluster load). It was considered that the flexibility of users, i.e. the ability to vary their consumption curve, is proportionally the same for all users, with the difference being that larger users can provide higher performance services for the entire DN. Reducing the number of actors simplifies the computational aspects of the problem and speeds up the solution.

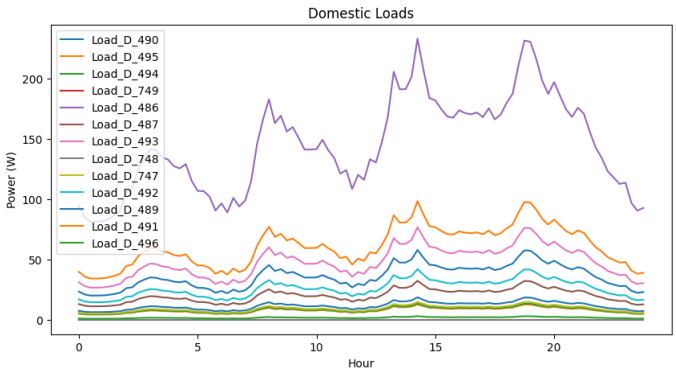


*Figure 66: Energy demand for domestic clusters*

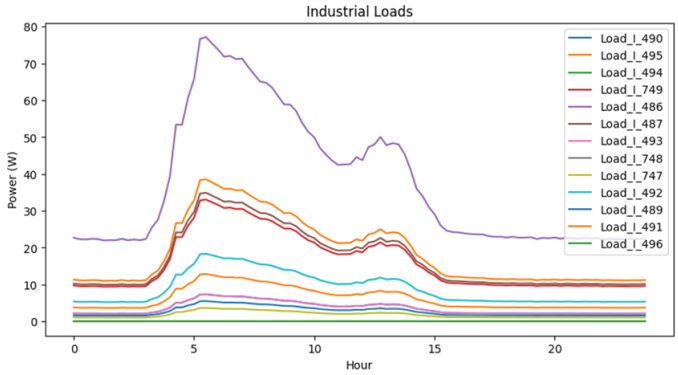


*Figure 67: Energy demand for industrial clusters*

It can be seen that the trend of domestic users peaks in the morning hours, and the two main peaks are around lunchtime and dinnertime. This is an averaged curve, which therefore considers full and part-time workers, students, or pensioners. The curve for industrial and commercial users presents a peak in the early hours of the day, corresponding to the start-up of engines and other consumer devices, and a slow decrease in consumption, interrupted only by a recovery around noon.

#### 3.3.2.2.2.1 Discretization of states

As the power demand continuously changes, it must be discretized, as a discrete state space is needed for training the optimizer in a reasonable time. The state space should be as small as possible in order to be completely explored by the optimizer so that the complete policy is learned. However, an excessive reduction of the time interval would increase the state space, imposing higher exploration time on the optimizer training process. After initial tests with quarter-hourly discretization, it was noted that an extremely large number of episodes were required by the optimizer to explore the state space, despite running on a very high-performance high performing compting cluster. Hence, it was decided to carry out hourly load discretization. An approach with much lower discretimization times, such as 15 seconds or less, would be desirable for electrical aspects (overcurrents, voltage issues…), for energy aspects, such as SCR or SSR, as the objective of the grid optimizer, there is no need to adopt short analysis times. In this respect, the Italian legislation also adopts hourly resolution times for the calculation of the SCR for the calculation of incentives for RECs [122]. Therefore, the states consist of the sum of all the loads, discretized by the hour. This approach ended up with 48 states, consisting of 2 vectors of 24 elements each (one for domestic consumers, another for industrial ones). Each state could take a continuous value in the range [0, 1], that is, the percentage over the total daily demand for each daily hour. Therefore, the range [0, 1] is also discretized into 10 bins. Besides, it is possible to apply a further normalisation by dividing the state value by a "load threshold" so that the possible states of demand in the range [0, 1] are constraints (to reduce the state space dimension) to those values with higher likelihood of being explored and applied by the optimizer. In this way, the simulator can explore more states in a reasonable time.

#### 3.3.2.2.3 Actions

The RL-based optimizer seeks to optimise the energy demand of the grid. To do so, the distribution of energy demand of each load is shifted throughout the day. This optimiser

uses four sets of discrete actions (Table 33). The first action set is the load selection: select one load from 8 available. The second action set determines the start and end time of the energy displacement. The third action set determines the percentage of energy that is shifted at different times. Three different energy shifts have been considered: 1%, 5%, and 10%. For example, if from 8:00 a.m. to 9:00 a.m. there is an energy demand of 10kW and it is chosen to make a 10% shift to the time slot between 9:00 a.m. and 10:00 a.m., this second-time slot will increase the power demand by 1kW, and the energy demand from 8:00 a.m. to 9:00 a.m. will decrease it by the same amount. This is resulting in a set of 147,456 possible actions.

*Table 33: Action subset*

| Action subset | Length |
|---|---|
| Domestic demand cluster selection | 4 |
| Industrial demand cluster selection | 4 |
| Domestic initial time slot | 24 |
| Industrial initial time slot | 24 |
| Final domestic time slot | 2 |
| Final industrial time slot | 2 |
| Demand shift for domestic cluster | 2 |
| Industrial shift for domestic cluster | 2 |

The energy demand shift presents several restrictions: i) the total energy demanded by a load must remain constant throughout the day, ii) the shift can only occur within 2 contiguous time slots, the displacement cannot be applied to any arbitrary distant time slots, iii) the demand cannot be negative. The power demand load describes the daily demand, with a 15-minute interval, resulting in a 96 values vector for a full day, in order to be aligned with the state discretization of 1 hour, the optimizer resamples the loads by averaging the samples within each hour.

#### 3.3.2.2.4 Rewards

The objective of the system is to optimise the operation of the grid. This version tries to maximise the SSR and SCR. The reward function is the mean of both parameters. In order to obtain greater flexibility during the training process, the reward is computed as a weighted average:

*Equation 31: Reward of the optimization problem*

$$R = \frac{1}{2}(\alpha \cdot SCR + (1-\alpha) \cdot SSR)$$

By tuning the $\alpha$ parameter, it's possible to address the optimisation needs, and promote SSR over SCR (or vice versa). In this way, we can force SCR and SSR to evenly contribute to the reward, by setting $\alpha = \frac{1}{2}$, or make reward equal to the SCR, by setting $\alpha = 1$.

#### 3.3.2.2.5 Agents

The optimization model includes agents for the training of types PPO, DQN, and DDQN [321]. The optimization model has been implemented using the Tensorforce RL framework. For training, some improvements have been conceived and implemented, including:

- Variable number of steps per episode: some experiments show that the reward fell down after some steps, incapable of going up for the rest of the episode. To avoid wasting time in the training process, the episode is concluded when obtained rewards go down a threshold of customizable 20%.
- Variable exploration time: the training process supports the configuration of a variable exploration rate, which can be diminished as the learning process progresses over more learning episodes.
- State density matrix: the optimization training process registers all the states visited by the agent, intended to give a clear vision of the agent's preferable combination of states, aiming to understand the reasons for the agent to choose such a state combination as optimal. This state's matrix consists of 48 columns, corresponding to the 24 hours of both domestic and industrial consumers, and 10 rows, corresponding to the 10 state bins available for each state.

#### 3.3.2.2.6 Grid Optimisation leveraging Demand Respons mechnism via Reinforcement Learning: Results

In order to evaluate the effectiveness of the ML tool developed, a portion of the Terni MV network was used as depicted in Figure 68, consisting of 14 nodes, one of which represents the primary substation, while the others represent secondary substations and 30 power lines. Each of the 13 secondary substations feeds a different capacity of industrial loads, for a total of 650 kW of installed power, domestic loads (3374 kW), and some of them have PV systems (3663 kW). Based on the historical data of the last 5 years, a yearly average curve of industrial and domestic loads and PV production is available, with a granularity of 15 minutes. These curves are used as a baseline in the optimisation tool. Experiments were conducted in an Atos high performance computing cluster of 12 nodes, with 720 cores each and a total memory of 2968 Gb. Experiments were conducted on 16 cores and 128 Gb RAM, lasting days to be completed.

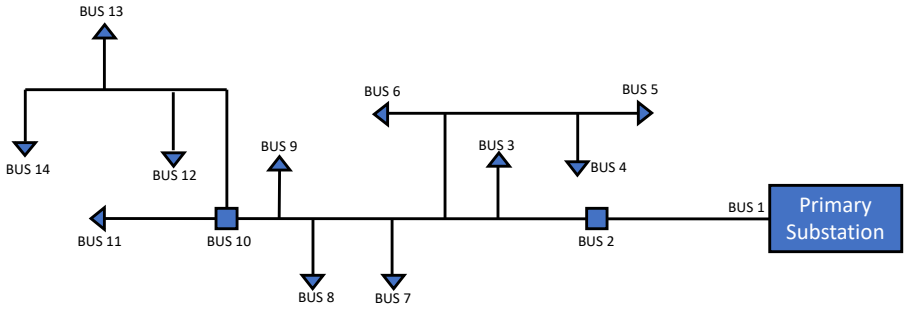


*Figure 68: Schematic diagram of the portion of the 20-kV grid used as a case study. Some nodes are connected via different sections of line, for example of the overhead and cable type, or with different typologies. For reasons of graphic clarity, they have not been distinguished here*

The grid optimisation model has been trained with the agent's hyperparameters shown in Table 34. In the experiment, $\alpha = 1$ was chosen, as from the DSO's point of view it is more convenient to implement a DR mechanism that favours SCR of local DER, to reduce RPF and reduce demand from the grid. High SCR means low grid losses. SSR, on the other hand, is more related to consumers and the possibility of becoming grid-independent.

*Table 34: Hyper parameters for grid optimisation models*

| Hyper-Parameter | Value |
|---|---|
| RL Algorithm | PPO |
| Learning Rate | 0.001 |
| Optimizer | Adam |
| Multistep | 10 |
| Batch size | 1 |
| Reward discount | 10% |
| $\alpha$ | 1 |
| Load threshold | 30% |

Initial experiments were conducted to determine each episode's optimal duration (i.e., #steps), resulting in 2000 steps. Also, as described before, better optimisation results were obtained by applying a normalised discretisation of the state space. Results show the agent is exploring the state space much better than if normalised discretisation would not be applied. Figure 69 shows the matrix space of visited loads after completing the experiment.

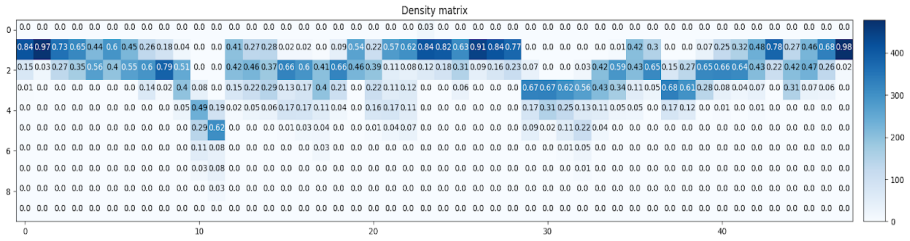


*Figure 69: Load state space*

As a result of the training, the reward is improved (Figure 70) after applying learnt actions on the user's demand load, resulting in better SCR. The SCR achieved, at around 52%, is very high, as the portion of the grid in question has an average daily production of 23.6 MWh and a consumption of 12.9 MWh, so the maximum SCR that can theoretically be achieved is 55%, which occurs in the case of completely zero energy absorption from the grid.

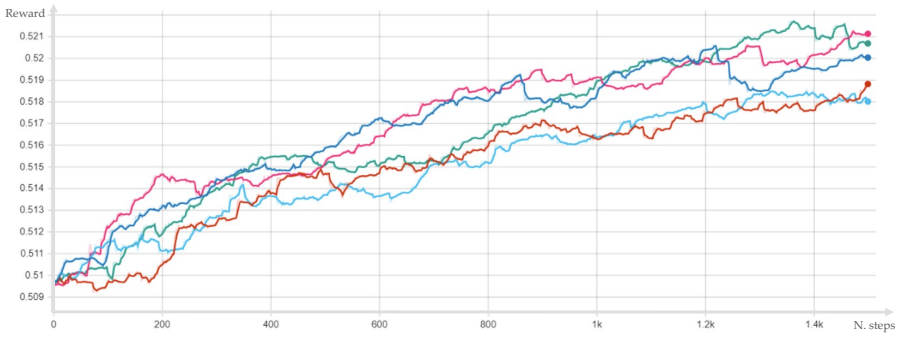


*Figure 70: Reward evolution over episodes considering α=1*

In Figure 71, domestic loads are shown before (i.e., left) and after being optimised (i.e., right) along the day hours in the x-axis. A similar trend is recognised for industrial loads. The optimised load shows a shape closer to the theoretical optimal one, with a bell-shape where the load is concentrated in the noon. For the optimizer reaching the optimal shape, extremely longer episode duration, beyond our computing capability, is required to exhaust the exploration of the

state space, in order to compute the optimal policy, but the initial training results, with our computational constraints, show progress in the right direction.

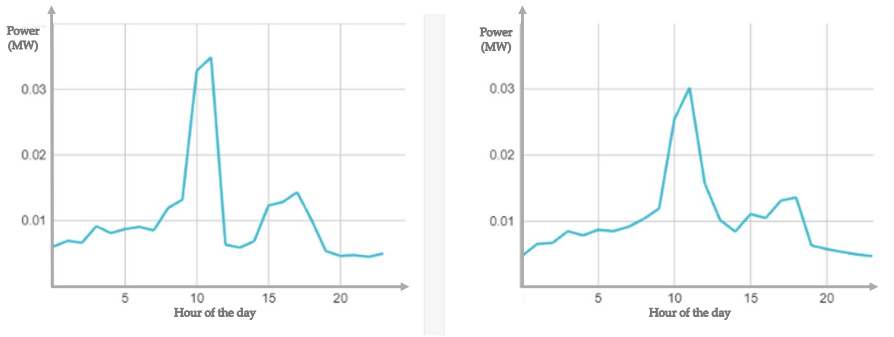


*Figure 71: Domestic demand load before (a) and after (b) the training*

Further experiments are required to improve the optimised SSR and SCR values, close to the theoretical ones, by reducing the dimension of the state space so that within the affordable computation time, the agent can exhaust the state space, searching for optimal user demand loads.

### 3.3.3 Predictive maintenance applied to power transformers

Predictive maintenance analytics applied to the electrical DN involve using data-driven techniques and advanced analytics to anticipate and prevent equipment failures, improve reliability, and reduce downtime. These analytics are crucial for modernizing the grid, ensuring its efficient operation, and reducing maintenance costs. The first step in predictive maintenance analytics is the collection of extensive data from various sensors and monitoring devices installed throughout the grid. These sensors can capture information about voltage levels, current, temperature, humidity, and other relevant parameters. Collected data is integrated into a centralized system, often referred to as a data historian or data warehouse. This allows for the consolidation of information from multiple sources, including substations, transformers, power lines, and other grid components. Before analysis, the collected data is cleaned and preprocessed to remove noise and inconsistencies. Data preprocessing may also involve data normalization, feature engineering, and the handling of missing data. Predictive maintenance analytics leverage ML algorithms to analyze historical and real-time data. These algorithms can identify patterns, anomalies, and early signs of equipment degradation or impending failures. Common techniques include regression analysis, clustering, classification, and time-series analysis. ML models can predict when specific grid components, such as transformers or circuit breakers, are likely to fail based on data patterns. These predictions are valuable for scheduling maintenance activities before an actual failure occurs. Real-time monitoring and analysis of equipment conditions are essential. Sensors continuously send data to predictive analytics models, which assess the current state of equipment and detect deviations from normal operating conditions. An asset health index or score is often assigned to individual grid components based on their condition. This index provides a quick overview of the health of assets and helps prioritize maintenance efforts. Predictive maintenance analytics generate optimized maintenance schedules, allowing utilities to plan and allocate resources efficiently. Maintenance activities can be scheduled during periods of lower demand to minimize service disruptions.

By implementing predictive maintenance analytics, utilities can enhance the reliability and efficiency of the electrical DN. This proactive approach reduces the risk of outages, minimizes maintenance costs, and contributes to a more robust and resilient grid infrastructure, ultimately benefiting both utilities and consumers. An example of predictive maintenance analytics service is presented in [IX], aimed to predict the electrical transformers' ageing in secondary substations. The correlation between the hot point temperature of the transformer and its degradation was the starting point for forecasting the component's working life, based on Arrhenius's theory. Moreover, by exploiting other data appropriately processed – mainly audio data – it was possible to estimate power data and forecast the transformer's ageing in a simple, cheap way. Efficient predictive maintenance of the transformers enables the substitution of the devices once their working life has expired and avoids high costs due to power interruptions. The developed model applies to oil-cooled secondary substation power transformers. The ageing of the transformer is strictly correlated to the temperature at the hot point. Still, since, in most cases, temperature-related measures are not available, it is necessary to calculate it by applying a thermal model of the transformer. Primarily, it’s necessary to calculate apparent power from raw power by extracting those values from the real-time smart meter. From apparent power, it is possible, through mathematical and physical models, to infer the hot-point temperature of the instrument and, from that, its degradation. The

Python library, named Prophet, allows the calculation of the aging [331], [255]. The use case also covered another eventual situation. Smart Meters are not available in every secondary substation, while acoustic sensors may be cheaper. So, theoretically, it is possible to use audio data to estimate power data and consequently, the ageing of the transformers. The tool used for this analytic service was the ML Regression Model. Still, first, it was necessary to identify an appropriate set of points (audio and electric data) that could be used to train the model. The power that had been inferred in this way wasthen used to predict in the same way as indicated for the normal workflow. All of the following implementation was done using Python, exploiting useful and common Data Science and ML libraries, such as Sci-Kit Learn [308], Pandas [247], etc.

#### 3.3.3.1 Transformer acoustic model

The acoustic emission of power transformers depends on numerous parameters, such as the type of transformer, type of cooling, age, presence of faults, etc. The vibration of the transformer housing and the emitted noise consists of a series of acoustic components that fall within the first 100 Hz frequency harmonics, i.e. there are typical values of 100 Hz, 200 Hz, 300 Hz, and 600 Hz, while there are rarely values above 1000 Hz [270]. The noise emitted by transformers can have a significant impact on the surrounding environment, especially near densely populated areas. The emission of transformer noise is caused by magnetostriction phenomena, i.e. vibrations of the mechanical components of the transformer due to electromechanical forces, the vibrations occur at a frequency that is twice the grid frequency, i.e. for a 50 Hz grid, such as the European grid, the vibrations and thus the emitted noise are at a frequency of 100 Hz [217]. Several articles in the literature address this topic, both through experimental cases and by investigating the physics of the phenomenon. In [157] the results of tests on 10 oil-cooled power transformers without load using the sound pressure method are presented, showing that the values are considerably lower than the legal limits and are affected by the value and quality of the voltage applied by the network. The no-load emission values, for transformers with voltage levels of 20kV / 400 V and a power between 40 and 150 kW, showed that as the size increases, the intensity of the emitted sound increases from 26 dB to 44 dB, but it is still below the legal limits [107]. In addition, since the transformers are equipped with a tap changer, it can be seen that a reduction in voltage by 10% reduces the noise level by approximately 15%, while an increase in voltage by 10% increases the emitted sound by almost 20%. The difference between no load and full load, at constant flux density is usually no greater than 1 or 2 dB. An exception to this is when special flux shields are placed inside a transformer tank to reduce stray flux effects. [117]. A similar analysis has been made in [346], where the transformers of the primary substations were analysed, which show significantly higher noise levels but still have a peak in the vicinity of 100 Hz, and in [217], where air-cooled transformers were analysed and tested instead. Part of the literature analyses suitable means of reducing noise escaping from secondary substations, e.g. through insulation or the design of substations in underground locations or further away from densely populated areas. The analysis of transformer noise emission provides some relevant information on the aging of transformers, based on existing models. Many faults are closely related to sound: If the sound of the transformer is louder than usual and there is a disordered sound, it may be caused by the loosening of the internal clamp or the iron core and other individual parts, which increases the vibration amplitude of the silicon steel sheet. If the dry-type transformer has a similar boiling sound,

the transformer winding may have a short circuit fault, or the tap changer may overheat due to poor contact. When there is discontinuous and abnormal noise in a dry-type transformer, it may be caused by poor contact in the high-voltage cabinet. If the sound intensity of the transformer is very strong and accompanied by an uneven popping sound, it may be the internal or surface insulation breakdown of the transformer. If partial discharge occurs inside or on the surface of the transformer, there will be "crackle" discharge sound in the sound. A large area of power transformer diagnostics relies on the analysis of partial discharges emitted by transformers at fault moments [143].

#### 3.3.3.2 Transformer aging model

The power flowing over the rated power, or the loading of the transformer, as well as the presence of defects on the internal components of the transformer and the grid segments near to it, all play a significant role in the ageing of electrical power transformers. The component most prone to degradation within the transformer is the electrical insulation between the windings. Degradation of dielectric performance occurs due to excessive temperatures and work hardening of the material, so the analysis of transformer aging is closely related to the transformer's thermal model [140]. Transformer aging is mainly assessed by calculating the hot point temperature, i.e. the maximum temperature that the oil reaches in the transformer. Various models can be found in the literature that relate the hot point temperature to the average oil temperature and ultimately to the power flowing through the transformer. The static parameters influencing the aging of the transformer are:

- nominal transformer power
- liters of oil in the tank
- power loss inside the transformer
- thermal capacity of the oil

On the other hand, from a dynamic point of view, aging depends on two parameters: electrical power flowing in the transformer and ambient temperature. Various models for calculating aging have been presented in [61], [271], [143], [109], [45].

#### 3.3.3.3 Regression Model

The solution implemented in this service consists of three different components: a grid search, a ML layer consisting of three different regressors, and one meta-regressor. The ML layer consists of three regression models: a polynomial regression model, a support vector regression, and an extreme gradient boosting regressor, commonly renamed XGBoost. The first step was to find the best parameters for all the models. To avoid arbitrary setting of the parameters, a grid search methodology was chosen, using the data to let the model find its best hyperparameters automatically. Then, each model was trained separately in order to evaluate the quality of single regressors. Finally, the stacking regressor was the meta-regressor chosen for this task, and it worked by using a model to make a prediction based on the predictions made by other estimators. In other words, each of the trained estimators returned a prediction that constituted the input of the meta-regressor, which was then responsible for returning the ultimate estimation.

### 3.3.3.4 Transformers Aging Prediction: Results

The outcome of this analysis is twofold: the forecasting module address the analysis of the loading of the secondary substations' transformers and the aging model determines the expected remaining life of the transformer, based on its health status, the current power flow and other physical parameters (noise emitted, temperature and humidity of the cabin). The forecasting module provides a domain expert with all the information needed to assess the transformer's condition, providing plots with the decreasing percentage, with a probabilistic forecast as illustrated in Figure 72. The module also provides weekly, yearly, and daily information on peak usage ranges, in order to modulate the usage of the substations.

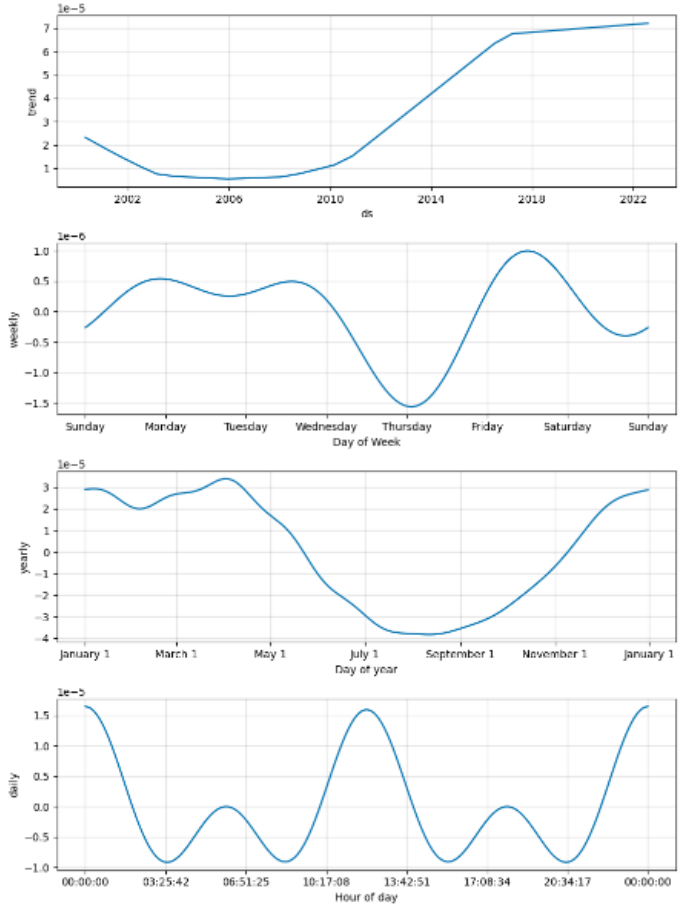


*Figure 72: Seasonality of usage of the transformer.*

ASM provides 10 secondary substations located in the distribution system, that collect power data from smart meters, power quality analysers, and acoustic and environmental (humidity and temperature) sensors installed in all secondary substations. All these data are available in real-time and are stored in a historic database on ASM's premises, working with MQTT protocol. Once the data are available, the analytic service applies some pre-processing steps in order to adapt the data to the model needs. For example, since there are no sensors that monitor the temperature of the oil in the transformer, but just the temperature of the cabin, it is necessary to calculate the hot-point temperature by applying some physical and mathematical models based on the ambient temperature and the power flow. As mentioned in the previous section, the pre-processing steps were required in order to adapt data to the requirements for the calculations. Two separate flows were applied in order to process audio or power data. For power, as indicated in the conceptual

diagram, it was necessary to apply a higher number of processing steps, in order to obtain the hot point temperature of the transformer. In the other case, audio data required only a general pre-processing, for example, to calculate the timestamp of the registration. To find a solution for the case in which power data are not available, a ML regression model capable of estimating power data from audio ones was trained. For this use case, the regressor is a meta-regressor, namely a stacking regressor. This type of algorithm is capable of taking the best prediction from other estimators and making another prediction using another regression model. First of all, it's useful to depict the initial situation, highlighting the set of points that were chosen to train the models. These data refer to a single transformer, but the mode has been applied to all the infrastructure. Figure 73 shows that there is a correlation between audio and power measurements. It was obtained by using a single transformer as a blueprint and then adding data taken from other sensors to cover all combinations. For a couple of specific and limited intervals of points, a data augmentation technique was required to improve the number of available features, but data simulated in this way did not exceed the threshold of 10% of data, to maintain a sort of balance between augmented data and real ones. The data were simulated in a strict interval, starting from the mean and the standard deviation calculated on the real power and audio data. Only 100 samples were be generated out of a total of 636 real and usable samples. The dataset created in this way also described a strong positive correlation (Pearson index= 0.75). From that, it is possible to start the training of each model.

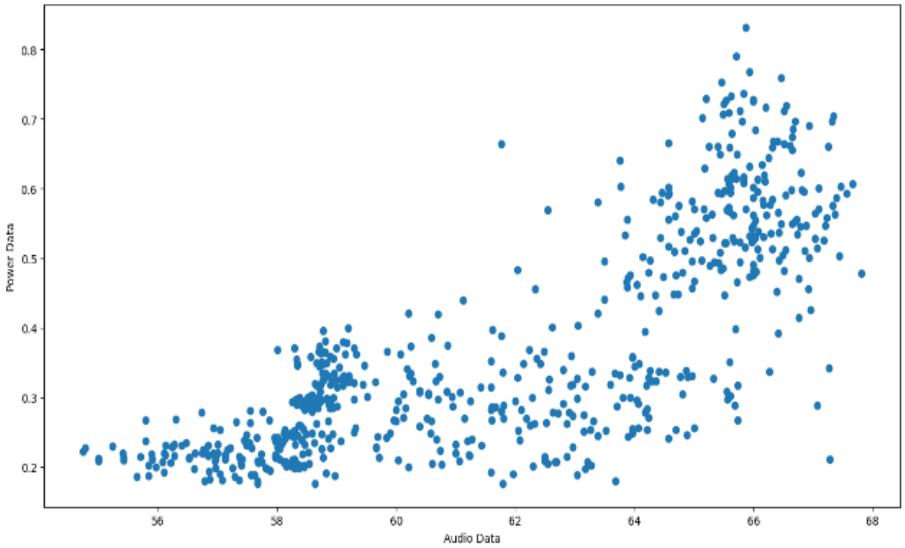


*Figure 73: Initial situation. Audio against power data.*

Figure 74 shows the training plots of the three estimators and the stacking regressor. To evaluate the performance of a regression, the most commonly used metrics are mean absolute error and mean squared error. Those metrics were used in association with the R2 coefficient to evaluate our models and to choose among other possibilities.

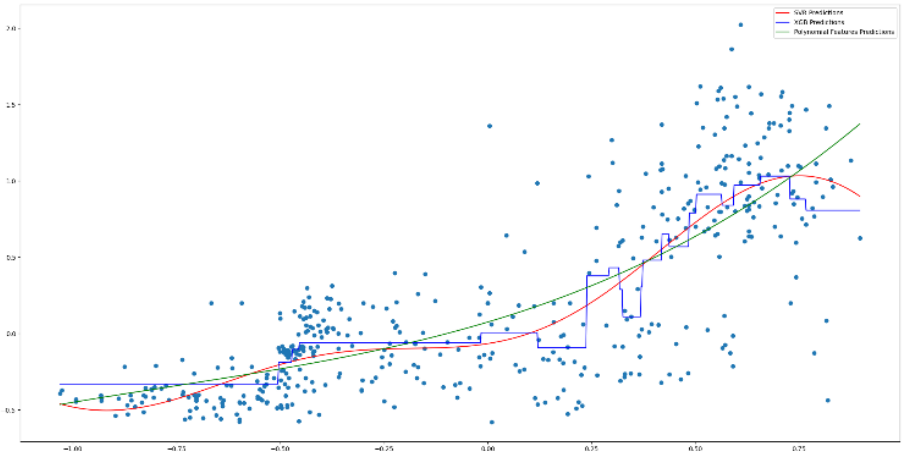

*Figure 74: Model training*

Figure 75 shows the prediction made by the regressor, with the relative metrics of the model. The data did not cover all the available sensors, but only a selection of them, in order to maintain the correlation. To improve the quality of the model a little, some data in a specific interval were simulated. The simulated data were less than a quarter of the initial data so the original situation was not affected too much by the injection of simulated data. Figure 75 depicts, on the left, the initial situation with the missing data section highlighted, and on the right the data with the addition of simulated ones.

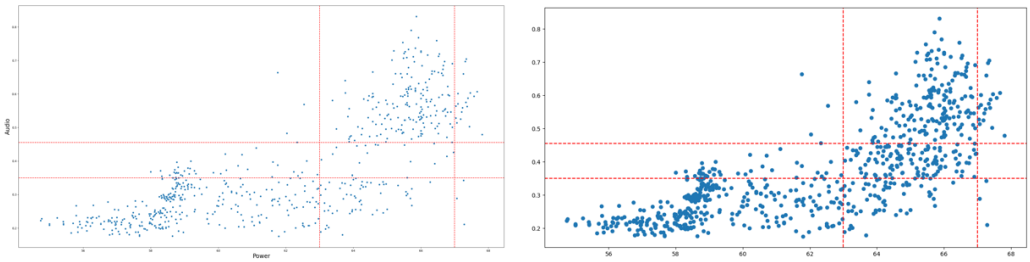

*Figure 75: Initial Data (on the left), Augmented Data (on the right)*

For reference, in Figure 76, the red line shows the prediction made by the polynomial regression model, the green line the support vector regressor model, and the blue line the XGBoost model. The output shows a good overall prediction, and the quality is confirmed by common metrics for the evaluation of regressors, which are mean absolute and mean squared errors. Table 35 reports the metrics of all the models illustrated in this paper.

*Table 35: Metrics of all ML models tested.*

| Metrics | Estimators | | | Stacking regressor |
|---|---|---|---|---|
| | SVR | XGBoost | Polynomial Model | |
| MAE | 0.221 | 0.237 | 0.211 | 0.0637 |
| MSE | 0.061 | 0.0734 | 0.567 | 0.00693 |

Lastly, the prediction is passed on to the stacking regressor, and the model outputs the final estimated power values. Since this was not a "linear" regression model, the depicted line is not as smooth as one might expect, but again, it shows good prediction based on the starting data we have.

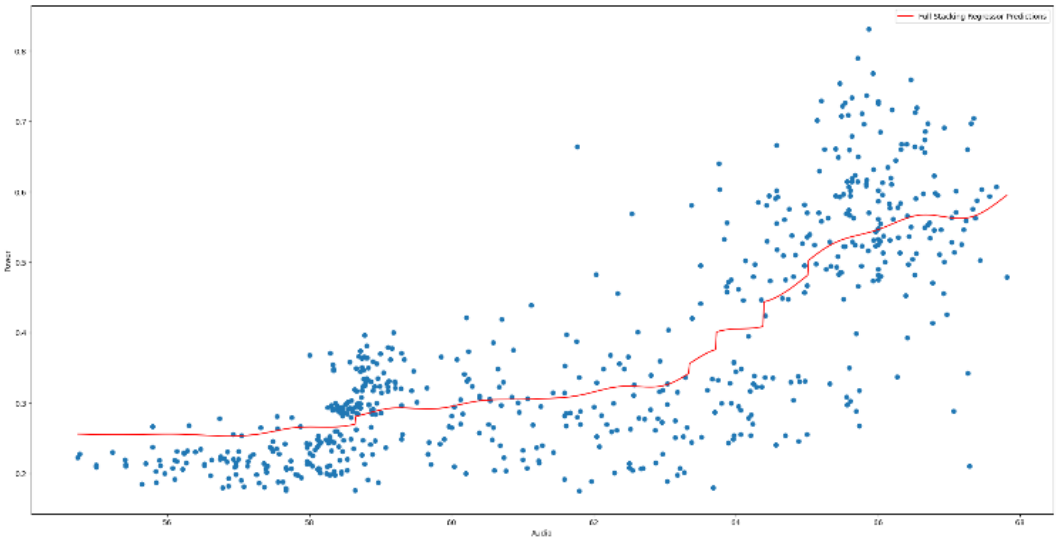

*Figure 76: Stacking Regressor Prediction.*

The outcome of this analytics service is the ageing prediction, depicted in Figure 77. As illustrated, the prediction also has a forecasted horizon, the most helpful part for a domain expert who needs to monitor the transformer's health.

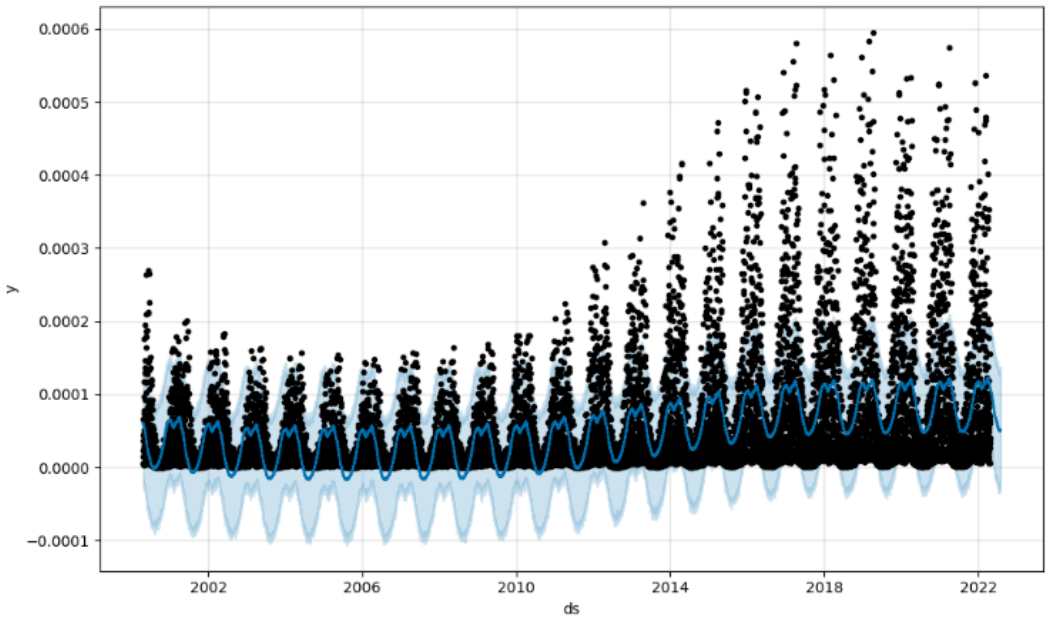


*Figure 77: Aging Forecasting Prediction.*

## 3.4 Big Data Management

The energy sector is currently undergoing a profound transformation driven by two key factors: the widespread adoption of RES and the active engagement of customers. This transformation is reshaping the industry's structure and giving rise to entirely new utility concepts. In an environment marked by a high penetration of RES, where the incremental energy costs are significantly decreasing, a novel type of relationship with customers is becoming a reality. Customers are evolving into active participants, often referred to as "prosumers." Within this digitized and service-centric energy ecosystem, data is expected to play an increasingly critical role.

In recent years, the growing adoption of information technologies, including the IoT, AI, 5G connectivity, and big data, has facilitated the shift from traditional power grids to the SGs. This paradigm shift is fueled by the availability of vast datasets generated at an unprecedented rate, both within the grid-owned assets (such as transformers, feeders, and PMUs) and non-grid-owned assets (including decentralized energy generation, smart residential buildings, industrial facilities, and community-level aggregated loads). This shift towards a more distributed architecture is giving rise to fresh innovation challenges. Furthermore, the integration of external data sources, including environmental, climate, geographic, financial, and socio-economic data, can empower novel energy analytics. This, in turn, provides energy stakeholders with more robust actionable insights and fosters improved decision-making.

The data within SGs are diverse, coming in varying resolutions, formats, and asynchronous forms, and are stored in different locations. These datasets are characterized by their high volume (often measured in terabytes), wide variety (ranging from structured to unstructured, and from synchronous to asynchronous), varying velocity (spanning real-time to different resolutions), veracity (including inconsistencies, redundancies, missing data, and potentially malicious information), and values (technical, operational, economic). Consequently, power grid management systems of the future will need to process enormous amounts of heterogeneous data. Thus, adopting a big data approach is essential for managing both real-time and historical data, extracting meaningful insights, and making data-driven decisions.

The growing momentum of big data technologies and the shift towards a data-driven economy offer a unique opportunity for the energy sector. This enables significant enhancements in grid reliability and efficiency, improved management of grid-connected assets, more accurate assessments of energy efficiency and RES investments, and attention to operational performance monitoring and citizen comfort. These trends, when coupled with AI, edge/IoT infrastructure management, and entrepreneurship, stimulate the creation of innovative energy services and applications.

For utilities, it is crucial to comprehend how the surge in data impacts their traditional operations and to devise strategies that unlock value from this vast and varied data pool. A recent survey involving 1,000 electric utility and industry respondents from 10 countries highlighted that most electric utilities acknowledge the importance of big data analytics for future SGs and new business opportunities. However, the implementation of big data analytics remains relatively low, with only 20% of utilities having partially adopted these technologies.

While various architectural and technological implementations for big data solutions in SGs have emerged, the development of a standardized and interoperable architecture for big data across smart energy grids has lagged behind. Furthermore, the presence of functional and organizational silos, combined with a lack of semantic and business interoperability, hampers the full potential of big data in the energy domain. Addressing these challenges is essential for harnessing the power of cross-domain data and providing a wide range of unprecedented services efficiently.

Efficiently handling this diverse data requires a precise understanding of its nature and the utilization of novel digital technologies (such as IoT, AI, cloud, and big data services) to process large datasets within acceptable timeframes and with due attention to safety and security. The absence of energy-focused data ownership and sovereignty management policies has, in many cases, hindered data sharing while respecting privacy and security. Additionally, the lack of data management provisions for near-real-time proactive analytics-based decision-making and control has limited the extraction of new value streams from big data. Traditional approaches to power system data management often focus solely on the most critical data required for immediate supervision and predefined operations, overlooking the potential benefits of big data.

The big data management problems and opportunities are in-deeph analysed in the BD4nRG European project [47].

## 3.5 The need for information security

Cyber-physical systems are composed of computation, communication and physical systems and processes, which integrate and coordinate heterogeneous components. SGs are one of the most complex cyber-physical system. Due to the increased usage of technologies in modern power systems, new types of threats emerge that are based on security vulnerabilities of the physical as well as the communication system. The interaction between both create new, previously unknown patterns of cyber-physical threats.

In a SG the energy management systems monitor and control the power flow process using SCADA systems, that usually hosts on dedicated communication infrastructures, consisting of WAN, FAN and LAN. Networked sensors in the system collect measurements and transmit the data to the control systems through remote terminal units in the SCADA system.

The integration of information technologies in the SG has resulted in a cyber infrastructure that is closely linked with the physical systems. Measurements and control commands are frequently exchanged between cyber and physical systems. Based on the measurements, operators determine the optimal control policies and issue the necessary control commands to coordinate actuators in the physical systems. In case of a fault, diagnostic logs are recorded to support the location, evaluation, mitigation and restoration during emergencies. Additionally, sensor measurements are processed by centralized and distributed computation devices deployed at different levels and locations in the SG.

The power grid increasingly relies on public communication infrastructures due to increased pressure for efficiency and cost reductions. Two-way communications between service providers and users are established through the advanced monitoring infrastructure system, which allows flexible DR patterns.

The safety of the power grid is obtained via a physical infrastructure and a cyber infrastructure, that work together to anable the security. Physical security is achieved for example through the presence of closed circuit cameras at sensitive points of the network or through the presence of fences and barriers for access to the infrastructure. Clearly it is not possible to use these devices for the entire length of the network, therefore contingency analyzes are often carried out to also limit the propagation of faults, if them occur. Cybersecurity is about protecting computer access points and assets from remote attacks. Defense against cyber attacks must be considered from an organic point of view and cybersecurity plays a leading role in the development of the SG. The use of secure protocols can protect the SCADA, while the use of dedicated telecommunication cables prevents attacks on sensitive parts of the network. Cybersecurity is closely linked to the physical configuration of the infrastructure and for this reason it is called a cyber-physical system. In security analysis, critical vulnerabilities are often revealed through scenarios where attackers are characterized with feasible resources, knowledge and objectives. The investigation of attack schemes often serves as the first step to establish security in a vulnerable system. While it is impossible to exhaust all potential attack schemes, the worst-case analysis is important to understand the feasibility and impact of a potential attack scenario. Extensive investigation of the SG security has revealed a significant number of attack schemes that could exploit critical vulnerabilities, potentially leading to severe disruptions and damages.

Essentially, a threat may be considered as a possible danger that could exploit a vulnerability and sidestep the security measures of a system. A threat can be associated to "intentional" damage, which means that the attack is intentionally caused. Instead, a threat can also be associated to an accidental damage. A cyber-threat is any circumstance or event with the potential to adversely impact organizational operations, organizational assets, or individuals through an information system via unauthorized access, destruction, disclosure, modification of information, and/or denial of service. Examples of differet threats are: malware, web based attacks, web application attacks, phishing, spam, denial of servics, randsomware, botnets, insider threat, physical manipulation, data breaches, identity theft, information leakage, exploit kits and cyber espionage.
Ensuring cybersecurity has emerged as a critical challenge in the pursuit of secure and dependable SGs [200], [298], [185], [352]. The primary cybersecurity threat vectors that can allow malicious attackers to gain access to a device or control network encompass external users accessing the network through the internet, improperly configured firewalls, unsecured wireless routers, wired modems, infected laptops outside the firewall, infected USB devices, programmable logic controllers, and insecure RS-232 serial links [68].

### 3.5.1 False data injection

The paper in reference [XVII] focuses on evaluating the repercussions of a voltage regulation mechanism in a case study when false data are introduced. The global surge in cybersecurity attacks targeting the energy sector has coincided with the widespread integration of DER into electrical grids, such as PV and wind power plants. The increasing reliance on communication networks to manage these complex systems has introduced new vulnerabilities to malicious threats [190], [55], [13], [264]. More data must be transmitted and processed to enhance interoperability and efficiency in forecasting and managing power generation, consumption, and storage [350]. The shift from passive grids to active grids, characterized by high RES penetration, presents technical challenges such as RPF, voltage stability, and increased interruptions [324], [94], [198].
Research into FDIA on SGs has gained significance in this context. Reference [112] emphasizes that most attacks on intelligent grids involve false data injection, and numerous detection algorithms have been developed [17], [207], [97], [211]. However, the impact of false data on power systems has received comparatively less attention. FDIA detection algorithms are often tested against manually crafted anomalous profiles that do not account for probabilistic scenarios [97]. Consequently, this document seeks to investigate how randomly generated false data could affect a smart DN employing a centralized voltage regulation framework to mitigate the effects of DER. While many papers in the literature have explored new voltage regulation strategies for DSOs to mitigate the impact of DER and load variations on grids [349], [294], [169], they often neglect cybersecurity aspects. Voltage regulation schemes are categorized based on communication architecture, including local control, centralized control, distributed control, and decentralized control [169]. The various voltage regulation schemes have been extensively studied in the literature, but cybersecurity considerations are frequently overlooked. For example, in [240], a decentralized control system is examined concerning the dynamic voltage regulation of a hybrid distribution transformer. In [129], DER are leveraged to maintain voltages within specified limits through local and centralized voltage control. [291], [197], [269] and [7] explore centralized voltage control schemes to

ensure voltage stability in active distribution grids, utilizing voltage source converters, on-load tap changers, and step voltage regulators. Reference [291] uses voltage fluctuations forecasting to optimize tap positions and maximize the minimum voltage margin. In [19], centralized voltage control is assessed about the impact of data falsification attacks, focusing on voltage measurements transmitted from the field to the control system. A two-step method based on ML techniques is proposed to detect false data injection in the context of an active grid, tested on a 240-bus real distribution system and the IEEE 123-node benchmark DN. Ref. [228] investigates a volt-var control system subjected to a cyberattack, considering varying levels of the attacker's knowledge about the control system, network topology, and monitoring system. The authors propose a game-theoretical approach to derive countermeasures for detecting and mitigating attacks. [350] studies the impact of false data injection on a centralized voltage control system in a DN with high PV penetration. The authors demonstrate that falsified measurements can lead to many voltage violations and propose a detection algorithm tested in a residential area with one feeder. [288] explores the impact of cyberattacks on the remedial action schemes of large transmission systems, offering metrics for evaluating the effects of malicious operations through simulations on synthetic Illinois 200-bus and South Carolina 500-bus systems. In [71], a formulation for detecting and characterizing cyberattacks is presented in the context of a control center for a transmission system network. The authors investigate the impact of false data on parameters used in calculating the optimal power flow, which is essential for grid management.
Unlike the previously mentioned papers, this study assesses the impact of FDIA by creating a false data generator simulating a wide range of attacks and their effects within an extensive DN. The paper introduces a voltage regulation framework based on a microgenetic algorithm for centralized voltage control, sending optimized setpoints to DER units to maintain voltage levels within acceptable limits. The IEEE 118-bus test system is employed, considering various false data attacks. These attacks are generated using a specially developed false data generator, differentiating this research from others by not manually defining false data and evaluating multiple attack scenarios.

#### 3.5.1.1 False Data Generator Model

The false data generator was implemented using a series of Python functions. It operates by taking a dataset as input, introducing various anomalies to some of the data, and then providing an altered dataset as output. This highly adaptable generator doesn't require additional adjustments when dealing with different data profiles. The model is constructed based on Pandas module data frames, where each variable within the data frame corresponds to a distinct electrical bus, and the values within these buses are subject to analysis. After identifying which users are affected by data falsification, anomalies are introduced by manipulating a subset of data points associated with an electrical user, which could be either a generation plant or a load. These values are altered using random parameters selected from predefined lists. The false data generator requires various parameters before creating the anomaly:

- Type of anomaly: Spot, Drift, or Mixed.
- Percentage of users subject to the cyber attack, $N_{false\_i}$
- Fraction of anomalies present per node, $N_{false\%}$
- Anomaly scale parameter, $\sigma(N_K)$
- Fraction of anomalies parameter, $\varphi(N_K)$

- Mean drift parameter, $\mu(N_K)$
- Drift spread parameter, $\gamma(N_K)$
- Typology of anomaly attack to the node NK, $A_{TYPE}(N_K)$
- Number of nodes subject to spot anomalies, $N_{A\ spot}$
- Number of lines subject to drift anomalies, $N_{A\ drift}$

The process of creating the anomaly is shown in Figure 78.

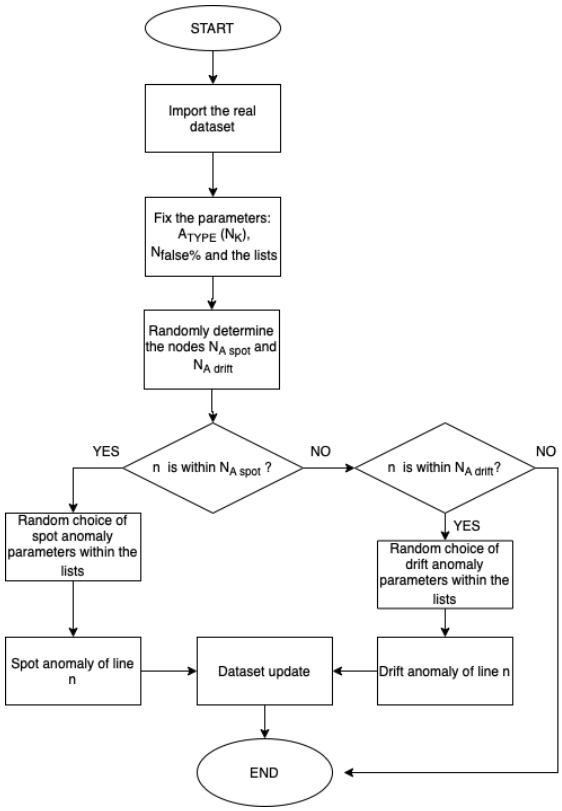


*Figure 78: False data generator algorithm*

For Spot type anomalies, first, the algorithm evaluates the minimum and maximum values of the input array related to a specific node $N_K$, from which the amplitude values are obtained as:

*Equation 32:*

$$\Delta_{arr}(N_K) = Arr_{max}(N_K) - Arr_{min}(N_K)$$

Where $\Delta_{arr}(N_K)$ is the maximum variation of values for the array relative to the $N_K$ node, and $Arr_{min}(N_K)$ and $Arr_{max}(N_K)$ are respectively the minimum and maximum value of the array referring to node $N_K$ data.

Based on the $\varphi(N_K)$ parameters, obtained by randomly extracting from φlist (list of all possible values for the anomaly fraction parameter) containing the permitted values for anomaly fraction, a portion of the timestamps is modified, extracted randomly by an amount equal to:

*Equation 33:*

$$N_{timestamps}(N_K) = \varphi(N_K) \cdot \Delta t$$

Where $N_{timestamp}(N_K)$ is the number of timestamps modified by the Spot anomalies in the analysis time-period Δt. These data are randomly increased or decreased according to Equation 34:

*Equation 34:*

$$x(N_K)_t^{False} = x(N_K)_t^{Real} \pm \sigma(N_K) \cdot \Delta_{arr}(N_K)$$

$x(N_K)_t^{False}$ is the false value of the array related to the node $N_K$ in the timestamp t and $x(N_K)_t^{Real}$ is the real value of the array related to the node $N_K$ in the timestamp t.

Drift-type anomalies vary the magnitude by raising or lowering the arrays' mean value from a specific time. First, a drift time $\tau_{drift}$ is set, chosen randomly within the analysis period Δt, at which the value of the quantity undergoes a shift, then the values of $\mu(N_K)$ and $\gamma(N_K)$ are defined, both obtained by randomly extracting from the lists $\gamma_{list}$ (list of all possible values for the spread drift parameter ) and $\mu_{list}$ (list of all possible values for the anomaly mean drift parameter), the first represents the percentage of mean drift, while the second represents the percentage change in the spread of the data.

In this type of anomaly, the values before $\tau_{drift}$ the magnitude remain the same, while for values after $\tau_{drift}$ the new value is evaluated as:

*Equation 35:*

$$x(N_K)_t^{False} = x(N_K)_t^{Real} + \frac{\sum_{\tau_{drift}}^{N_{after}} x(N_K)_t^{Real}}{(N_{after} - \tau_{drift})} \cdot \frac{\mu(N_K)}{100} \cdot \left(1 + \frac{\gamma(N_K)}{100}\right)$$

Where $N_{after}$ represents the number of timestamps after the drift time.

In the case of a mixed typology of anomaly, 50% of the nodes involved have a Spot data falsification, while the remaining 50% have a Drift type falsification. In Figure 79 two typologies of anomalies are shown.

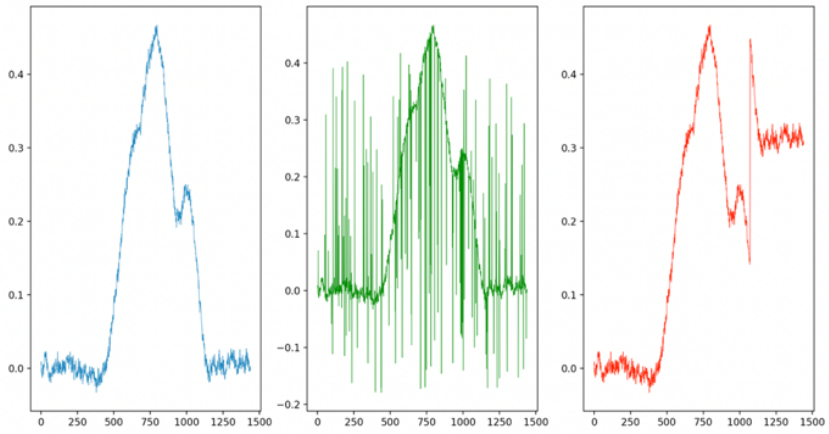

*Figure 79: Left) Real Trend; Center) Trend with Spot anomalies; Right) Trend with Drift anomalies*

### 3.5.1.2 Centralized Voltage Regulation Framework

The model for the centralized voltage regulation system is centered around the capability to remotely adjust the operating parameters of DER to maintain the desired voltage profile of the grid. With the increasing integration of DER, it is anticipated that operators will adopt such a voltage regulation framework to prevent frequent disruptions resulting from voltage deviations. Specifically, in the future, operators may fine-tune the reactive power

exchange without impacting active power generation, adhering to the limits specified by the capability diagrams of renewable-based generators. In the context of DR, there is potential for leveraging network services flexibility in an automated manner. Similar mechanisms for regulation support from DER are either being implemented or have been defined in existing networks or standards. For example, the Italian Grid Codes identify specific plants that operators can automatically disconnect to ensure system security [333]. According to the German grid code for LV grid connections, new PV installations with less than 30 kW capacity, which cannot be controlled remotely, are required to limit their output to 70% of their rated power. Additionally, remote control of active power output at the request of the system operator is mandated for all DERs rated above 100 kW connected to the grid [150]. The Chinese energy storage connection code GB36547-2018 stipulates that the system operator can send set-points and should work toward effective voltage management. The current version of IEEE Std 1547 specifies a requirement for all conformant DERs to respond to control signals (local and/or remote) limiting their active power output, with no DER size threshold for this requirement. In [XVII], it was assumed that the regulation framework could be applied to a MV network, with generators connected to the substations of the network. The regulation framework is implemented in the Octave environment using the Matpower package. Each substation is represented as a power demand node in the load flow analysis, accounting for local power consumption and production contributions.The key steps of the regulation framework are illustrated in Figure 80. Initially, load flows are computed for the specific timestamp being analyzed. Subsequently, the voltage regulation is activated if certain inequalities are not met for each node within the network:

*Equation 36:*

$$0.95 \leq V_i \leq 1.05, \forall i \in [1, N_{SS}]$$

where Vi is the voltage at the secondary substation characterized by the index i.

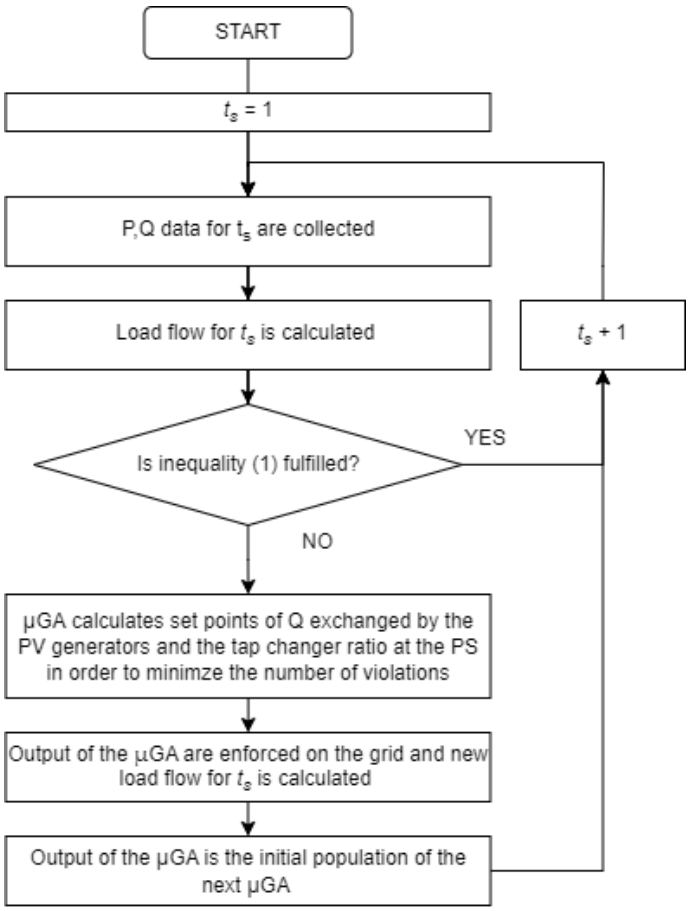


*Figure 80: Flowchart of the voltage regulation framework*

According to Figure 80, if Equation 36 is not fulfilled, the regulation is activated. The implemented regulation exploits the reactive production or absorption of RES. The reactive power exchanges have to fulfill the typical capability diagram of the PV generator, as in [100]. In detail, the maximum Q that a DG system can provide ($Q_{max}$) to the grid should be calculated according to the following equation, considering an operating point characterized by an active power production greater or equal to the 10% of the apparent power $S_n$:

*Equation 37:*

$$Q_{max} = P_n \cdot 0.484 \text{ (overexcited mode)}$$

where Pn is the nominal power of the DG system.

The minimum Q absorbed by the DG system (Qmin) is calculated with the following equation.

*Equation 38:*

$$Q_{min} = -P_n \cdot 0.484 \text{ (under excited mode)}$$

When the active power production is under 10% of the Pn, the reactive power cannot be exchanged with the grid. These limits are also shown in Figure 81.

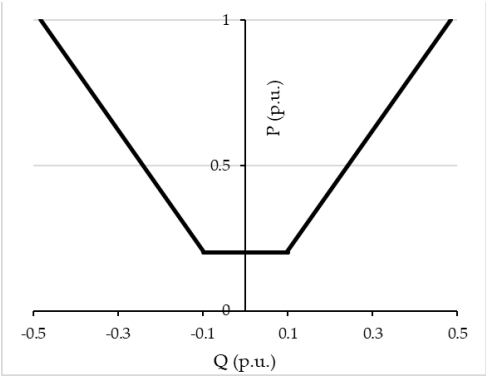

*Figure 81: Capability curve assumed for DG in the voltage regulation framework*

The voltage regulation model acquires the active and reactive profiles of load and generation by each secondary substation and performs the load flow, considering the topology of the grid and the interconnection with the HV system as the reference bus. Then, according to Equation 34 the total number of violations is calculated. In case of violation occurrence, the model tries to reduce the number of violations using the reactive power support by DG. As reported in Figure 80, the optimization technique used for this nonlinear problem is based on a micro genetic algorithm, implemented by the authors in the open-source Octave environment and coupled with Matpower. The usage of micro genetic algorithm enables to address the solution of nonlinear problems with adequate performance, even during real-time operation. The algorithm initializes a random sample of individuals with the values in p.u. of reactive power for each substation to be optimized. The evolution via survival of the fittest is adopted, and the selection scheme used is tournament selection with a shuffling technique for choosing random pairs for mating. The routine includes binary coding for individuals, jump mutation, creep mutation, and the option for a single-point crossover; a restart mechanism with elitism is also implemented. The population size is fixed to 5 individuals. Each individual has several genes equal to the number of secondary substations + 1; the number of secondary substations describes the reactive power exchanges of the generators, while the last gene corresponds to the tap changer of the transformer of the primary substation. The objective function to be minimized by the micro genetic algorithm is defined as the number of violations. Two stopping criteria are implemented: the algorithm is stopped as soon as the number of voltage violations is nihil or the maximum number of generations is reached. Therefore, in each iteration, the micro genetic algorithm performs the load flow of the DN to evaluate the number of remaining violations after implementing the combination of setpoints in terms of reactive power exchanged by the DERs. It is worth highlighting that the performances (i.e., a reduced number of generations and the related execution times) are dramatically improved by exploiting the solution of the previous iteration for the current calculation. Leveraging this recursive behavior, micro genetic algorithm suggests a minimum amount of changes; moreover, generations start only if the solution of the previous timestamp causes a violation during the new timestamp. The entire procedure is repeated for each timestamp according to the case study. To evaluate the voltage deviations, the following indices are calculated after the execution of the voltage regulation:

- $TV_{1.05}$ is the number of timestamps during which the maximum network voltage is higher than 1.05;

- $TV_{1.1}$ is the number of timestamps during which the maximum network voltage exceeds 1.1.
- $TV_{1.15}$ is the number of timestamps during which the maximum network voltage exceeds 1.15.

#### 3.5.1.3 False data injection in a test network

The impact of false data on voltage regulation is assessed through a case study involving a 118-node DN, as described in [128]. The network's topology is illustrated in Figure 82, which initially emphasizes its radial structure comprising four primary feeders and a primary substation identified by a red square marker. Each node corresponds to a secondary substation with several connected customers. This particular case study was chosen as an intriguing test system due to its inclusion of lengthy feeders. Such a configuration is representative of scenarios where voltage-related issues may emerge, particularly in the presence of significant RPF. Notably, this case study does not include current limits on the branches. Therefore, when considering higher flowing currents, such as when assuming a certain level of DER penetration, it is assumed that these currents remain within the line's specified limits and protection thresholds.

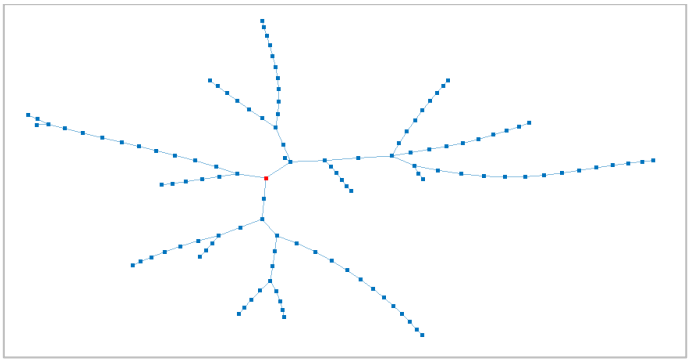

*Figure 82: Case study topology (red marker corresponds to the PS)*

Following the establishment of the network topology, power profiles were formulated. A yearly load profile was utilized for the passive loads, as outlined in [2]. This profile is in p.u. and was subsequently adjusted to align with the loads assigned to the nodes in the original network from [128]. Additionally, a coefficient ranging randomly from 0.85 to 1.15 was applied to this profile. Using these load profiles, it was assumed that the loads would consume 290 MWh annually, with an average peak load of 0.19 MW at the nodes. In addition to the existing passive loads, PV generators were installed at all nodes. Regarding the power profiles of these generators, an openly accessible dataset from [234] was employed. The sizes of these PV plants are pivotal parameters for determining their impact on voltage profiles, and, consequently, the need for frequent regulation. In this context, a substantial deployment of PV plants was considered, capable of supplying approximately 40% of the energy consumption. This was achieved by assigning sizes to the PV generators ranging from 3 to 4 times the peak power of the load profile at each node. The installed generators collectively produced 444 MWh annually, delivering 120 MWh to the loads, resulting in a RPF of 324 MWh at the primary substation. While the simulated conditions may appear extreme, they reflect scenarios in regions with low load density but high potential for RES installations, such as areas with favorable exposure, minimal authorization constraints, available open land, and significant adoption of agro

PV plants. These regions often feature a fragile network infrastructure susceptible to voltage issues, as evidenced by continuous RPF reported by network operators at their primary substations.
Following the definition of the reference profiles and the sizes to be considered, production and consumption profiles were sampled at one-minute intervals. For clarity, the analysis concentrates on a single day when the RPF was at its peak, and the most significant voltage deviations were observed. Consequently, the overall consumption and production profiles under examination are depicted in Figure 83.

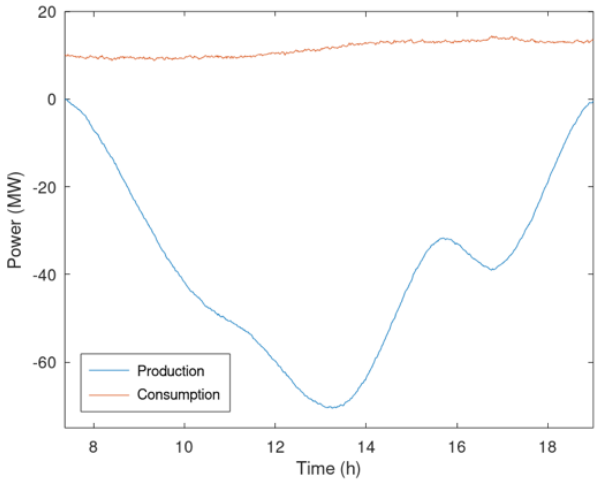


*Figure 83: Global power profiles in case of production peak, used in the case study*

Results were obtained by simulating the voltage regulation process, which was performed every minute based on the power profiles of the substations. Specifically, the impact on voltage profiles was initially assessed when the received data was accurate and reliable. Subsequently, multiple sets of false data were introduced to assess their detrimental effects on the effectiveness of voltage regulation and the overall network stability.
The voltage regulation framework inputs the active power and reactive power values of the nodes, along with the active power injected by the generators. These profiles are intentionally falsified to examine the consequences of FDIA. Furthermore, voltage regulation can adjust the transformer ratio at the primary substation, essentially varying the secondary voltage, as well as modulating the reactive power exchanged by PVs. Assuming that the secondary voltage at the primary substation remains at 1 p.u., the voltage regulation comes into effect whenever the voltage exceeds 1.05 p.u. or falls below 0.95 p.u. Figure 84 illustrates the trends in maximum and minimum voltage levels when regulation is actively applied. When regulation is not in effect, voltage levels are assumed to be the same as those calculated for the baseline scenario, where regulation is not enforced, and the secondary voltage at the PS is set at 1 p.u. It is important to note that the maximum voltage level always remains below 1.1 p.u. Due to the enforcement of regulations. Operators typically impose this limit to identify potential network violations. The beneficial effects of the voltage regulation framework can also be observed by examining $TV_{1.05}$, which corresponds to 67.8%. However, when the impacts of voltage regulation are factored in, this value decreases to 7.4%.

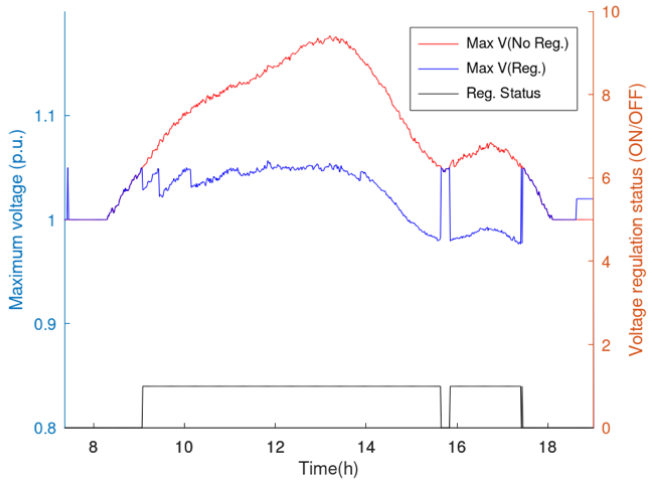


*Figure 84: Case study voltage regulation*

The attack scenarios simulated in this paper are characterized by a distributed manipulation of consumption and production data at the secondary substations. In detail, the power profiles of the production power plant and the overall power demand at secondary substations are manipulated. Results were calculated considering the two types of threats previously described (i.e., drift and spot anomalies) and their mixed combination. Moreover, an increasing amount of manipulated measurements was considered for the simulation; notably, it was simulated that 25%, 50% or 75% of the nodes are affected by the anomalies.

#### 3.5.1.4 Results: Impact of FDIA in a distribution grid

This section presents the simulation results considering the case study and load profiles previously presented, assuming that an increasing number of profiles are manipulated. The evaluation of the impact of false data is carried out considering 2 main sets of simulations. a first set regards some attacks that manipulate up to 25 % of the measurements, while a second set regards those attacks that massively manipulate the measurements, namely 50 % and 75 % of the data are falsified. The results are presented by calculating mean values, standard deviation of the voltages and the defined indices $TV_{1.05}$, $TV_{1.1}$, and $TV_{1.15}$.

##### 3.5.1.4.1 FDIA affecting 25 % of the measurements

The first set of simulations regards the effects of manipulating 25% of the measurements applying a mixed anomaly; 10 simulations randomly assigned the set of profiles to be manipulated. The overall results are shown in Table 36, which reports the average values collected from the 10 simulations; furthermore, these are compared with those calculated when the voltage regulation framework does not exploit manipulated data. Considering statistical parameters, it can be highlighted that the manipulated data cause notable effects on voltage regulation; on average, 6 % of the timestamps report voltage violations on the network (i.e., voltage overcome 1.1 p.u. in at least one node). It is worth highlighting that false data are processed during all the timestamps. Therefore, the VR framework can still solve voltage issues. Indeed, considering that the lack of VR leads to TV1.05 higher than 1.05, equal to 67.8 %, on average, 30 % of the voltage violations are still solved by the regulation procedure.

*Table 36. Main results comparing average effects of 10 simulations with 25% of manipulated measurements and true data processed by VR framework.*

| | Max | Min | Mean | SD | $TV_{1.05}$ | $TV_{1.1}$ |
|---|---|---|---|---|---|---|
| True Data | 1.056 | 0.941 | 0.982 | 0.0233 | 7.4 % | 0.0 % |
| Attack on 25% Nodes | 1.127 | 0.945 | 0.991 | 0.0261 | 31.5 % | 6.0 % |

The average voltage of the nodes is reported in Figure 85. The figure shows the individual effects of the 10 simulated anomalies and the profile calculated without manipulation, which is taken as a reference. Figure 86 highlights that the longest feeders (i.e., those with the highest numbers of nodes) have the highest voltages and the highest differences among results (i.e., the maximum difference is about 0.03 p.u.). Moreover, some nodes have a voltage lower than the reference; this behavior is due to the lack of disruptive anomalies on the feeder that do not jeopardize the voltage regulation framework.

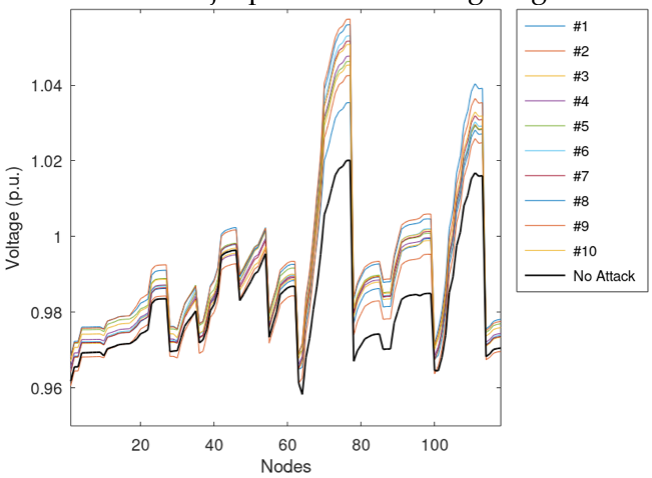


*Figure 85: Average Voltage of the nodes assuming that 25% of measurements are manipulated*

A specific timestamp is also reported in Figure 86 as an example that shows the voltages calculated during the timestamp associated with the maximum voltage in the case of real data. In this case, it can be seen a violation on voltage higher than 1.1 p.u.

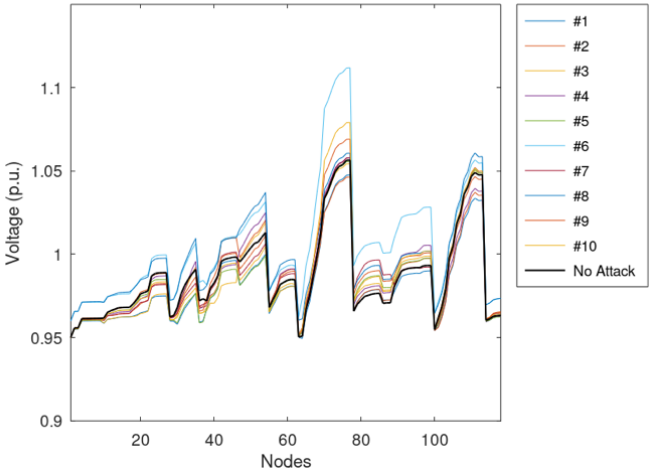


*Figure 86: The voltage of the nodes during the maximum violation assuming that 25% of measurements are manipulated*

Figure 87 shows the maximum network voltage during the simulated time period considering the false data that cause maximum and minimum violations, identified as min and max attack, respectively. This figure highlights that a specific combination of false

data does not cause voltage violations, while the most disruptive falsification leads to violations.

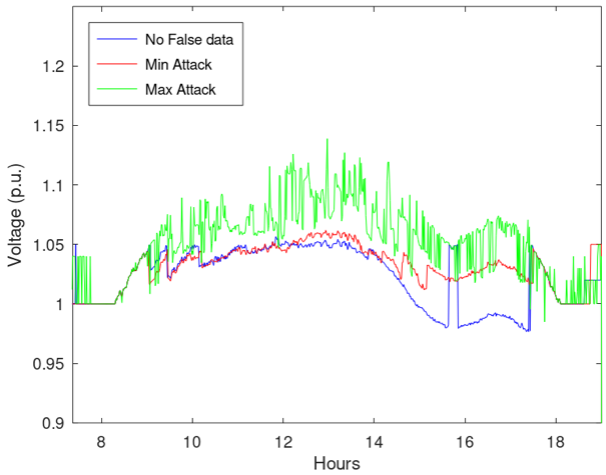


*Figure 87. Maximum network voltage during the timestamps considering maximum and minimum violations assuming that 25% of measurements are manipulated.*

#### 3.5.1.4.2 Massive widespread of False data injection attacks

An additional set of simulations regards the effects of an increasing amount of falsified measurements. Notably, it simulated the effects of spot and drift anomalies when applied to 50% or 75% of measurements. The main results of these simulations are collected in Table 37, which shows the notable impact on the voltages caused by incorrectly processed data; in particular, calculated violations overcome even 1.15 p.u.

*Table 37. Main results considering a combination of anomalies and percentage of falsified measurements*

| | **True Data** | **Attack on 50% of measurements** | | **Attack on 75% of measurements** | |
|---|---|---|---|---|---|
| Manipulation type | N/A | Spot | Drift | Spot | Drift |
| Max | 1.056 | 1.164 | 1.181 | 1.252 | 1.215 |
| Min | 0.941 | 0.923 | 0.941 | 0.886 | 0.891 |
| SD | 0.023 | 0.029 | 0.028 | 0.040 | 0.039 |
| $TV_{1.05}$ | 7.4% | 48.4% | 64.4% | 63.7% | 65.1% |
| $TV_{1.1}$ | 0.0% | 15.0% | 29.6% | 31.4% | 31.0% |
| $TV_{1.15}$ | 0.0% | 0.6% | 2.3% | 11.7% | 13.3% |

Similarly to the previous simulations, the average voltages of the nodes are reported in Figure 87, while Figure 89 shows the voltages during the most critical timestamps identified during the regular operation. Considering Figure 89, it can be noted that the spot anomaly does not cause any voltage issues on the network if applied to half of the measurements; the drift anomaly has a higher impact on the network, causing overvoltages. Moreover, considering the average effects on the network presented in Figure 88, it can be shown that drift anomalies can have a higher impact on the DN weakening the voltage regulation framework. It is worth noting that the profile associated with a lower number of falsified profiles has produced a higher voltage profile on average, even if violations are more frequent in the case of a higher number of falsified profiles. Indeed, a more comprehensive set of falsified measurements lead to higher standard deviation values, namely, overvoltages are more frequent and more intense. Moreover,

taking advantage of the evaluation of a wide set of values, it was found that the distribution of false profiles that introduce low measurement variations is more dangerous than concentrated threats that introduce the highest differences from the actual measurement.

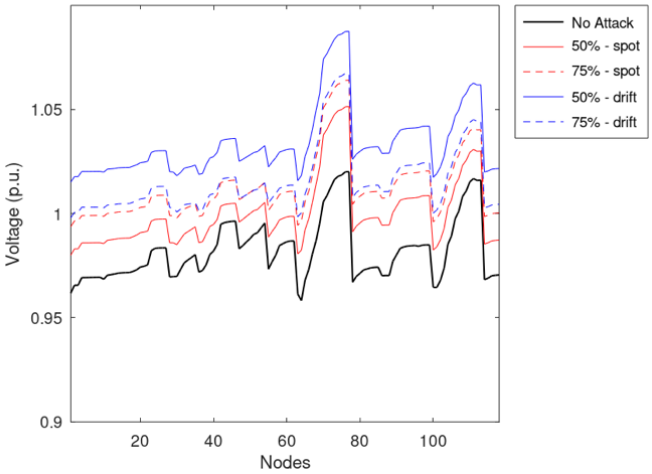


*Figure 88. Average Voltage of the nodes assuming respectively that 50% and 75% of measurements are manipulated.*

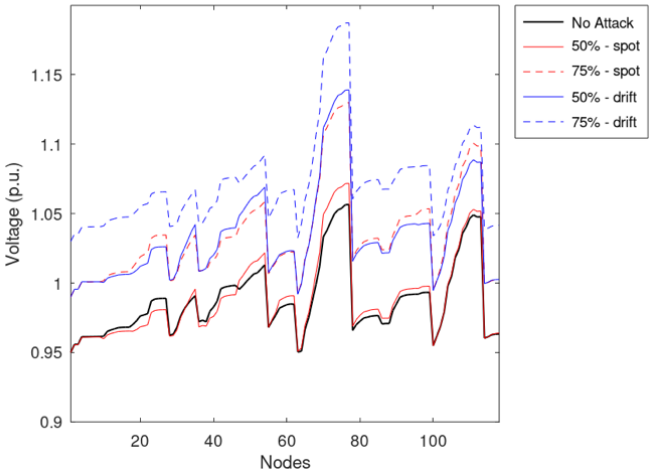


*Figure 89. The voltage of the nodes during the maximum violation assuming respectively that 50% and 75% of measurements are manipulated.*

Figure 90 and Figure 91 report the maximum network voltages calculated for all the timestamps. These figures show that the effects of drift anomalies are more disruptive than the spot anomalies.

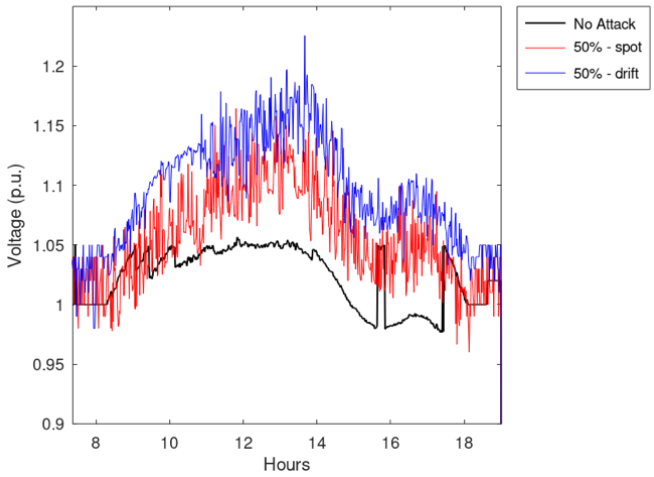


*Figure 90. Maximum network voltage during the timestamps considering half of the measurements falsified.*

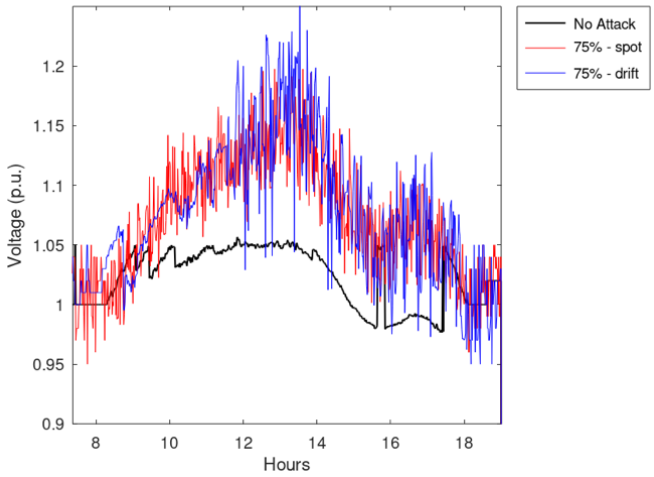


*Figure 91. Maximum network voltage during the timestamps considering 75% of the measurements falsified.*

# 4 Mobility as a service provider for the electrical network

## 4.1 Prospectives for electrical mobility in the energy transition

The energy transition involves a radical change in the mobility sector, with the emergence of new platforms such as car sharing and the spread of light vehicles in cities, as well as the conversion of the vehicle fleet to EVs [252] shows that as of 2019, almost 2.3 million EVs, both plug-in hybrids and battery EVs, have been registered, a growth of 9 % compared to the previous year, and this growth is set to continue in the near future, considering that various national and international policies limit the use of diesel- and petrol-powered vehicles after 2035.

The spread of EVs is spread all over the world, with most vehicles in China, Europe, the USA and Japan. In Italy, electric cars account for 0.9 % of registrations (17,000), with 70 % of vehicles present in the north, according to 2019 figures. It is estimated that there are around 9,100 public EVCSs in Italy, with 9 % of them being fast. In the future, this is expected to grow to between 47,000 and 7,000 in 2030, plus between 1.8 million and 3.8 million private EVCSs.

As the world shifts towards sustainable energy solutions, electric mobility has gained significant traction for the following reasons: 1) EVs contribute to lower carbon emissions, supporting global efforts to combat climate change; 2) the integration of EVs into the energy grid can promote the use of RES, contributing to a more diverse and sustainable energy mix; 3) the growing EV market presents economic opportunities for industries involved in the production of EVs, battery technologies, and charging infrastructure; 4) EVs can provide grid flexibility and enabling DR capabilities. Through smart charging solutions and vehicle-to-grid technologies, EVs can support grid stability and optimization.

Many governments are offering incentives and implementing supportive policies to encourage the adoption of EVs. These initiatives include tax incentives, subsidies, and the development of charging infrastructure, fostering a favorable environment for electric mobility.

These prospects indicate a promising future for electric mobility, emphasizing its pivotal role in the global transition towards a more sustainable and environmentally conscious energy landscape, but at the same time the complexities of such a large transition, the impact on the electricity grid and the economic aspects are also current challenges.

### 4.1.1 The role of electric vehicles in providing plexibility to the distribution grid

Electric mobility is an important enabler for flexibility services for the DN, mainly because vehicles are generally parked for a long period of time and can recharge at times of the day when it is most convenient for the grid.

EVs can provide flexibility to the energy DN in several ways. The first way is to charge vehicles intelligently, i.e. by using charging management systems that take into account the availability of energy from RES or peaks in the grid's power, this approach corresponds with the application of DR mechanisms for EVs, shifting recharging to the most convenient times. Vehicles can also feed electricity into the grid at times of particular need by breaking down storage to feed other sensitive loads, the so-called vehicle-to-grid. Intelligent use of storage allows them to be used, taking care not to shorten their lifespan or damage the cars, to provide ancillary services to the grid, such as voltage support or congestion management.

Finally, it is common to use EVCSs within RECs or microgrids to act as active instruments of the microgrid to limit the flow of power exchanged with the external grid.
In summary, e-mobility offers significant potential to improve the flexibility and resilience of DN, helping to better manage demand, integrate RES and reduce power surges. These benefits are key to supporting the transition to a more sustainable energy system.

## 4.2 E-mobility impact on the distribution grid

In the past decade, EVs have seen a significant increase in adoption, and there are strong expectations for even more substantial growth in the years ahead. This trend is having a notable impact on the DN as the electricity demand is rising rapidly. This increased demand is putting stress on power cables and transformers, leading to higher peak power loads. EVs have been rapidly gaining popularity, and local governments have introduced various incentive policies to encourage their adoption. In 2020, approximately 10 million EVs were on the road, accounting for 4.6% of all vehicles sold. Looking ahead to 2030, the International Energy Agency forecasts a range of 145 to 230 million EVs, constituting approximately 7% to 12% of the total vehicle market [141]. In the European Union, the transportation sector is responsible for 30% of greenhouse gas emissions, with 72% of those emissions attributed to road transportation. To address this, there is a growing emphasis on promoting sustainable mobility options, including electric and hydrogen-powered vehicles [VI], [326], [35], is needed to reduce pollutant emissions by 55% in 2030 compared to 1990 data [329], [66]. EVs contribute to greater environmental sustainability in the transportation sector and play a crucial role in advancing the adoption of RES. They also constitute a significant and economically vital sector within the industry. Nevertheless, EVs have disadvantages, including elevated costs, lengthy charging periods, and limited driving range. It's important to note that EVs notably influence DN, elevating the overall electrical demand, introducing harmonics, and potentially straining power lines and transformers. [90], [79], [133], [141]. The scientific literature in this research domain primarily focuses on three key aspects:

1. Charging technologies.
2. Optimal placement of EVCSs.
3. The effects of EVs demand on the electrical grid [137].

Adverse effects of EVCSs on the electrical grid encompass issues like voltage instability, increased load demand, power quality problems, and overheating and overloading of transformers. In [302], the authors tackle the challenge of optimising the design and sizing of DNs while considering EV demand to minimise overall costs. They consider both the sizing and degradation of transformers in this analysis. In [245] and [299], the impact of EVCSs on the power quality of the network is explored using OpenDSS, emphasising a significant increase in harmonics. Various methodologies, such as Monte Carlo simulations and gaussian mixture models, are employed to conduct these analyses. In a series of studies [90], [166], [32], [30], authors delve into the ramifications of electric mobility on LV distribution feeders. They primarily examine aspects like increased power flow and voltage instability. These investigations involve case studies conducted in Switzerland, Iran, and California, assessing different charging technologies. To mitigate the adverse effects of EVCSs on the power grid, specific research papers propose strategies for scheduling EV charging. These include implementing DR mechanisms or utilising vehicle-to-grid technology to provide ancillary services to the DN [24], [257].

Two studies have been presented to analyse the impact of mobility on the grid; in the first case, the impact of ultra-fast EVCS has been considered [IV], while in the second case, a new DN for the city of Terni, separated to the main one that supplies all the other loads, has been designed [V].

### 4.2.1 Impact of ultrafast electric vehicle chargin stations

This research aims to assess the impact of ultrafast EVCS on DN. As a case study, it examines a parking area in Terni, equipped with six ultrafast 500 kW EVCSs. The analysis uses Italian projections for adopting EVs and data from the open-access ACN-Data database to estimate the load demand, including that from EVs, from 2020 to 2030. Introducing EVCSs amplifies the power draw from the primary substation, leading to overloads on LV lines. However, it's noted that voltage profiles consistently remain within acceptable parameters. The study also investigates the potential role of local DER equipped with EESS, revealing a positive impact on the SCR of the EV parking area.
The research encompasses three distinct scenarios for electric mobility development and two plausible load increase scenarios. These scenarios shed light on the consequences of ultrafast EVCSs regarding power consumption, voltage fluctuations, and potential overloads. This study focuses on 500 kW liquid-cooled EVCSs, which, while emerging in the market, are presently limited in deployment. These devices offer a notable advantage in rapid recharging times, comparable to conventional internal combustion engine vehicles, taking just a few minutes. References related to 500 kW EVCSs can be found in [340], [75], [76], [59]. The case study presented in the paper spans 11 years, from 2020 to 2030, and considers evolving trends in electricity consumption and the adoption of EVs. The simulation, through OpenDSS, utilises actual data provided by ASM to model the DN, load demands, and PV generation. Additionally, the daily load profiles of the EVCSs are based on actual data obtained from the publicly accessible ACN-Data database.

#### *4.2.1.1 E-mobility scenarios and analysis*

In this research, a model has been made to evaluate the impact of 500 kW EVCS on the electrical DN. The development of the model involved a sequence of three key steps:

1. Examination of electricity consumption and EVs adoption scenarios, focusing on the city of Terni.
2. Analysis of EVs consumption patterns over time, drawing upon data provided by the ACN-Data dataset [26].
3. Conducting a power flow analysis with OpenDSS.

In the subsequent subsections, these three steps are explained.

##### 4.2.1.1.1 Electrical demand scenarios

The Italian Transmission System Operator, hypothesises two scenarios for the electricity consumption trend [307]: business as Usual and Advanced development rate growth; trends of aggregate electrical energy consumption normalised for the year 2020 are plotted in Figure 92. In the business as usual scenario, the load increases with an average 0.41 %/year rate, reaching the normalised value of 104.50 % in 2030; in the advanced scenario, the rate is 0.87 %/year, reaching 109.65 % in 2030. Growth rates reported in [307] at the national level also represent the city of Terni. Based on [252], three scenarios with the different spread of EVs and EVCSs in Italy from 2020 to 2030 are considered: base

development scenario, which foresees the maintenance of current growth trends; moderate development scenario, in line with car manufacturers' development plans and the Italian Integrated National Energy and Climate Plan [146]; accelerated development scenario, which requires the presence of relevant support mechanisms. Figure 93 shows the trends at the national level of the three scenarios, normalised on the total number of EVs in Italy in 2020, i.e., 128,000, and the number of EVCSs in 2020, i.e., 24,794.

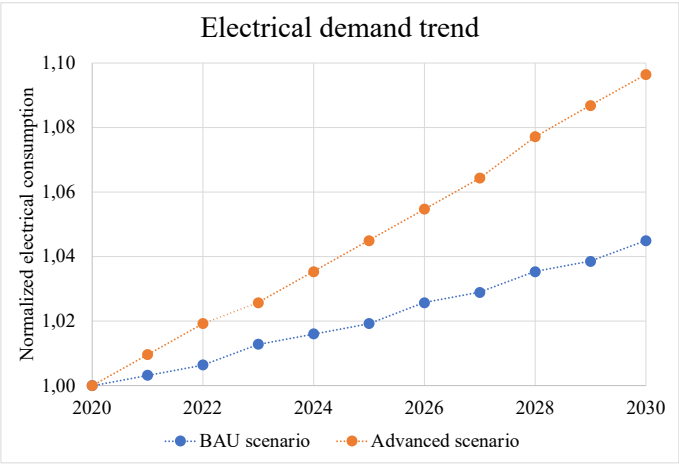


*Figure 92: Business as Usual and Advanced development scenarios of electrical demand trend based on [307], normalised on 2020 value*

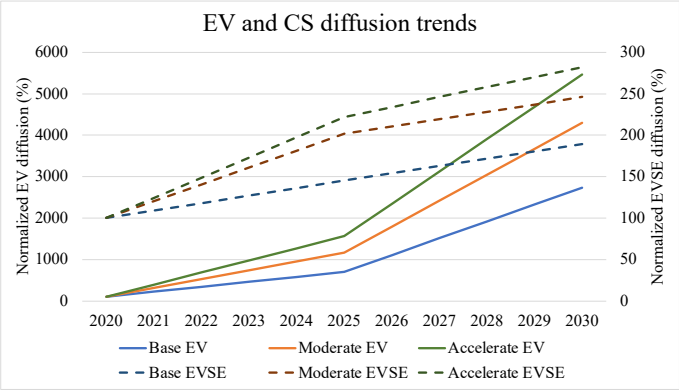


*Figure 93: EVs and EVCSs diffusion in three scenarios normalised on 2020 values.*

The base scenario envisages 3.5 million EVs in 2030, with a 2,730% increase in 10 years and 47,000 EVCSs (189% increase). In the moderate scenario, EVs in 2030 are 5.5 million, with a 4,290% increase, and EVCSs are 61,000, with a 246% increase. The accelerated scenario considers about 7 million EVs in 2030, with a 5,460% increase and 70,000 EVCSs, i.e., a 282% increase concerning the 2020 value. As from [146], the most significant growth in all scenarios is performed in 2025 – 2030. In Italy, the ratio between the number of EVs and the number of EVCSs in 2020 is about 5. In the base, moderate and accelerated scenarios, it is expected to reach values of 70, 90, and 100 in 2030. Installation of public EVCSs is expected to accelerate significantly between 2020 and 2025 due to national policies and grow more slowly until 2030. In this study, only public EVCSs are considered, even if, in Italy, a large part of EV owners use private charging points, which at present are about 70% of the total EVCSs; in 2025, it will be 60%, and in 2030 will be about 45 %. According to [252], in the model, about 48.6% of all recharging sessions occur in public EVCSs.

#### 4.2.1.1.2 Distribution of vehicle power consumption over time

The model's distribution over time of EV load demand is based on historical data and development scenarios. To define the time consumption pattern, an analysis of the typical weekly EV load demand was studied using ACN Data and other open-access data sources [26], [359]. A total of 66,745 charging session data from 2015 to 2021 were collected, and relevant information concerning the time of access to recharging and the amount of energy required for each recharge was evaluated. As shown in Figure 94, the weekly distribution of energy required for EV recharges is roughly constant during weekdays, decreases on Fridays, and is significantly less on weekends.

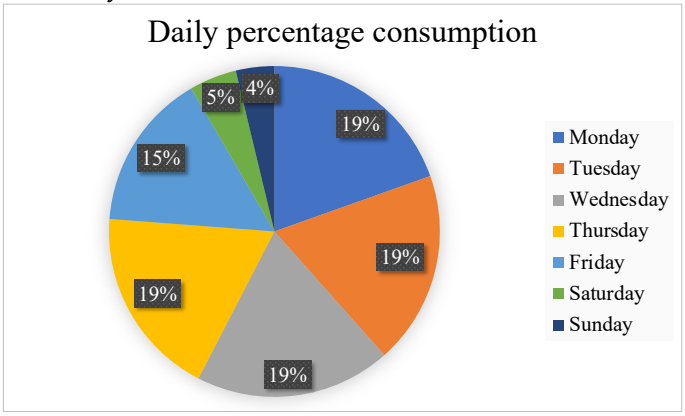


*Figure 94: Percentage of energy required on the total weekly demand.*

The data collected by ACN Data were divided according to the time of arrival and the amount of energy required, with a granularity of 1 minute. Figure 95 reports the time of arrival trend, assuming that EVCSs are open from 6:45 a.m. to midnight.

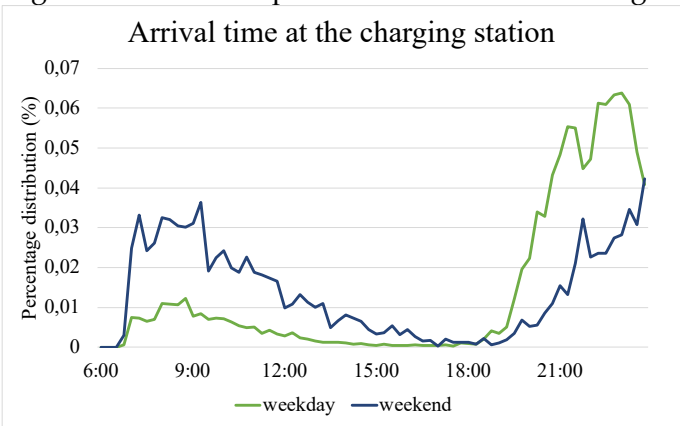


*Figure 95: The typical trend of the percentage distribution of arrival times at EVCSs day by day.*

Figure 95 shows that the pattern of arrival times over time follows a constant trend on weekdays, with a significant peak in the evening hours (78.3% of charging sessions are from 8 PM onwards), while on the weekend, the pattern is more distributed, with a peak in the morning hours (44.7% from 7 to 11 AM) and a peak in the evening hours (34.5% from 8 PM onwards). The evaluation of EV energy demand requires evaluating the average daily EV consumption. Using available data in the literature, the authors supposed an average annual mileage for each EV of 14,200 km/year [281] and an average EV efficiency of about 0.195 kWh/km [83], so the annual energy demand for each EV is about 2,769 kWh/year. Once defined the number of EVs and EVCSs in the location under study, using the above-reported data, the model evaluates how many vehicles on average

use a EVCS and which is the annual energy demand. Each EV's arrival time is calculated based on the distribution in Figure 95. In contrast, the duration of each charging session is estimated using the daily share of energy consumption (Figure 94) and the energy required by EVs depending on the arrival time. Lastly, the power absorbed in each charging session has been randomly reduced to consider limiting factors such as lesser needs of the user, technological limits of the car, and power transients, so the average value of absorbed charging power is about 250 kW.

#### 4.2.1.1.3 Distribution grid analysis using OpenDSS

The impacts of EVCSs on the electrical DN were analysed using OpenDSS. Detailed power flow analyses spanning the 2020-2030 period with a 1-minute granularity show how the different scenarios could affect voltage and current trends in the network over time.

### *4.2.1.2 Electric vehicle trends baseline*

To assess how the presence of 500 kW EVCSs affects the electricity DN, data provided by ASM were used. It was decided to simulate a 9-bus system: three secondary substations supply a parking area with six ultrafast 500 kW EVCSs connected to the MV/LV transformer by an LV underground power cable. In addition, a 50 kW PV plant and a 60 kW/55 kWh EESS are connected to one secondary substation. The three substations are supplied by a dedicated MV power cable starting from the MV busbars of the primary substation. The rest of the DN is represented by an aggregate load directly connected to the primary substation. The one-line diagram of the simulated system is depicted in Figure 96, whereas Table 38 and Table 39 report the primary data of transformers and underground power cables.

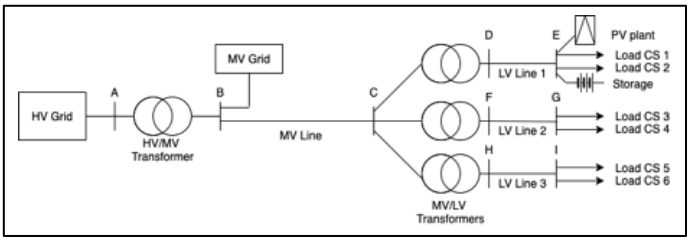


*Figure 96: One-line diagram of the simulated system*

*Table 38: Transformers electrical characteristics*

| | **HV/MV Transf.** | **MV/LV Transf.** |
|---|---|---|
| Connections | Yy | Dyg |
| S (MVA) | 25 | 1.25 |
| Vn1 / Vn2 (kV) | 132 / 20.8 | 20 / 0.4 |
| No load Losses (%) | 0.06 | 0.1075 |
| Load Losses (%) | 0.49 | 0.9625 |
| Max tap ratio | 1.15 | - |
| Min tap ratio | 0.85 | - |
| Xcc (%) | 14.6 | 6.0 |
| Earth Resistance (Ω) | - | 5 |

*Table 39: Underground power cables characteristic*

| | in MV | in LV |
|---|---|---|
| Nominal conductor area (mm²) | 185 | 240 |
| Positive sequence resistance (ohm/km) | 0.128 | 0.0978 |
| Positive sequence inductance (ohm/km) | 0.119 | 0.176 |
| Ampacity (A) | 479 | 556 |
| Length (km) | 0.8 | 0.05 |

The MV underground power cable has a smaller cross-section than LV power cables since, in this specific application, currents flowing through cables are a limiting aspect. In the case study, a 50 kW LV-connected PV plant supplies the EVCSs. PV and inverter have been simulated using available technical data of real devices [223], [74]. In contrast, PV generation has been calculated using historical data on radiation and temperature in Terni. The calculated PV profile over one year is shown in Figure 97.

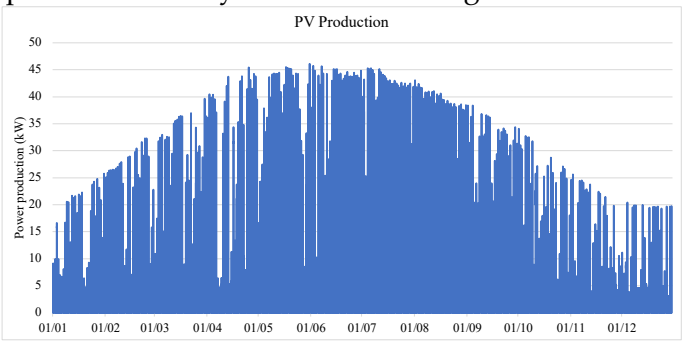


*Figure 97: PV generation profile during one year*

To increase SCR and reduce over-currents, the PV is equipped with a 55 kWh/60 kW EESS, which injects power when the power output from secondary substation (bus D) is more significant than 100 kW and absorbs power when the power output from secondary substation is almost zero. MV-busbar demand is connected at 20 kV, and in 2020, the recorded power profile ranged between -108 kW (power injected in the PS) and 11,282 kW. A graphical representation of the recorded annual active and reactive power in 2020 at the MV busbars of the primary substation is in Figure 98:

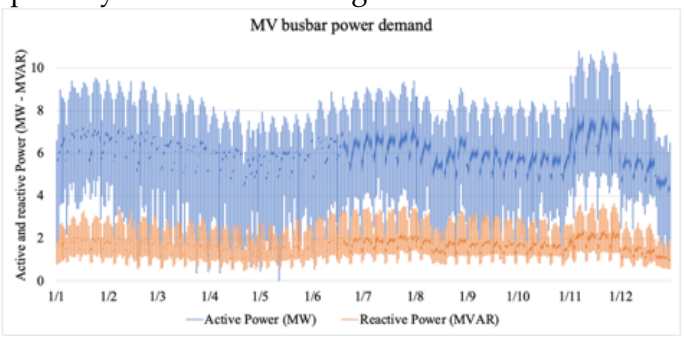


*Figure 98: MV power demand in 2020 (bus B).*

In the case study, demand is considered to increase during the 11 years according to the two scenarios already shown. To assess the electric demand forecast for vehicle power supply in the case study, an analysis was made, taking into account actual data and national scenarios scaled at the municipal level. Based on research on the register of vehicles and EVCSs, in Terni in 2021, there were 88 EVs and 9 public EVCSs [195]. Figure 99 shows Terni's expected number of EVs and EVCSs from 2020 to 2030. The number of

EVs is estimated to increase in 2030 to 1,547 in the base development scenario, with a maximum of 3,095 in the accelerated development scenario. For EVCSs, the difference will be more limited, i.e., between 17 and 25. Since 51.4% of the users supply their EVs from private charging points and the average annual energy required by EVs is 2,769 kWh, each EVCS will supply 44 EVs in the base scenario and 59 EVs in the accelerated scenario. The amount of energy required per year is significant, up to 163 MWh per EVCS per year, i.e., a total of 4.097 GWh is needed to supply all the electric mobility, accounting for about 1% of the current annual demand supplied by ASM and approximatively corresponding to the annual consumption of 1,500 households.

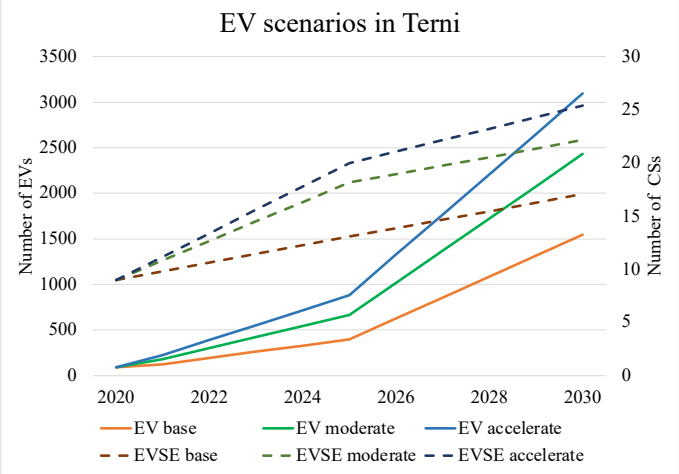


*Figure 99: EVs and EVCSs in the considered scenarios in Terni from 2020 to 2030*

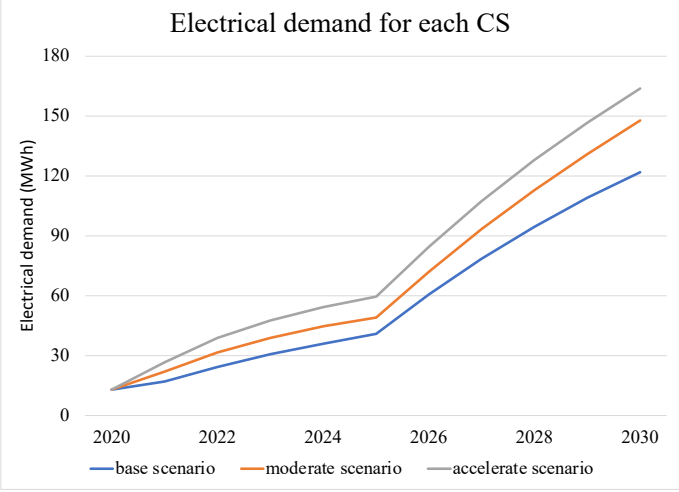


*Figure 100: Annual electrical demand for each EVCSs*

### 4.2.1.3 500 kW EVCSs impact on the distribution grid

Through OpenDSS, the trends of all electrical parameters over time in all circuit elements were obtained. In the following, the results of power and energy in the primary substation are first shown; then, bus voltage profiles and branch currents are analysed. Lastly, the role of PV and EESS in ensuring SCR is investigated. The OpenDSS model of the system runs quite fast: power flow calculations in 11 years with a 1-minute granularity for all different analyses performed required about 130 minutes.

#### 4.2.1.3.1 Primary substation energy and power trends

The amount of energy absorbed from the primary substation is distinguished based on development scenarios of electric mobility and consumption electrification. Figure 101 shows that the energy supplied by the primary substation almost exclusively depends on the electrical consumption scenario. In the business as usual scenario, 50.7 GWh were supplied in 2020, whereas 53.8 GWh will be required in 2030, while the advanced scenario in the same year reaches 56.4 GWh. The impact of electric mobility on the total load demand ranges from 0.16% in 2020 to 1.29% and 1.74% in 2030, respectively, in the base and accelerated scenarios. In terms of power supplied by the primary substation, over the 11 years, peak power is expected to increase from the current value of 11.04 MW to 12.40 MW and 13.23 MW, respectively, in the business as usual scenario and the advanced scenario. The EVCSs have a significant impact on the supplied power. Indeed, a EVCS rated 500 kW is much more impactful for the power than the energy required. The power required by the six EVCSs is 3.30% in 2020 (with a maximum power required of 0.41 MW) and will weigh up to 16.48% in 2030 (with 2.18 MW of maximum power required for EVs).

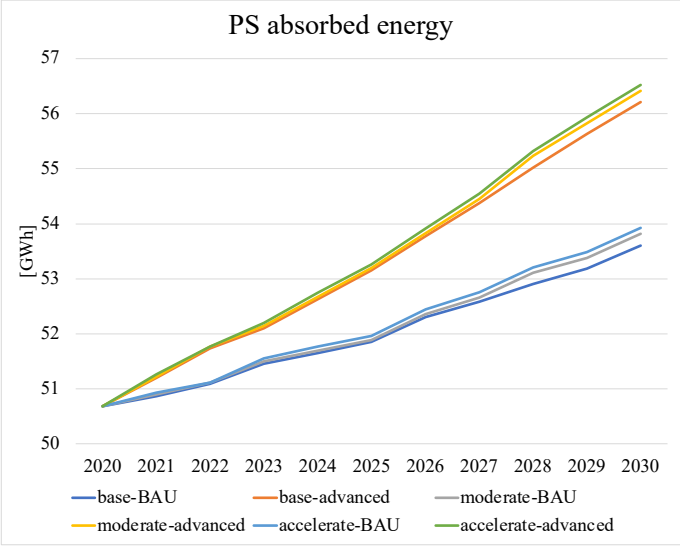


*Figure 101: Amount of energy demand for each year in primary substation in six different energy scenarios*

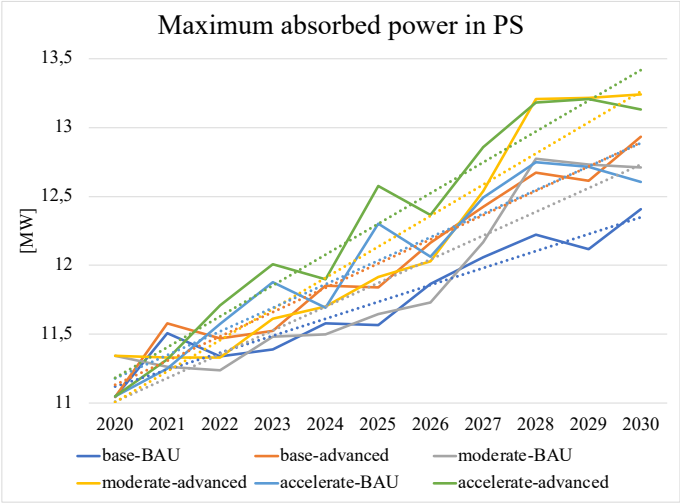


*Figure 102: Maximum power demand in primary substation for each year and linear trends for six scenarios*

#### 4.2.1.3.2 Voltage and current trends

The analysed network comprises 9 buses, and through OpenDSS, various analyses have been made on the voltage in all buses and the current in all branches. The average voltage of buses A and B is highly constant over time. The average voltage of buses C, D, E, F, G, H, and I is always in an acceptable range so that no over- or under-voltages are detected in the performed analysis. The current along the MV underground power cable increases from about 11.6 A in 2020 to over 59.6 A in 2030, while the currents along the LV underground power cables are between 1,149 A and 1,453 A. No overloads on the MV underground power cable are detected, while there are several overloads in the LV lines supplying the parking area. among LV underground power cables, the least loaded one is LV Line 1, equipped with EESS and PV. Figure 103 reports the percentage of time with overcurrents in LV lines. Frequently, there are overloads in the LV line due to the high power of the EVCSs, which is why LV lines have a cross-section larger than MV lines. Indeed, assuming for LV lines, a 70 mm$^2$ cross-section would have obtained overloads up to 9% of the time, while using 240 mm$^2$ cables, overloads occur for less than 3.5% of the time. In addition, one way to reduce overloads would be to increase the operating voltage.

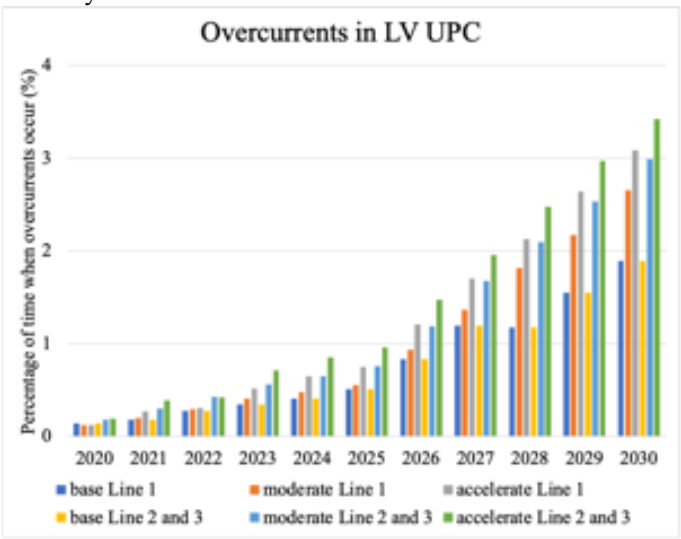


*Figure 103: Percentage of time with overcurrents in LV underground power cables in six simulated scenarios*

Figure 104 shows the trends of some electrical parameters in bus E, where two EVCSs, the PV and the EESS, are connected. Three selected days in the accelerated–advanced scenario, namely from the 1$^{st}$ to the 3$^{rd}$ of February in 2020, 2025, and 2030, are chosen to show the influence of both conventional and EVCS load demand increase over the years. Voltage decreases over the years, even if values lower than 0.9 p.u. are never detected. Current increases at the same rate over time of load, whereas the tap ratio of the HV/MV transformer slowly increases, well below the maximum tap ratio value of 1.15.

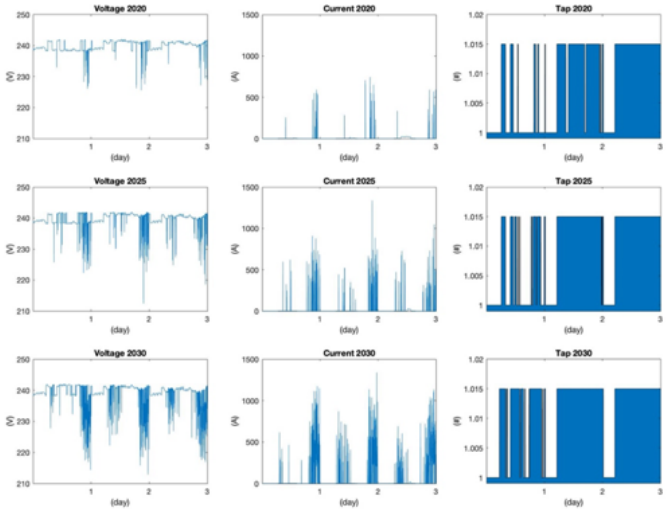


*Figure 104: Trends over time during three selected days (from the 1st to the 3rd of February in 2020, 2025, and 2030) in the accelerated–advanced scenario: column 1: bus E voltage; column 2: bus E current; column 3: tap ratio of the HV/MV transformer.*

#### 4.2.1.3.3 PV plant and storage roles

A 50 kWp PV system in the parking area is installed in bus E, which either supplies the EVCSs on-site or sends power to the PS. A 55 kWh - 60 kW EESS is also installed to increase the SCR of the RES produced by the PV. PV generation is 74,406 kWh annually, partly fed into the grid and partly consumed on-site. As shown in Figure 105, SCR is about 24.25% in 2020, increasing in 2030 to 54.3% in the base development scenario, 60.2% in the moderate development scenario, and 62.3% in the accelerated development scenario. The EESS allows increasing SCR considerably, up to 21.9% more.

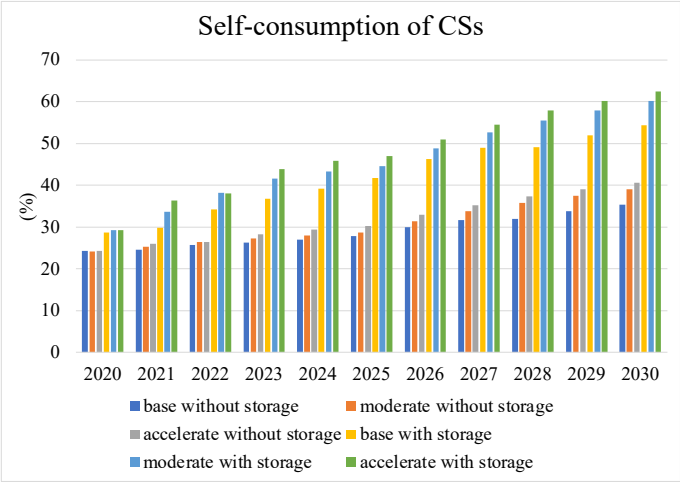


*Figure 105: Self-consumption of EVCSs, with or without EESS*

### 4.2.2 Design of a medium voltage network dedicated to supply electric mobility

The study reported in [V] focuses on the feasibility of expanding the existing DN to effectively and securely accommodate EVs. The widespread adoption of electric mobility presents a significant challenge for DNs due to the connection of high-capacity and unpredictable loads and the increasing demand for rapid recharging, which can result in power quality issues. The research proposes establishing a dedicated network exclusively designed to supply EVs. This approach aims to mitigate the impact of electric mobility on the existing grid while concurrently enhancing the flexibility and resilience of the power system. A section of the Terni DN was examined as a case study, comprising two primary substations and 18 secondary substations. The study assessed the network's capacity to cater to EVs and determined the maximum number of vehicles the system can accommodate. Utilising power flow and fault analysis conducted with OpenDSS, the most suitable configurations were identified. Additionally, the study investigated the system's performance during a primary substation disconnection, revealing that the proposed solution significantly enhances grid resilience.

#### *4.2.2.1 Tools and steps for the grid design*

To provide the necessary infrastructure for electric mobility, a proposition is made to design a new 20 kV grid onto the existing one. This approach serves two essential purposes: firstly, it helps prevent significant disruptions to the existing MV grid, and secondly, it offers the flexibility required for accommodating the increasing demand for EV charging, which would otherwise be challenging to achieve. Public EVCSs consume range from 22 kW for slower charging to over 100 kW for rapid direct current charging. Future projections indicate a rising demand for such services. The network's design to support EV recharging infrastructure relies on assessing the hosting capacity of HV / MV transformers situated in primary substations. This means that the available power margin, relative to the maximum load, is entirely allocated to supply EVCS, thus eliminating the need for installing new HV/MV transformers.

The power grid created to supply the charging infrastructure can adopt a radial configuration (more straightforward to manage) or a meshed layout (offering greater reliability). In this study, specific criteria are employed to identify appropriate grid configurations in operation, which include the following:

- HV/MV transformer loading consistently lower than the rated power;
- bus voltages always within the range of 0.9-1.1 p.u.
- Branch loadings are always lower than branch capacities;
- Three-phase short circuit current in each MV bus lower than the breaking capacity of circuit breakers already installed at the MV side of HV/MV transformers.

Based on such criteria, a comparison between the possible network configurations in operation has been made, identifying the most suitable for this service. For each configuration, power flow and short circuit calculations have been performed using OpenDSS [283]: the maximum load condition is simulated in the study to obtain conservative results. A flow chart illustrating the methodology adopted in the study is reported in Figure 106.

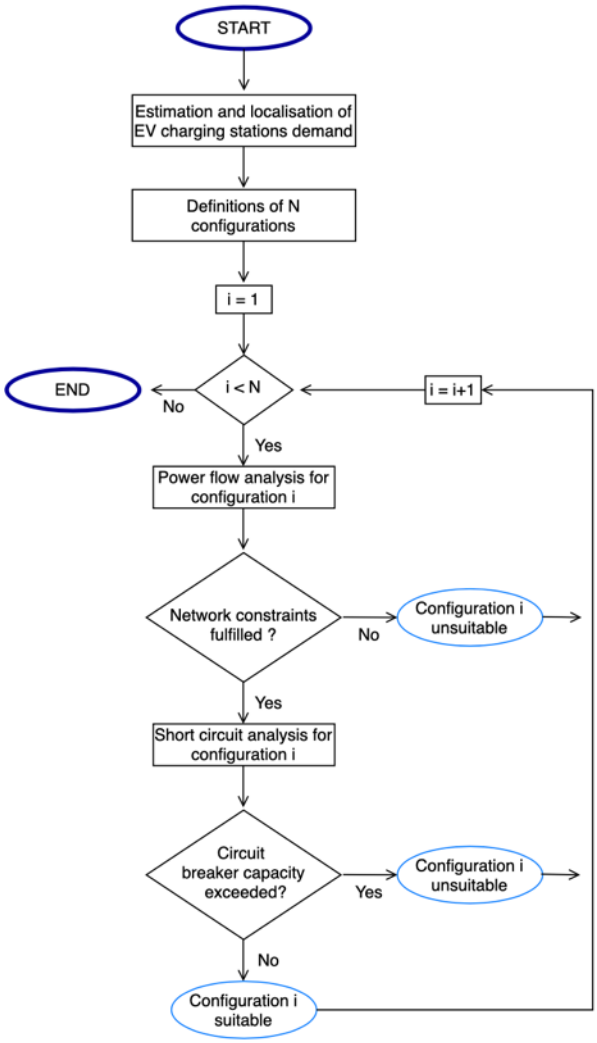


*Figure 106: Flow chart of the methodology for the deisign of a new MV network dedicated to EVs*

#### 4.2.2.2 Grid features and configurations tested

The portion of the DN under study is located in the city centre and connected to two primary substations, named CPA and CPB. CPA has 2 HV/MV transformers installed, and CPB has 3 transformers. The main features of the transformers and the related supplied load are reported in Table 40.

*Table 40: Main features of available HV/MV transformers*

| Primary substation | Transf. | Rated power (MVA) | Maximum active load (MW) | Maximum reactive load (MVAR) |
|---|---|---|---|---|
| CPA | TR1 | 25 | 12.41 | 1.26 |
| CPA | TR2 | 25 | 14.79 | 1.49 |
| CPB | TR1 | 25 | 17.05 | 7.59 |
| CPB | TR2 | 25 | 14.21 | 6.51 |
| CPB | TR3 | 25 | 12.79 | 3.34 |

The aggregate loading factor of the network is 57.7%, whereas the maximum loading factor is 63.8% for TR1 in CPB. From an N-1 perspective, considering 4 out of 5 transformers in operation, the aggregate hosting capacity is about 44 MVA, of which half

is reserved for public EVCSs. In contrast, the remainder is spared to cope with possible load demand increase and private EVCSs. Based on a preliminary analysis carried out in collaboration with ASM ì, 18 EV charging areas connected to the LV DN have been identified, each supplied by an 1250 kVA secondary substation [21], and equipped with ten 50 kW EVCSs, ten at 22 kW and two at 320 kW. The choice of such infrastructure allows for different EV charging times (slow, fast and ultra-fast) and costs. EVCSs available on the market have been selected, whose manufacturers' data are listed in [20] and [312]. The configuration of each charging area allows the simultaneous recharging of 22 EVs, and therefore, up to 396 EVs in the whole grid, corresponding to 22.5 MVA. The proposed grid is equipped with 12.7/22kV, 240 mm² three core underground power cables, and simulations are performed both with aluminium and copper conductors; main conductors parameters (positive and zero sequences, denoted by subscripts 1 and 0, respectively) are listed in Table 41 [237]. The 240 mm² cable cross-section has been preferred to 150 mm² and 185 mm² due to the higher ampacity, whereas no voltage violation has also been noticed for these two smaller section value.

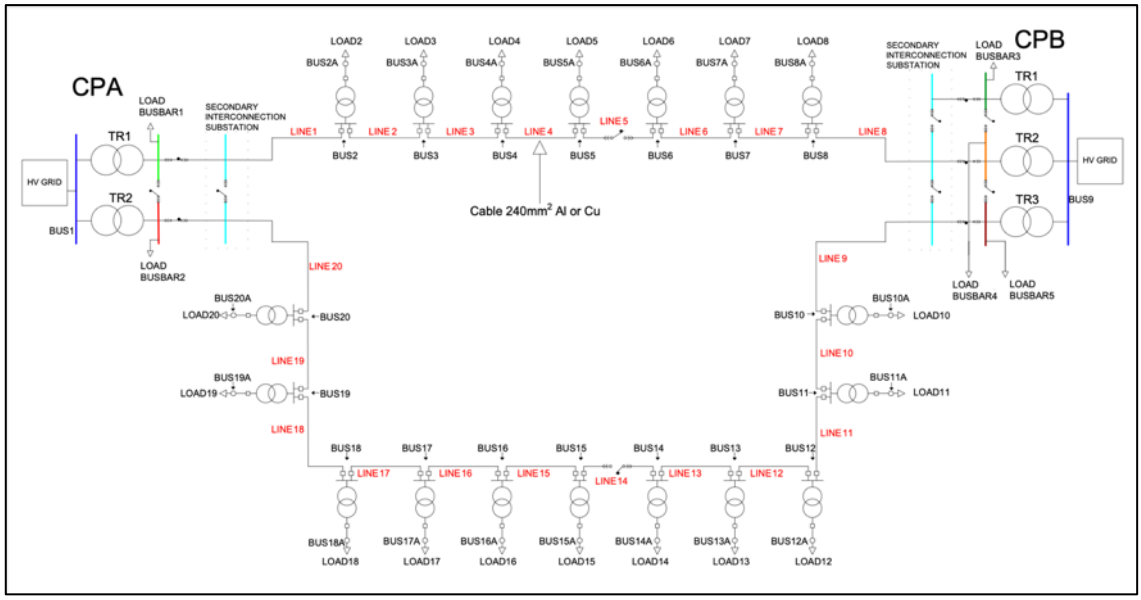


*Figure 107: Network topology for the studied configuration*

*Table 41: The main electrical parameters of the 240 mm² underground power cable*

| | Al | Cu |
|---|---|---|
| $R_1$ (ohm/km) | 0.161 | 0.098 |
| $X_1$ (ohm/km) | 0.102 | 0.101 |
| $C_1$ (nF/km) | 298 | 305 |
| $R_0$ (ohm/km) | 0.520 | 0.468 |
| $X_0$ (ohm/km) | 0.055 | 0.054 |
| Ampacity (A) | 316 | 398 |

As shown in Figure 107, the portion of the network supplying the 18 secondary substations is composed of 2 separate three-phase lines, connected to both primary substations through interconnection cabins. The upper line, 6.7 km long, is composed of 8 branches and the lower one, 9.9 km long, is divided into 12 branches: the average length of each line

section is 0.83 km. Disconnectors have been placed in the middle of both the upper and lower lines. All transformers are currently equipped with circuit breakers with a 12.5 kA breaking capacity. In the case study, 9 possible network configurations were analyzed, 4 in closed-ring (loop) operation and 5 in open-ring (radial) operation. Since TR1 installed in CPB is the most loaded transformer during the year, in the analyzed configurations it is the least used. Table 42 describes each configuration, also showing which transformers are used to supply the network.

*Table 42: Grid configurations analysed*

| N. | Config. | Involved Transf. | Description |
|---|---|---|---|
| 1 | Closed-ring | TR1 (CPA) TR2 (CPA) TR2 (CPB) TR3 (CPB) | Loop operation with power supplied by both PSs with 2 transformers in parallel. |
| 2 | Closed-ring | TR1 (CPA) TR2 (CPA) | Loop operation with power supplied only by CPA through 2 transformers in parallel. |
| 3 | Closed-ring | TR2 (CPB) TR3 (CPB) | Loop operation with power supplied only by CPB through 2 transformers in parallel. |
| 4 | Closed-ring | TR1 (CPB) TR2 (CPB) TR3 (CPB) | Loop operation with power supplied only by CPB through 3 transformers in parallel. |
| 5 | Open-ring | TR1 (CPA) TR2 (CPA) TR2 (CPB) TR3 (CPB) | Radial operation with 2 separate lines fed by both PSs, with disconnectors in the middle of the lines closed. Interconnection SSs with busbar disconnectors open. |
| 6 | Open-ring | TR1 (CPA) TR2 (CPA) TR2 (CPB) TR3 (CPB) | Radial operation of 2 grid sections, with disconnectors in the middle of the lines open. Interconnection SSs with busbar disconnectors closed. |
| 7 | Open-ring | TR1 (CPA) TR2 (CPA) TR2 (CPB) TR3 (CPB) | Radial operation of 4 grid sections, with disconnectors in the middle of the lines open.Interconnection SSs with busbar disconnectors open. |
| 8 | Open-ring | TR1 (CPA) TR2 (CPA) | Radial operation of 2 grid sections fed only by CPA, with disconnectors in the middle of the lines closed. Interconnection SSs with busbar disconnectors open. |
| 9 | Open-ring | TR2 (CPB) TR3 (CPB) | Radial operation of 2 grid sections fed only by CPB, with disconnectors in the middle of the lines closed. Interconnection SSs with busbar disconnectors open. |

#### *4.2.2.3 Simulation results: the design of a MV network dedicated to EVs*

##### 4.2.2.3.1 Electric mobility impact on the distribution grid

The proposed electric mobility infrastructure has a 22.5 MVA peak load, corresponding to 35.8% of the power peak of the current grid and 20.4% of the installed capacity in the primary substation. The proposed infrastructure allows for to recharge of 396 EVs simultaneously and Figure 108 shows the aggregate number of EVs that can be recharged over one year. This number is calculated according to the EV average consumption in a year and the average EVCSs occupancy factor, defined as the ratio between the yearly average number of EVCSs in operation and the number of installed EVCSs. Currently, assuming 14,200 km travelled in a year [63] and conversion efficiency of 0.195 kWh/km [83], the energy consumption of an EV is about 2,769 kWh/year. Based on this analysis, it is evaluated that the system can recharge 42,888 EVs, assuming an occupancy factor equal to 0.5 and an average consumption equal to 2,500 kWh/year. This number seems adequate for the needs of the entire population of Terni, which is about 110,000 inhabitants.

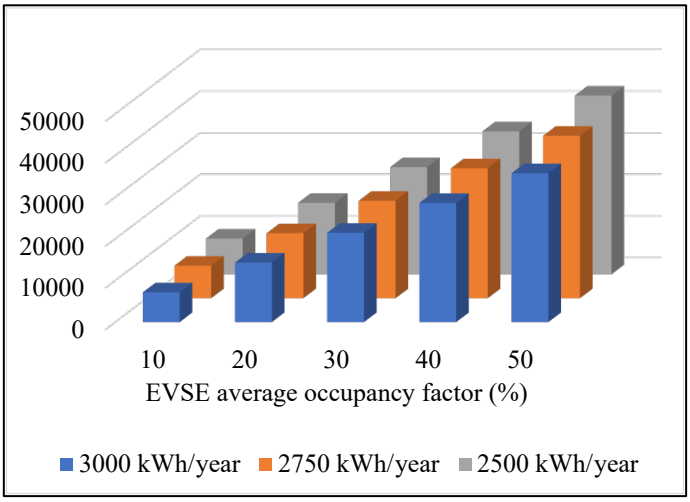


*Figure 108: Number of EVs that the infrastructure can recharge in a year as a function of the EVCSs occupancy factor and the average yearly consumption of EVs*

#### 4.2.2.3.2 Grid configurations for power electric mobility

The analysis is performed using OpenDSS, assuming the maximum load for each HV/MV transformer and a 0.96 power factor and 0.8 utilisation factor for the EVCSs; results are reported in Table 43. HV/MV transformers loading, $S_{max}$, is always larger than 20 MVA, and for configurations 2, 3, 8 and 9, the rated capacity is exceeded (highlighted in red) regardless of using aluminium or copper conductors. The maximum current in the network, $I_{max}$, is more significant than cable ampacity in five configurations with aluminium conductors (configurations 2, 3, 4, 8 and 9, highlighted in red) and two configurations with copper conductors (configurations 8 and 9, highlighted in red). Thanks to on-load tap changers installed in each HV/MV transformer, bus voltages never exceed threshold values. Lastly, the maximum three-phase fault current, $I_{cc,\,max}$, exceeds the 12.5 kA breaking capacity in configurations 1 and 4 (loop operation). In summary, the results suggest that configurations 5, 6 and 7 are suitable (all are open-ring configurations). In contrast, closed-ring configurations are all unsuitable due to transformer overloading or due to the breaking capacity of the circuit breakers. Amongst the three suitable configurations, performances are very similar, with the exception of $I_{cc,\,max}$ value in configuration 7, which is about half the value in configurations 5 and 6: this indicates configuration 7 as the most suitable (highlighted in blue). Moreover, since practically the same results are obtained in the case of aluminium and copper conductors, configuration 7, equipped with 240 mm² aluminium conductor underground power cable, is selected due to cost-effectiveness.

*Table 43: Power flow and Fault Analysis results*

| Grid config. | | $S_{max}$ in HV/MV transf. (MVA) | $I_{max}$ (A) | $V_{min}$ (p.u.) | System power losses (kW) | $I_{cc,max}$ (kA) |
|---|---|---|---|---|---|---|
| 1 | Al | 20.56 | 211.9 | 1.037 | 937 | 14.1 |
| | Cu | 20.49 | 210.5 | 1.037 | 893 | 14.5 |
| 2 | Al | 26.32 | 337.5 | 0.999 | 842 | 9.3 |
| | Cu | 26.24 | 335.3 | 1.008 | 706 | 9.3 |

| | | | | | | |
|---|---|---|---|---|---|---|
| 3 | Al | 27.68 | 331.7 | 1.002 | 1191 | 9.2 |
| | Cu | 27.60 | 332.1 | 1.010 | 1060 | 9.2 |
| 4 | Al | 24.97 | 331.1 | 1.004 | 1288 | 12.8 |
| | Cu | 24.92 | 329.4 | 1.011 | 1158 | 12.8 |
| 5 | Al | 21.93 | 207.8 | 1.040 | 937 | 8.0 |
| | Cu | 20.55 | 217.6 | 1.043 | 893 | 8.2 |
| 6 | Al | 20.62 | 212.5 | 1.007 | 953 | 9.4 |
| | Cu | 20.04 | 211.5 | 1.010 | 909 | 9.0 |
| 7 | Al | 20.71 | 212.5 | 1.033 | 937 | 4.9 |
| | Cu | 20.54 | 211.7 | 1.034 | 894 | 5.0 |
| 8 | Al | 28.01 | 402.8 | 0.999 | 1172 | 5.0 |
| | Cu | 27.88 | 399.5 | 1.011 | 1023 | 5.0 |
| 9 | Al | 29.32 | 406.7 | 0.990 | 1351 | 4.9 |
| | Cu | 29.18 | 402.4 | 1.002 | 1200 | 4.9 |

Figure 109 qualitatively shows power flows in the branches of the network: the thickness of the line is proportional to the power flowing, and the maximum value is about 6 MW.

#### 4.2.2.3.3 Network resilience

Even if the proposed network only supplies public EVCSs in regular operation, since the network connects the two primary substations, in case one of the two primary substations is disconnected from the HV network, it is possible to supply its load by using the remaining substation, thus significantly increasing the grid resilience. Figure 110 reports results obtained adopting an extremely conservative approach, i.e. each HV/MV transformer supplies its maximum load (in this case, the EVCS are not connected, otherwise transformers in the sound primary substation would be overloaded). Results show that if CPA/CPB is faulty, it is possible to supply about 70%/40% of its load by CPB/CPA; moreover, results do not differ significantly if aluminium or copper conductor is installed.

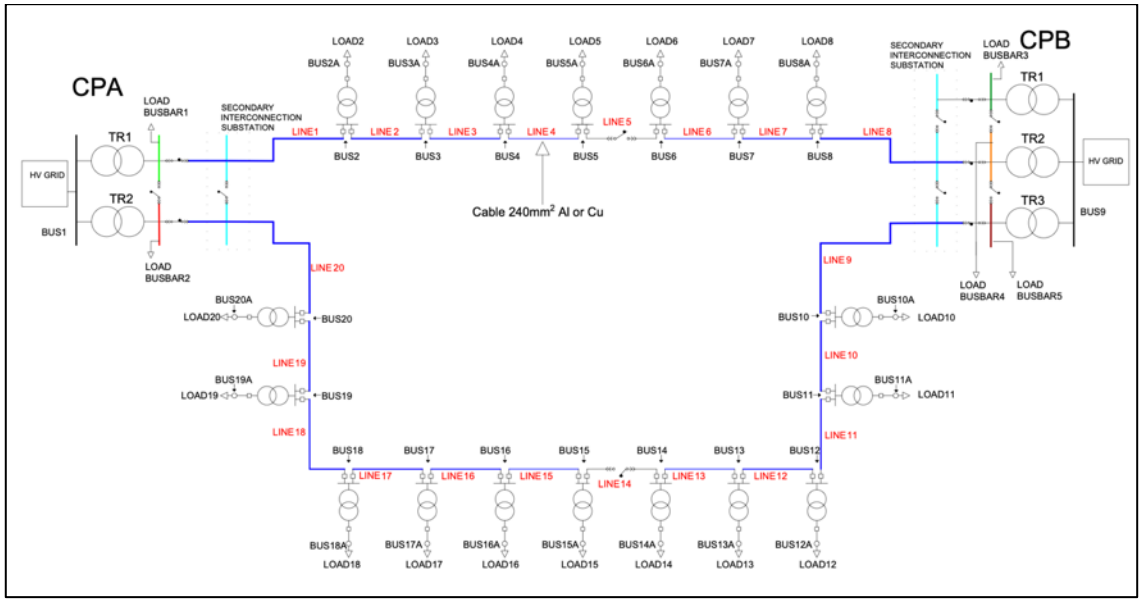


*Figure 109: Power flow results for configuration 7. The blue lines' thickness is proportional to each branch's active power flow*

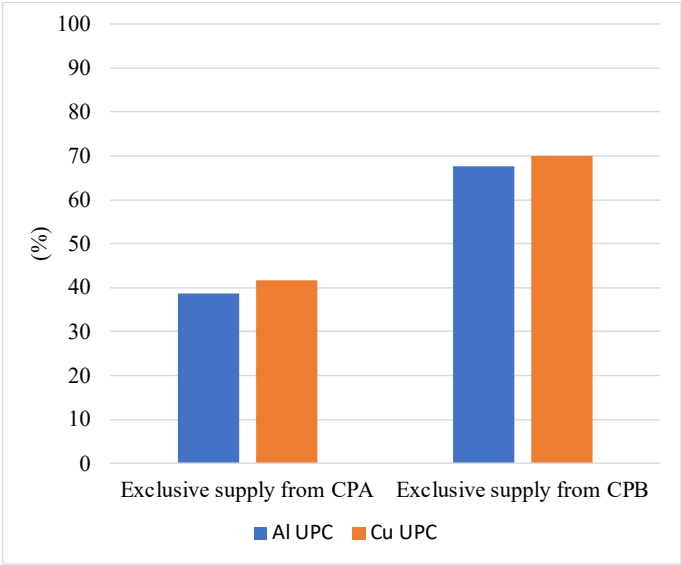


*Figure 110: Load (per cent of the rated capacity of the faulty primary substation) that can be supplied using the remaining substation, in the case of underground power cable with aluminium and copper conductors*

#### 4.2.2.3.4 One year of dynamic analysis

Results reported in the previous subsection are obtained simulating only the maximum load condition for each HV/MV transformer (maximum load conditions are not contemporary during the year for each transformer, so this assumption is highly conservative), i.e., with an aggregate 72.16 MVA load demand. In 2021, the maximum load was 47.2 MVA, with an average value of 21.4 MVA and was more significant than 30 MVA only 12.09% of the time. Then, a power flow study over one year is performed, using, for loads at primary substation busbars, the load demands recorded by the DSO in a ten-minute resolution and simulating the EVCSs always at maximum load: results for configuration 7 equipped with aluminium conductors show that the average transformer loading is 32.03%, whereas the average line loading is 5.09%. The presence of EVs also significantly impacts the reduction of RPF due to RES generation, which decreases from

35.7 GWh to 15.9 GWh, thus providing several benefits for the management of the grid. The increase in the grid resilience is even more significant: it is possible to fully supply with only one primary substation all loads, including the EVCSs, 74.9% of the year. If the EVCSs are excluded, this value increases to almost 100% of the year.

## 4.3 The role of company electric vehicle fleets

Company fleets play an important role in the spread of electric mobility, as medium/large companies often have a vehicle utilisation that does not require them to cover large distances and the range of an EV can be adequate. In addition, if they also have a PV or other generation plant, these companies can be configured as energy districts. The intelligent management of energy flows, e.g. through the flexibility provided by EVs, can lead to significant savings and environmental benefits. There are some examples of optimisation models in the literature, such as George and Xia [116], that created an optimisation model based on queueing networks to determine the ideal fleet size. In [132], the effects of EV adaption were evaluated in Denmark, Finland, Germany, Norway, and Sweden. The combined electricity and road transportation system was studied using the Balmoral deterministic partial equilibrium mode, and they found that EVs can potentially lessen the requirement for new coal and natural gas power facilities. Vehicle to grid technology, in a large-scale scenario, can have several benefits in terms of emissions reduction [303], support for the electric supply network [179], [123], and financial gains for EV owners [330]. Other indicators mentioned in the literature by Barth and Todd [44] include "vehicle-to-trip ratio," "number of relocations," and "number of trips,". The interplay between RES and EVs also attracted attention when examining smaller-scale systems. For instance, in [273], authors analyse the scenario of two Scandinavian cities and find that PV can almost entirely cover the number of EVs required in the summer but that the temporal match might be improved in other cases. California's energy system is the subject of research by McCarthy et al. [220] on the effects of EVs. Using a spreadsheet-based dispatch model, the authors categorise California's generation units according to technology. According to the findings, greenhouse gas emissions in the transportation sector can significantly decrease.

A part of the literature delve into the analysis of impediments and facilitating factors affecting the transition of corporate fleets to EVs, substantiating their findings through surveys. The principal drivers behind this shift include environmental benefits, user-friendliness, the desire to be at the forefront, cost savings on refuelling, anticipation of regulatory changes, enhancement of public perception, and the allure of government incentives, as evidenced in [39]. Nevertheless, the decision to embrace EVs within a corporate fleet primarily hinges on the influence of subjective norms and the inquisitiveness of company executives. In [22], the authors shed light on the primary obstacles to adopting electric mobility within companies based on interviews with 30 Swiss companies. Among these barriers, the most significant include a limited driving range, substantial initial investment costs, and a scarcity of widespread charging infrastructure. A number of major corporations are presently transitioning their entire fleets to EVs [39] - [22].

To mitigate the impact on the electricity DN, it is essential to implement intelligent management of EV charging. This management strategy is intricately linked to the existing charging infrastructure and service features. In scholarly literature, numerous articles examine the repercussions of EVs on the electricity DN, encompassing aspects such as heightened energy demand, peak power requirements, and the introduction of harmonics. Additionally, various technologies, such as vehicle-to-grid systems and DR mechanisms, are under investigation [94], [136], [90]. Furthermore, researchers have assessed the support provided by complementary enabling technologies, as demonstrated in [47], [91].

In the academic sphere, only a few papers have focused on corporate EV fleets [114], [251]. A German research [253] addresses how EVs can replace an existing company fleet. Three distinct scenarios are delineated: i) powering the fleet exclusively through the grid, ii) utilising both local RES and the grid to power the EVs, and iii) scheduling EV charging to coincide with periods of reduced network stress. A mixed-integer linear programming formulation to jointly perform the routing of the EVs and the scheduling of their charge/discharge operation has been presented by Triviño-Cabrera et al. [335]. Additionally, numerous research that relates to the objective of this work has been conducted. For instance, Lee and Bomsma [193] devised an approximation dynamic programming strategy known as the least square Monte Carlo method to solve a dynamic and stochastic optimisation problem for short-term electric car operation. Wu et al. [347] also investigated energy management strategies for EVCSs with multiple types of chargers, and they also designed a fuzzy logic guiding system to assign the EVs to the appropriate charging spots based on their charging urgency levels, which can reduce operation costs by over 50% in comparison to the immediate charging scheme. In a related study, Tuchnitz et al. [337] developed a reinforcement learning-based charging coordination system for a fleet of scalable EVs that do not require any knowledge of future information, such as arrivals, departures, or the energy consumption of the EVs.
In the following, two original studies on electric fleets for companies are presented in detail [XV], [XIII], in which the optimal scheduling of charging is analysed in order to have a limited impact on the electricity grid and to minimise the costs for EV owners.

### 4.3.1 Design and policy for a electric vehicles company's fleet

In [XIII], the researchers have examined various criteria for effectively managing the recharging of ASM Terni's corporate vehicle fleet. Following an analysis of the fleet's current energy consumption and the service characteristics it offers, diverse management strategies were assessed with the objectives of reducing the number of EVCSs, ensuring employee comfort, and enhancing the utilisation of local RES. The research employs a case study approach that leverages data from the fleet responsible for maintaining and operating the service network to evaluate the consequences of widespread EV adoption within the fleet. Currently, the technical service fleet is powered by conventional fossil fuels, specifically oil and diesel, consisting of 86 light vehicles and vans utilised by technicians for their daily tasks, including maintenance and emergency repairs. Monitoring of this fleet is indirect in nature, as refuelling can only occur at the headquarters, where a limited number of refuelling points are available. Each refuelling event is meticulously documented, capturing details such as the date and time of refuelling, the current mileage of the vehicle, and the vehicle's unique identifier. A comprehensive dataset has been extracted from the refuelling database, spanning a period of 1760 days, starting from January 1, 2015, through October 26, 2019, encompassing a total of 16,414 recorded refuelling operations.

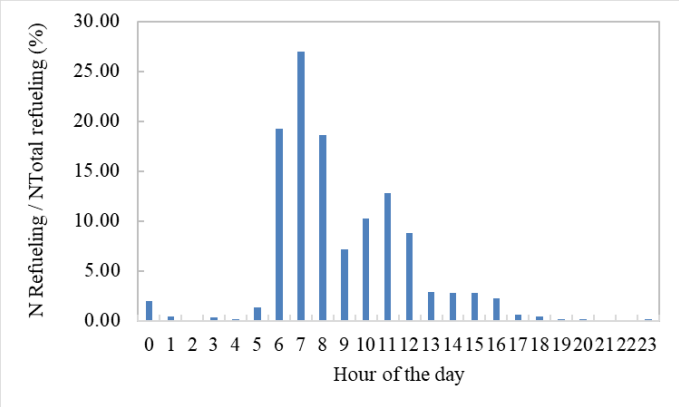


*Figure 111: Distribution of refuelling of ASM vehicles according to the hour of the day*

The dataset has been utilised to gain insights into the real-world operational conditions of a fleet. Specifically, the data have been instrumental in understanding vehicle mileage and relevant behavioural patterns, which are essential for formulating a new policy for managing an electric company fleet. In this context, Figure 111 illustrates the distribution of refuelling occurrences over the course of a day. It is evident that a significant number of refuellings take place between 6:00 and 8:00 (approximately 65% of all recorded refuellings). Based on this graph, it can be inferred that the current practice involves refuelling vehicles at the start of their activities. An analysis of the time intervals between refuellings reveals substantial variance. However, the first quartile of the fleet experiences intervals shorter than 7.9 working days, while the second quartile corresponds to intervals of 14.6 days. Upon examining the dataset, the average mileage of the vehicles has been determined. Specifically, data analysis indicates that the fleet covers an average daily distance of about 33 kilometres, with a standard deviation of 23 kilometres. The probability distribution of this data is depicted in Figure 112.

The proposed charging infrastructure is slated to be installed at the ASM headquarters. Figure 113 illustrates an example of the SoC and power trends during the charging process of an EV, from 12% to 100%.

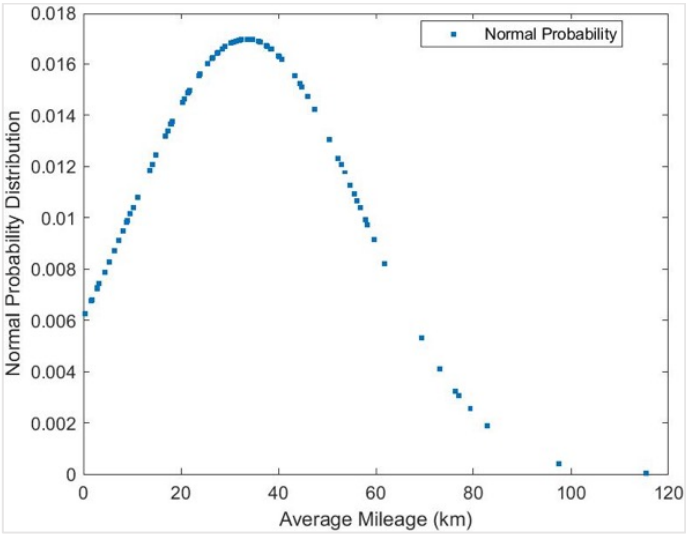


*Figure 112: Distribution of mileage considering data acquired in the case study*

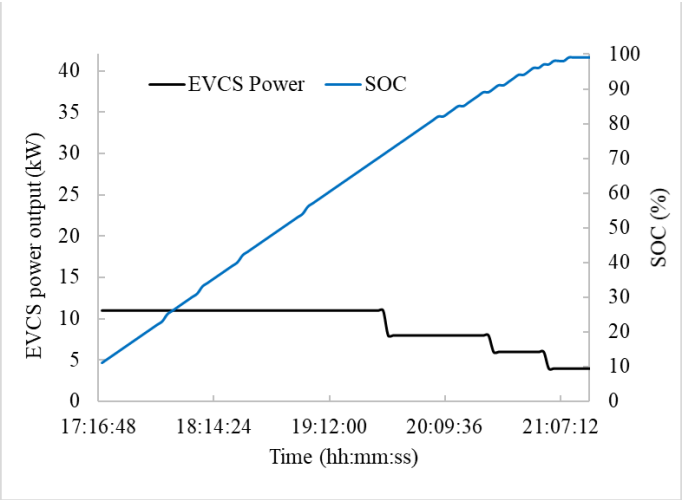


*Figure 113: The SOC and the charging profile measured in the EV and EVCS of ASM*

#### 4.3.1.1 Company fleet scenarios and criteria

This research assess the implications of substituting 50 disel-engine vehicles with EVs. Within this paper, the authors have examined two different design solutions:

- Design 1: Leveraging and improving existing EV charging infrastructure based on a fixed number of fast EVCS, where vehicles charge according to a probabilistic function dependent on their SoC. For the sake of clarity, one EVCS corresponds to one plug for the EV.
- Design 2: Each EV has its own 3 kW EVCS located in the parking area. The charging sessions are centrally managed and exploited to increase the district's SSR by using the energy of the PV plant.

Moreover, a company fleet is also characterised by the policy through which vehicles are managed. Indeed, company policies can be extremely different.

##### 4.3.1.1.1 Design 1: 22 kW electric vehicle charging stations

Concerning Design 1, using a fixed number of 22 kW EVCSs, two policies have been simulated and are defined as follows:

- Policy 1: When a user comes back from a trip, he has to look for a free charging point according to the probability P1(SOC) in Figure 114, based on the SOC value; when the trip is not approaching a charging probability distribution, P(SOC) is also assigned.
- Policy 2: When a user comes back from a trip, he has to look for a free charging point according to the probability P1(SOC) in Figure 114, based on the SOC value; when the trip is not approaching a charging probability distribution, red P(SOC) is also assigned.

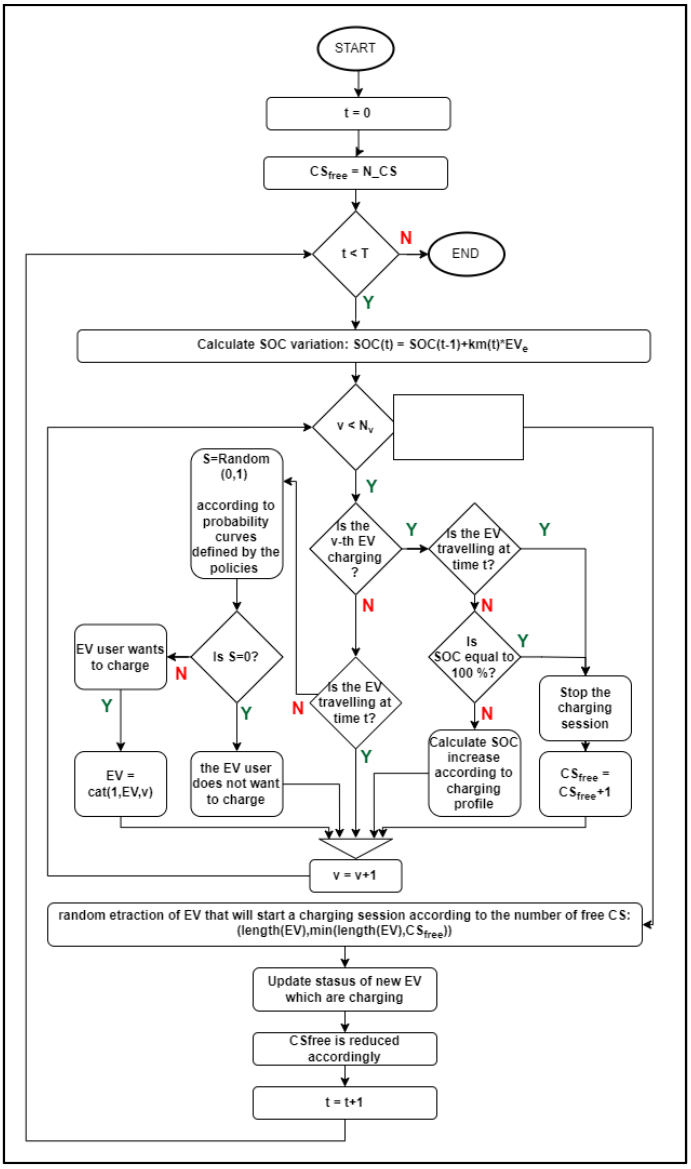


*Figure 114: Flowchart for assigning an EVCS to an EV for Design 1*

Policy 1 would require campaigns to increase users' awareness and enforce a charging session if it is lower than 40 %. Policy 2 is less strict and simulates more lascivious recharging management: it requires recharging only when SOC is less than 20%, whereas, for higher values, the probability is much lower. Nihil probability implies a company rule that forces users not to charge EVs for that specific SOC. Moreover, Design 1 is based on the following assumptions:

1. Charging sessions can start only during working hours from 7:30 to 13:00 and from 14:00 to 17:00.
2. Assigned EVCS is defined based on the flowchart shown in Figure 114,
3. When SOC is equal to 100 %, it is assumed that the EV can be disconnected to allow a new charging session.
4. The charging profile is defined based on the historical data collected for the EV already included in the company fleet; the related profile is shown in Figure 113.

All these inputs and assumptions are modelled in the simulations to evaluate the behaviour of the EV user and the corresponding SOC variation. The adequate number of

EVCS is verified a posteriori, namely, the number of EVCS would be inadequate if SOC were lower than 10 % in more than 500 timestamps for all EVs. Considering that the simulations involve 1000 days sampled every 15 min and 50 EVs, SOC can be lower than 10 % only in 0.1 ‰ of the timestamps. Only the simulation for which the minimum number of EVCS satisfies this tolerance have been reported.

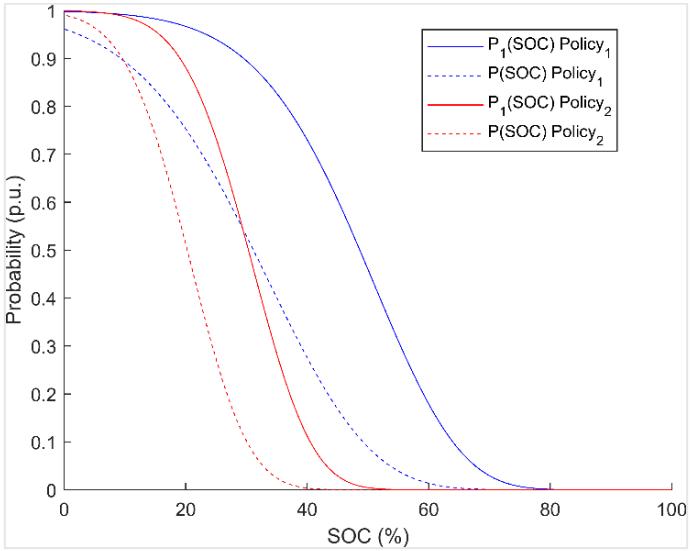


*Figure 115: Different probabilities of starting a charging session according to the actual SOC curves depend on the adopted policy*

#### 4.3.1.1.2 Design 2: 3 kW EV charging stations

Concerning Design 2, using a slow EVCS (3 kW) for each EV, two policies have been defined; both require that users connect the EV at the end of the trip. The activation of charging sessions is centrally managed; nevertheless, two different strategies have been evaluated:

- Policy 1: Recharging is carried out in parked EV when there is a surplus of energy produced by the PV compared to the district's demand, thus withdrawing self-produced energy, or when EVs fall below the safety threshold, set at 45% SOC, by drawing directly from the DN.
- Policy 2: Compared to Policy 1, night-time charging is favoured here because, in addition to RES self-consumption, daily recharge is applied when SOC<20%, while nightly recharge is applied when SOC<50%.

Design 2 is scheduled to maximise SCR; recharging with the DN only occurs when the SOC falls below a set threshold. For the management of the charging sessions in Design 2, a centralised control is applied which evaluates how many and which vehicles to charge based on which are available at the park station, how much surplus energy is produced by the PV compared to the needs of the district and the SOC of the vehicles. Figure 116 shows the algorithm for determining charging in Policy 1 and the additional conditions in Policy 2 (highlighted in blue).

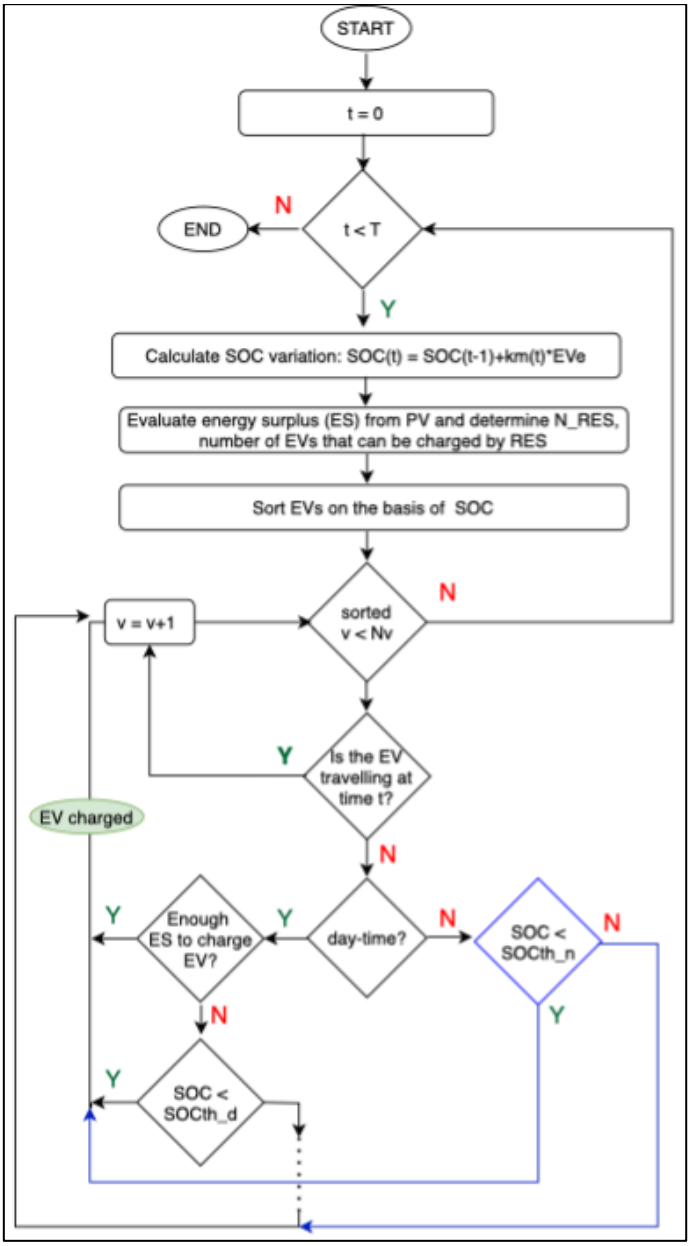


*Figure 116: Flowchart for determining charging sessions for Design 2*

#### 4.3.1.1.3 Electrical Fleet Modelling

Fleet modelling is strongly based on the measurement previously presented; other technical features of the fleet behaviour have been identified by interviewing the vehicles' users in order to understand the common practices about vehicle usage. Concerning the technical modelling of the EV fleet, the following aspects have been considered in the model:

- Daily mileage is assigned to each EV, it is based on probability distribution, as reported by Figure 112;
- Trips duration is defined as a random number based on the standard distribution (average value is 6 h, the standard deviation is 1.5 h);
- Every day, a certain number of trips is assigned to the EV, it ranges from 0 to 2;
- Trips can start in the morning as well as in the afternoon, trips duration and mileage are equally distributed. In all cases, working hours are from 7:30 to 13:00 and from 14:00 to 17:00.

Concerning the presented simulations, some reference EV and EVCS have been considered; in particular, in the simulations it has been considered a 52 kWh battery able to ensure an autonomous range of 265 km assuming an efficiency of 0.19 kWh/km. The EVCS model corresponds to that already installed in the ASM headquarters, therefore, its characterization follows the trends presented in Figure 113. The model has been implemented using MATLAB.

#### 4.3.1.2 Impact of company fleet management on the distribution grid

This section presents the results of the simulations that are carried out based on the model previously described. Therefore, input data are randomly generated based on the probability distribution presented previously; these are used to simulate SOC variation according to mileage and charging sessions. Strategies for charging sessions are defined according to policies previously described, notably, the following scenarios are presented:

- Two scenarios based on Design 1 (i.e., a limited number of 22 kW EVCS).
- Two scenarios based on Design 2 (i.e., all EVs have a low charger at their disposal).

The configurations have been tested by simulating 50 EVs that travel 1000 days. Concerning Design 1, Table 44 shows the minimum number of EVCS that is sufficient to supply 50 EVs. Regarding Policy 1, 8 EVCS would be sufficient to supply the fleet; Policy 2 requires at least 12 EVCS. The main results of the simulations are summarized in Table 45.

*Table 44: Model input*

| | **Policy 1** | **Policy 2** |
|---|---|---|
| Number of simulated days | 1000 | 1000 |
| Number of EV | 50 | 50 |
| Number of timestamp for every EV for which SOC is lower than 10 (‰) | 0.001 | 0.08 |
| Minimum number of EVCS for supplying the EVs | 8 | 12 |

*Table 45: Simulation results (design 1, policy 1)*

| | **Policy 1** | | **Policy 2** | |
|---|---|---|---|---|
| Model Output | Mean | SD | Mean | SD |
| Daily energy for charging session (kWh) | 286.3 | 46.13 | 286.8 | 88.9 |
| Mileage (km) | 30.5 | 16.1 | 30.5 | 16.1 |
| EV SOC (%) | 73.38 | 15.16 | 63.54 | 19.94 |
| Daily recharging sessions | 16.58 | 3.03 | 10.95 | 3.23 |
| Charging duration (h) | 2.13 | 0.89 | 2.86 | 1.16 |
| Days between two charging sessions for a EV | 2.5 | 0.08 | 3.90 | 0.14 |

Figure 116 - Figure 118 shows some comparisons between the two policies. Figure 116 reports the distribution of the average number (in p.u.) of the busy plugs of the EVCS and the average power profiles of the EVCS when a certain policy is applied; frequencies of daily energy are reported in Figure 117; finally, Figure 118 reports the SOC variation of two EVs as an example. Figure 117 shows that EVCS are often busy in the afternoon, this

is because users have ended their activities. From 10:00 to 11:00, the EVCS are frequently free because EVs are travelling, as well as from 14:00 to 15:00. Considering the corresponding average power profiles of EVCS, Policy 1 causes higher peak powers even if the installed capacity is lower than Policy 2. Moreover, according to Table 45, the daily energy has a greater standard deviation if Policy 2 is applied; indeed, this policy is less strict and does not encourage charging sessions for high SOC. Figure 117 is coherent with these results, showing that daily energy has greater variance when Policy 2 is applied.

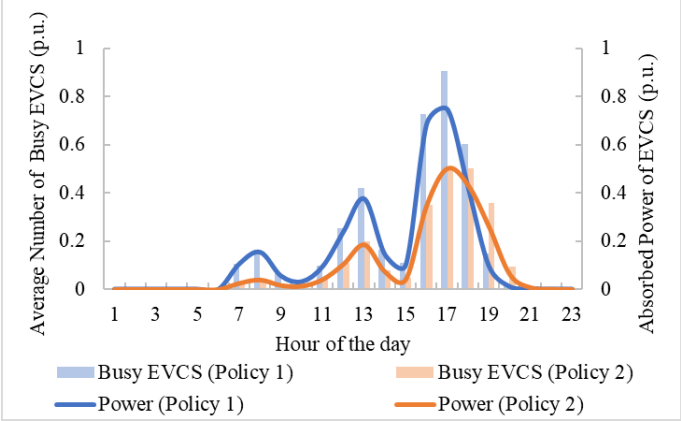


*Figure 117: Percentage of busy EVCS and average power profile when Policy 1 and Policy 2 are applied*

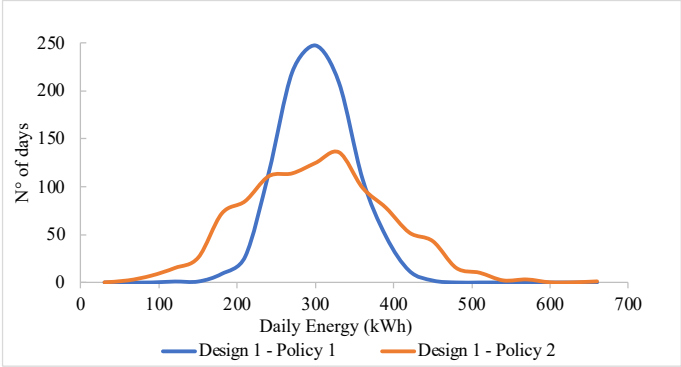


*Figure 118: Frequency of daily energy when Policy 1 and Policy 2 are applied (Design 1)*

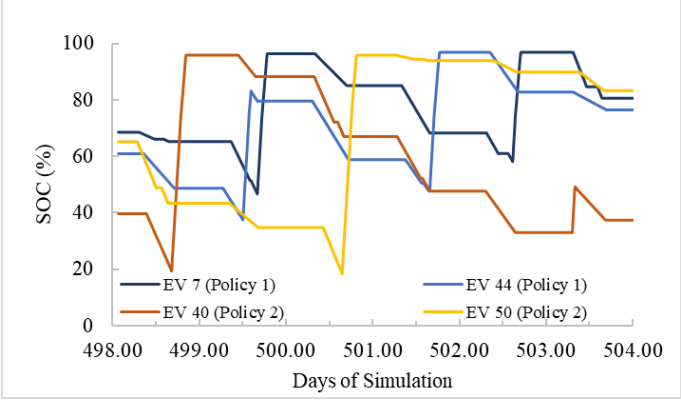


*Figure 119: SOC variation of 2 EVs during 5 days with Design 2 when Policy 1 and Policy 2 are applied*

Concerning SOC variation, Table 45 reports that Policy 1 keeps fleet SOC between 40 % and 100 % (i.e., according to standard deviation) whilst Policy 2 causes a significant variation of SOC from 20 % to 100 % (ref. Table 46). This difference is also shown in Figure

119. The two policies significantly change the fleet management; indeed, when Policy 1 is applied, EVs are frequently charged (i.e., every 2.5 days) in comparison with Policy 2 (i.e., every 3.9 days). Policy 2 is similar to the current management of the fleet, notably the user refuels the vehicle when its tank is almost empty as well as refuelling is done every 14 working days on average, nevertheless, SOC is often lower than 40 %, and the corresponding travel distance could be so much reduced that it could arise range anxiety issues and usage barriers. Even strict management of EVCS, as proposed by the first case, has some positive aspects; it increases the exploitation of the installed EVCS as well as reduces energy variance; in addition, range anxiety issues are avoided because of the high average SOC of EV. Nevertheless, this policy would require a campaign to increase users' awareness since it would significantly change their habits. Concerning Design 2, the charging infrastructure is located directly inside the parking area, with each parking space equipped with a simple 3 kW EVCS. The two policies differ because in the first one the aim is to maximise the SCR of local RES, while in the second one the aim is to reduce the cost of charging, exploiting both RES and absorbing energy at night, when the cost is generally lower as well as to reduce the overall peak of the district. Figure 120 shows the number of charging sessions over time and the recharging power within an average day. In Policy 1, the sessions are mainly distributed over the evening and night hours, with the average daily maximum number of vehicles recharged simultaneously being 13 (corresponding to 39 kW). In Policy 2, the majority of vehicles are recharged during the night, leaving the rest of the day only to recharge through surplus energy; the average daily maximum number of vehicles recharged simultaneously is 36 (corresponding to 108 kW). Energy from RES is concentrated in the central hours of the day, which are characterised by an excess of RES production. Figure 121 shows the trend of the SOC of 2 EVs in 4 days, for both Policy 1 and Policy 2. It can be seen that the handling is extremely different than for Design 1 and the charging is slower. The vehicles have on average SOC and standard deviation values respectively of 43.84 % and 7.56% (Policy 1) or 47.36 % and 8.64% (Policy 2).

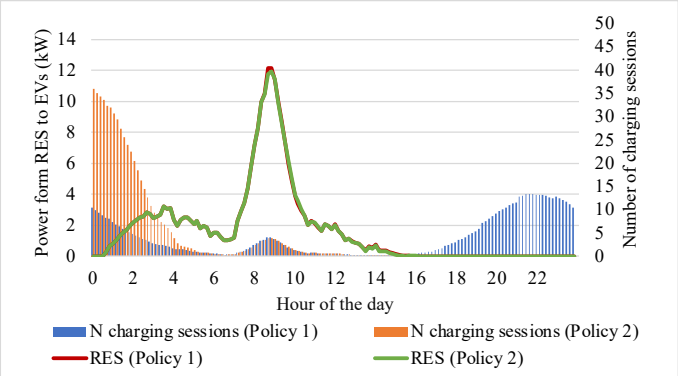


*Figure 120: The daily average number of charging sessions and power flows from RES to EVCS in Design 2: Policy 1 and Policy 2*

Figure 122 shows the district's electricity balance, which includes the office building and warehouse as well as a 185 kW PV and EV fleet. Charging management allows increasing the district SCR and SSR, with consequent economic benefits. As shown in Table 46, these values are respectively increased by 5.9 % and decreased by 2.4%, while RPF is reduced to 70.8 % in both policies.

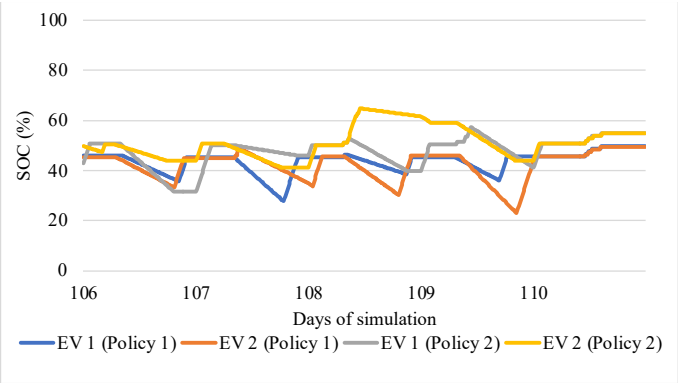


*Figure 121: SOC variation of 2 EVs during 5 days with Design 2 when Policy 1 and Policy 2 are applied*

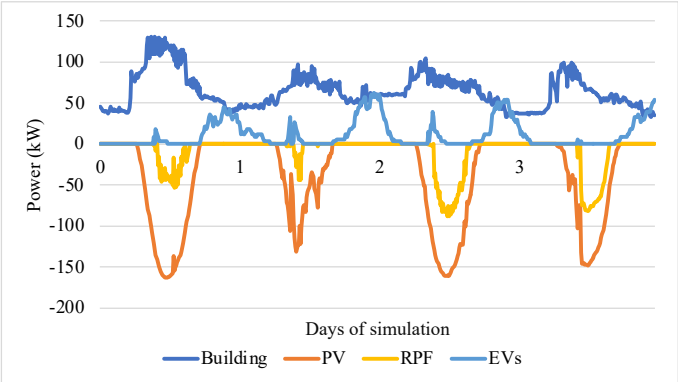


*Figure 122: Electrical balance of the energy district (Design 2, Policy 1) during four days*

*Table 46: Simulation results (design 2)*

| | **RPF (MWh/year)** | **SCR (%)** | **SSR (%)** |
|---|---|---|---|
| Without EVs | 51.5 | 79.7 | 31.2 |
| Design 2 | 36.5 | 85.6 | 28.8 |

### 4.3.2 Optimizing electric vehicle company fleet management in an energy district

Paper in reference [XV] introduces a novel model designed to optimize EV fleet charging schedules within the context of an energy district. Specifically, the aim is to minimize unmet demand, ultimately increasing the profit of the system operator while upholding a predefined service level. The developed model is further validated using real-world data obtained from a multi-utility company that operates within an energy district and deploys fleets for various services. This study assesses the optimal scheduling of an EV fleet, with the objectives of cost reduction, emissions reduction, and maximizing the energy district's SCR.

#### *4.3.2.1 EV Fleet Management Model in An Energy District*

##### 4.3.2.1.1 Optimized EV management

A simplified representation of the model used to represent the EV fleet is illustrated in Figure 123. This optimization approach is applicable to energy districts that encompass RES generation, passive loads, and a substantial fleet of vehicles frequently in use throughout the day. The primary objective of the optimization model is to minimize costs, taking into account the variability in energy prices for consumption and revenues from energy injection, which can fluctuate on an hourly basis. Ultimately, the optimizer aims to determine the most cost-effective sequence of charging sessions by deciding the optimal moment to connect each vehicle to a EVCS, adhering to predefined constraints.

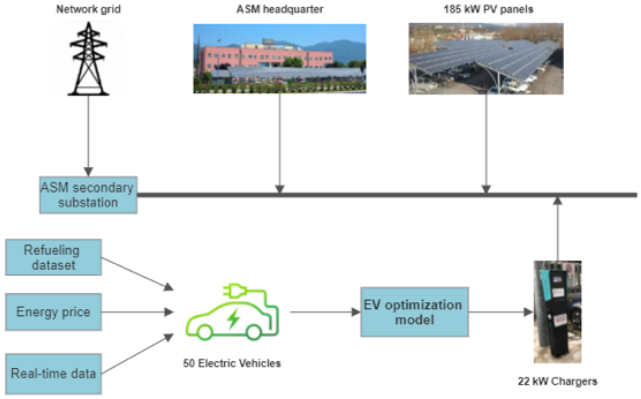


*Figure 123: Optimization model for EV scheduling in an energy district*

The technical analysis is formulated as a mixed integrer linear programming optimization problem and implemented on Matlab environment, exploiting the free open-source Yalmip package [356]. The Gurobi optimization solver [124] is integrated with Yalmip to solve the optimization problem. The optimization minimizes the overall cost over the year, as expressed in the objective function. The objective function of the problem is the following:

*Equation 39:*

$$obj = \sum_{t=1}^{T} (r_t \cdot ESC_t + c_t * (\sum_{v=1}^{N^{EV}} ECV_{t,v} - ESC_t))$$

Where $r_t$ is the revenue for injected electrical energy during a certain timestamp t (€/kWh), T is the number of timestamps, $ESC_t$ is the electrical energy self-consumed by the district (kWh), $c_t$ is the cost for consumed electrical energy during timestamp $t$ (€/kWh), $N^{EV}$ is the number of EVs in the fleet, $ECV_{t,v}$ is the energy consumed by one vehicle during one

timestamp (kWh), and $EEV_{t,v}$ is the energy available in one vehicle during one timestamp (kWh).
Since the available energy is firstly tried to be used for self-consumption in the building before being used to charge EVs, the amount of SCR by the district is calculated from the total amount of energy consumed by EVs as in Equation 39. The optimization problem is solved considering a constraint about the variation of the available energy in the battery of the EV (i.e., the residual capacity of the battery):
*Equation 40:*

$$EEV_{t,v} = EEV_{t-1,v} - EV^{eff} \cdot KM_{t,v} + ECV_{t,v} \cdot A_{t,v} \qquad \forall t > 1, v$$

Where $EV^{eff}$ is the rated efficiency of the EV (kWh/km), $KM_{t,v}$ is the distance travelled by an EV during timestamp $t$ (km), and $A_{t,v}$ is the availability of EV to be charged during timestamp t (can be 0 or 1).
The following constraint limits the SCR of the district so that $ESC_t$ cannot be higher than the minimum between produced ($EP_t$) and consumed energy ($EC_t$); moreover, the self-consumed energy cannot be negative:
*Equation 41:*

$$0 \leq ESC_t \leq \min\left(EP_t,\ EC_t + \sum_{v=1}^{N^{EV}} ECV_{t,v}\right), \forall t$$

Another constraint defines the maximum amount of energy that can be drawn by an EV during a charging session, with $P^{CS}$ the nominal power of the EVCS (kW) and $N^{ts}$ the number of analysed timestamps in one hour.
*Equation 42:*

$$0 \leq ECV_{t,v} \leq P^{CS}/N^{ts}, \qquad \forall t, v$$

Similarly, the residual capacity of the battery EEV cannot overcome the rated capacity of the vehicle ($EB_v^{MAX}$), as it is defined by the following constraint:
*Equation 43:*

$$0 \leq EEV_{t,v} \leq EB_v^{MAX}, \qquad \forall t, v$$

The last constraint ensures that the number of charging session during one timestamp t cannot overcome the number of EVCS ($N^{CS}$) installed in the district:
*Equation 44:*

$$\left|\cup_{v=1}^{N^{EV}} ECV_{t,v} \neq 0\right| \leq N^{CS} \quad \forall t$$

Considering constraint in Equation 40, the optimization problem requires the initialization of the EEV for the initial timestamp for all the EVs. Therefore, the initial residual capacities of the batteries of the fleet are defined according to the equation:
*Equation 45:*

$$0.22 \cdot EB_v^{MAX} \leq EEV_{1,v} \leq 0.75 \cdot EB_v^{MAX},$$

According to the objective function in Equation 39 and the related constraints in Equation 40 – Equation 45, the optimization problem provides as output the following variables:

- Self-consumed energy of the district during the analysed timestamps and charging.
- Electrical energy consumed by the EVs during the analysed timestamps.

- Variation of the energy available in the batteries of the EVs during the analysed timestamps.

#### 4.3.2.1.2 Not Opimezd EV management

In order to assess if the optimized strategy could significantly improve the energy district efficiency, a not optimized strategy has been defined. The vehicle management strategy used in the non-optimized scenarios follows simplified criteria, namely, if the SOC is less than 20 % there is always charging, if the EV has a SOC of less than 30 % there is 80 % chance of charging, if the EV has a SOC of less than 50 % there is 60 % chance of charging, and if the EV has a SOC of more than 50 % the probability of recharging drops to 20 %. This simulated the ability of the responsible operator to choose whether to do recharging depending on the circumstances. In the recharge management algorithm, it was arranged that in each timestamp the EVs with a lower SOC would have priority in choosing whether or not to recharge, according to the previously stated probability, in order to simulate in this way, the urgencies encountered by the different operators.

### *4.3.2.2 Optimised fleet management results*

#### 4.3.2.2.1 Energy district and EV modeling

The company's headquarters can be regarded as a compact energy district, comprising two PV arrays of 185 kWp and 60 kWp, an EESS featuring a 72 kWh, two buildings spanning 6,800 square meters each, and a warehouse spanning 1,300 square meters. The baseline electricity demand within this setup fluctuates between 50 kW and 90 kW, while peak demand ranges from 120 kW to 170 kW. The building's HVAC system is equipped with a building energy management system, and there are two private EVCSs alongside one public EVCS on-site. ASM operates a 86 conventional vehicles fleet for several activities of the multi-utility. A comprehensive dataset encompassing 1,760 days, starting from January 1, 2015, to October 26, 2019, has been compiled, consisting of a total of 16,414 refueling operations. These dataset outcomes are also utilized in this research. It is noteworthy that, on average, a vehicle covers a daily distance of approximately 33 km, while the standard deviation for daily mileage is 23 km.
In addition the PV profile and load building demand of ASM is provided based on the first week of 2022 in Figure 124.

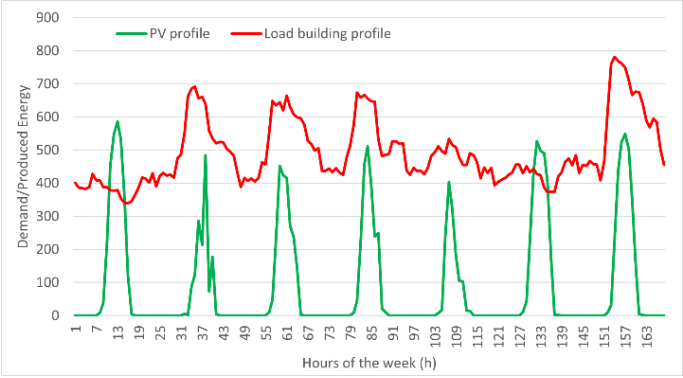


*Figure 124: Hourly variation of the costs and revenue of the energy price*

#### 4.3.2.2.2 Cost and revenues modelization

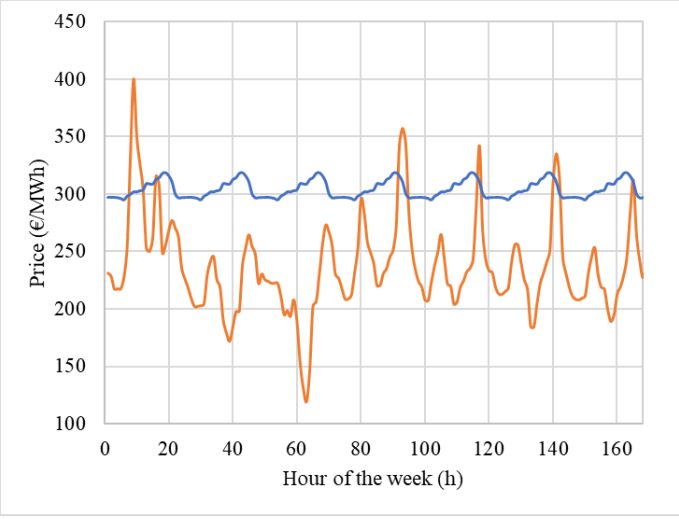


*Figure 125: Hourly variation of the costs and revenue of the energy price*

It has been considered that revenues and costs of exchanged energies are variable during the day; notably, it has been assumed that these parameters change every hour. An example of the hourly variation is shown in Figure 125, which represents one week of hourly variation of cost for withdrawn energy and revenue for injected energy. Energy cost is based on the tariffs provided by the Italian Authority [37] whilst its hourly variation is based on the open dataset [306]; the second is based on the public variation in 2022 of the unified Italian price available in [152].

In the following, the results collected by applying the optimization model on the energy district considering one year of operation assuming different amounts of $N_{EVCS}$ are reported. Moreover, it has been simulated the current size of the PV in the district (i.e., 185 kW) and an increased size (i.e., 370 kW) assuming that the current plant can be increased by installing additional or more efficient panels. Table 47 reports the 6 scenarios evaluated applying the optimizer (Scenario 1 – 6); moreover, it includes 6 additional scenarios that assess the not optimized behaviour of the fleet (i.e., Scenario 7 – 12). Each scenario assesses the same input data, namely, mileage variation of 50 EVs, produced power for 1 kW of PV size, and consumed energy by the passive loads. Moreover, PCS is equal to 22 kW and assumed constant in this paper. Other relevant parameters were considered in the simulations; notably, $EV^{eff}$ and $EB_v^{MAX}$ are equal to 0.13 kWh/km and 44 kWh, respectively.

*Table 47: Analysed scenarios*

| Scenario ID | $N_{EVCS}$ | Size of the PV | Optimization algorithm |
|---|---|---|---|
| 1 | 3 | 185 | Yes |
| 2 | 4 | 185 | Yes |
| 3 | 5 | 185 | Yes |
| 4 | 3 | 370 | Yes |
| 5 | 4 | 370 | Yes |
| 6 | 5 | 370 | Yes |
| 7 | 3 | 185 | No |
| 8 | 4 | 185 | No |
| 9 | 5 | 185 | No |
| 10 | 3 | 370 | No |
| 11 | 4 | 370 | No |
| 12 | 5 | 370 | No |

Given that the optimization problem primarily revolves around cost reduction, it's valuable to present an overview of the total annual expenditures as assessed across various scenarios. These findings are summarized in Table 48, encompassing all the scenarios considered in the study. The costs remain unaffected by the number of EVCS, which ranges from 3 to 5. However, the optimization of charging sessions demonstrates the potential for substantial cost reductions. Specifically, when considering the current PV array size (Scenarios 1 - 3 and 7 - 9), the optimized procedure results in a 10% reduction in costs. In contrast, when an expanded PV array size is taken into account (Scenarios 4 - 6 and 10 - 12), the impact on cost reduction is even more pronounced, with a reduction of approximately 25%.

*Table 48: Total costs assessed by the scenarios*

| Scenario ID | Total cost (€) |
|---|---|
| 1 | 41,072 |
| 2 | 41,082 |
| 3 | 41,068 |
| 4 | 19,658 |
| 5 | 19,582 |
| 6 | 19,533 |
| 7 | 45,684 |
| 8 | 45,649 |
| 9 | 45,668 |
| 10 | 26,010 |
| 11 | 26,046 |
| 12 | 25,979 |

The cost reduction can be also seen in the energy balance of the energy district. Table 49 reports the SCR of the district, the percentage of produced energy that is injected into the grid, and the average energy consumed during a charging session.

*Table 49: Energy district balance*

| Scenario ID | SCR (%) | Injected energy into the grid (%) | Average energy per charging session (kWh) |
|---|---|---|---|
| 1 | 92.15 | 7.85 | 7.44 |
| 2 | 92.13 | 7.87 | 5.91 |
| 3 | 92.13 | 7.87 | 6.95 |
| 4 | 61.77 | 38.23 | 10.96 |
| 5 | 61.90 | 38.10 | 9.94 |
| 6 | 62.34 | 37.66 | 8.60 |
| 7 | 81.37 | 18.37 | 22 |
| 8 | 81.72 | 18.27 | 22 |
| 9 | 81.93 | 18.06 | 22 |
| 10 | 53.86 | 46.14 | 22 |
| 11 | 54.00 | 46.00 | 22 |
| 12 | 53.92 | 46.07 | 22 |

Some details about Scenarios 3 and 6 are shown in Figure 126 and Figure 127 which report the trend of the energy self-consumed for the entire year.

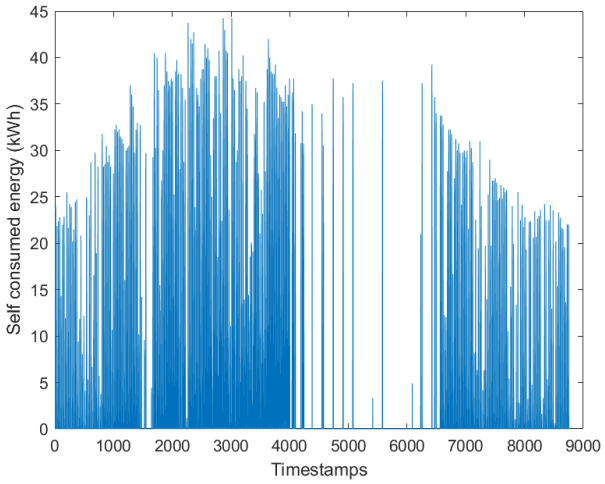


*Figure 126: Self-consumed energy during one year (Scenario 3)*

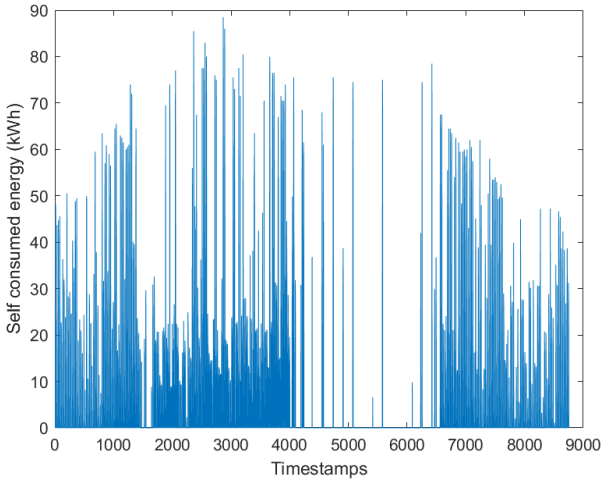


*Figure 127: Self-consumed energy during one year (Scenario 6).*

Further findings are detailed in Table 50, which provides information on the average duration between two consecutive charging sessions, the mean SOC of the vehicles, and its standard deviation. Additionally, in Figure 128, the variation in the available battery energy is depicted for the same EVs under Scenario 1 and Scenario 4. Based on the results presented, it can be inferred that an optimized scenario would lead to a reduction in the average SOC, decreasing from 75% to 48%. However, it's important to note that optimized charging sessions, while more frequent, are of shorter duration compared to the non-optimized scenario, as indicated in Table 50.

*Table 50: EV status during the simulated scenarios*

| Scenario ID | Average time interval between recharges (h) | Average SOC (%) | SOC standard deviation (%) |
|---|---|---|---|
| 1 | 210.79 | 48.97727 | 18.36364 |
| 2 | 167.51 | 54.02273 | 22.02273 |
| 3 | 186.57 | 51.52273 | 19.54545 |
| 4 | 311.17 | 44.84091 | 17.22727 |

| | | | |
|---|---|---|---|
| 5 | 282.12 | 43.88636 | 15.45455 |
| 6 | 232.96 | 41.59091 | 11.56818 |
| 7 | 539.07 | 75.27273 | 14.52273 |
| 8 | 541.07 | 75.20455 | 14.54545 |
| 9 | 540.41 | 75.25 | 14.63636 |
| 10 | 543.10 | 74.93182 | 14.59091 |
| 11 | 539.74 | 75.29545 | 14.54545 |
| 12 | 540.41 | 75.09091 | 14.56818 |

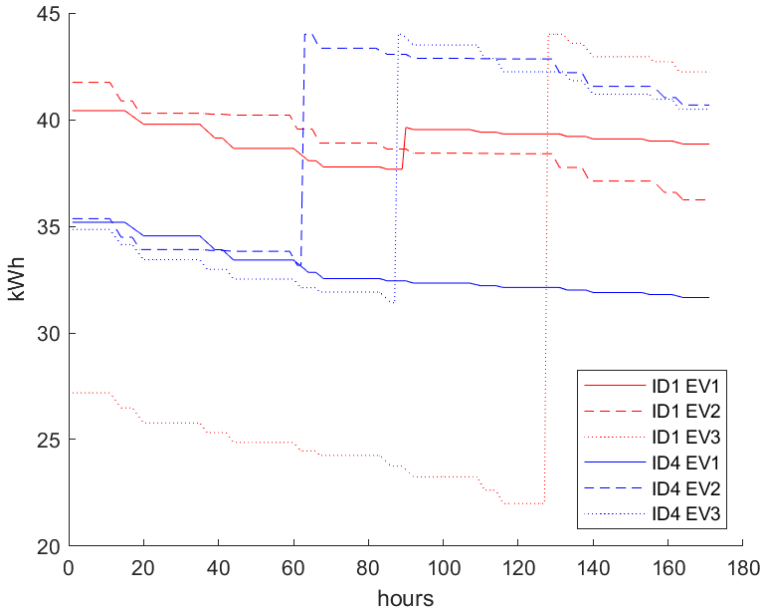


*Figure 128: Variation of the Energy available in the battery of the same EV in case of different scenarios*

# 5 Integration of the hydrogen carrier with the electricity sector

## 5.1 Perspectives of hydrogen in the European panorama

Hydrogen is worldwide seen as the fuel of the future, capable of increasing the process of replacing fossil fuels, enabling the integration and development of RES, reducing pollutant emissions and facilitating energy independence. Hydrogen can be used in a large number of different fields of application, including industrial and transport area, storage for the energy system and as an energy carrier, and has received a lot of interest in recent years, in addition to sustainability reasons, for its high calorific value (120 MJ/kg).
Hydrogen is a key energy vector for the European and international perspective in decarbonisation processes, as it is estimated [142] that to reach a zero-emission scenario in 2050, hydrogen will have to account for up to 20 % of final consumption and will be produced either through electrolysers, using RES, or from fossil sources combined with carbon capture and storage mechanisms.
Hydrogen has applications in various consumer sectors: energy production, energy storage, mobility, chemical production, and other industrial uses.
Several countries are competing for technological dominance and the development of a hydrogen chain. Japan is currently the leader in the hydrogen economy and in 2019 presented the "Strategic Road Map for Hydrogen and Fuel Cell" [62]. China has developed a policy of incentives for the development of hydrogen mobility and the construction of electrolysers to achieve climate neutrality in 2060 [221]. South Korea intends to achieve leadership in the production of fuel cells for vehicles and stationary applications, aiming to produce 6.2 million fuel cell EV and 15 GW of fuel cells in 2040 [316], [176]. The European Union published its hydrogen strategy in 2020 [86], with a target of 40 GW of electrolysers in 2030. The creation of a hydrogen supply chain would allow countries to reduce fossil dependency on oil and other limited resources (such as uranium or lithium) and to set up a new supply chain, suitable to create jobs and wealth.
At the Italian level, guidelines for the national hydrogen strategy have been published [222], which include for 2030 real targets for use in heavy mobility and for use in maritime and rail transport, for 2050, there are plans to extend applications to hard-to-abate industrial sectors and light mobility.
One of the main interests for hydrogen is its ability to integrate with RES, i.e. it is possible to store energy in the form of hydrogen (power to gas) and then use it, staggered in time, for the aforementioned applications. In this way, it inserts a chemical storage system into the grid that can guarantee high volumes, with efficient conversions; in this way, it is possible to realise both storage with a daily time horizon and seasonal storage.
One of the factors currently limiting the spread of hydrogen is the high cost of electrolysers.

## 5.2 Impact of hydrogen mobility on the electricity grid

The mobility sector is responsible for 27% of $CO_2$ emissions worldwide with 8.2 Gt of $CO_2$ every year; also, local pollutants and their health impacts cannot be neglected [178], [89]. Based on 2013 European data, the transport sector contributed 13% of primary PM10 emissions and 15% of PM2.5 emissions; it is also the largest source of $NO_x$ emissions, with 46%. In addition, noise and other emissions types must be considered in the impact of traditional vehicles on the quality of life. All these pollutants would be dramatically reduced by adopting alternative mobility technologies. In the EU Green Deal, the Commission decided to phase out petrol and diesel cars from 2035 [87], so that vehicle conversion will become a regulatory requirement. The sustainable mobility of the future will be realised mainly through EVs and fuel cell EVs. Despite a much more limited current development, higher prices and much lower conversion efficiency, fuel cell EVs present specific advantages over EVs, notably a longer range and a shorter recharging time, similar to the performances of conventional vehicles. Fuel cell EVs have an overall conversion efficiency of about 50%, as compared with 90% for EVs. Concerning the safety issues of these vehicles, the US National Fire Protection Agency has declared that alternative fuel vehicles, such as fuel cell EVs and EVs, are no more dangerous than heat engine vehicles [73]. In scientific and grey literature, sustainable energy system scenarios forecast that in 2050 hydrogen and its derivates (ammonia, methanol, synthetic fuels) will cover 21% of transport demand, contributing to a 26 % reduction in $CO_2$ emissions to achieve carbon neutrality [149].

In literature, many papers propose an optimization of the microgrid energy management including the hydrogen vector, as in [343] where the dual optimisation of energy management and component size of a port in France is investigated, which also includes an electrolyser and hydrogen storage. In [243], the authors show a mixed integer linear programming optimisation of the operating costs of a microgrid located on Stromboli (Italy), which integrates RES, an electrolyser, stationary fuel cells and an EESS. Other papers report an optimization study of an fuel cell EV fleet. In [192], the authors elaborate on a mixed integer linear programming to optimise the installation and the operation cost of hydrogen-powered trucks, used for road transport between France and Germany; hydrogen production is ensured by the nuclear power plant and wind energy. In [219], several MW electrolysers are compared to see how an optimized production chain can be set up to supply fuel cell EVs. Few papers perform an optimization model for a microgrid including an fuel cell EV fleet, like [33] that investigates the techno-economic analysis of a microgrid equipped with heat, power and hydrogen; the electrolysers and fuel cell EVs are considered to provide a flexibility lever. A similar case study is presented in [108], in which the implementation of hydrogen systems is studied considering the hydrogen blending into the methane network. The hydrogen fleet as a flexibility source is analysed also in other studies, like [31], [103]. Few papers consider large fleet case studies; in [339] a Canadian microgrid a design study is carried out for the islanded operation of 2 days duration, equipped with electrolyser, wind and solar sources and 38 fuel cell EVs. Details of all costs are given and the sizes have been designed through mixed integer linear programming optimisation. In addition, a detailed failure mode and effect analysis is carried out. The authors of [225] provide a detailed dataset of vehicles, evaluating a technical-economic comparison with the endothermic fleet. Many contributions are supported by long terms scenarios where different cost trends and parameter variations

are considered; in this respect, reference [304] reviews the feasibility of current hydrogen technologies for mobility; reference [106] quantifies the impact of uncertainty on the transition to green hydrogen identifying cost of electrolysers, capacity factor and gas price as critical factors. Reference [164] assesses the energy and environmental effects of the hydrogen energy supply chain on the Korean energy system considering scenarios influenced by the development level of key technologies, the contribution of RES to the power generation sector, and the importance of each hydrogen production method. Reference [336] considers the widespread of hydrogen buses in combination with an increasing share of production from wind and solar farms. Reference [6] identifies the decarbonizing benefits of hydrogen in transport using hydrogen whilst reference [310] points out that hydrogen could be important to decarbonise industry and transport considering several scenarios. Finally, the review [104] identifies several key challenges to achieving a net-zero economy by 2050.

Based on literature reviews, an original paper has been presented [XIV], that shows a model to forecast the total cost of microgrid management, related to a company equipped with a hydrogen fleet. A multiparametric analysis is carried out considering the economic trends related to investment and operational costs. The microgrid management is optimized through a mixed integer linear programming. The study is carried out over a time frame of 21 years, considering economic parameters variation over time, as the hydrogen price and energy sale benefits, based on literature trends. The microgrid management evaluation is investigated through an extended multiparametric analysis (91,125 scenarios are overall reported in the paper). The case study is represented by the real microgrid of ASM.

### 5.2.1 Energy district equipped with a hydrogen fleet model

The model presented in this paper delineates the energy equilibrium within a locality encompassing an operational microgrid, hydrogen electrolyser, and a fleet powered by hydrogen. Furthermore, this model facilitates the establishment of optimal energy management plans for each scenario, conducts a technical-economic appraisal of the energy district, and assesses energy expenses between 2030 and 2050. Figure 129 illustrates the principal components of the energy district, with particular emphasis on energy and hydrogen flow dynamics.

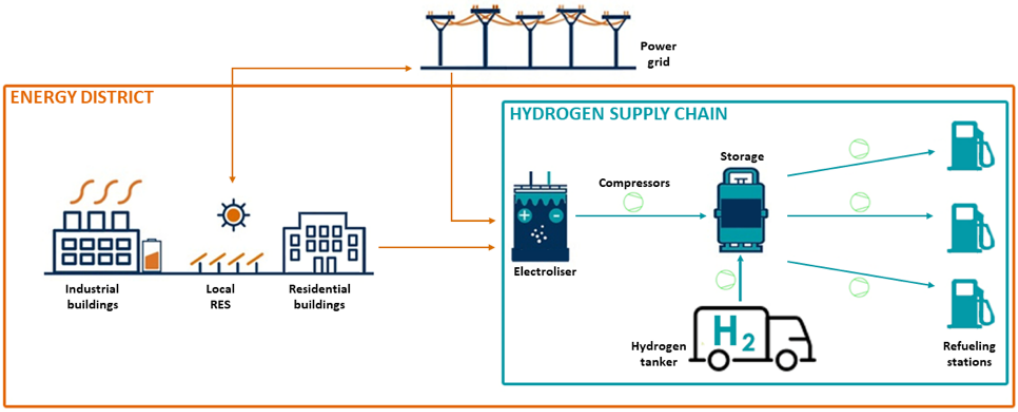


*Figure 129: District model: electrical energy (orange lines) and hydrogen flows (blue lines)*

On one aspect, the energy flows within the system encompass the building's consumption and the local energy production from RES (such as a PV plant). Additionally, it involves the utilisation of the electrolyser and interaction with the DN. As depicted in Figure 129, the hydrogen system encompasses an electrolyser and a hydrogen storage system within the district to provide fuel for fuel cell EVs through a refuelling station and an external refuelling service. It's important to emphasise that various auxiliary components play a critical role in deploying the hydrogen system, including compressors necessary to achieve the required pressure levels. Based on literature findings, a predefined set of pressure levels (as shown in Table 51) was considered for all simulation scenarios, which assumed that the system would adhere to the highest efficiency standards and the latest technical norms. The electrolyser's conversion efficiency was set at 0.2 $Nm^3/kWh$ by product catalogue available on the market.

*Table 51: Pressure levels of district components*

| Component | Electrolyser | Refuelling system | hydrogen storage system | Vehicle tank |
|---|---|---|---|---|
| Pressure (bar) | 30 | 200 | 500 | 700 |

To date, hydrogen production is mainly carried out by steam reforming methane, but to make the proposed model more sustainable, it integrates electricity from RES and the power grid to produce hydrogen using electrolysers. The electrolyser was modelled as a simple hydrogen source, considering a conversion coefficient $\eta_e$ from energy (kWh) to hydrogen volume ($m^3$). The electrolyser can operate in different operation modes. It can be powered by self-generated RES, with RPF energy to maximise SCR of the district or absorb energy from the grid. Different solutions can be applied to the storage system. As reported in [149], hydrogen can be stored in four different ways: i) in gaseous form in high-pressure cylinders, ii) in liquid, iii) chemical absorption within solids, and iv) physical absorption within solids. Concerning this work, special cylindrical containers in which compressed gas is inserted have been considered; pressure ranges from 350 to 700 bars whilst the lower heating value reaches up to 5.6 MJ/l.
First of all, in order to size the storage vessel, the hydrogen consumption during the day was linearized and the total annual mileage for each vehicle were considered also a constrain of the model. In order to trigger fuel cell EV refueling, a simple probabilistic evaluation was implemented in order to sort by priority order the vehicles that could require the refueling. Four levels of priority were identified, assigning the highest probabilities to refuel fuel cell EV with the emptiest tanks. The vehicle order was needed due to the limited refueling points of the infrastructure. The initial tank hydrogen level was randomised to represent a reasonable vehicles condition. Therefore, the model is able to study the framework operation during a defined discretized time period, evaluating the hydrogen consumption, production and exchange. The illustrated model was implemented in the GNU Octave environment. The characteristics of the different components and the frequency of refueling with the tanker truck were set, but the initial tank hydrogen level and the vehicle refueling time were not fixed. Therefore, the simulation was repeated several times to take into account the variability of these parameters. The hydrogen storage system capacity was calculated considering the

maximum variation of the hydrogen level in the simulations. In fact, the initial hydrogen storage system size was set as a great value.
The model presented in [XIV] assesses the electrical energy and hydrogen balances considering the components described above (e.g., fuel cell EV demand, Tank level, production from RES) and their technical constraints; moreover, it calculates the cash flow of the district as to the hydrogen system; finally, the model identifies the optimal energy management plan of the district every day. The technical and economic constraints taken into account by the model are the following:

- Purchased hydrogen price (€/l)
- Revenue from electrical energy injection in the DN (€/kWh)
- Price of electrical energy absorption from the DN (€/kWh)
- Cost of the electrolyser installation (€/kW)
- Cost of the PV installation (€/$kW_P$)
- Cost of the hydrogen storage installation (€/l)
- Cost of the fuel cell EVs fleet purchase (€)
- Nominal power of the electrolyser (kW)
- Nominal power of the PV ($kW_P$)
- Electrical energy associated to energy surplus each timestamp
- Electrical energy consumed by the electrolyser each timestamp

As output, the optimal energy management plan reports a set of six variables, which correspond to the optimized management of each component of the district: i) the energy injected in the DN in year $y$ in day $t$ (kWh), $EI_{y,t}$, ii) the energy consumed by the electrolyser in year $y$ in day $t$ (kWh) $EC_{y,t}$, iii) the energy supplied by the DN for $H_2$ production in year $y$ in day $t$ (kWh), $EP_{y,t}$; iv) The hydrogen volume supplied by the tank in year $y$ in day $t$ (l), $H_{y,t}$; v) a binary variable for tanker operation in year $y$ in day $t$, $B_{y,t}$; vi) the level of hydrogen storage system in year $y$ in day $t$ (l) $L_{y,t}$.
The technical analysis is formulated as a mixed integer linear programming optimization problem and implemented on Matlab environment [218], exploiting the Yalmip package [356]. The Cplex10 [139] solver is integrated with Yalmip to solve the optimization problem. The optimization minimizes the overall cost among the year, as expressed in the objective function. The objective function ($obj_y$) of the mixed integer linear programming problem is the following:
*Equation 46: Objective function of the mixed integer linear programming problem in hydrogen mobility fleet*

$$obj_y = \sum_{t=1}^{T} (-g_y^{DN} \cdot EI_{y,t} + c_y^{H_2} \cdot B_{y,t} \cdot L_n \cdot 0.9 + c_y^P \cdot EP_{y,t})$$

Where T is the total number of days in one year, $g_y^{DN}$ is the revenue from energy injection in the DN (€/kWh), $c_y^{H_2}$ is the purchased hydrogen price (€/l), $L_n$ is the nominal level of the hydrogen storage system and $c_y^P$ is the electricity price in year y (€/kWh). The constraints of the mixed integer linear programming problem are reported below:
*Equation 47:*

$$0 \leq EP_{y,t} \leq Max\_EP_{y,t}, \ \forall y, t$$

Where $Max\_EP_{y,t}$ is the maximum of energy supplied by the DN for $H_2$ production (kWh).
*Equation 48:*

$$0 \leq L_{y,t} \leq Max\_EC_{y,t},\ \forall y, t$$

Where $Max\_EC_{y,t}$ is the maximum of energy consumed by the electrolyser in year $y$ in day $t$ (kWh).

*Equation 49:*

$$EI_{y,t} \geq 0,\ \forall y, t$$

*Equation 50:*

$$REV_{y,t} = EC_{y,t} + EI_{y,t},\ \forall y, t$$

Where $REV_{y,t}$ is total energy surplus at timestamp t in the district.

*Equation 51:*

$$L_{y,t} = L_0 - HV_{y,t} + \varepsilon \cdot EC_{y,t} + B_{y,t} \cdot L_n \cdot 0.9, \quad \forall y, t$$

Where $L_0$ is the initial level of the hydrogen storage system, $HV_{y,t}$ is the total hydrogen demand by fuel cell EVs at timestamp t, $\varepsilon$ is the conversion coefficient of the electrolyser.

*Equation 52:*

$$0 \leq L_{y,t} \leq L_n, \forall y, t$$

The tanker operation is managed considering a refuelling of 90% of the nominal hydrogen storage capacity, as in Equation 51. The binary variable is defined in this way:

- $B_{y,t} = 1\ ,\ \forall y, t$ when the tanker is in operation.
- $B_{y,t} = 0,\ \forall y, t$ when the tanker is not in operation.

Electrolyser behaviour is determined based on its size. Indeed, for each step of the optimization (i.e., one day) the following equation is applied to calculate $Max\_EP_{y,t}$ and $Max\_EC_{y,t}$, based on the nominal power of the electrolyser ($P_n^{EL}$).

*Equation 53:*

$$P_n^{EL} \cdot 24 = Max\_EP_{y,t} + Max\_EC_{y,t}\ , \forall y, t$$

It is worth mentioning that these constraints are evaluated taking into account the 10-minutes production and consumption profiles of the energy district. For each timestamp, the electrolyser available power, corresponding to its rated power, can be derived by the local energy surplus or by the DN. In this way, the total available electrolyser energy consumption can be distinguished into two parts, expressed in kWh, as in Equation 53. Equation 50 fixes the amount of electrical energy sold and the electrolyser absorption to the local RES in the energy district for each timestamp. Equation 52 limits the variation of hydrogen storage level from 0 to the nominal value $L_n$.

The main outputs of the mixed integer linear programming problem are:

- Daily DN energy profile among the year;
- Daily electrolyser electrical energy and hydrogen production profile among the year;
- Number of tanker operations and total hydrogen volume supplied by the tanker;
- Daily hydrogen storage level among the year.

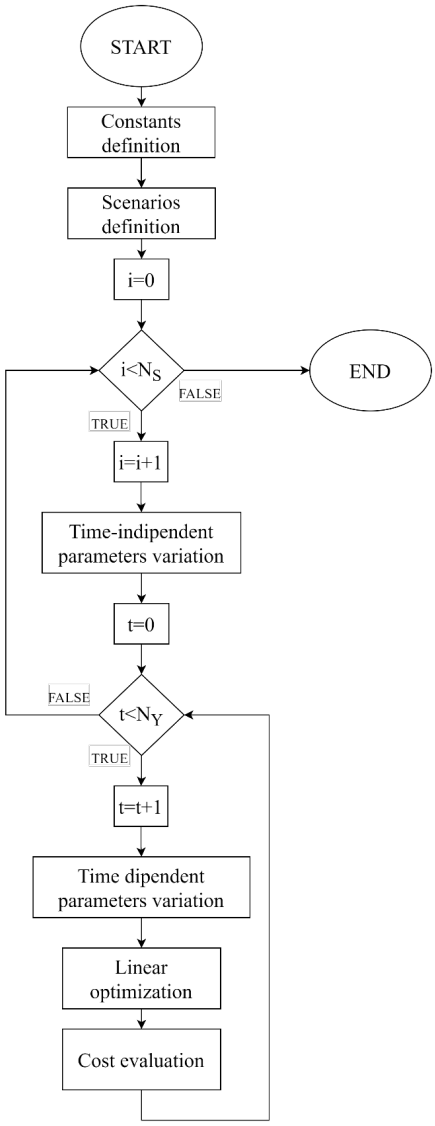


*Figure 130: Flowchart of the overall algorithm*

The presented model has been exploited in an algorithm (Figure 130) to carry out multi-parametric analysis and evaluate long-term scenarios. At the beginning of the algorithm, the constants of the model are defined. Among them, the daily energy surplus in the district and the fuel cell EVs requests profiles are loaded, considering the available dataset. After the constants' definition, all the combinations of the parameters are built to start a loop related to the parameters' variation. In this way, all the scenarios are initialised, corresponding to a total number of scenarios, $N_S$. When all scenarios are analysed, the algorithm ends. A second loop is placed in a cascade to apply the technical and economic analysis for each of the 2030-2050 time frame. Every scenario presents a number of itarations equal to the number of years, $N_Y$ (e.g., 21), in which some time-dependent parameters are varied. The technical analysis is made as a mixed integer linear programming optimization problem, in which the operating management of the energy district is optimised among the specific year. The electrical energy flow is distributed between the DN and electrolyser; the hydrogen flow is managed considering the tank

operations. The economic evaluation is carried out through the electrical energy/hydrogen profiles over all the years.

#### 5.2.1.1 Economic scenarios and evaluation methods

To carry out a comprehensive economic analysis, the price of hydrogen and the other components involved in the system were researched in the scientific literature [64], [49], [314] and [280]. Considering the large investments that are being made globally in this sector, as well as the great challenge of the energy transition, the prices of electrolysers, as well as the prices of hydrogen and PV plants, are expected to decrease quickly [138]. Therefore, given the uncertainty of this transition period, several various scenarios are necessary to simulate district operation when the hydrogen fleet will be applied. Evaluating economic variables, all OPEX and CAPEX have been identified and considering that technologies are not yet fully mature for the inclusion of integrated energy disposals with a hydrogen fleet, it was decided to assess the economic viability of intervention from 2030, lasting until 2050, i.e., for 21 years, almost corresponding to the lifetime of the electrolyser.

OPEX has been analysed with scenarios from 2030 to 2050, identifying five trends for each operational cost: i) hydrogen price (€/kg), ii) revenue from the RPF injected in the DN (€/kWh) and price of electrical energy absorption from the DN (€/kWh). Figure 131 shows the OPEX cost trend.

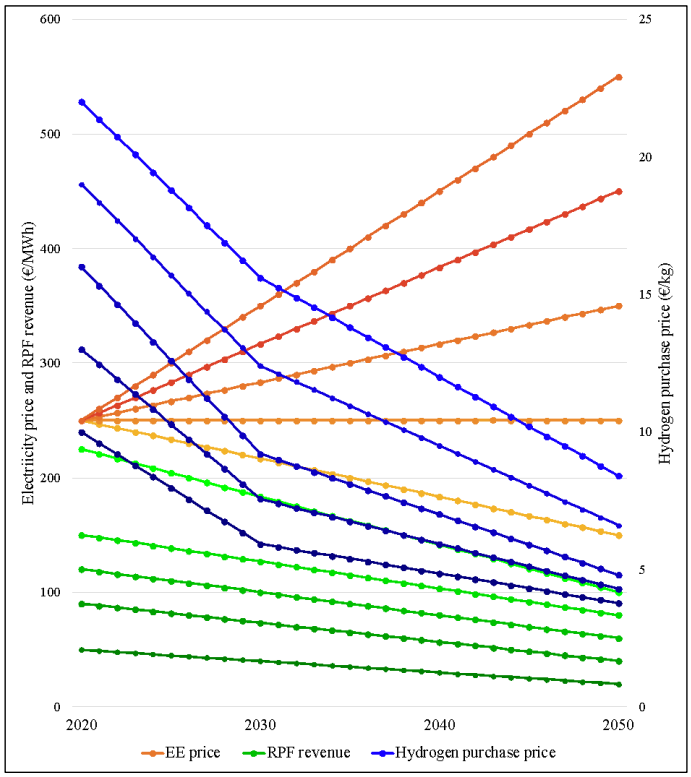


*Figure 131: The lines represent the OPEX parameter cost trends between 2030 and 2050. Five red lines show the hydrogen purchase price yearly trends, five blue lines show the electrical energy price trends, and five green lines show the RPF revenue trends*

The price reported is only the price of green hydrogen, because, from 2030 onwards, the cost of hydrogen produced from this source will become more and more advantageous than the others [49]. The hydrogen purchase price is estimated to decrease, reaching a value of 3.78 €/kg in the most favourable trend and 8.40 €/kg in the least favourable trend. The gain from RPF is also expected to decrease due to policies encouraging self-consumption, in some scenarios even down to 0.02 €/kWh. Finally, forecasting the electrical energy price is highly uncertain, so upward trends of up to 0.55 €/kWh in 2050 and downward trends of up to 0.15 €/kWh in 2050 were analysed.
Concerning the investment costs of PV, electrolyser, hydrogen storage and fuel cell EVs, minimum, average and maximum values related to 2030 have been identified and depicted in Table 52.

*Table 52: CAPEX at 2030 related to district components*

| COMPONENT | Minimum CAPEX | Average CAPEX | Maximum CAPEX |
|---|---|---|---|
| Electrolyser | 350 €/kW | 638 €/kW | 925 €/kW |
| PV plant | 294 €/kW | 508 €/kW | 721 €/kW |
| Hydrogen storage | 8 €/l | 11 €/l | 14 €/l |
| Fuel cell EV fleet | 30.8 M€ | 33.6 M€ | 36.4 M€ |

The depreciation is determined considering a debt interest of 3 %, an equity interest of 10 %, a percentage of capital coming from bank debt of 80 % and a percentage of capital coming from the equity of 20 %. As result, a weighted average cost of capital, WACC, of 4.4% and a depreciation coefficient in 21 years, $\alpha_{WACC}$, equal to 0.074 were obtained, as specified by Equation 54.

*Equation 54:*

$$\alpha_{t,WACC} = \frac{WACC \cdot (1 + WACC)^t}{(1 + WACC)^t - 1}$$

Each year the investment cost was depreciated using Equation 55:

*Equation 55:*

$$Annual\ depreciation\ cost = \alpha_{WACC} \cdot Investment\ cost$$

Finally, for each year the following equations calculate the overall costs, considering both OPEX and CAPEX, to compare scenarios.

*Equation 56:*

$$C_y^{TOT} = \alpha \cdot (c^{PV} \cdot + c^{HS} \cdot L_n + c^{EL} \cdot P_n^{EL}) + c_y^{H_2} \cdot (\sum_{t=1}^{T} HV_{y,t} - \varepsilon \cdot \sum_{t=1}^{T} E_{y,t}^{EL}) - g_y^{DN} \cdot EI_{y,t}$$

Where $c^{PV}$ is the cost of the PV installation (€/kWp), $c_y^{HS}$ cost of HS installation (€/l), $c^{EL}$ is the cost of the electrolyser installation (€/kW) and $E_{y,t}^{EL}$ is the energy consumed by the electrolyser at timestamp t.

### 5.2.2 Deployment of a fuel cell electricl vehicles fleet in Terni

The optimization algorithm was evaluated on the headquarters of ASM. ASM Terni is responsible for the local door-to-door waste collection in Terni, covering an area of 211 $km^2$ and serving 110,000 citizens on average. The waste collection in the city is carried out by a devoted company fleet which consists of 143 endothermic engine vehicles, that are normally refuelled at the ASM headquarters. Therefore, the authors assumed that the hydrogen refuelling system will be installed in this location. Concerning the algorithm implementation, ASM headquarters already comprises some facilities (i.e., offices and warehouses) with a total load of about 650 MWh yearly. Furthermore, a 500 kW PV plant produces 684 MWh/year, with a SCR of 39.5 %.

The energy district structure is shown in Figure 129, with an electrical load consisting of offices, warehouses and utility rooms, a PV generation and the hydrogen system infrastructure, composed of an electrolyser, an hydrogen storage and four refuelling stations.

As for the fleet needs, historical data were used to hypothesize the hydrogen needs of the new fuel cell EV fleet. The fuel cell EVs fleet has been modelled as a heterogeneous aggregation of vehicles, that consumes hydrogen from the energy district hydrogen storage. The hydrogen request profile from fuel cell EVs is evaluated through an algorithm on the GNU Octave environment. The fleet was simulated considering parameters like the number and the typologies of fuel cell EVs, the tank size, the pressure level and the annual mileage of each vehicle, the efficiency and the weekly working time for each vehicle category. The hydrogen consumption was linearized over the time of each timestamp (10 minutes) and the annual mileage of each vehicle, real data provided by ASM, was considered as the model constraint. fuel cell EV charging session, in each timestamp, takes place probabilistically according to four identified priority levels, dependent on the fuel cell EV tank filling level. The main features of the fleet are reported in Table 53.

*Table 53: Case study vehicle features*

| **Vehicle category** | **Number of Vehicles** | **Tank size (l)** | **Weekly Work hours (h)** | **Fuel cell EV efficiency (l/km)** |
|---|---|---|---|---|
| Light vehicle | 13 | 120 | 48 | 0.25 |
| Medium-weight vehicle | 33 | 300 | 48 | 0.45 |
| Heavy vehicle | 97 | 600 | 48 | 0.70 |

The following figure shows the annual mileage of ASM fleet vehicles

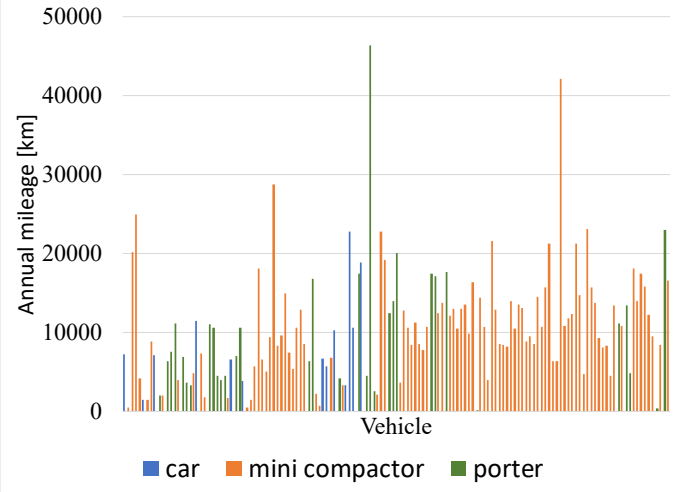


*Figure 132: Annual mileage of ASM fleet*

In the case study, vehicle mileage ranges from 190 km and 46,362 km every year, average and standard deviation values are respectively of 10,596 km, and 7,148 km. Light vehicles are those that travel the shortest distance per year (8,901 km), while heavy vehicles are the most used (10,896 km). The waste management fleet has, to date, annual consumption of about 508 $m^3$ of diesel fuel. Performing an economic analysis of the district, including the fleet, the building consumption and the production of the 500 kW PV it results that the annual OPEX cost is 881 k€/year, considering a diesel price of 1.6 €/l, electrical energy price of 250 €/MWh and RPF gain of 115 €/MWh. The costs are distributed as follows: the cost for the fuel and maintenance of the fleet is 812 k€, the cost for the electrical energy for the district is 94 k€ and the income from feeding RPF into the grid is 25 k€. CAPEX is due exclusively to the cost of the fleet, which is about 28 M€ and, in compliance with the depreciation coefficient expressed Equation 54, has an annual depreciation cost of 2.07 M€/year.
The hydrogen consumption required after the fleet conversion was calculated over time and a monthly trend is shown in Figure 134. Each year the fleet would require 1,127 $m^3$ at 500 bars of hydrogen, which corresponds to about 45.832 tons. For the case study, it is considered to supply the electrolyser with the energy surplus from the PV plant, which is studied in different sizes.

#### 5.2.2.1 Considerations on the hydrogen storage size

In [VI], the authors carried out a study, made with GNU Octave, to see what size hydrogen storage should be within the district. For the study, based on the resources of the area and the available space, three types of operation were assumed, as shown in Table 54. In the first scenario the electrolyzer is fed by the power produced in excess by the PV system compared to the demands of the headquarter, avoiding the introduction of RPF into the grid. In the second scenario the electrolyzer is connected in series to a 180 kW PV system and converts all the electricity into hydrogen. Finally, in the third scenario, the electrolyzer absorbs constant power from the grid, regardless of on-site production, always working at the nominal power of 100 kW.

*Table 54: Electrolyser operating modes*

| Operating modes | Description |
|---|---|
| Scenario I | The electrolyser is powered by the RPF produced by a 180 kW PV system. |
| Scenario II | The electrolyser is powered in series by a 180 kW PV system. |
| Scenario III | The electrolyser is powered by absorbing a constant power of 100 kW from the grid. |

In order to evaluate the feasibility in converting the ASM's waste collection fleet to hydrogen-powered vehicles, 500 simulations were carried out to determine the hydrogen storage size, the hydrogen production during two intermittent operation modes (RPF and PV production) and a continuous one (electricity from the grid) as well as the number of refueling stations.

#### 5.2.2.1.1 Size of the Hydrogen storage vessel

First and foremost, the capacity of the hydrogen storage was determined for each operation mode, considering four refueling stations. Figure 133 shows the results of the simulations.

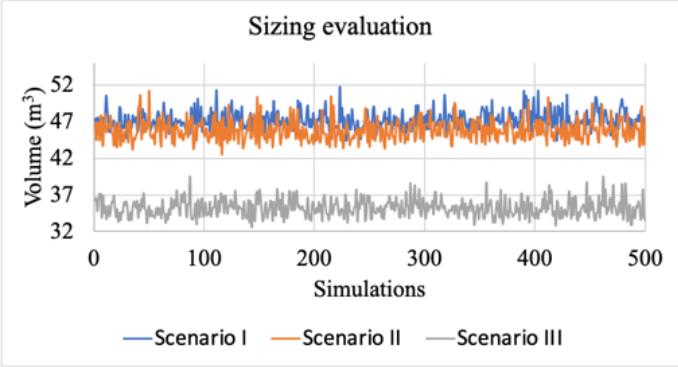


*Figure 133: Sizing evaluation in the 500 simulations in the three scenarios, considering 4 refueling points.*

The average values analysis highlights that the greater size is related to Scenario I, with a medium value of 47.12 $m^3$, due to the limited impact of electrolyser operation. Scenario III requires the minimum average value of 35.25 $m^3$, due to the high hydrogen production from the electrolyser, as reported in Table 55. During the simulations it was noted that the maximum size occurs in Scenario I, with 51.74 $m^3$, while the minimum reservoir that occurred in one simulation took place in Scenario III, with 32.62 $m^3$.

*Table 55: Vessel Sizing Results*

| Operating mode | Scenario I | Scenario II | Scenario III |
|---|---|---|---|
| Maximum size ($m^3$) | 51.74 | 51.18 | 39.53 |
| Medium size ($m^3$) | 47.12 | 45.79 | 35.25 |
| Minimum size ($m^3$) | 44.32 | 42.51 | 32.62 |
| $H_2$ self-sufficiency (%) | 3.80 | 9.40 | 30.70 |

Considering an average value of 500 simulations, the fleet requires 1,127 $m^3$ at 500 bars of hydrogen each year, which corresponds to about 45.832 tons. Figure 134 shows, as an example, the trend of the hydrogen tank filling level in one year for Scenario II, where every two weeks the storage system is completely filled by a tanker truck.

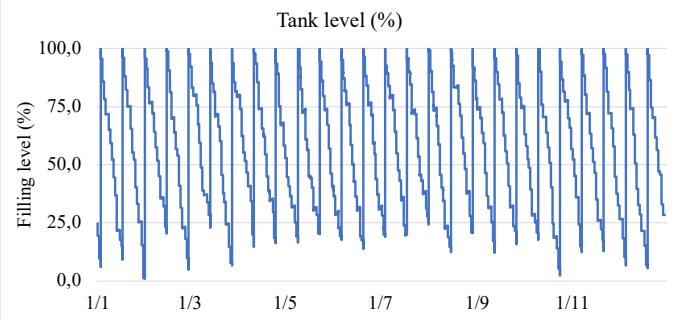


*Figure 134: Filling level of hydrogen storage system in Scenario II.*

As shown in Figure 134 the hydrogen level profile presents a reasonable periodic trend, influenced by the refueling sessions and the electrolyser operation.

#### 5.2.2.1.2 Hydrogen produced by electrolysis

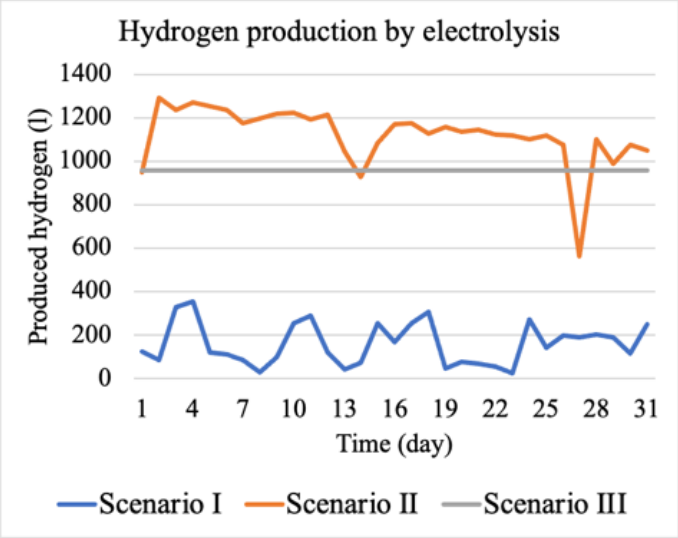


*Figure 135:Amount of hydrogen injected by the electrolyser into the tank at 500 bar day by day in August, for the three scenarios.*

To evaluate the amount of hydrogen produced by the electrolyser and its profile due to the intermitted generation of ASM's PV arrays, historical data were used in the simulation. Figure 135 shows the production of hydrogen by the electrolysis in August for the three scenarios. It is worth highlighting that only during the summer months the hydrogen production in Scenario II overcome that one of Scenario III, due to the seasonal variation of PV plants. Moreover, the graph shows that the operation of the electrolyser is highly variable over time if powered by intermittent RES generation even though it can provide an unquestionably useful service to the electricity grid, absorbing RPF and avoiding load increase or voltage drops. Based on the simulations, the hydrogen produced in Scenario I is about 42.66 $m^3$ (about 1,733 kg) at a pressure of 500 bar, that corresponds to the 3.8 % of the hydrogen consumption of the fleet. The percentage is low due to the electrolyser

management, that activates the production only in case of a RPF in the secondary substation linked to ASM headquarters. In Scenario II, hydrogen is generated from all the energy produced by a PV system of 180 kW of nominal power, with a hydrogen generated of 105.88 m3 at 500 bar, covering 9.39 % of the hydrogen consumed. Finally, in Scenario III the hydrogen generated from the electrolyser is 346.72 $m^3$ at 500 bar, corresponding to 30.7 % of the whole demand.
As to the water demand during the electrolysis, an amount of water between 15.6 $m^3$ (Scenario I) and 126.8 $m^3$ (Scenario III) has to be used to produce the amount of hydrogen needed by the ASM's fuel cell EV fleet.

#### 5.2.2.1.3 Impact of the number of refueling stations

To evaluate the impact of the number of refueling stations on the size of the storage vessel, simulations were performed for Scenario I and the results are summarized in Table 56.

*Table 56: Impact of the number of refuelling stations on hydrogen storage capacity*

| **Hydrogen storage capacity ($m^3$)** | | | |
|---|---|---|---|
| Refueling points | 4 | 6 | 8 |
| Maximum | 51.74 | 52.52 | 51.86 |
| Medium | 47.12 | 47.19 | 47.14 |
| Minimum | 44.32 | 44.07 | 43.98 |

Since the storage capacity does not change significantly in case of 4, 6 or 8 refueling stations, this parameter has negligible effects on the storage vessel size. In fact, the higher value corresponds to 52.52 $m^3$ in case of 6 refueling points, which differs only of about the 1.5% with respect to the minimum value of the sizing evaluation.

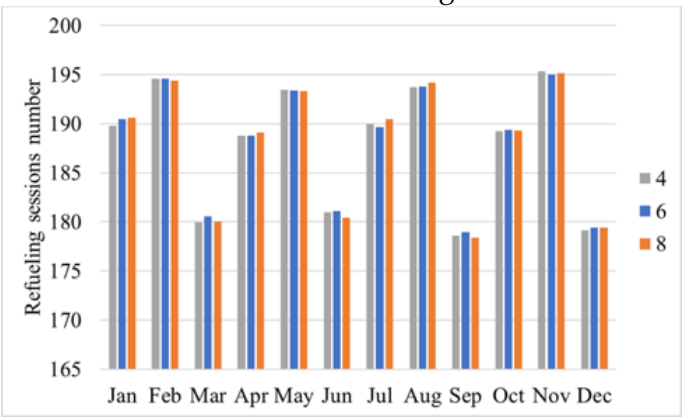


*Figure 136: Average number of refueling performed each month considering hydrogen vehicles and refueling points number (Scenario I).*

The number of timestamps characterized by almost one refueling session are distributed among the months, as expected, because the seasonal variation related to work conditions was avoided. The average monthly number of refueling sessions is shown in Figure 136, according to the number of refueling points.
In accordance with that, a 47 $m^3$ hydrogen storage was used within this district for the optimization problem.

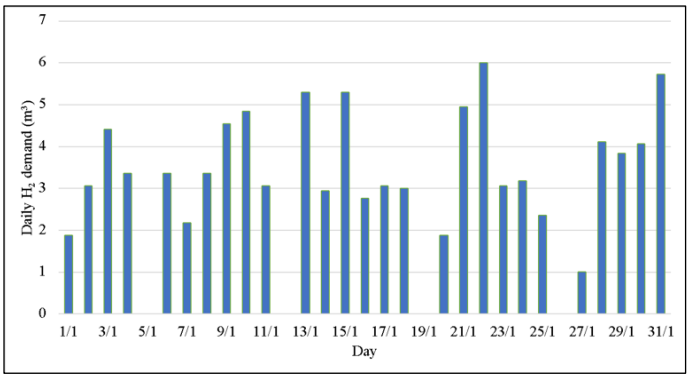


*Figure 137: Hydrogen fleet daily consumption during the month of January 2030*

To date, the ASM district has a 500 kW PV plant, but it has been studied what could happen by increasing its size up to 1500 kW. Higher sizes are not applicable because of the lack of space in the district. Concerning the electrolyser size, it was decided to limit the study to only three scenarios, one concerning the electrolyser sizeable to cover the first quartile of the energy surplus power, counting only non-zero values, one concerning the second quartile of the energy surplus power and finally one concerning the third quartile of the energy surplus. Table 57 shows the sizes used for the case study.

*Table 57: Case study PV and electrolyser sizes*

| | Minimum electrolyser (kW) | Average electrolyser (kW) | Maximum electrolyser (kW) |
|---|---|---|---|
| PV I (500 kW) | 70 | 159 | 442 |
| PV II (750 kW) | 101 | 249 | 689 |
| PV III (1500 kW) | 191 | 499 | 1,475 |

### 5.2.3 Technical-economical optimisation of the fuel cell electric vehicle fleet

This section presents and discusses results gathered from the implementation of the model and the algorithm in the case study. Results are firstly distinguished between analyses performed on OPEX, both technical and economic and analyses performed CAPEX; finally, results of these two analyses are combined providing concluding remarks. Table 58 shows the list of all the variables used in this study. Five and six parameters were respectively chosen, some concerning external data (i.e., independent from the district) and others concerning system design parameters. It is worth highlighting that the model is capable of evaluating different energy districts as well as different external conditions; nevertheless, results are already promising in respect of similar energy districts, namely those owned by the waste management company that is operating in a medium-size city, as in this case study.

*Table 58: OPEX and CAPEX scenarios*

| OPEX scenarios | N. | CAPEX scenarios | N. |
|---|---|---|---|
| PV size | 3 | PV size | 3 |
| electrolyser size | 3 | Electrolyser size | 3 |
| Hydrogen purchase price | 5 | PV investment cost | 3 |
| RPF revenue | 5 | electrolyser investment cost | 3 |
| Electrical energy purchase price | 5 | Hydrogen storage investment cost | 3 |
| | | Fuel cell EV fleet cost | 3 |

In the following the results are shown: first, the average annual behaviour at the level of comparison between the 1125 operational scenarios and the 729 investment scenarios is investigated, then the 21-year trend for some specific scenarios is shown, and so the annual trend of the technical parameters in a sample scenario is depicted.

#### *5.2.3.1 Comparison of annual costs in the scenarios*

In the study, several scenarios are investigated to perform the multiparametric analysis. The results show the total operating technical parameters and costs as well as the investment cost of the ASM district considering the new hydrogen fleet.

#### *5.2.3.2 Comparison of technical parameters*

Within the district, hydrogen and electrical energy flows are distinguished, the magnitude of which depends on the size of the PV, the size of the electrolyser and the price trends considered.

Concerning the hydrogen flow, each year the fuel cell EVs fleet's consumption is about 1,127 $m^3$, while the energy inputs are distributed between the hydrogen imported from outside by tanker trucks, $H_{2,TANKER}$, (covering between 53% and 99.6% of the annual demand, with an average value of 92.8%), the hydrogen produced by the electrolyser using energy from local RES, $H_{2,RES}$, (between 0.4% and 13.4%, with an average value of 6.0%) and the hydrogen produced by the electrolyser using energy from the DN, $H_{2,DN}$ (between 0 % and 34.7%, with an average of 1.1%).

$H_{2,TANKER}$ is almost constant, with a slight decrease as the hydrogen price increases, i.e., the average number of annual refuelling goes from 26.1 to 23.6 when the hydrogen price

scenario goes from cheapest to most expensive. $H_{2,RES}$ and $H_{2,DN}$ increase as the hydrogen price increases, although they always have small values. An increase in the electrolyser size causes the share of $H_{2,RES}$ to increase from 2.9 to 8.9 % of annual demand. The hydrogen balance does not undergo any variation when varying the PV size since costs mainly determine the flows. Figure 138 shows three examples of hydrogen balance. Sample I concerns the scenario where the percentage of hydrogen importation from outside is the highest and is determined by having the lowest hydrogen price among those considered, i.e., on average, 5.9 €/kg. Sample II is the median scenario concerning the hydrogen importation percentage and is determined by having the maximum hydrogen price, i.e., on average 14.3 €/kg; finally, Sample III is the minimum hydrogen importation scenario and is characterised by having the maximum hydrogen price and the minimum electrical energy price, i.e., on average 0.18 €/kWh.

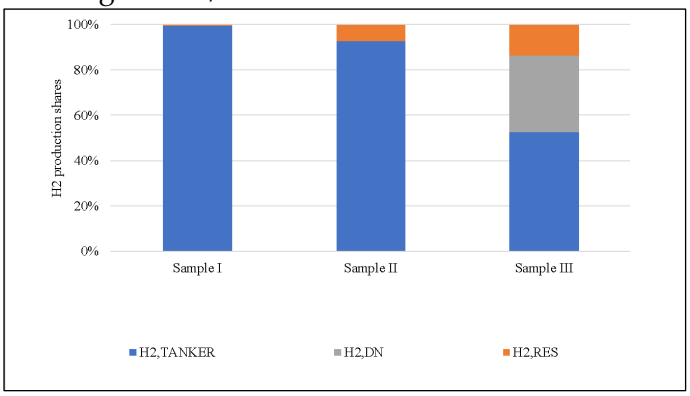


*Figure 138: District hydrogen balance in three extreme scenarios*

Concerning the electrical energy balance, it is necessary to consider both the production through the PV and the supply from the DN in addition to the consumption of the building (of 646 MWh/year) and the consumption for the electrolysis. Increasing the size of the PV from the current 500 kW to 750 kW and 1500 kW results in annual production of 684 MWh, 1026 MWh and 2052 MWh, respectively, of which 39%, 28% or 15% is self-consumed by the building, while the remaining can be sold to the DN or can be converted into hydrogen by the electrolyser. This simplified assumption has neglected the effect of scaling up on the capacity factor; the primary rationale is that the capacity factor could also be affected by other parameters (e.g., not uniform space and shadowing) not considered in the model. An amount of energy is also taken from the DN used to power the building and possibly to increase the hydrogen production from the electrolyser. The consumption of the electrolyser increases as the hydrogen price increases, i.e., starting from 15% of the district consumption in the cheapest hydrogen trend, it goes up to 39.7% in the most expensive hydrogen price trend. An increase in the electrolyser size produces an increase in the amount of self-produced hydrogen, i.e., compared to the district consumption, the electrolyser goes from absorbing 14.7 % in the case of the smallest electrolyser size to absorbing 33.8 % in the case of the largest electrolyser. The greater size of the PV does not increase the amount of electrical energy injected into the electrolyser. Figure 139 shows the average electrical energy balance obtained in the 500 kW, 750 kW and 1500 kW PV configurations, respectively.

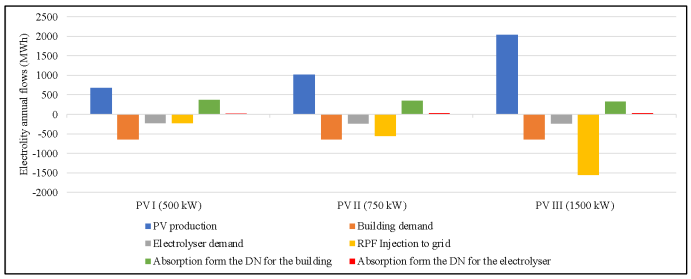


*Figure 139: District electrical energy balance as PV size changes*

Table 59 shows the average number of $H_{eq}$ of electrolyser operation in the different design configurations. The average number of $H_{eq}$ of operation is relatively low, especially as the size of the electrolyser and the size of the PV plant increase, making it more challenging to amortize the investment cost.

*Table 59: Electrolyser equivalent operating hours in different configurations*

| | 1st electrolyser size (kWh/kW) | 2nd electrolyser size (kWh/kW) | 3rd electrolyser size (kWh/kW) |
|---|---|---|---|
| PV I (500 kW) | 1,505 | 1,419 | 746 |
| PV II (750 kW) | 1,078 | 956 | 479 |
| PV III (1500 kW) | 634 | 505 | 223 |

Considering all the parameters, within the limits of the assumed values, the increase of the RPF revenue causes slightly more electrical energy to be sold to the EG, reducing the SCR of the district and with the decrease of hydrogen production from the electrolyser. The electrical energy price does not affect, except in the case of very low cost, the amount of electrical energy drawn from the grid to self-produce hydrogen.

#### 5.2.3.2.1 Comparison OPEX

The operating costs are determined by the hydrogen purchased price and the electrical energy balance, i.e., the cost of supplying the building, electrical energy absorption for running the electrolyser and the revenue for injecting RPF into the EG.

Given the variety of variable parameters taken into account, it is worth focusing on their effect on the average OPEX over 20 years which is calculated for each scenario. Firstly, Figure 140 a) shows the distribution of the number of scenarios in relation to the OPEX; in particular, each bar length represents the number of scenarios for which OPEX is between the corresponding value in the x-axis and the previous one. Based on these data, the OPEX average value is 436 k€, the median value is 414 k€, the standard deviation is 100 k€, maximum and minimum values are 699 k€ and 243 k€, respectively. It is worth mentioning that maximum OPEX is obtained for scenarios with a 500 kW PV plant and an electrolyser of 70 kW, while the minimum OPEX is obtained for a scenario with a 750 kW PV plant and an electrolyser of 689 kW.

Therefore, if compared with the current OPEX of the ASM waste collection fleet (881 k€/year), the average OPEX of the fuel cell EV fleet for the period between 2030 and 2050 is almost 436k€/year (49.4%) demonstrating that even in the most economically unfavourable case among those considered, the forecast OPEX is lower than the current one. It, therefore, appears that environmental sustainability associated with optimal management also implies economic sustainability. The fact that the CAPEX significantly affects the total cost only in part reduces the importance of this result.

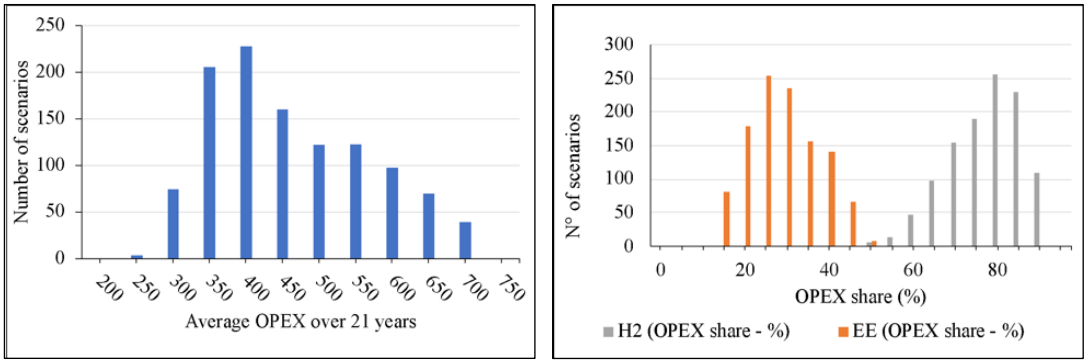


a) b)

*Figure 140: a) Average OPEX over 21 years for all the scenarios; b) Distribution of OPEX share (EE and Hydrogen)*

Concerning the OPEX shares, it has been evaluated that hydrogen expenditure ranges from 48 % up to 94 % of the total amount, average and median values are 74 % and 76 %, respectively; distribution of OPEX share for hydrogen price is reported in Figure 140 b). Moreover, expenditure for electrical energy consists of two elements, namely electrical energy bill for the building and electrical energy absorbed by the electrolyser from the grid. On the one hand, the first element is on average 26 % of the total amount of OPEX, it ranges from 10 % to 48 % (Figure 140 b); on the other hand, energy for the electrolyser is nihil in the majority of the scenarios (i.e., in many cases energy absorption for the electrolyser is not convenient), but it is notable when the highest hydrogen price and the lowest electrical energy price are applied. In that case, it has been evaluated as a notable contribution to hydrogen production from the electrolyser absorbing from the DN, in terms of costs OPEX share ranges from 6 % to 45 % considering the variation of the remaining input parameters (i.e., size of the PV plant, size of the electrolyser, revenue from injected electrical energy). The highest values have been calculated for the biggest size of the electrolyser, in particular, Figure 141 highlights the variable contributions to OPEX for different electrolyser sizes, contributions below 5 % of the OPEX are not reported. It is worth mentioning that for each size of PV, 3 sizes of electrolyser are assessed, therefore, the circles in Figure 141 represent the total amount of OPEX for a certain pair of electrolyser and PV sizes corresponding to different scenarios; triangles correspond to the OPEX share for the electrical energy absorbed from the grid for producing hydrogen. Concerning the OPEX share, variations among the scenarios are negligible as well as it does not increase when the electrolyser size is bigger than 500 kW. As shown in this graph, a size maximization of PV is not convenient relative to the scale of the pilot site (i.e., waste management company in a medium-sized city).

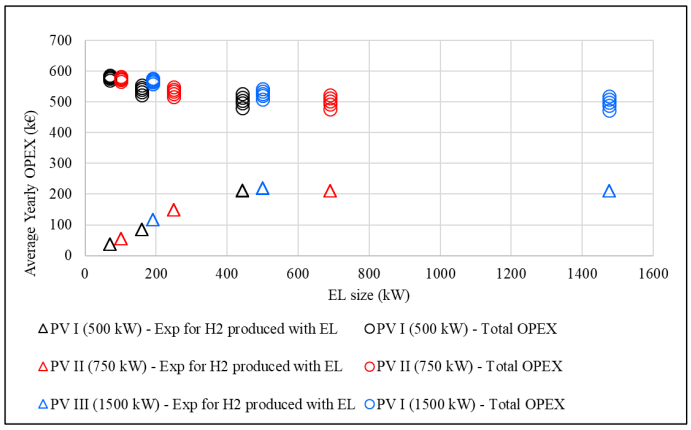


*Figure 141: Average yearly expenditure considering 45 scenarios defined by highest hydrogen price and lowest electrical energy price; triangles correspond to the expenditure for producing hydrogen by using electrolyser; circles correspond to the total amount of OPEX spent every year on average*

The following analysis investigates the influence of the parameters, notably the size of the PV plant, the size of the electrolyser, the prices of the hydrogen and the electrical energy as well as revenue from energy injection. Correlation coefficients have been firstly evaluated for the OPEX in relationship with the prices of the hydrogen and the electrical energy and the revenue from energy injection; correlation coefficients are 0.92, 0.33 and 0.03, respectively. Further analysis and graphs are reported about parameter influence. In line with the correlation coefficients and the hydrogen balance, OPEX strongly depends on the hydrogen price for which five scenarios have been identified. Figure 142 a) reports the average OPEX over 21 years corresponding to the five price trends of the hydrogen, notably each bar is as high as the number of scenarios for which OPEX is within the limits defined by the x-axis; each colour defines a certain hydrogen price and the group of 225 scenarios since 1125 scenarios were identified through the combination of all parameters. Moreover, the black line is the reference distribution and it is calculated as one-fifth of the distribution extracted from Figure 142, where parameter influence is not assessed.

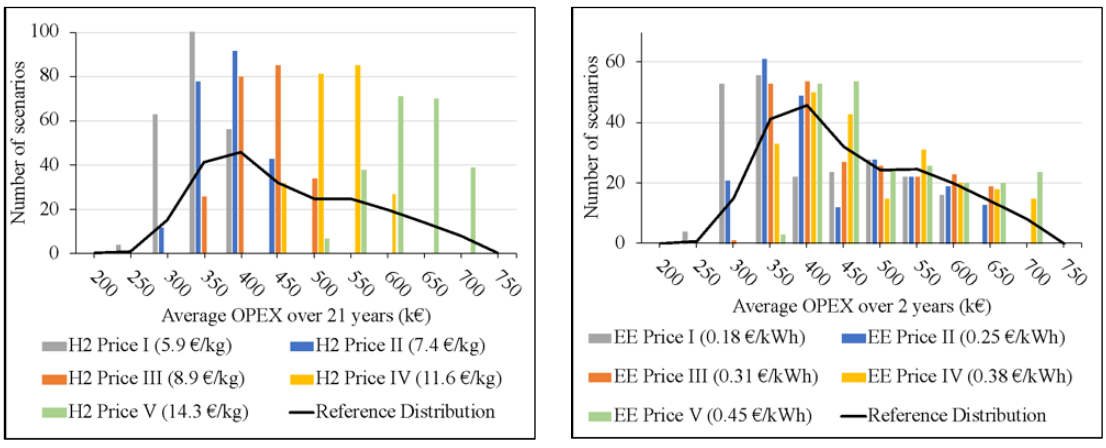


a) b)

*Figure 142: Average OPEX over 21 years in relation to the price of hydrogen. The average price of the hydrogen is included in the legend; b) Average OPEX over 20 years in relation to the cost of electrical energy (EE). The average cost of the electrical energy is included in the legend*

According to the graph, OPEX increases significantly when the unitary cost is higher as well as distribution paths are greatly different from distribution reference. In particular, for the extreme scenarios characterized by the highest unitary cost all the calculated OPEX

overcome the median value calculated for all the scenarios as in Figure 140 a) (i.e., 414 k€); conversely, the scenarios related to the lowest unitary cost cause OPEX lower than the median value in all the simulated cases. Finally, when the intermediate unitary cost is applied, 47 % of the scenarios report OPEX higher than 414 k€.

Figure 142 b) shows the impact of the cost of electrical energy on the simulations, graph has been obtained following the approach already presented in Figure 142 a). The OPEX evaluation takes into account the overall expenditure for the electrical energy supply of the district (i.e., building consumption are included in the calculation). As shown in the graph, this parameter partially influences the scenario distribution; on the one hand, when the lowest cost is applied, 63 % of scenarios reports OPEX lower than the median value, 414 k€; on the other hand, when the highest cost is simulated, 79 % of scenarios is characterised by OPEX higher than the benchmark.

Following the approach adopted for Figure 142, Figure 143 a) shows the OPEX distribution related with the revenues for electrical energy injected in the DN. According to the graph, this parameter does not influence the scenario distribution; indeed, when the highest unitary revenue is applied, the median value of OPEX is equal to the benchmark, 414 k€, if the lowest cost is applied, 56 % of scenarios reports OPEX higher than the median value calculated for all the scenarios.

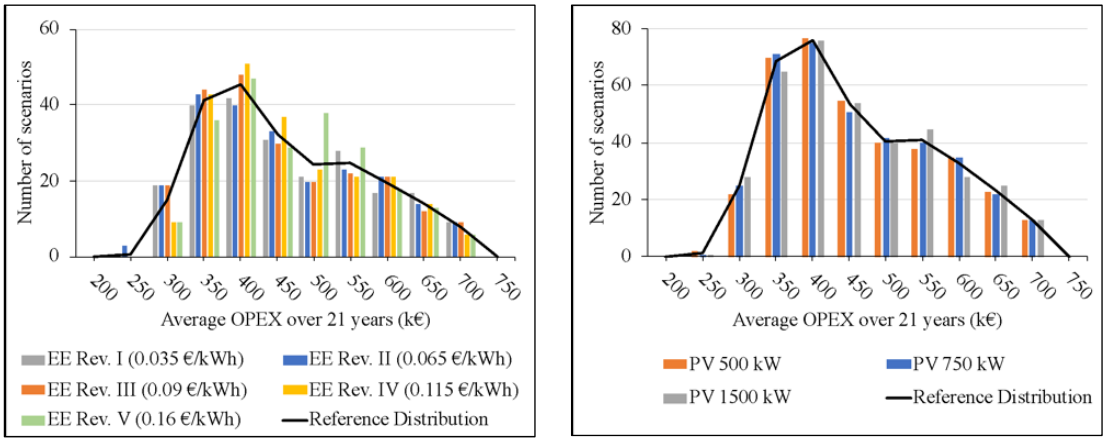


a) b)

*Figure 143: a) Average OPEX over 20 years in relation to revenues for electrical energy injected in the DN. Average revenue is included in the legend; b) Average OPEX over 20 years in relation to the size of the PV plant*

Figure 143 b) shows the average OPEX over 20 years corresponding to the 3 sizes of the PV plant, the black line is the reference distribution and it is calculated as one-third of the distribution extracted from Figure 140 a), where parameter influence is not assessed. As shown in the graph, the three clusters of scenarios are slightly different among them and the reference distribution, nevertheless it is worth mentioning that 53 % of scenarios calculated for the highest size of PV plant provides OPEX lower than the median value calculated for all the scenarios as in Figure 140 a). Finally, the evaluation of the impact of the electrolyser sizes is reported in Figure 144; according to the figures, when the highest size of electrolyser for each PV size it can be stated that 55 % of the scenarios are under the benchmark.

The size of the PV has a very limited impact on OPEX, indeed, moving from 500 kW to 1500 kW of installed PV allows to reduce the OPEX on average by only 2.7 %.

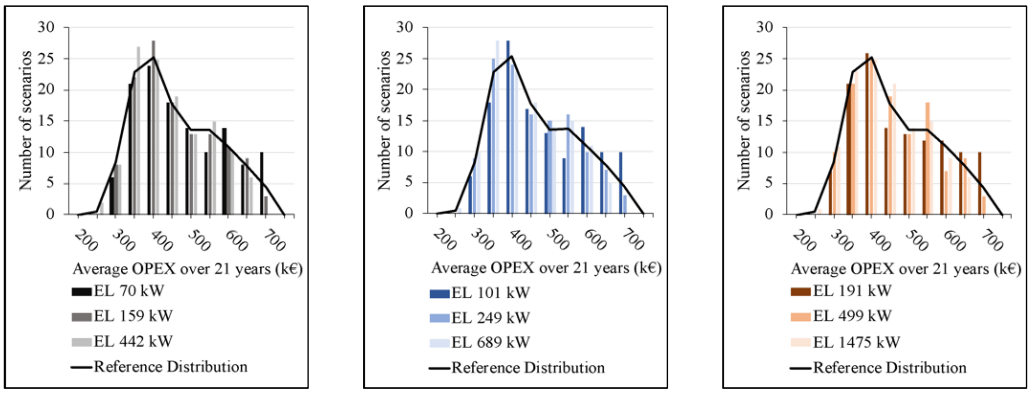


a) b) c)

*Figure 144: a) Average OPEX over 20 years in relation to the size of the electrolyser (PV plant equal to 500 kW); b) Average OPEX over 20 years in relation to the size of the electrolyser (PV plant equal to 750 kW); c) Average OPEX over 20 years in relation to the size of the electrolyser (PV plant equal to 1,500 kW)*

#### 5.2.3.2.2 Comparison CAPEX

During the analysis, 729 investment cost analysis scenarios were considered, which have a decidedly significant impact on total costs. The investment costs are due to the purchase of PV, electrolyser, hydrogen storage and fuel cell EVs fleet. The following table shows a summary of the data from the CAPEX analysis, and Figure 145 shows the CAPEX depreciation in relation with the size of PV and electrolyser.

*Table 60: CAPEX analysis results*

| | PV cost (k€) | Electrolyser cost (k€) | Hydrogen storage cost (k€) | Fleet cost (k€) | CAPEX (k€) |
|---|---|---|---|---|---|
| Minimum | 147 | 24 | 376 | 30,810 | **31,357** |
| Average | 465 | 274 | 517 | 33,611 | **34,868** |
| Maximum | 1,081 | 1,364 | 658 | 36,411 | **39,515** |

The fleet cost has a weight ranging from a minimum of 90.85 % to a maximum of 98.52 % of the total cost, which is also a symptom of the fact that fuel cell EVs are currently really expensive and that the ASM fleet has several special vehicles, dedicated to waste collection and therefore very expensive. Excluding the cost for the fleet, the cost of PV, electrolyser and hydrogen storage come up to an average percentage weight of 35.7 %, 18.8 % and 45.5 % respectively. Figure 145 shows the average CAPEX values varying the PV and electrolyser sizes. The value of CAPEX varies over a narrow range as PV and electrolyser have much less weight than fleet cost in determining it.

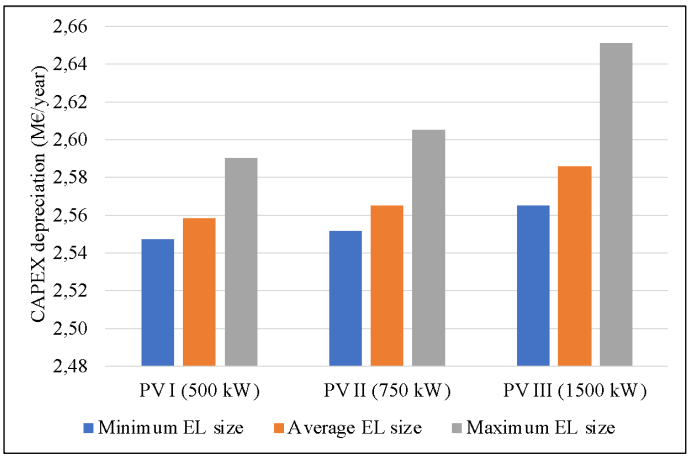


*Figure 145: Average CAPEX values as a function of PV and electrolyser size*

The purchase and depreciation of assets can take place in ways other than those indicated here, such as assets already owned and depreciated, different financial and tax rates, incentives, non-repayable loans, for this reason, it was decided not to analyse excessively this topic.

#### 5.2.3.2.3 Overall cost considerations

Making a comparison between OPEX and CAPEX, annualizing the investment costs, through Equation 56, CAPEX covers a portion of total costs ranging from 76.85% to 91.98%. The total cost has a value, depending on the parameters, ranging from a minimum of 2,580 k€ up to 3,549 k€. On average the total annual cost for the district is 3,017 k€, with a standard variation of 24.6 k€. Although there is not a big difference between the different technical parameters, the average total cost is lower (2,990 k€) for the scenarios with 500 kW PV and maximum size electrolyser, while it is higher (3,064 k€) for the configurations with 1500 kW PV and the maximum size electrolyser.

Comparing the values obtained from the simulations with the current cost of the district with the diesel fleet, it results that the forecasted cost ranges from 87.4 % to 120.2 %, with an average value of 102.2 %. This value is encouraging for the development and sustainability of hydrogen technology.

The average breakdown of all the costs, with all the parameters involved, is presented in Figure 146. The most significant factors are the fleet, which has an annual cost equal to 82.6 % of the total (in the current diesel fleet it has a percentage weight of 70.2 %), and the hydrogen purchase, which weighs on average 10.5 %. The values shown in Figure 146 are averages among all the scenarios considered, so the values can significantly vary from case to case. The revenue from the RPF, not represented in the figure, is averagely worth 0.43% of the annual total costs.

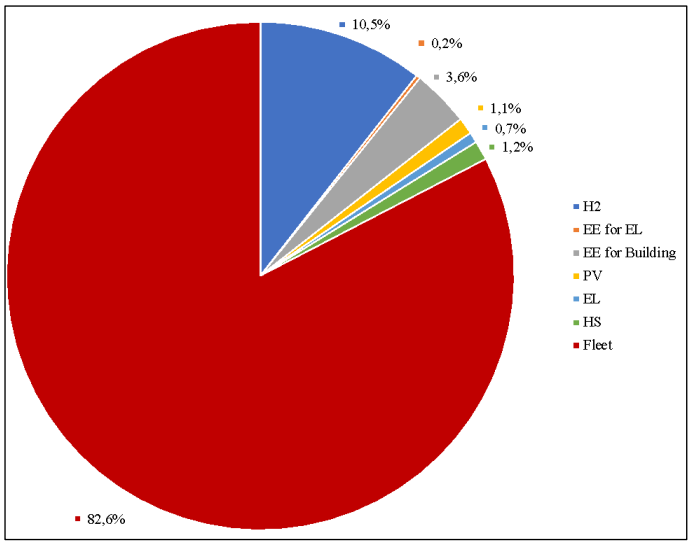


*Figure 146: Distribution of total cost (CAPEX and OPEX)*

### 5.2.3.3 Parameter trends over 21 years

In the analysis performed, several years of operation of the district are considered, from 2030 to 2050, in which, as already expressed in paragraph 2.1.1, the prices change over time. The mixed integer linear programming was performed year by year, so each year can be considered independent of the previous one and may have different results. Considering the assumptions, the production from the PV, the consumption of the fleet and the district do not change from year to year, while only the external prices vary in line with the five trends. Based on the results, it is noticed that two situations could happen, the first one, much more common and represented also in Figure 147 a), representing the scenario with median OPEX, in which the values are maintained almost constant over time, with light random variations or due to small differences of the costs. Otherwise, it can verify the case expressed in Figure 147 b), in which the decrease in the hydrogen price, which initially started from a very high value, causes to go from the first years in which it is not convenient to import hydrogen from outside, but only to absorb electrical energy that will then be converted with the electrolyser, to the following years in which the behaviour is reversed and hydrogen is completely imported, except for a small percentage of $H_{2,RES}$.

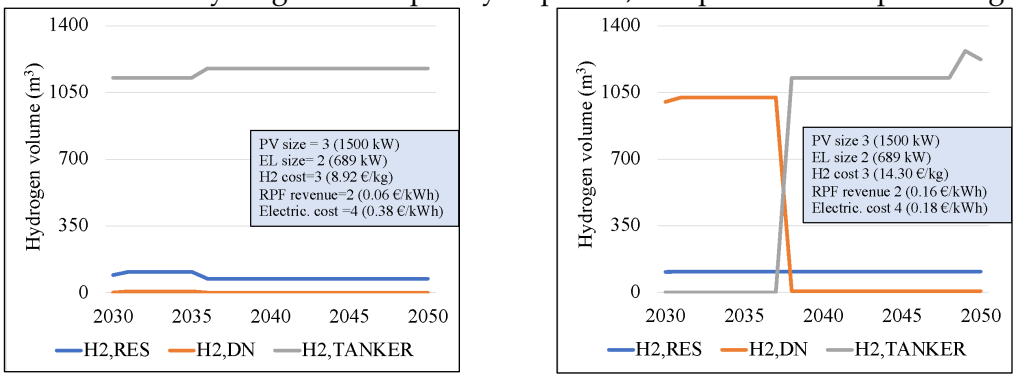


*Figure 147:a) 21-years trend for an operative scenario with parameters almost constant in time; b) 21-years trend for an operative scenario with highly variable parameters over time.*

### 5.2.3.4 Monthly parameters trend

In the study performed, for each of the 1,125 operational scenarios analyzed, a day-by-day optimization of the district was performed, to know when the tanker arrives, how much hydrogen is produced by the electrolyser, and how much electrical energy the district absorbs from the DN. Figure 148 and Figure 149 show what is the trend of the tank filling level and the hydrogen and electrical energy balances in the time frame of three months of 2030 for the scenario with median OPEX, i.e. the scenario with 1,500 kW PV plant, 689 kW electrolyser and taking into account the price trends as shown in the figures.

The tank filling curve of the hydrogen storage has a cyclical behaviour and fills up about twice a month thanks to the intervention of the tanker, while the electrolyser contributions only serve to slightly delay the tanker refilling frequency. The production from electrolyser has a rather irregular behaviour and has an increase in the seasons with higher irradiation and PV production.

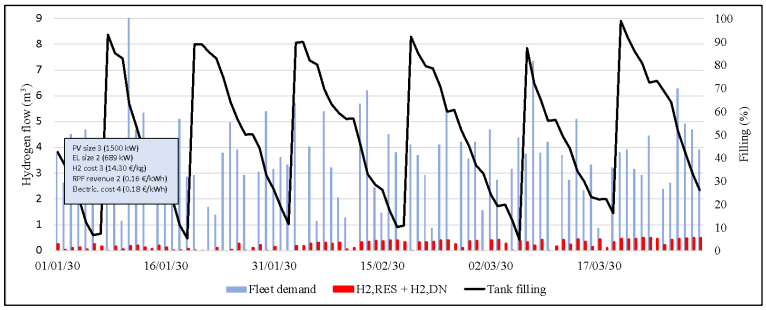


*Figure 148: Day-by-day hydrogen balance for three months. Data from the scenario with median OPEX value.*

Figure 149 shows that using the 1,500 kW PV size results in a high energy surplus, which is only partially absorbed by the electrolyser or the building, while a large part is fed into the DN as RPF. Although there is high energy surplus, the electrolyser does not absorb all the electrical energy because, except for very high hydrogen costs and very low RPF sales costs, it is not cost-effective to convert all the energy surplus to hydrogen.

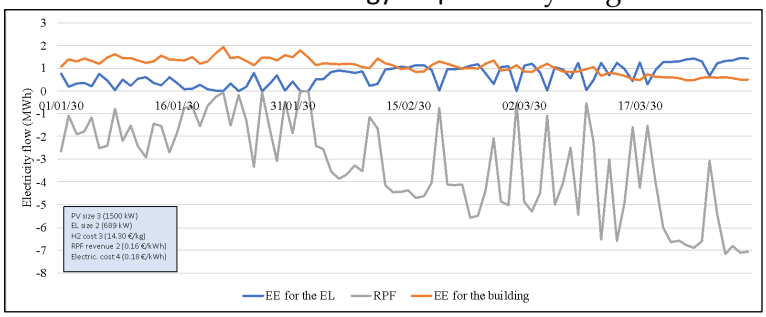


*Figure 149: Day-by-day electrical energy (EE) balance for three months. Data from the scenario with median OPEX value*

# 6 The emergence of renewable energy communities and self-consumption groups

## 6.1 European and Italian regulatory framework

The increased frequency of extreme weather events and other increasingly visible effects of climate change and global warming urgently pose the need for adequate and effective action. The objectives set for 2030 and 2050 through the Paris Agreement of 2015 have led the European Union to define a common energy strategy with the aim of achieving high energy efficiency targets in the end uses of energy and buildings, promoting the use of energy from RES and regulating the internal electricity market.

From these objectives was born the Clean Energy for all Europeans Package, approved in May 2019: a set of four European directives and four regulations, which aims to implement the necessary energy transition by ensuring access to clean energy for all European citizens. Subsequently, it emerged the need to update these directives as part of the European Green Deal. The crisis following the war between Russia and Ukraine has led to strong volatility in gas prices and has pushed the European Community to launch a further plan, which takes the name of REPowerEU, with a further increase in the objectives of renewable capacity, up to 45% of the electricity mix, and the reduction of consumption of natural gas.

In Italy, RECs are defined by recent legislative decrees that allow a virtual aggregation of the users that are supplied by the same primary substation. Moreover, the community has to involve newborn RES power plants that virtually supply the participants. The self-consumption within the community is promoted by calculating the so-called shared electricity (i.e., the minimum value chosen between energy hourly consumed and produced). According to the measured shared energy, a contribution, identified as the sum of the avoided transportation costs, is paid to the RECs. Moreover, in the next 20 years, a premium tariff is assigned to self-consumer groups for shared energy.

The legislation [187] defines the characteristics that RECs must have in terms of their legal form and their respective entities. The legislation is in the process of being finalised, but it is considered that the RECs is made up of subjects under the same primary substation and with a maximum generation power of 1 MW.

The estimates underlying the planning of the Italian National Recovery and Resilience Plan investments foresees of a potential contribution of 2 GW of installed capacity from RES due to the formation of RECs in the period 2022-2026, representing 7% of the renewable capacity necessary to achieve the 2030 objectives.

Many researchers have studied the response of high PV penetration in different kinds of DNs. In [268] the impact of a diffused installation of PV systems in a typical suburban Canadian DN. In their work, the RES were evenly distributed among all the households and found that the grid was poorly affected by this distribution. References [323], [VII] report that the SCR of individual domestic customers are on average lower than 30%. This data analysis highlights the need for collaborating mechanisms among prosumers and nearby consumers. Also, statistical approaches have been used. In [161] a stochastic simulation has been carried out on three different DNs in Sweden. In this work minor overvoltages have been detected while consistent RPF towards the MV grid were present. Higher penetration of PV has been studied in [14] with a Monte Carlo simulation on a DN in the UK. In their work emergers the importance of the granularity of the data. Using the hourly average power instead of the quarter-hour average power underestimates the

overvoltage and overload frequency. Less attention has been posed to the MV grid with fewer and more recent studies. In [208] a study on a real MV network showed that the DG can help the power grid in limiting some overloads. Along with the technical feasibility of the PV introduction, there is also an economic issue. In a deregulated electricity market, most of the initial investment is in charge of private initiatives. Here the profitability of the PV system is strongly affected by country-specific conditions such as solar irradiance, grid fees, national incentives, and more. Many of these aspects have been treated in [158] among the single country condition a factor that was common in all the countries was the importance of the RECs. Study [158], highlights the importance of SCR, which allowed to significantly reduce the total electricity cost. Different studies have been focused on the optimization of the REC to maximise their effectiveness in total cost reduction [126], [155]. Many studies have been carried out on the issue of the profitability of the REC highlighting their effectiveness and the importance of the scale of the community [93].

## 6.2 The social, economic and technical benefits of energy communities

RECs offer a range of significant benefits that can be classified as socual, economical and technical.

The social benefits go beyond just addressing environmental concerns. These benefits contribute to building more sustainable, resilient, and inclusive societies. First, the RECs empower local residents to take control of their energy production and consumption. They encourage REC members to actively participate in decision-making processes related to energy, fostering a sense of ownership and control over their energy future. The development and maintenance of RES projects, such as solar and wind farms, create job opportunities within the community. These jobs can range from installation and maintenance to research and development, offering stable employment and boosting the local economy. RES projects often involve a diverse range of community members, promoting social cohesion. These projects bring together various stakeholders, including local governments, landowners, and energy cooperatives, to collaborate on a shared goal. In the meantime, the development of RES projects can provide educational opportunities for community members, and increase awareness of sustainability. As a direct consequence of the use of renewable energy, there is less environmental impact, and a reduction in air pollution. Finally, participating in a REC often fosters a sense of purpose and pride among its members. Knowing that they are contributing to a more sustainable and environmentally friendly future can boost community morale.

From the economic point of view, the RECs can positively impact both at local and regional level. These benefits arise from the development, deployment, and maintenance of RES technologies within a community. One of the most notable economic benefits of RECs is the creation of jobs. These RECs often require a skilled workforce for the construction, operation, and maintenance of RES installations. Local residents can find employment opportunities in these sectors. Developing renewable energy projects often necessitates significant investments in infrastructure, manufacturing, and technology. This results in increased local spending on goods and services, such as construction materials, equipment, and local suppliers. This boosts the local economy and supports small businesses. RECs generate revenue through the sale of excess energy, this income can be reinvested into community projects, services, or infrastructure, helping to fund local initiatives, and, in the meantime, by generating their own RES, REC members reduce their electricity bills and are less subject to the price volatility. Finally, properties located within RECs can experience an increase in value and become more attractive to potential buyers.

Finally, from the technical point of view, the RECs provide a step towards the adoption of the SGs, introducing technologies that enable real-time monitoring, control, and optimization of energy distribution. In such a way it's possible to enhance grid stability, reduce energy losses, and allow for better integration of RES into the DN. The RECs often employ advanced control and automation systems that optimise energy management, and remote monitoring and maintenance systems, allowing for real-time performance tracking and remote troubleshooting, reducing downtime and maintenance costs. RES technologies, such as wind and solar, possibly integrated with EESS, can be used to match energy demand. This flexibility allows for more efficient energy production and reduces the need for additional power plants, especially during peak demand periods.

## 6.3 The benefits of Renewable Energy Communities in the context of Terni

The paper [X] analyzes, through a Python code that exploits OpenDSS, the impact of the inclusion of 30 RECs in the electricity DN of Terni, highlighting what can be the benefits and disadvantages from the point of view of the DSO and what can be the gains for the subjects that make up the community. Various scenarios were considered, taking into account the renewable targets envisaged by the RepowerEU plan, and different behaviour of consumers were analyzed.

### 6.3.1 Modelling a Renewable Energy Community

The examination relies on the approach outlined in Figure 150. A network model was constructed using OpenDSS. To enhance flexibility and leverage the software's capabilities, it was chosen to interface with it through the py-dss-interface package, which invokes the software via Python. The primary parameters employed in the simulations are as follows:

- the grid model that ASM provided and it follows the actual structure of the MV network,
- the load profile measured at secondary substations of the grid for one year.

The goal of the simulations is to assess the impact of the REC on the DN and the operational cash flows of the REC varying the following parameters:

- Participation degree refers to the total energy absorbed by each MV load node by the users participating in the collective self-consumption schemes. Participation in DR mechanisms has been modelled through storage, adequately sized and configured.
- According to Italian regulations, it has been assumed that the REC cannot be established without the deployment of additional PV plants.

RECs have been established by grouping various load profiles based on proximity, with a preference for loads connected to the same MV node as the PV system rather than nodes not part of the same load node.

Institutions provide economic incentives for energy shared by the same PV system among members connected at different points within an MV network downstream of the same primary substation. This aligns with the transposition of European directives RED II and IEM through subsequent Italian legislative decrees. For incentive calculation purposes, the following table of incentives is considered, assuming, for simplicity's sake, a negligible variation in the zonal price:

*Table 61: Incentive for Self-Consumed Energy*

| Power PV (kW) | Reward for self-consumed energy (€/MWh) |
|---|---|
| P > 600 | 100 |
| 200 < P < 600 | 110 |
| P < 200 | 120 |

In alignment with European energy policies and their implementation in Italy, four scenarios have been formulated for 2030. Initially, as by [278] and [276], an examination was conducted to assess the potential variations in consumption between 2023 and 2030. These variations were attributed to increasing electrification and improved energy

efficiency. Subsequently, an evaluation was performed to determine how many PVs could proliferate. In these scenarios, grounded in the RepowerEU initiative, consumption is projected to increase by 13.2%, rising from 318 TWh to 360 TWh in Italy, with an anticipated installation of 85 GW of PV plants.
The analysis considers three levels of user engagement in RECs, enabling users to temporarily shift a fraction of their rated power, ranging from one-tenth for 30 minutes to one-tenth for 60 minutes and one-tenth for 90 minutes.
To assess the impact on the DN, the following parameters are taken into account:

- The total energy produced,
- RPF in the primary substations,
- SCR,
- SSR,
- Network losses.

The formulas for the SCR and SSR are as indicated in Equation 2and Equation 3. These indices are calculated both for each REC and for the entire network.

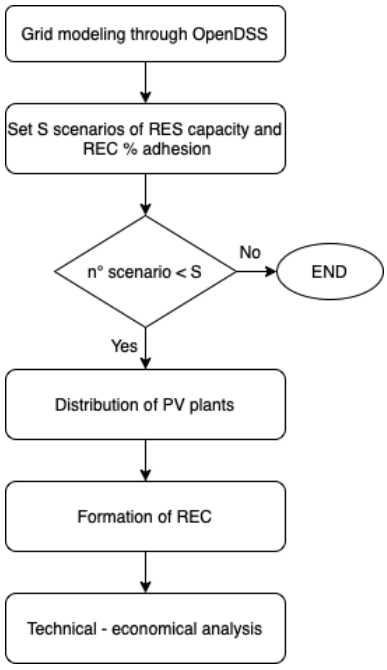


*Figure 150: The methodology applied to the study*

### 6.3.2 Virtual energy communities in the city of Terni

The study focuses on a segment of Terni's MV network, specifically the portion supplied by one of the three primary substations within the network. This section comprises 316 MV nodes and 309 branches. The MV nodes correspond to MV users or secondary substations, while the underlying networks, such as LV, are not considered and are simulated as load nodes. The analyzed network includes two 120/20.5 kV transformers with a rated power of 25 MVA each. A network segment operates at 10 kV, utilizing a 6 MVA MV/MV transformers. Within this network are 309 lines and 316 nodes, out of which 168 function as load nodes. All transformers are equipped with on-load tap changers. This grid section currently hosts approximately 10 MW of distributed PV generators and a 9 MW biomass plant. The results pertain to a one-week period, during which the average

profiles for each load node, based on annual quarterly data provided by ASM, are utilized, as depicted in Figure 151.

The current condition of the case study was also assessed to serve as a baseline for comparison with the identified scenarios. Currently, there are no energy flows toward the primary substation, no overvoltages or undervoltages at the loads, and no line overloads, mainly due to the actions of the tap changer. Energy consumption within this grid segment amounts to 1123 MWh, while distributed PV systems generate 286 MWh, resulting in a SSR of 25.46% and a SCR of 100%, attributed to the relatively limited availability of RES. Network losses account for 1.86% of the demand, equivalent to 23.69 MWh.

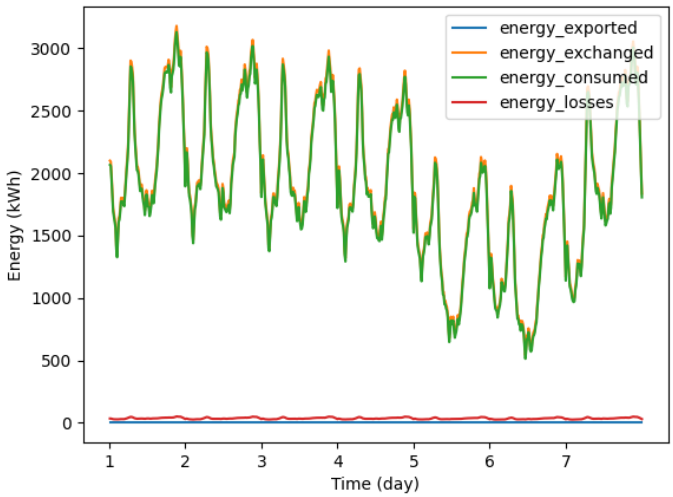


*Figure 151: Power flow analysis in an average week in the current state*

### 6.3.3 Technical benefits for the Distribution System Operator and economic benefits for the end users

First, as indicated in the methodology, the impact of the increase of the RES has been considered, with an increase in the load of 13.2% due to the electrification and the installation of additional 16 MW PV plants. Then, the overall generation capacity is 26 MW. For each scenario, it was chosen to create 30 RECs in the network under consideration. For the calculation of the incentive, Table 61 was considered.

*Table 62: Features of the 30 RECs*

| Name | PV size (kW) | Domestic load size (kW) | Industrial load size (kW) |
|---|---|---|---|
| CER 1 | 69 | 22 | 16 |
| CER 2 | 151 | | 72 |
| CER 3 | 85 | 64 | |
| CER 4 | 85 | 43 | |
| CER 5 | 71 | 20 | 27 |
| CER 6 | 71 | | 46 |
| CER 7 | 184 | 93 | |
| CER 8 | 185 | | 95 |
| CER 9 | 28 | 3 | 4 |
| CER 10 | 122 | | 61 |

| | | | |
|---|---|---|---|
| CER 11 | 186 | 81 | |
| CER 12 | 171 | 86 | |
| CER 13 | 122 | 28 | 27 |
| CER 14 | 112 | 22 | 39 |
| CER 15 | 68 | 34 | 9 |
| CER 16 | 68 | | 40 |
| CER 17 | 78 | 34 | 10 |
| CER 18 | 123 | 27 | 31 |
| CER 19 | 70 | 28 | 25 |
| CER 20 | 88 | 62 | |
| CER 21 | 111 | 84 | |
| CER 22 | 70 | 15 | 15 |
| CER 23 | 33 | | 21 |
| CER 24 | 90 | 82 | |
| CER 25 | 110 | 45 | 12 |
| CER 26 | 36 | 13 | |
| CER 27 | 56 | 51 | |
| CER 28 | 101 | 82 | |
| CER 29 | 136 | | 85 |
| CER 30 | 28 | 10 | |

Table 62 overviews the RECs composition. It's important to note that the load curves are assumed to be uniform for industrial and residential loads based on typical profiles for each load category, without variations for specific loads. Notably, the power generated by the PV systems often exceeds the installed load capacity. However, in terms of energy consumption, the load consumes an average of 215% more energy than what is produced by the PV systems. In the 2030 grid simulation, each node within the analyzed MV network hosts a PV generation plant, but only 30 of these plants form RECs. The selection of nodes for the RECs was made randomly within the network, with proximity and load capacity being key considerations.

A comparison with the current network reveals that by 2030, with PV production increased to 26 MW, power production during an average week reaches 745 MWh, while power demand amounts to 1272 MWh. This results in a SSR of 46.70% and a SCR of 81.26%. RPF registers at 139 MWh and network losses account for 23.73 MWh. Figure 152 illustrates the power trends during an average week, depicting the introduction of 16 MW of additional PV plants (only the new plants are represented by the orange curve, while the existing ones are "hidden" in the green curve). The energy exchanged with the national transmission grid generally indicates a positive sign, signifying energy absorption. Still, it becomes negative during the central daylight hours, indicating energy export due to the PV peak. Figure 153 illustrates the power trends and how consumption and generation do not align temporally for a single REC.

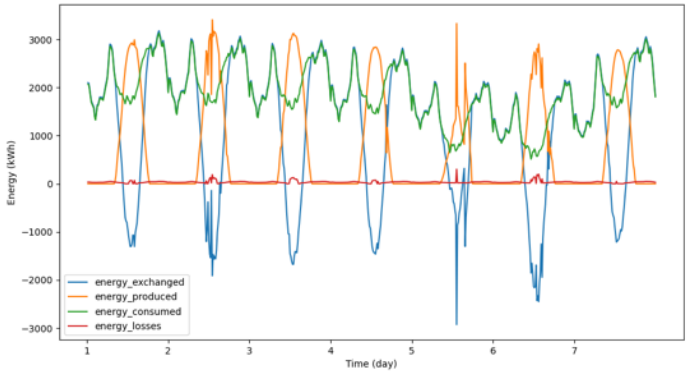


*Figure 152: Power flow analysis in an average week in the 2030 scenario for the whole DN, without considering the presence of DR*

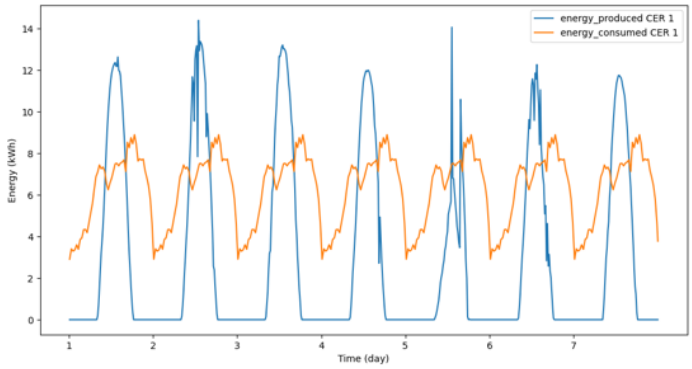


*Figure 153: Power flow analysis in an average week in the 2030 scenario for a REC, without considering the presence of DR*

Subsequently, an examination was conducted to assess the potential impacts of different management strategies for RECs, wherein users adjust their behavior to varying degrees, resulting in benefits for themselves (in economic terms) and the network—this adjustment aimed at reducing RPF and network losses. Three scenarios were considered, each involving a 10% load shifting percentage for 30, 60, or 90 minutes.

Figure 154 illustrates the trend of power flows within the network, as detected at the primary substation, when users engage in DR mechanisms, with 60% of the load participating. The curve bears similarities to the one presented in Figure 152, albeit with a slight shift in the load curve to align more closely with the generation curve. The advantages of this mechanism become more apparent in Table 63, where it is observed that the SCR and the SSR experience a modest increase as DR participation grows. Concurrently, network losses decrease proportionally.

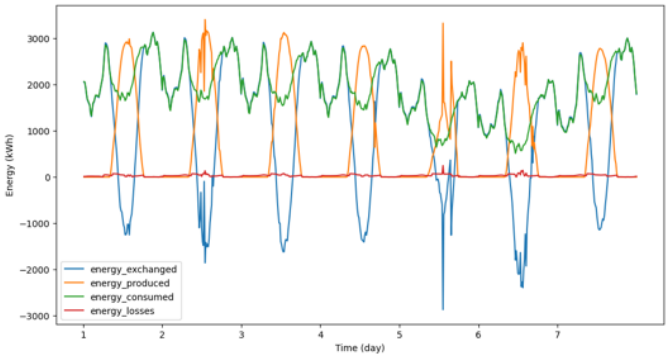


*Figure 154: Power flow analysis in an average week in the 2030 scenario for the whole DN, considering the presence of DR and adhesion of 60%.*

*Table 63: Impact on the distribution grid in the scenarios for an averaged week*

| Name | 2023 Current situation | 2030 without DR | 2030 with DR 30 min | 2030 with DR 60 min | 2030 with DR 90 min |
|---|---|---|---|---|---|
| E.prod. (MWh) | 286 | 745 | 745 | 745 | 745 |
| E.cons. (MWh) | 1123 | 1272 | 1272 | 1272 | 1272 |
| SCR (%) | 100.00 | 81.26 | 81.35 | 81.73 | 82.06 |
| SSR (%) | 22.10 | 46.70 | 46.74 | 47.03 | 47.29 |
| Grid losses (%) | 1.861 | 1.864 | 1.863 | 1.738 | 1.58 |
| RPF (MWh) | 0.00 | 139.59 | 138.95 | 136.13 | 133.63 |

In the present situation, the presence of PV plants is quite limited, contributing to only 22.1% of the energy consumed, and all of this energy is fully absorbed within the grid. In 2030 the scenario envisions sufficient production to cover 46.7% of the total load, achieving a SCR of 81.26%. Consequently, there's an increase in RPF, accompanied by a slight uptick in losses.

By effectively utilizing RECs, users can adjust their energy consumption patterns to align with RES production. The scenarios examined, involving load shifting for 30, 60, and 90 minutes, exclusively for REC users (which collectively represent an installed load of only 1.6 MW), demonstrate an enhancement in overall grid performance. This improvement results in a reduction in the SCR, an increase in the SSR, and a decrease in losses. Figure 155 compares the current load profile and the one that would be realized with the ability to shift up to one-tenth of the installed load's power within a 90-minute window. This illustration underscores a more pronounced alignment between load demand and RES generation.

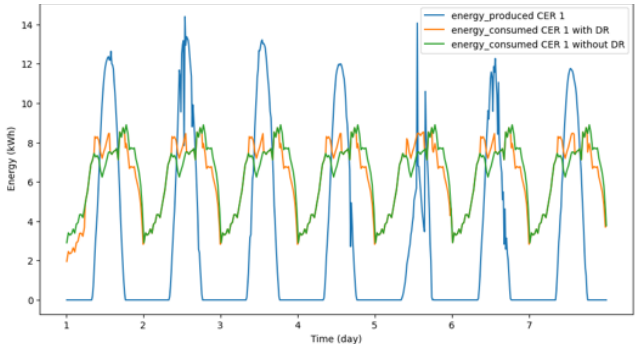


*Figure 155: Power flow analysis in an average week in the 2030 scenario for a REC, considering DR with a participation of 60% of the power demand*

*Table 64: Technical-economical results for each REC*

| Name | SCR without DR (%) | SCR DR-30 min (%) | SCR DR-60 min (%) | SCR DR-90 min (%) | Cash flow DR 60% (€/year) |
|---|---|---|---|---|---|
| **CER 1** | 75,01 | 75,42 | 77,23 | 78,64 | 3419 |
| **CER 2** | 78,91 | 79,17 | 81,96 | 84,38 | 9539 |
| **CER 3** | 78,34 | 78,86 | 82,8 | 86,24 | 3614 |
| **CER 4** | 60,80 | 61,70 | 63,94 | 66,18 | 3630 |
| **CER 5** | 87,84 | 87,85 | 90,49 | 92,19 | 3528 |
| **CER 6** | 94,27 | 94,26 | 96,71 | 98,38 | 3840 |
| **CER 7** | 59,22 | 60,12 | 62,48 | 64,75 | 8018 |
| **CER 8** | 82,71 | 82,86 | 85,06 | 87,22 | 11209 |
| **CER 9** | 43,05 | 43,82 | 45,07 | 46,28 | 1201 |
| **CER 10** | 81,60 | 81,79 | 83,93 | 86,03 | 7410 |
| **CER 11** | 53,31 | 54,24 | 56,38 | 58,38 | 7956 |
| **CER 12** | 58,93 | 59,84 | 62,19 | 64,45 | 7454 |
| **CER 13** | 66,31 | 66,87 | 68,85 | 70,5 | 6318 |
| **CER 14** | 78,99 | 79,27 | 81,56 | 83,55 | 6136 |
| **CER 15** | 69,94 | 79,58 | 73,24 | 76,00 | 2928 |
| **CER 16** | 66,79 | 67,54 | 70,06 | 72,62 | 2915 |
| **CER 17** | 71,35 | 71,88 | 74,1 | 76,01 | 3671 |
| **CER 18** | 68,94 | 69,56 | 72,19 | 74,41 | 6778 |
| **CER 19** | 82,45 | 82,74 | 85,42 | 88,01 | 4293 |
| **CER 20** | 75,03 | 75,55 | 78,53 | 81,10 | 3619 |
| **CER 21** | 78,15 | 78,61 | 81,78 | 84,34 | 4397 |
| **CER 22** | 64,66 | 65,27 | 67,18 | 68,75 | 3614 |
| **CER 23** | 70,56 | 71,29 | 74,07 | 76,74 | 1409 |
| **CER 24** | 87,39 | 87,53 | 91,16 | 94,25 | 3042 |
| **CER 25** | 67,25 | 67,83 | 70,09 | 71,98 | 5203 |
| **CER 26** | 46,63 | 47,61 | 49,37 | 50,83 | 1433 |
| **CER 27** | 87,62 | 87,75 | 91,37 | 94,97 | 1890 |
| **CER 28** | 81,69 | 82,06 | 85,45 | 88,41 | 3856 |
| **CER 29** | 67,90 | 68,57 | 71,27 | 73,56 | 5814 |
| **CER 30** | 48,22 | 50,90 | 60,62 | 67,02 | 1828 |

Table 64 shows, for each REC, the SCR is when no flexibility resources are used and when there is a shift of loads up to 30, 60, 90 minutes. On average, shifting loads can achieve SCRs 5.74% higher. In addition, the approximate operating cash flow was calculated, which includes the public incentive on shared energy within the REC, the purchase of electricity for consumers, and the sale of the energy produced by the PVs. The higher the SCR, the higher the income from the incentive, up to an average increase of 936€ per year.

# 7 Conclusion

The electricity distribution grid is undergoing a period of major change to meet the pressing demands for sustainability, security and resilience.
This PhD thesis addressed the fundamental challenge of increasing the flexibility of the electricity distribution network through a transversal approach, with particular emphasis on the case study of the Terni distribution network. The results obtained from the research underline the importance of advanced power grid management, particularly in a context where renewable and distributed energy resources are becoming increasingly widespread.

The main energy sectors involved in the research carried out and shown in this thesis concerned the electric mobility sector, power-to-gas, with a focus on hydrogen, and the spread of energy districts in the form of renewable energy communities.
The integration of flexibility resources is not separated from the development of enabling technologies, i.e. the emergence of algorithms, models and platforms that allow the management of sensors, IoT devices and the monitoring and control infrastructure.
Several innovative algorithms were presented, some of which are based on machine learning, such as consumption and generation forecasting, optimization of power flows in assets and predictive maintenance in power transformers.
The tools developed have been validated within the case study of the Terni distribution network, managed by ASM Terni, which is an innovation hub and in which numerous technologies are tested within numerous European projects.
Original researches were shown in the text, as reported in 17 papers published in journals or presented at international conferences.

In conclusion, the thesis demonstrates that increasing energy flexibility in the distribution networks is an achievable goal through a holistic approach that includes detailed local analysis, integration of distributed energy resources, advanced management strategies and active stakeholder involvement. This contribution is crucial to address future energy challenges and promote a transition to a sustainable and resilient energy system. The conclusions of this research are a step forward in the direction of smarter and more flexible power grids, ready to meet the challenges of the era of renewable energy and decentralization.

# 8 Published material


[I] A. Geri et al., "Distributed generation monitoring: a cost-effective Raspberry Pi-based device", 2022, 2nd International Conference on Innovative Research in Applied Science, Engineering and Technology (IRASET), 2022, pp. 1-6, doi: 10.1109/IRASET52964.2022.9737768.

[II] A. Geri, F.M. Gatta, M. Maccioni, J. Dell'Olmo, F. Carere, M.A. Bucarelli, P. Poursoltan, N. Hadifar, M. Paulucci, A Low-Cost Smart Monitoring Device for Demand-Side Response Campaigns. In: Yang, XS., Sherratt, S., Dey, N., Joshi, A. (eds) Proceedings of Seventh International Congress on Information and Communication Technology. Lecture Notes in Networks and Systems, vol 448. Springer, Singapore. https://doi.org/10.1007/978-981-19-1610-6_52

[III] E. Sarmas; S. Strompolas; V. Marinakis; F. Santori; M.A. Bucarelli; H. Doukas. An Incremental Learning Framework for Photovoltaic Production and Load Forecasting in Energy Microgrids. Electronics 2022, 11, 3962. https://doi.org/10.3390/electronics11233962

[IV] M. A. Bucarelli, A. Geri, M. Maccioni, F. M. Gatta, T. Bragatto and M. Paulucci, "Impact of ultrafast EV charging stations on the electrical distribution grid: a case study in Terni," 2023 IEEE International Conference on Environment and Electrical Engineering and 2023 IEEE Industrial and Commercial Power Systems Europe (EEEIC / I&CPS Europe), Madrid, Spain, 2023, pp. 1-6, doi: 10.1109/EEEIC/ICPSEurope57605.2023.10194699

[V] M. A. Bucarelli, A. Palmieri, A. Geri, F. M. Gatta, M. Maccioni and M. Paulucci, "Design of a New MV Network to Supply Electric Vehicle Charging Stations: A Real Case Study in Terni," 2022 IEEE International Conference on Environment and Electrical Engineering and 2022 IEEE Industrial and Commercial Power Systems Europe (EEEIC / I&CPS Europe), 2022, pp. 1-6, doi: 10.1109/EEEIC/ICPSEurope54979.2022.9854571

[VI] M. A. Bucarelli, F. Carere, T. Bragatto and F. Santori, "Exploiting RES for Hydrogen mobility: a new scenario for the company's fleet management", 2021 12th International Renewable Energy Congress (IREC), 2021, pp. 1-6, doi: 10.1109/IREC52758.2021.9624830

[VII] M. A. Bucarelli, F. Carere, T. Bragatto and F. Santori, "Moving towards self-consumption and self-sufficiency: COVID-19 impact in the city of Terni", 2021 IEEE International Conference on Environment and Electrical Engineering and 2021 IEEE Industrial and Commercial Power Systems Europe (EEEIC/I&CPS Europe), 2021, pp. 1-6, doi: 10.1109/EEEIC/ICPSEurope51590.2021.9584539.

[VIII] M.A. Bucarelli, M. Ghoreishi, F. Santori, Quantitative assessment of barriers to innovation in Smart Grids in Europe, AEIT 2023 International Annual Conference, Roma, Italy, 2023, in press.

[IX] M.A. Bucarelli, S. Cipolla, A. Natalini, F. Santori, V. Marinakis, E. Sarmas, M. Mammina. Application of Big Data analytics in the electrical sector: a real case study, The Fourteenth International Conference on Information, Intelligence, Systems and Applications (IISA 2023), University of Thessaly, Volos, Greece, 10-12 July 2023, in press.

[X] M.A. Bucarelli, T. Bragatto, A. Curci, M. Maccioni, J. Dell'Olmo, A. Geri, M. Paulucci, Technical–economic Impact of the Deployment of Renewable Energy Communities: An Italian Case Study, AEIT 2023 International Annual Conference, Roma, Italy, 2023, in press.

[XI] M.A. Bucarelli; M. Ghoreishi; F. Santori; J. Mira; J. Gorroñogoitia. Impact of an ML-Based Demand Response Mechanism on the Electrical Distribution Network: A Case Study in Terni. Electronics 2023, 12, 3948. https://doi.org/10.3390/electronics 12183948

[XII] M.A.Bucarelli, F.M. Gatta, D. Agostini, M. Maccioni, A. Geri, M. Paulucci, Investigating the impact of short-circuit faults in different neutral configurations: a real case study, AEIT 2023 International Annual Conference, Roma, Italy, 2023, in press.

[XIII] T. Bragatto, M. A. Bucarelli, F. Carere and F. Santori, "Transition to Electric Vehicles in a Company's fleet: Design and Policy on a Case Study," 2022 7th International Conference on Smart and Sustainable Technologies (SpliTech), 2022, pp. 1-6, doi: 10.23919/SpliTech55088.2022.9854223.

[XIV] T. Bragatto, M. A. Bucarelli, F. Carere, A. Cavadenti, F. Santori, "Optimization of an energy district for fuel cell electric vehicles: Cost scenarios of a real case study on a waste and recycling fleet", International Journal of Hydrogen Energy, 2022, ISSN 0360-3199, https://doi.org/10.1016/j.ijhydene.2022.08.114

[XV] T. Bragatto, M. A. Bucarelli, M. Ghoreishi and F. Santori, "Optimizing EV Company Fleet Management in an Energy District," 2023 AEIT International Conference on Electrical and Electronic Technologies for Automotive (AEIT AUTOMOTIVE), Modena, Italy, 2023, pp. 1-6, doi: 10.23919/AEITAUTOMOTIVE58986.2023.10217236.

[XVI] T. Bragatto, M.A. Bucarelli, F. Carere, M. Cresta, F.M. Gatta, A. Geri, M. Maccioni, M. Paulucci, P.

Poursoltan, F. Santori, Near real-time analysis of active distribution networks in a Digital Twin framework: A real case study, Sustainable Energy, Grids and Networks, Volume 35, 2023, 101128, ISSN 2352-4677, https://doi.org/10.1016/j.segan.2023.101128.

[XVII] T. Bragatto, M.A. Bucarelli, M.S. Bucarelli, F. Carere, A. Geri, M. Maccioni, False Data Injection Impact on High RES Power Systems with Centralized Voltage Regulation Architecture. Sensors. 2023; 23(5):2557. https://doi.org/10.3390/s23052557

*Publications - Deliverables*

I have also co-authored the deliverables of the European Projects in which ASM Terni has participated and which are cited in this work.

# References


[1] 2012/148/EU: Commission Recommendation of 9 March 2012 on preparations for the roll-out of smart metering systems. Available online at: https://op.europa.eu/en/publication-detail/-/publication/a5daa8c6-8f11-4e5e-9634-3f224af571a6/language-en

[2] A report prepared by the Reliability Test System Task Force of the Application of Probability Methods Subcommittee, "IEEE Reliability Test System," IEEE Trans. Power Apparatus and Systems, Vol. PAS-98, No. 6, pp. 2047-2054, Nov. 1979.

[3] A. Agga, A. Abbou, M. Labbadi, Y. El Houm, I. H. O. Ali, Cnn-lstm: An efficient hybrid deep learning architecture for predicting short-term photovoltaic power production, Electric Power Systems Research 208 (2022) 107908.

[4] A. Bouaichi, A. Alami Merrouni, C. Hajjaj, H. Zitouni, A. Ghennioui, A. El Amrani, and C. Messaoudi, "In-situ inspection and measurement of degradation mechanisms for crystalline and thin film PV systems under harsh climatic conditions", Energy Procedia, Volume 157, 2019, pp 1210-1219,

[5] A. Cataliotti, V. Cosentino, D. di Cara, and G. Tinè, "LV Measurement Device Placement for Load Flow Analysis in MV Smart Grids," IEEE Transactions on Instrumentation and Measurement, vol. 65, no. 5, 2016. Available: https://ieeexplore.ieee.org/document/7321815/.

[6] A. Chapman, et al. A review of four case studies assessing the potential for hydrogen penetration of the future energy system, International Journal of Hydrogen Energy, Volume 44, Issue 13, 2019, pp. 6371-6382, ISSN 0360-3199, https://doi.org/10.1016/j.ijhydene.2019.01.168.

[7] A. Dutta, S. Ganguly and C. Kumar, "MPC-Based Coordinated Voltage Control in Active Distribution Networks Incorporating CVR and DR," in IEEE Transactions on Industry Applications, vol. 58, no. 4, pp. 4309-4318, July-Aug. 2022, doi: 10.1109/TIA.2022.3163108.

[8] A. Fuller, Z. Fan, C. Day, and C. Barlow, "Digital Twin: Enabling Technologies, Challenges and Open Research," IEEE Access, vol. 8, 2020, doi: 10.1109/ACCESS.2020.2998358.

[9] A. Ghosal and M. Conti, "Key Management Systems for Smart Grid Advanced Metering Infrastructure: A Survey," IEEE Commun. Surv. Tutorials, vol. 21, no. 3, pp. 2831–2848, Jul. 2019.

[10] A. Hernandez-Matheus, et al., A systematic review of machine learning techniques related to local energy communities, Renewable and Sustainable Energy Reviews, Volume 170, 2022, 112651, ISSN 1364-0321, https://doi.org/10.1016/j.rser.2022.112651.

[11] A. Mendes et al. (2012). Barriers to Social Innovation. A deliverable of the project: "The theoretical, empirical and policy foundations for building social innovation in Europe" (TEPSIE).

[12] A. Monti, C. Muscas, and F. Ponci, Phasor Measurement Units and Wide Area Monitoring Systems: From the Sensors to the System. Elsevier Inc., 2016.

[13] A. Mustafa, B. Poudel, A. Bidram and H. Modares, "Detection and Mitigation of Data Manipulation Attacks in AC Microgrids," in IEEE Transactions on Smart Grid, vol. 11, no. 3, pp. 2588-2603, May 2020, DOI: 10.1109/TSG.2019.2958014.

[14] A. Navarro, L. F. Ochoa, and D. Randles, "Monte Carlo-based assessment of PV impacts on real UK low voltage networks," IEEE Power Energy Soc. Gen. Meet., 2013.

[15] A. Noorwali, R. Rao, and A. Shami, "Modeling and delay analysis of wide area network in smart grid communications," 2016 4th IEEE Int. Conf. Smart Energy Grid Eng. SEGE 2016, pp. 347–352, Oct. 2016.

[16] A. Piantini, Analysis of the effectiveness of shield wires in mitigating lightning-induced voltages on power distribution lines, Electric Power Systems Research, Volume 159, 2018, Pages 9-16, ISSN 0378-7796, https://doi.org/10.1016/j.epsr.2017.08.022.

[17] A. S. Musleh, G. Chen and Z. Y. Dong, "A Survey on the Detection Algorithms for False Data Injection Attacks in Smart Grids," in IEEE Transactions on Smart Grid, vol. 11, no. 3, pp. 2218-2234, May 2020, doi: 10.1109/TSG.2019.2949998.

[18] A. Saad, S. Faddel, T. Youssef, and O. A. Mohammed, "On the Implementation of IoT-Based Digital Twin for Networked Microgrids Resiliency against Cyber Attacks," IEEE Trans Smart Grid, vol. 11, no. 6, 2020, doi: 10.1109/TSG.2020.3000958.

[19] A. Teixeira, G. Dán, H. Sandberg, R. Berthier, R. B. Bobba and A. Valdes, "Security of smart distribution grids: Data integrity attacks on integrated volt/VAR control and countermeasures," 2014 American Control Conference, 2014, pp. 4372-4378, DOI: 10.1109/ACC.2014.6859265.

[20] ABB Electric Vehicle Charging Infrastructure Catalog. Available online at: https://new.abb.com/ev-charging?_ga=2.195974188.1856219891.1643034143-853351252.1643034143&_gl=1*fw3r62*_ga*ODUzMzUxMjUyLjE2NDMwMzQxNDM.*_ga_46ZFBRSZNM*MTY0MzAzNDE0Mi4xLjAuMTY0MzAzNDE0Mi4w

[21] ABB Secondary Substations Catalog. Available online at: https://library.e.abb.com/public/4da8d0dee20f40a99ed6eb87e9286858/UniPack-G%20Catalog%20Rev%20C.pdf

[22] ABB, ABB announces transition to all-electric vehicle fleet in the UK, available online at: https://new.abb.com/news/detail/67386/abb-announces-transition-to-all-electric-vehicle-fleet-in-the-uk

[23] Abbas, Ahmar. Grid Computing: A Practical Guide to Technology and Applications, Charles River Media. Inc., Hingham, MA, 2004.

[24] Abdulgader Alsharif, Chee Wei Tan, Razman Ayop, Abdulhakeem Dobi, Kwan Yiew Lau, A comprehensive review of energy management strategy in Vehicle-to-Grid technology integrated with renewable energy sources, Sustainable Energy Technologies and Assessments, Volume 47, 2021, 101439, ISSN 2213-1388, https://doi.org/10.1016/j.seta.2021.101439.

[25] Abhishek Tiwari, Naran M. Pindoriya, Automated Demand Response in Smart Distribution Grid: A Review on Metering Infrastructure, Communication Technology and Optimization Models, Electric Power Systems Research, Volume 206, 2022, 107835, ISSN 0378-7796, https://doi.org/10.1016/j.epsr.2022.107835.

[26] Adaptive Charging Network Dataset. Available online at: https://ev.caltech.edu/dataset

[27] AFTER Method from Research on the Energy System – RSE SpA, Resilience in the Electrical System, Editrice Alkes, Milan, 2017, pp 86-94

[28] Ahmed Fawzy Gad, "PyGAD: An Open-Source Python Library for Building the Genetic Algorithm and Training Machine Learning Algorithms pygad.readigital twinhedocs.io," 2020

[29] Akifumi Yamanaka, Kazuyuki Ishimoto, Influence of a shield wire flashover on the indirect lightning performance assessment of distribution lines, Electric Power Systems Research, Volume 223, 2023, 109614, ISSN 0378-7796, https://doi.org/10.1016/j.epsr.2023.109614.

[30] Alan Jenn, Jake Highleyman, Distribution Grid Impacts of Electric Vehicles: A California Case Study, iScience, 2021, 103686, ISSN 2589-0042, https://doi.org/10.1016/j.isci.2021.103686

[31] Alavi F. et al., Fuel cell cars in a microgrid for synergies between hydrogen and electricity networks, Applied Energy, Volume 192, 2017, p. 296-304, ISSN 0306-2619, https://doi.org/10.1016/j.apenergy.2016.10.084.

[32] Ali-Mohammad Hariri, Maryam A. Hejazi, Hamed Hashemi-Dezaki, Investigation of impacts of plug-in hybrid electric vehicles' stochastic characteristics modelling on smart grid reliability under different charging scenarios, Journal of Cleaner Production, Volume 287, 2021, 125500, ISSN 0959-6526, https://doi.org/10.1016/j.jclepro.2020. 125500

[33] Amir Saman Godazi Langeroudi, Majid Sedaghat, Samaneh Pirpoor, Ramin Fotouhi, Mohamad Amin Ghasemi, Risk-based optimal operation of power, heat and hydrogen-based microgrid considering a plug-in electric vehicle, International Journal of Hydrogen Energy, Volume 46, Issue 58, 2021, Pages 30031-30047, ISSN 0360-3199, https://doi.org/10.1016/j.ijhydene.2021.06.062.

[34] Ana Cabrera-Tobar, Eduard Bullich-Massagué, Mònica Aragüés-Peñalba, Oriol Gomis-Bellmunt, Capability curve analysis of photovoltaic generation systems, Solar Energy, Volume 140, 2016, pp. 255-264, ISSN 0038-092X, https://doi.org/10.1016/j.solener.2016.11.014.

[35] Andrew Brown, "Sustainable Mobility," in Green Technologies and the Mobility Industry, SAE, 2011, pp.145-145.

[36] Archana. Modelling Barriers for Smart Grid Technology Acceptance in India. Process Integr. Optimization Sustain, 2022.

[37] Arera, electrical prices and tariffs, available online at: https://www.arera.it/it/prezzi.htm

[38] ASM Terni website, available online at: https://www.asmterni.it

[39] Atos, Atos commits to all-electric company car fleet by 2024. Available online at: https://atos.net/en/2021/press-release/general-press-releases_2021_03_31/atos-commits-to-all-electric-company-car-fleet-by-2024

[40] ATPdraw, available online at: https://www.atpdraw.net

[41] B. Parrish et al., On demand: Can DR live up to expectations in managing electricity systems?, Energy Research & Social Science, Volume 51, 2019, Pages 107-118, ISSN 2214-6296, https://doi.org/10.1016/j.erss.2018.11.018.

[42] B. Parrish, P. Heptonstall, R. Gross, B. K. Sovacool, A systematic review of motivations, enablers and barriers for consumer engagement with residential demand response, Energy Policy, Volume 138, 2020, 111221, ISSN 0301-4215, https://doi.org/10.1016/j.enpol.2019.111221.

[43] Balijepalli, VSK Murthy, et al. SmartGrid initiatives and power market in India. In: IEEE PES General Meeting. IEEE, 2010. p. 1-7.

[44] Barth, M., Todd, M., 1999. Simulation model performance analysis of a multiple station shared vehicle system. Transport. Res. C Emerg. Technol. 7 (4), 237–259

[45] BD4NRG analytic model, http://bd4nrg.epu.ntua.gr:8088/.

[46] BD4NRG analytics toolbox, available online at: https://analyticstoolbox.bd4nrg.eu/

[47] BD4NRG: Big Data for Next Generation Energy, European Project, available online at: https://www.bd4nrg.eu

[48] Bifet, A.; Gavalda, R.; Holmes, G.; Pfahringer, B. Machine Learning for Data Streams: With Practical Examples in MOA; MIT Press: Cambridge, MA, USA, 2018.

[49] BloombergNEF, Hydrogen Economy Outlook Key messages, 20/03/2020, Available online at: https://data.bloomberglp.com/professional/sites/24/BNEF-Hydrogen-Economy-Outlook-Key-Messages-30-Mar-2020.pdf

[50] Borou S, et al. Bardisbanian H Enhanced IoT federated deep learning/reinforcement ML. IoT NGIN report. https://iot-ngin.eu/wp-content/uploads/2023/01/IOT-NGIN_D3.3_V1.0_PENDING_EC_APPROVAL.pdf

[51] Bourlard, H.; Kamp, Y. Auto-association by multilayer perceptrons and singular value decomposition. Biol. Cybern. 1988, 59, 291–294.

[52] BRIGHT: Boosting DR through increased communIty-level consumer engaGement by combining Data-driven and blockcHain technology Tools with social science approaches and multi- value service design European Project, available online at: https://www.brightproject.eu

[53] Buitinck, L.; Louppe, G.; Blondel, M.; Pedregosa, F.; Mueller, A.; Grisel, O.; Niculae, V.; Prettenhofer, P.; Gramfort, A.; Grobler, J.; et al. API design for machine learning software: Experiences from the scikit-learn project. In Proceedings of the ECML PKDD Workshop:

Languages for Data Mining and Machine Learning, Prague, Czech Republic, 23–27 September 2013; pp. 108–122.

[54] C. Antal et al., "Blockchain based decentralized local energy flexibility market," Energy Reports, vol. 7, 2021, doi: 10.1016/j.egyr.2021.08.118.

[55] C. Cameron, C. Patsios, P. C. Taylor and Z. Pourmirza, "Using Self-Organizing Architectures to Mitigate the Impacts of Denial-of-Service Attacks on Voltage Control Schemes," in IEEE Transactions on Smart Grid, vol. 10, no. 3, pp. 3010-3019, May 2019, DOI: 10.1109/TSG.2018.2817046.

[56] C. Gungor et al., "A Survey on Smart Grid Potential Applications and Communication Requirements," in IEEE Transactions on Industrial Informatics, vol. 9, no. 1, pp. 28-42, Feb. 2013, doi: 10.1109/TII.2012.2218253.

[57] C. Nemes, M. Adochitei, F. Munteanu, A. Ciobanu, and O. Neagu, "Self-consumption enhancement on a low-voltage grid-connected photovoltaic system," 2018 IEEE International Energy Conference (ENERGYCON), 2018, pp. 1-6.

[58] C. S. Holling, Resilience and stability of ecological systems, Ecology, vol. 4, no. 1, pp. 1–23, 1973

[59] Carrie Hampel, CHAdeMO 3.0 supports charging with "over 500 kW", Electrive.com, 2020. Available online at: https://www.electrive.com/2020/04/28/chademo-3-0-supports-charging-with-over-500-kw/

[60] Chai KH, Yeo C., Overcoming energy efficiency barriers through systems approach - A conceptual framework. Energy Policy 2012;46:460–72. doi:10.1016/j.enpol.2012.04.012.

[61] Chandran, Lekshmi R., et al. A review on status monitoring techniques of transformer and a case study on loss of life calculation of distribution transformers. Materials Today: Proceedings, 2021, 46: 4659-4666.

[62] Chaube, A.; Chapman, A.; Shigetomi, Y.; Huff, K.; Stubbins, J. The Role of Hydrogen in Achieving Long Term Japanese Energy System Goals. Energies 2020, 13, 4539.

[63] Chris Hardesty, Average Miles Driven Per Year: Why It Is Important, available online at https://www.kbb.com/car-advice/average-miles-driven-per-year/

[64] Christensen A. Assessment of Hydrogen Production Costs from Electrolysis: the United States and Europe, 04/06/2020, Available online at https://theicct.org/publications/assessment-hydrogen-production-costs-electrolysis-united-states-and-europe

[65] Claudia Antal et al., Blockchain-based decentralized local energy flexibility market, Energy Reports, Volume 7, 2021, Pages 5269-5288, ISSN 2352-4847, https://doi.org/10.1016/j.egyr.2021.08.118.

[66] CO2 emissions from cars: facts and figures (infographics), 18/04/2019, available online at https://www.europarl.europa.eu/news/en/headlines/society/20190313STO31218/co2-emissions-from-cars-facts-and-figures-infographics

[67] Conejo, A.J.; Baringo, L. Power System Operations; Springer International Publishing AG: Cham, Switzerland, 2018

[68] Cybersecurity considerations for electrical distribution systems", Eaton, November 2016, available online:https://www.eaton.com/ecm/idcplg?IdcService=GET_FILE&allowInterrupt=1&RevisionSelectionMethod=LatestReleased&Rendition=Primary&dDocName=WP152002EN.

[69] D. A. Reed, K. C. Kapur, and R. D. Christie, Methodology for assessing the resilience of networked infrastructure, IEEE Syst. J., vol. 3, no. 2, pp. 174–180, Jun. 2009.

[70] D. E. Rumelhart, G. E. Hinton and R. J. Williams, "Learning internal representations by error propagation," San Diego, California: Institute for Cognitive Science, University of California., 1985.

[71] D. K. Molzahn and J. Wang, ''Detection and characterization of intrusions to network parameter data in electric power systems,'' IEEE Trans. Smart Grid, vol. 10, no. 4, pp. 3919–3928, Jul. 2019.

[72] D. P. Kingma and J. Lei Ba, "ADAM: A method for stochastic optimization," 2014.

[73] D'Allegro, CNBC https://www.cnbc.com/2019/02/21/musk-calls-hydrogen-fuel-cells-stupid-but-tech-may-threaten-tesla.html

[74] David Bromberg, Inverter Efficiency Curve, Available online at: https://help.aurorasolar.com/hc/en-us/articles/115001389928-Inverter-Efficiency-Curves

[75] DC charging cables for fast charging stations, Phoenix Contact. Available online at: https://www.phoenixcontact.com/en-us/products/charging-technology-for-e-mobility/dc-charging-cables

[76] DC UltraFast Charger, Energcharge. Available online at: https://enercharge.at/wp-content/uploads/2020/08/TD_UFC_2020-0709v8-ENG.pdf

[77] E. Bionda, A. Maldarella, F. Soldan, G. Paludetto and F. Belloni, "Covid-19 and electricity demand: focus on Milan and Brescia distribution grids," 2020 AEIT International Annual Conference (AEIT), 2020, pp. 1-6, doi: 10.23919/AEIT50178.2020.9241083.

[78] E. Ferko, A. Bucaioni, and M. Behnam, "Architecting Digital Twins," IEEE Access, vol. 10, pp. 50335–50350, 2022, doi: 10.1109/ACCESS.2022.3172964.

[79] E. Veldman and R. A. Verzijlbergh, "Distribution Grid Impacts of Smart Electric Vehicle Charging From Different Perspectives," in IEEE Transactions on Smart Grid, vol. 6, no. 1, pp. 333-342, Jan. 2015, DOI: 10.1109/TSG.2014.2355494

[80] EC, Study on Tariff Design for Distribution Networks, Directorate-General for Energy, European Commission, Directorate B – Internal Energy Market, Brus-sels, 2015.

[81] Eklas Hossain, Shidhartho Roy, Naeem Mohammad, Nafiu Nawar, Debopriya Roy Dipta, Metrics and enhancement strategies for grid resilience and reliability during natural disasters, Applied Energy, Volume 290, 2021, 116709, ISSN 0306-2619, https://doi.org/10.1016/j.apenergy.2021.116709.

[82] Elagtal, Ibrahem A. et al.. Smart Grid Technology for Better Integration of Renewable Energy Resources. Solar Energy, 10: 1.

[83] Electric vehicle database, available online at https://ev-database.org

[84] Empowering the digitalisation of Energy transition, available online at: https://www.eebus.org

[85] Energy Policies of IEA Countries: Italy 2016 Review, available online at: https://www.iea.org/reports/energy-policies-of-iea-countries-italy-2016-review

[86] EU Commission. A Hydrogen Strategy for a Climate Neutral Europe. 2020. Available online: https://ec.europa.eu/energy/sites/ener/files/hydrogen_strategy.pdf

[87] Euronews, EU wants to tax aviation fuel and phase out polluting cars by 2035, Available online at: www.euronews.com/2021/07/14/carbon-tax-alternative-fuels-brussels-unveils-drastic-measures-to-slash-emissions-by-2030

[88] European Commission, 2011. Biodiversity strategy. http://ec.europa.eu/environment/nature/biodiversity/strategy/index_en.htm

[89] European Environmental Agency, Towards clean and smart mobility: Transport and environment in Europe, 2016, DOI: 10.2800/090074, ISBN 978-92-9213-739-7

[90] F. Carere et al., "Electric Vehicle Charging Rescheduling to Mitigate Local Congestions in the Distribution System," 2021 IEEE Madrid PowerTech, 2021, pp. 1-6, DOI: 10.1109/PowerTech46648.2021.9494882

[91] F. Carere et al., "Flexibility - enabling technologies using electric vehicles," 2020 EEEIC / I&CPS Europe, 2020, pp. 1-6, doi: 10.1109/EEEIC/ICPSEurope49358.2020.9160781

[92] F. Carere, T. Bragatto and F. Santori, "A Distribution Network during the 2020 COVID-19 Pandemic," 2020 AEIT International Annual Conference (AEIT), 2020, pp. 1-6.

[93] F. Ceglia, P. Esposito, E. Marrasso, and M. Sasso, "From smart energy community to smart energy municipalities: Literature review, agendas and pathways," 2020.

[94] F. M. Gatta et al., "Electric Mobility Hosting Capacity assessment in Terni distribution network," 2021 EEEIC / I&CPS Europe, 2021, pp. 1-6, DOI: 10.1109/EEEIC/ICPSEurope51590.2021.9584815.

[95] F. Tao, M. Zhang, Y. Liu, and A. Y. C. Nee, "Digital twin driven prognostics and health management for complex equipment," CIRP Annals, vol. 67, no. 1, 2018, doi: 10.1016/j.cirp.2018.04.055.

[96] F. Tossani, F. Napolitano, A. Borghetti, C.A. Nucci, A. Piantini, Yun-Su Kim, Sun-Kyu Choi, Influence of the presence of grounded wires on the lightning performance of a medium-voltage line, Electric Power Systems Research, Volume 196, 2021, 107206, ISSN 0378-7796, https://doi.org/10.1016/j.epsr.2021.107206.

[97] F. Ünal, A. Almalaq, S. Ekici and P. Glauner, "Big Data-Driven Detection of False Data Injection Attacks in Smart Meters," in IEEE Access, vol. 9, pp. 144313-144326, 2021, doi: 10.1109/ACCESS.2021.3122009.

[98] F. Ye, Y. Qian, and R. Q. Hu, "Energy efficient self-sustaining wireless neighborhood area network design for smart grid," IEEE Trans. Smart Grid, vol. 6, no. 1, pp. 220–229, Jan. 2015.

[99] F. Zavoda, C. Abbey, Y. Brissette, and R. Lemire, "Universal IED for distribution smart grids," IET Conf. Publ., vol. 2013, no. 615 CP, 2013.

[100] F.M. Gatta, A. Geri, S. Lauria, M. Maccioni, Improving high-voltage transmission system adequacy under contingency by genetic algorithms, Electric Power Systems Research, Volume 79, Issue 1, 2009, Pages 201-209, ISSN 0378-7796, https://doi.org/10.1016/j.epsr.2008.05.013.

[101] Fagan J et al. From policy to implementation – the race to build a smart grid. Pillsbury Winthrop Shaw Pittman LLP 2009 (May 7).

[102] FAN, Zhong, et al. Smart grid communications: Overview of research challenges, solutions, and standardization activities. IEEE Communications Surveys & Tutorials, 2012, 15.1: 21-38.

[103] Farahani S. et al. Hydrogen-based integrated energy and mobility system for a real-life office environment, Applied Energy, Volume 264, 2020, 114695, ISSN 0306-2619, https://doi.org/10.1016/j.apenergy.2020.114695.

[104] Faran Razi, Ibrahim Dincer, Challenges, opportunities and future directions in hydrogen sector development in Canada, International Journal of Hydrogen Energy, Volume 47, Issue 15, 2022, Pages 9083-9102, ISSN 0360-3199, https://doi.org/10.1016/j.ijhydene.2022.01.014.

[105] FastAPI, [Online]. Available: https://fastapi.tiangolo.com.

[106] Fazeli R et al., Recognizing the role of uncertainties in the transition to renewable hydrogen, International Journal of Hydrogen Energy, https://doi.org/10.1016/j.ijhydene.2022.06.122

[107] Federal Pacific, Understanding Transformer Noise, available online at: https://federalpacific.com/wp-content/uploads/2019/01/2016-FP-Understanding-Transformer-Noise.pdf

[108] Fragiacomo P., Genovese M., Technical-economic analysis of a hydrogen production facility for power-to-gas and hydrogen mobility under different renewable sources in Southern Italy, Energy Conversion and Management, Volume 223, 2020, 113332, ISSN 0196-8904, https://doi.org/10.1016/j.enconman.2020.113332.

[109] Franchek, Michael A.; Woodcock, David J. Life-Cycle considerations of loading transformers above nameplate rating. In: 65th Annual International Conference of Doble Clients. 1998.

[110] Friedman, H., & Sreedharan, P. (2010). Wiring the smart grid for energy savings: mechanisms and policy considerations. ACEEE Summer Study Energy Eff Build.

[111] G. Dileep, A survey on smart grid technologies and applications, Renewable Energy, Volume 146, 2020, Pages 2589-2625, ISSN 0960-1481, https://doi.org/10.1016/j.renene.2019.08.092.

[112] G. Liang, J. Zhao, F. Luo, S. R. Weller and Z. Y. Dong, "A Review of False Data Injection Attacks Against Modern Power Systems," in IEEE Transactions on Smart Grid, vol. 8, no. 4, pp. 1630-1638, July 2017, doi: 10.1109/TSG.2015.2495133.

[113] G. Morales-España, R. Martínez-Gordón, and J. Sijm, "Classifying and modelling demand response in power systems," Energy, vol. 242, 2022, doi: 10.1016/j.energy.2021.122544.

[114] G. Napoli et al., Freight distribution with electric vehicles: A case study in Sicily. Delivery van development, Transportation Engineering, Volume 3, 2021.

[115] Gardner, M.W.; Dorling, S. Artificial neural networks (the multilayer perceptron)—A review of applications in the atmospheric sciences. Atmos. Environ. 1998, 32, 2627–2636.

[116] George, D.K., Xia, C.H., 2011. Fleet-sizing and service availability for a vehicle rental system via closed queueing networks. Eur. J. Oper. Res. 211 (1), 198–207

[117] Girgis, Ramsis S.; Bernesjo, Mats; Anger, Jan. Comprehensive analysis of load noise of power transformers. In: 2009 IEEE Power & Energy Society General Meeting. IEEE, 2009. p. 1-7.

[118] Global Solar Atlas website, available online at: https://globalsolaratlas.info/map

[119] Grafana. Available online at: https://grafana.com/.

[120] Grids, Smart; Vision, E. T. P. strategy for Europe's electricity networks of the future. European Commission, 2006.

[121] GSE, "Rapporto statistico Solare Fotovoltaico 2019 " (in Italian, Solar Photovoltaic Statistical Report 2019), June 2020. Available online on https://www.gse.it/documenti_site/Documenti%20GSE/Rapporti%20statistici/Solare%20Fotovoltaico%20-%20Rapporto%20Statistico%202019.pdf

[122] GSE, Gruppi di autoconsumatori di energia rinnovabile che agiscono collettivamente e comunità di energia rinnovabile (in Italian, Self-consuming renewable energy groups acting collectively and renewable energy communities), Available online at: https://www.gse.it/servizi-per-te/autoconsumo/gruppi-di-autoconsumatori-e-comunita-di-energia-rinnovabile/documenti

[123] Guille, C., Gross, G., 2009. A conceptual framework for the vehicle-to-grid (V2G) implementation. Energy Pol. 37, 4379–4390

[124] Gurobi, Gurobi Optimization, LLC. Gurobi Optimizer Reference Manual, 2023, https://www.gurobi.com

[125] H. A. Park, G. Byeon, W. Son, H. C. Jo, J. Kim, and S. Kim, "Digital twin for operation of microgrid: Optimal scheduling in virtual space of digital twin," Energies (Basel), vol. 13, no. 20, 2020, doi: 10.3390/en13205504.

[126] H. Awad and M. Gül, "Optimisation of community shared solar application in energy efficient communities," 2018.

[127] H. Golpˆıra, S. Bahramara, Internet-of-things-based optimal smart city energy management considering shiftable loads and energy storage, Journal of Cleaner Production 264 (2020) 121620.

[128] H. R. E. H. Bouchekara, Y. Latreche, K. Naidu, H. Mokhlis, W. M. Dahalan, M. S. Javaid, "Comprehensive Review of Radial Distribution Test Systems for Power System Distribution Education and Research", Resource-Efficient Technologies, 3(3), pp. 1—12, 2019. DOI: 10.18799/24056537/2019/3/196 D-19, H.13

[129] H. S. Bidgoli and T. Van Cutsem, "Combined Local and Centralized Voltage Control in Active Distribution Networks," in IEEE Transactions on Power Systems, vol. 33, no. 2, pp. 1374-1384, March 2018, DOI: 10.1109/TPWRS.2017.2716407.

[130] H. Wang, K. A. Alattas, A. Mohammadzadeh, M. H. Sabzalian, A. A. Aly, A. Mosavi, Comprehensive review of load forecasting with emphasis on intelligent computing approaches, Energy Reports 8 (2022) 13189–13198.

[131] He, J.; Mao, R.; Shao, Z.; Zhu, F. Incremental Learning in Online Scenario. In Proceedings of the IEEE/CVF Conference on Computer Vision and Pattern Recognition (CVPR), Seattle, WA, USA, 16–19 June 2020.

[132] Hedegaard K, Ravn H, Juul N, Meibom P. Effects of electric vehicles on power systems in Northern Europe. Energy 2012;48:356–68. https://doi.org/10.1016/j.energy.2012.06.012

[133] Hoang Nguyen, Cishen Zhang, Md Apel Mahmud, Smart Charging and Discharging of Electric Vehicles to Support Grid with High Penetration of Renewable Energy, IFAC Proceedings Volumes, Volume 47, Issue 3, 2014, Pages 8604-8609, ISSN 1474-6670, ISBN 9783902823625, https://doi.org/10.3182/20140824-6-ZA-1003.02109

[134] Horizon 2020 European Research and innovation Funding programmes. Available online at: https://research-and-innovation.ec.europa.eu/funding/funding-opportunities/funding-programmes-and-open-calls/horizon-2020_en

[135] Horizon Europe Research and innovation Funding programmes. Available online at: https://research-and-innovation.ec.europa.eu/funding/funding-opportunities/funding-programmes-and-open-calls/horizon-europe_en

[136] Hu, Junjie & Morais, Hugo & Sousa, Tiago & Lind, Morten. (2016). Electric vehicle fleet management in smart grids: A review of services, optimization and control aspects. Renewable and Sustainable Energy Reviews. 56. 1207-1226. 10.1016/j.rser.2015.12.014.

[137] Hussain Shareef, Md. Mainul Islam, Azah Mohamed, A review of the stage-of-the-art charging technologies, placement methodologies, and impacts of electric vehicles, Renewable and

Sustainable Energy Reviews, Volume 64, 2016, Pages 403-420, ISSN 1364-0321, https://doi.org/10.1016/j.rser.2016.06.033.

[138] Hydrogen in the EU's Economic Recovery Plans, Hydrogen Europe, Available online at: https://www.hydrogeneurope.eu/wp-content/uploads/2021/07/Hydrogen-Europe_EU-Recovery-Plan-Analysis_FINAL.pdf

[139] IBM ILOG CPLEX Optimization Studio V12.10, documentation available online at: https://www.ibm.com/it-it/products/ilog-cplex-optimization-studio.

[140] IBRAHIM, K., et al. Reliability calculations based on an enhanced transformer life expectancy model. Ain Shams Engineering Journal, 2022, 13.4: 101661.

[141] IEA (2021), Global EV Outlook 2021, IEA, Paris https://www.iea.org/reports/global-ev-outlook-2021

[142] IEA (2023), Global Hydrogen Review 2023, IEA, available online at: https://www.iea.org/reports/global-hydrogen-review-2023

[143] IEEE guide for loading mineral-oil-immersed transformers and step-voltage regulators. IEEE Std. C57.91 (Revision of IEEE Std C57.91-1995); 2011. p. 1– 123.

[144] Igor Borges de Oliveira Chagas, Marcelo Aroca Tomim, Co-simulation applied to power systems with high penetration of distributed energy resources, Electric Power Systems Research, Volume 212, 2022, 108413, ISSN 0378-7796, https://doi.org/10.1016/j.epsr.2022.108413.

[145] I-NERGY: Artificial Intelligence for Next Generation Energy European project, available online at: https://i-nergy.eu

[146] Integrated National Energy and Climate Plan, MISE, 2020. Available online at: https://www.mise.gov.it/images/stories/ documenti/PNIEC_finale_17012020.pdf

[147] Ioannis Antonopoulos, Valentin Robu, Benoit Couraud, Desen Kirli, Sonam Norbu, Aristides Kiprakis, David Flynn, Sergio Elizondo-Gonzalez, Steve Wattam, Artificial intelligence and machine learning approaches to energy demand-side response: A systematic review, Renewable and Sustainable Energy Reviews, Volume 130, 2020, 109899, ISSN 1364-0321, https://doi.org/10.1016/j.rser.2020.109899.

[148] IoT-NGIN: Next Generation IoT as part of Next Generation Internet European project, available online at https://iot-ngin.eu

[149] IRENA (2021), World Energy Transitions Outlook: 1.5°C Pathway, International Renewable Energy Agency, Abu Dhabi.

[150] IRENA (2022), Grid codes for renewable powered systems, International Renewable Energy Agency, Abu Dhabi. ISBN: 978-92-9260-427-1

[151] ISO 23247-2:2021 Automation systems and integration — Digital twin framework for manufacturing — Part 2: Reference architecture."

[152] Italian electrical market, available online at: https://www.mercatoelettrico.org/it/

[153] J. B. Samson, K. A. Fredrick, M. N. Sathiya, R. C. Joy, W. J. Wesley, and S. S. Samuel, "Smart Energy Monitoring Using RaspberryPi," 2019. Available online at: https://ieeexplore-ieee-org.ezproxy.uniroma1.it/document/8819743/.

[154] J. Han, Q. Hong, Z. Feng, M. Syed, G. Burt, and C. Booth, "Design and Implementation of a Real-Time Hardware-in-the-Loop Platform for Prototyping and Testing Digital Twins of Distributed Energy Resources," Energies (Basel), vol. 15, no. 18, p. 6629, Sep. 2022, doi: 10.3390/en15186629.

[155] J. Hicks and N. Ison, "An exploration of the boundaries of 'community' in community renewable energy projects: Navigating between motivations and context," 2017.

[156] J. L. Carlson et al., Resilience: Theory and Applications. Argonne, IL, USA, Feb. 2012.

[157] J. Mina Casaran, D. Navas, D. Echeverry-Ibarra. (2017). Evaluation of the audible noise level on distribution transformers using the Sound Pressure Method. Revista Facultad de Ingeniería. 26. 71-82. 10.19053/01211129.v26.n45.2017.6051. ICONTEC, "NTC 5978 Electrotécnia: Transformadores monofásicos y trifásicos valores de referencia de los niveles de emisión sonora." 2013.

[158] J. Radl, A. Fleischhacker, F. H. Revheim, G. Lettner, and H. er, "Comparison of Profitability of PV Electricity Sharing in Renewable Energy Communities in Selected European Countries."

[159] J. Wang, L. Ye, R. X. Gao, C. Li, and L. Zhang, "Digital Twin for rotating machinery fault diagnosis in smart manufacturing," Int J Prod Res, vol. 57, no. 12, 2019, doi: 10.1080/00207543.2018.1552032.

[160] J. Watson et al. Conceptual framework for developing resilience metrics for the electricity, oil, and gas sectors in the United States, Sandia Nat. Lab., Albuquerque, NM, USA, Tech. Rep. SAND2014-18019, 2014.

[161] J. Widén, E. Wäckelgård, J. Paatero, and P. Lund, "Impacts of distributed photovoltaics on network voltages: Stochastic simulations of three Swedish low-voltage distribution grids," Electr. Power Syst. Res., vol. 80, pp. 1562–1571, 2010.

[162] J. Zheng, D. W. Gao, and L. Lin, "Smart meters in smart grid: An overview," IEEE Green Technol. Conf., pp. 57–64, 2013.

[163] J.-F. Uhlenkamp, J. B. Hauge, E. Broda, M. Lütjen, M. Freitag, and K.-D. Thoben, "Digital Twins: A Maturity Model for Their Classification and Evaluation," IEEE Access, vol. 10, pp. 69605–69635, 2022, doi: 10.1109/ACCESS.2022.3186353.

[164] Jaewon Choi, Dong Gu Choi, Sang Yong Park, Analysis of effects of the hydrogen supply chain on the Korean energy system, International Journal of Hydrogen Energy, Volume 47, Issue 52, 2022, Pages 21908-21922, ISSN 0360-3199

[165] Jie Song, Marc Cheah-Mane, Eduardo Prieto-Araujo, Oriol Gomis-Bellmunt, Short-circuit analysis of grid-connected PV power plants considering inverter limits, International Journal of Electrical Power & Energy Systems, Volume 149, 2023, 109045, ISSN 0142-0615, https://doi.org/10.1016/j.ijepes.2023.109045.

[166] Jochen Stiasny, Thierry Zufferey, Giacomo Pareschi, Damiano Toffanin, Gabriela Hug, Konstantinos Boulouchos, Sensitivity analysis of electric vehicle impact on low-voltage distribution grids, Electric Power Systems Research, Volume 191, 2021, 106696, ISSN 0378-7796, https://doi.org/10.1016/j.epsr.2020.106696

[167] K. Ashok, D. Li, D. Divan, and N. Gebraeel, "Distribution transformer health monitoring using smart meter data," 2020 IEEE Power Energy Soc. Innov. Smart Grid Technol. Conf. ISGT 2020, Feb. 2020.

[168] K. C. Budka, J. G. Deshpande, T. L. Doumi, M. Madden, and T. Mew, "Communication network architecture and design principles for smart grids," Bell Labs Tech. J., vol. 15, no. 2, pp. 205–227, Sep. 2010.

[169] K. E. Antoniadou-Plytaria, I. N. Kouveliotis-Lysikatos, P. S. Georgilakis and N. D. Hatziargyriou, "Distributed and Decentralized Voltage Control of Smart Distribution Networks: Models, Methods, and Future Research," in IEEE Transactions on Smart Grid, vol. 8, no. 6, pp. 2999-3008, Nov. 2017, DOI: 10.1109/TSG.2017.2679238.

[170] K. Gairaa, S. Benkaciali, M. Guermoui, Clear-sky models evaluation of two sites over Algeria for pv forecasting purpose, The European Physical Journal Plus 134 (10) (2019) 1–17.

[171] K. M. Alam and A. el Saddik, "C2PS: A digital twin architecture reference model for the cloud-based cyber-physical systems," IEEE Access, vol. 5, 2017, doi: 10.1109/ACCESS.2017.2657006.

[172] K. S. Reddy, M. Kumar, T. K. Mallick, H. Sharon, and S. Lokeswaran, "A review of Integration, Control, Communication and Metering (ICCM) of renewable energy based smart grid," Renew. Sustain. Energy Rev., vol. 38, pp. 180–192, Oct. 2014.

[173] K. Sha, N. Alatrash, and Z. Wang, "A Secure and Efficient Framework to Read Isolated Smart Grid Devices," IEEE Transactions on Smart Grid, vol. 8, no. 6, 2017. Available online at: https://ieeexplore-ieee-org.ezproxy.uniroma1.it/document/7419260/.

[174] K. Sharma and L. Mohan Saini, "Performance analysis of smart metering for smart grid: An overview," Renewable and Sustainable Energy Reviews, vol. 49, pp. 720–735, Sep. 2015, doi: 10.1016/J.RSER.2015.04.170.

[175] K. Wang, X. Qi, H. Liu, A comparison of day-ahead photovoltaic power forecasting models based on deep learning neural network, Applied Energy 251 (2019) 113315.

[176] Kan, S. South Korea's Hydrogen Strategy and Industrial Perspectives. 2020. IFRI, Édito Énergie, 25 March 2020. Available online at: https://www.ifri.org/sites/default/files/atoms/files/sichao_kan_hydrogen_korea_2020_1.pdf.

[177] Katoch, S., Chauhan, S.S. & Kumar, V. A review on genetic algorithm: past, present, and future. Multimed Tools Appl 80, 8091–8126 (2021). https://doi.org/10.1007/s11042-020-10139-6

[178] Kelland, K. Diesel Exhaust Fumes Can. Cause Cancer, WHO Says; Reuters Agency: London, UK, 2012.

[179] Kempton, W., Tomic, J., 2005b. Vehicle-to-grid power implementation: from stabilizing the grid to supporting large-scale renewable energy. J. Power Sources 144 (1), 280–294

[180] Knight M, Brownell N. How does smart grid impact the natural monopoly paradigm of electricity supply? Grid-Interop Forum, at the conference in Chicago in December 2010.

[181] Koukaras P. et al., A Tri-Layer Optimization Framework for Day-Ahead Energy Scheduling Based on Cost and Discomfort Minimization, Energies 2021, 14, 3599. https://doi.org/10.3390/en14123599.

[182] Krishnamurthy D., Opendssdirect.py. Available online at: https://github.com/dss-extensions/OpenDSSDirect.py.

[183] Kserve. Available online at: https://kserve.github.io/website/0.10/.

[184] Kubeflow. Available online at: https://www.kubeflow.org/.

[185] Kundur, Deepa & Feng, Xianyong & Mashayekh, Salman & Liu, S. & Zourntos, Takis & Butler-Purry, K.L.. (2011). Towards modelling the impact of cyber attacks on a smart grid. IJSN. 6. 2-13. 10.1504/IJSN.2011.039629.

[186] L. D. Gitelman, M. v. Kozhevnikov, and D. D. Kaplin, "Asset management in grid companies using integrated diagnostic devices," International Journal of Energy Production and Management, vol. 4, no. 3, 2019, doi: 10.2495/EQ-V4-N3-230-243.

[187] L. Esposito, G. Romagnoli, Overview of policy and market dynamics for the deployment of renewable energy sources in Italy: Current status and prospects, Heliyon, Volume 9, Issue 7, 2023, e17406, ISSN 2405-8440, https://doi.org/10.1016/j.heliyon.2023.e17406.

[188] L. I. Minchala-Avila, J. Armijos, D. Pesántez, and Y. Zhang, "Design and Implementation of a Smart Meter with Demand Response Capabilities," Energy Procedia, vol. 103, pp. 195–200, Dec. 2016, doi: 10.1016/J.EGYPRO.2016.11.272.

[189] L. M. Antunes Caseiro, Power system resilience (end user) and critical infrastructure, Editor(s): Jorge García, Encyclopedia of Electrical and Electronic Power Engineering, Elsevier, 2023, Pages 218-232, ISBN 9780128232118, https://doi.org/10.1016/B978-0-12-821204-2.00097-0.

[190] L. Sheng, G. Lou, W. Gu, S. Lu, S. Ding and Z. Ye, "Optimal Communication Network Design of Microgrids Considering Cyber-Attacks and Time-Delays," in IEEE Transactions on Smart Grid, vol. 13, no. 5, pp. 3774-3785, Sept. 2022, DOI: 10.1109/TSG.2022.3169343.

[191] L. Zheng, R. Su, X. Sun, S. Guo, Historical pv-output characteristic extraction based weather-type classification strategy and its forecasting method for the day-ahead prediction of PV output, Energy 271 (2023) 127009.

[192] Lahnaoui, A., Wulf, C., & Dalmazzone, D. Building an optimal hydrogen transportation system for mobility, focus on minimizing the cost of transportation via truck. Energy Procedia, 142, 2072–2079. https://doi.org/10.1016/J.EGYPRO.2017.12.579

[193] Lee, Sangmin, and Trine Krogh Boomsma. "An approximate dynamic programming algorithm for short-term electric vehicle fleet operation under uncertainty." Applied Energy 325 (2022): 119793

[194] Liubov Dumarevskaya, Jason R. Parent, Electric grid resilience: The effects of conductor coverings, enhanced tree trimming, and line characteristics on tree-related power outages, Electric Power Systems Research, Volume 221, 2023, 109454, ISSN 0378-7796, https://doi.org/10.1016/j.epsr.2023.109454.

[195] Location of all electric vehicle charging stations in Terni. Available online at: https://it.chargemap.com/cities/terni-IT

[196] M. Abdel-Basset, H. Hawash, R. K. Chakrabortty, M. Ryan, Pv-net: An innovative deep learning approach for efficient forecasting of short-term photovoltaic energy production, Journal of Cleaner Production 303 (2021) 127037.

[197] M. Ahmed, R. Bhattarai, S. J. Hossain, S. Abdelrazek and S. Kamalasadan, "Coordinated Voltage Control Strategy for Voltage Regulators and Voltage Source Converters Integrated Distribution System," in IEEE Transactions on Industry Applications, vol. 55, no. 4, pp. 4235-4246, July-Aug. 2019, doi: 10.1109/TIA.2019.2902524.

[198] M. Delfanti, D. Falabretti, M. Fiori, M. Merlo, Smart Grid on field application in the Italian framework: The A.S.SE.M. project, Electric Power Systems Research, Volume 120, 2015, Pages 56-69, ISSN 0378-7796, https://doi.org/10.1016/j.epsr.2014.09.016.

[199] M. E. Baran and F. F. Wu, "Network reconfiguration in distribution systems for loss reduction and load balancing," in IEEE Transactions on Power Delivery, vol. 4, no. 2, pp. 1401-1407, April 1989, doi: 10.1109/61.25627

[200] M. Govindarasu and P. W. Bauer, "Special section on keeping the smart grid safe," IEEE Power Energy Mag., vol. 10, no. 1, pp. 16–17, Jan./Feb. 2012.

[201] M. J. Mayer, Benefits of physical and machine learning hybridization for photovoltaic power forecasting, Renewable and Sustainable Energy Reviews 168 (2022) 112772.

[202] M. J. Mayer, D. Yang, Pairing ensemble numerical weather prediction with ensemble physical model chain for probabilistic photovoltaic power forecasting, Renewable and Sustainable Energy Reviews 175 (2023) 113171.

[203] M. Kunicki, S. Borucki, D. Zmarzły, and J. Frymus, "Data acquisition system for on-line temperature monitoring in power transformers," Measurement, vol. 161, p. 107909, Sep. 2020, doi: 10.1016/J.MEASUREMENT.2020.107909.

[204] M. Latifi, A. Khalili, A. Rastegarnia, W. M. Bazzi, and S. Sanei, "A Robust Scalable Demand-Side Management Based on Diffusion-ADMM Strategy for Smart Grid," IEEE Internet of Things Journal, vol. 7, no. 4, pp. 3363–3377, Apr. 2020, doi: 10.1109/JIOT.2020.2968539.

[205] M. M. Albu, M. Sănduleac, and C. Stănescu, "Syncretic Use of Smart Meters for Power Quality Monitoring in Emerging Networks," IEEE Transactions on Smart Grid, vol. 8, no. 1, 2017, Available online at: https://ieeexplore-ieeeorg.ezproxy.uniroma1.it/document/7536160/.

[206] M. Mayilvaganan and M. Sabitha, "A cloud-based architecture for Big-Data analytics in smart grid: A proposal," 2013 IEEE Int. Conf. Comput. Intell. Comput. Res. IEEE ICCIC 2013, 2013.

[207] M. R. Habibi, H. R. Baghaee, T. Dragičević and F. Blaabjerg, "Detection of False Data Injection Cyber-Attacks in DC Microgrids Based on Recurrent Neural Networks," in IEEE Journal of Emerging and Selected Topics in Power Electronics, vol. 9, no. 5, pp. 5294-5310, Oct. 2021, doi: 10.1109/JESTPE.2020.2968243.

[208] M. R. Maghami, J. Pasupuleti, and C. M. Ling, "A Static and Dynamic Analysis of Photovoltaic Penetration into MV Distribution Network," Process. 2023, Vol. 11, Page 1172, vol. 11, no. 4, p. 1172, Apr. 2023.

[209] M. Rastegar, "Impacts of residential energy management on reliability of distribution systems considering a customer satisfaction model," IEEE Transactions on Power Systems, vol. 33, no. 6, 2018, doi: 10.1109/TPWRS.2018.2825356.

[210] M. S. Hoosain and B. S. Paul, "Smart homes: A domestic demand response and demand side energy management system for future smart grids," 2017. Available online at: https://ieeexplore.ieee.org/document/7931852/.

[211] M. Sănduleac et al., "Using Frequency measurements for data consistency assessment related to malicious data injection in distribution related ICT systems," 2018 International Symposium on Fundamentals of Electrical Engineering (ISFEE), 2018, pp. 1-5, doi: 10.1109/ISFEE.2018.8742414.

[212] M. Sanduleac et al., "Next Generation Real-Time Smart Meters for ICT Based Assessment of Grid Data Inconsistencies," Energies 2017, Vol. 10, Page 857, vol. 10, no. 7, p. 857, Jun. 2017.

[213] M. Shinozuka et al. Resilience of integrated power and water systems, in Proc. Seismic Eval. Retrofit Lifeline Syst., 2003, pp. 65–86.

[214] M. Vallés et al., Regulatory and market barriers to the realization of DR in electricity distribution networks: A European perspective, Electric Power Systems Research, Volume 140, 2016, Pages 689-698, ISSN 0378-7796, https://doi.org/10.1016/j.epsr.2016.04.026.

[215] M. Z. Degefa, I. B. Sperstad, and H. Sæle, “Comprehensive classifications and characterizations of power system flexibility resources,” Electric Power Systems Research, vol. 194. 2021. doi: 10.1016/j.epsr.2021.107022.

[216] M. Zahurul Huq and S. Islam, “Home area network technology assessment for demand response in smart grid environment.”

[217] Marcsa, Daniel. (2019). Noise and Vibration Analysis of a Distribution Transformer. Przeglad elektrotechniczny. 1. 174-177. 10.15199/48.2019.12.38.

[218] MATLAB R2021a, documentation. Available online at: https://it.mathworks.com/products/new_products/release2021a.html.

[219] Matute G. et al., Techno-economic modelling of water ELs in the range of several MW to provide grid services while generating hydrogen for different applications: A case study in Spain applied to mobility with FCEVs. 2019, International Journal of Hydrogen Energy. 44. 17431-17442. 10.1016/j.ijhydene.2019.05.

[220] Mccarthy RW, Yang C, Ogden J. Impacts of Electric-drive Vehicles on California’s Energy System; n.d

[221] Meng, Xiangyu & Gu, Alun & Wu, Xinguo & Zhou, Lingling & Zhou, Jian & Liu, Bin & Mao, Zongqiang. (2020). Status quo of China hydrogen strategy in the field of transportation and international comparisons. International Journal of Hydrogen Energy. 46. 10.1016/j.ijhydene.2020.11.049.

[222] Ministero delle imprese e del made in Italy, Strategia Nazionale Idrogeno, Linee guida preliminari (in italian, National hydrogen strategy, preliminar guidelines), available online at: https://www.mimit.gov.it/images/stories/documenti/Strategia_Nazionale_Idrogeno_Linee_guida_preliminari_nov20.pdf

[223] Mitsubishi Electric MLU series Photovoltaic Modules, PV-MLU255HC 255Wp and PV-MLU250HC 250 Wp. Available online at https://www. mitsubishielectricsolar. com/images/uploads/documents/specs/MLU_spec_sheet_250W_255W.pdf

[224] Muhammad Kamran, Chapter 3 - Power grids, Editor(s): Muhammad Kamran, Fundamentals of Smart Grid Systems, Academic Press, 2023, Pages 71-131, ISBN 9780323995603, https://doi.org/10.1016/B978-0-323-99560-3.00005-3.

[225] Muhammad Mansoor, Michael Stadler, Hans Auer, Michael Zellinger, Advanced optimal planning for microgrid technologies including hydrogen and mobility at a real microgrid testbed, International Journal of Hydrogen Energy, Volume 46, Issue 37, 2021, Pages 19285-19302, ISSN 0360-3199, https://doi.org/10.1016/j.ijhydene.2021.03.110.

[226] Muhammad Waseem, Saeed D. Manshadi, Electricity grid resilience amid various natural disasters: Challenges and solutions, The Electricity Journal, Volume 33, Issue 10, 2020, 106864, ISSN 1040-6190, https://doi.org/10.1016/j.tej.2020.106864.

[227] N. Bazmohammadi et al., “Microgrid Digital Twins: Concepts, Applications, and Future Trends,” IEEE Access, vol. 10, 2022, doi: 10.1109/ACCESS.2021.3138990.

[228] N. Bhusal, M. Gautam and M. Benidris, "Detection of Cyber Attacks on Voltage Regulation in Distribution Systems Using Machine Learning," in IEEE Access, vol. 9, pp. 40402-40416, 2021, DOI: 10.1109/ACCESS.2021.3064689.

[229] N. G. Paterakis, O. Erdinç, A. G. Bakirtzis, and J. P. S. Catalão, “Optimal household appliances scheduling under day-ahead pricing and load-shaping demand response strategies,” IEEE Trans Industr Inform, vol. 11, no. 6, 2015, doi: 10.1109/TII.2015.2438534.

[230] N. Good et al., Review and classification of barriers and enablers of DR in the smart grid, Renewable and Sustainable Energy Reviews, Volume 72, 2017, Pages 57-72, ISSN 1364-0321, https://doi.org/10.1016/j.rser.2017.01.043.

[231] N. Mogles et al., “How smart do smart meters need to be?,” Build. Environ., vol. 125, pp. 439–450, Nov. 2017.

[232] Nancy M.P. et al., Barriers and drivers to sustainable business model innovation: Organization design and dynamic capabilities, Long Range Planning, Volume 53, Issue 4, 2020, 101950, ISSN 0024-6301, https://doi.org/10.1016/j.lrp.2019.101950.

[233] Nemoto, T., & Beglar, D. (2014). Developing Likert-scale questionnaires. In N. Sonda & A. Krause (Eds.), JALT2013 Conference Proceedings. Tokyo: JALT.

[234] NREL, Solar Power Data for Integration Studies. Available online at https://www.nrel.gov/grid/solar-power-data.html

[235] O. Elma and U. S. Selamoğullari, “An overview of demand response applications under smart grid concept,” 2017. Available online at: https://ieeexplore.ieee.org/document/7935802/.

[236] Obinna, U., Joore, P., Wauben, L., & Reinders, A. (2017). Comparison of two residential Smart Grid pilots in the Netherlands and in the USA, focusing on energy performance and user experiences. Applied energy, 191, 264-275.

[237] Olex cables datasheet, available online at https://www.olex.com.au/products.html

[238] P. Gupta, R. Singh, Pv power forecasting based on data-driven models: a review, International Journal of Sustainable Engineering 14 (6) (2021) 1733–1755.

[239] P. J. Maliszewski and C. Perrings, Factors in the resilience of electrical power distribution infrastructures, Appl. Geogr., vol. 32, no. 2, pp. 668–679, 2012.

[240] P. Kou, D. Liang, R. Gao, Y. Liu and L. Gao, "Decentralized Model Predictive Control of Hybrid Distribution Transformers for Voltage Regulation in Active Distribution Networks," in IEEE Transactions on Sustainable Energy, vol. 11, no. 4, pp. 2189-2200, Oct. 2020, DOI: 10.1109/TSTE.2019.2952171.

[241] P. Koukaras et al., “A tri-layer optimization framework for day-ahead energy scheduling based on cost and discomfort minimization,” Energies (Basel), vol. 14, no. 12, 2021, doi: 10.3390/en14123599.

[242] P. Li, K. Zhou, X. Lu, S. Yang, A hybrid deep learning model for short-term PV power forecasting, Applied Energy 259 (2020) 114216.

[243] P. Marocco, D. Ferrero, E. Martelli, M. Santarelli, A. Lanzini. (2021). An MILP approach for the optimal design of renewable battery-hydrogen energy systems for off-grid insular communities. Energy Conversion and Management. 245. 114564. 10.1016/j.enconman.2021.114564.

[244] P. Thorsnes et al., Consumer responses to time varying prices for electricity, Energy Policy, Volume 49, 2012, Pages 552-561, ISSN 0301-4215, https://doi.org/10.1016/j.enpol.2012.06.062.

[245] Pablo Rodríguez-Pajarón, Araceli Hernández, Jovica V. Milanović, Probabilistic assessment of the impact of electric vehicles and nonlinear loads on power quality in residential networks, International Journal of Electrical Power & Energy Systems, Volume 129, 2021, 106807, ISSN 0142-0615, https://doi.org/10.1016/j.ijepes.2021.1 06807.

[246] Pandapower. Available online at: http://www.pandapower.org/

[247] Pandas, available online at: https://pandas.pydata.org

[248] Panteli, M., Trakas, D. N., Mancarella, P., & Hatziargyriou, N. D. (2017). Power Systems Resilience Assessment: Hardening and Smart Operational Enhancement Strategies. Institute of Electrical and Electronics Engineers. Proceedings , 105(7), 1202 - 1213. https://doi.org/10.1109/JPROC.2017.2691357

[249] Pascanu, R., Mikolov, T., & Bengio, Y. (2013, May). On the difficulty of training recurrent neural networks. In International conference on machine learning (pp. 1310-1318). Pmlr.

[250] Pedregosa, F.; Varoquaux, G.; Gramfort, A.; Michel, V.; Thirion, B.; Grisel, O.; Blondel, M.; Prettenhofer, P.; Weiss, R.; Dubourg, V.; et al. Scikit-learn: Machine learning in Python. J. Mach. Learn. Res. 2011, 12, 2825–2830.

[251] Pinto, B. et al. Fleet Transition from Combustion to Electric Vehicles: A Case Study in a Portuguese Business Campus. Energies 2020, 13, 1267

[252] Politecnico di Milano, Smart monitoring report, 2020. Available online at: https://www.energystrategy.it/es-download/

[253] Potential of Using Medium Electric Vehicle Fleet in a Commercial Enterprise Transport in Germany based on Real-World GPS Data

[254] Prometheus. Available online at: https://prometheus.io/ .

[255] Prophet. Available online at: https://facebook.github.io/prophet/

[256] Pypower, Available online at: https://pypi.org/project/PYPOWER/

[257] Qian Hu, Haiyu Li, Siqi Bu, The Prediction of Electric Vehicles Load Profiles Considering Stochastic Charging and Discharging Behavior and Their Impact Assessment on a Real UK Distribution Network, Energy Procedia, Volume 158, 2019, Pages 6458-6465, ISSN 1876-6102, https://doi.org/10.1016/j.egypro.2019.01.134.

[258] R. Ahmed, V. Sreeram, Y. Mishra, M. Arif, A review and evaluation of the state-of-the-art in PV solar power forecasting: Techniques and optimisation, Renewable and Sustainable Energy Reviews 124 (2020) 109792.

[259] R. B. D’Agostino and E. S. Pearson, "Tests for Departure from Normality. Empirical Results for the Distributions of b2 and √b1," in Biometrika, 1973, p. 613–622.

[260] R. Cloutier, G. Muller, D. Verma, R. Nilchiani, E. Hole, and M. Bone, “The concept of reference architectures,” Systems Engineering, vol. 13, no. 1, 2010, doi: 10.1002/sys.20129.

[261] R. Darbali-Zamora, J. Johnson, A. Summers, C. Birk Jones, C. Hansen, and C. Showalter, “State estimation-based distributed energy resource optimization for distribution voltage regulation in telemetry-sparse environments using a real-time digital twin,” Energies (Basel), vol. 14, no. 3, 2021, doi: 10.3390/en14030774.

[262] R. Deblasio and C. Tom, “Standards for the Smart Grid,” 2008 IEEE Energy 2030 Conference, pp. 1–7, 2008.

[263] R. Dey and F. M. Salem, "Gate-Variants of Gated Recurrent Unit (GRU) Neural," Department of Electrical and Computer Engineering, 2017

[264] R. Liu, C. Vellaithurai, S. S. Biswas, T. T. Gamage and A. K. Srivastava, "Analyzing the Cyber-Physical Impact of Cyber Events on the Power Grid," in IEEE Transactions on Smart Grid, vol. 6, no. 5, pp. 2444-2453, Sept. 2015, DOI: 10.1109/TSG.2015.2432013.

[265] R. Moghaddass and J. Wang, “A Hierarchical Framework for Smart Grid Anomaly Detection Using Large-Scale Smart Meter Data,” IEEE Transactions on Smart Grid, vol. 9, no. 6, 2018. Available online at: https://ieeexplore-ieee- org.ezproxy.uniroma1.it/document/7908945/.

[266] R. Morello, C. de Capua, G. Fulco, and S. C. Mukhopadhyay, “A smart power meter to monitor energy flow in smart grids: The role of advanced sensing and iot in the electric grid of the future,” IEEE Sensors Journal, vol. 17, no. 23, pp. 7828–7837, Dec. 2017, doi: 10.1109/JSEN.2017.2760014.

[267] R. Sharifi, S. H. Fathi, and V. Vahidinasab, “A review on Demand-side tools in electricity market,” Renewable and Sustainable Energy Reviews, vol. 72. 2017. doi: 10.1016/j.rser.2017.01.020.

[268] R. Tonkoski, D. Turcotte, and T. H. M. El-Fouly, “Impact of High PV Penetration on Voltage Profiles in Residential Neighborhoods,” IEEE Trans. Sustain. ENERGY, vol. 3, no. 3, 2012.

[269] R. Tonkoski, L. A. C. Lopes and T. H. M. El-Fouly, "Coordinated Active Power Curtailment of Grid Connected PV Inverters for Overvoltage Prevention," in IEEE Transactions on Sustainable Energy, vol. 2, no. 2, pp. 139-147, April 2011, DOI: 10.1109/TSTE.2010.2098483.

[270] R.S. Ming, J. Pan, M.P. Norton, S. Wende, H. Huang, The sound-field characterisation of a power transformer, Applied Acoustics, Volume 56, Issue 4, 1999, Pages 257-272, ISSN 0003-682X, https://doi.org/10.1016/S0003-682X(98)00036-X.

[271] Radakovic, Z.; Cardillo, E.; Feser, K. The influence of transformer loading to the aging of the oil–paper insulation. In: Proceedings of the 13th International Symposium High Voltage Engineering, Rotterdam, The Netherlands. 2003.

[272] Ramaswamy PC et al. Barriers and recommendations for enabling ICT based intra-grid control applications in smart Grids. In: Proceedings of the IEEE conference at San Diego, CA. Published in Power and Energy society General meeting 22–26 July 2012. http://dx.doi.org/10.1109/PESGM.2012. 6345081.

[273] Rashidizadeh-Kermani H, Najafi HR, Anvari-Moghaddam A, Guerrero JM. Optimal decision-making strategy of an electric vehicle aggregator in short-term electricity markets. Energies 2018;11(9):2413

[274] Raspberry pi 3 model b, 2015. Available online at: https://www.raspberrypi.com

[275] Ratcliff, R. Connectionist models of recognition memory: Constraints imposed by learning and forgetting functions. Psychol. Rev. 1990, 97, 285.

[276] Renewable Energy Report 2022 produced by Energy & Strategy. Available online at: https://cdn.motor1.com/pdf-files/rer22.pdf visisted on 31/07/2023

[277] Report on non-technical barriers for smart energy solutions. Report by the e-harbours expert group on Smart Energy Networks; March 2013.

[278] RES acceleration is boosted by the networks. Available online at: https://www.elettricitafutura.it/public/editor/News/2022/2022.07.20_Tech%20Watch_Reti_Slide EF.pdf visited on 31/07/2023.

[279] Rick Wallace Kenyon, Barry Mather, Bri-Mathias Hodge, Coupled transmission and distribution simulations to assess distributed generation response to power system faults, Electric Power Systems Research, Volume 189, 2020, 106746, ISSN 0378-7796, https://doi.org/10.1016/j.epsr.2020.106746.

[280] Rinnovabilandia, Quanto paga il GSE l'energia immessa in rete? (in italian, How much does the GSE pay for energy fed into the grid?) Available online at: http://www.rinnovabilandia.it/quanto-paga-il-gse-energia-immessa-in-rete-prezzo-zonale-a-kwh-aeeg/

[281] Rob Hull, What range anxiety? Nissan says owners of electric vehicles travel 390 miles MORE on average a year than drivers of petrol and diesel cars, Thisismoney.co.uk, 2021. Available online at: https://www.thisismoney.co.uk/money/cars/article-9659615/Electric-car-owners-390-miles-year-petrol-diesel.html

[282] Robins, A. Catastrophic forgetting, rehearsal and pseudorehearsal. Connect. Sci. 1995, 7, 123–146.

[283] Roger C.Dugan, Davis Montenegro, Electric Power Research Institute, Open Distribution System Simulator (OpenDSS) Reference Guide, June 2020

[284] Rolf Egert, Jörg Daubert, Stephen Marsh, Max Mühlhäuser, Exploring energy grid resilience: The impact of data, prosumer awareness, and action, Patterns, Volume 2, Issue 6, 2021, 100258, ISSN 2666-3899, https://doi.org/10.1016/j.patter.2021.100258.

[285] Rumelhart, D.E.; Hinton, G.E.; Williams, R.J. Learning representations by back-propagating errors. Nature 1986, 323, 533–536.

[286] S. Bahrami and A. Sheikhi, "From Demand Response in Smart Grid Toward Integrated Demand Response in Smart Energy Hub," IEEE Transactions on Smart Grid, vol. 7, no. 2, 2016. Available online at: https://ieeexplore.ieee.org/document/7206579/.

[287] S. Bajaj, S. Charan Teja, and P. K. Yemula, "Computer vision based energy monitoring system using Meter Image Capturing System (MICAPS)," 2020 1st Int. Conf. Power, Control Comput. Technol. ICPC2T 2020, pp. 246–249, Jan. 2020.

[288] S. Basumallik, S. Eftekharnejad, and B. K. Johnson, ''The impact of false data injection attacks against remedial action schemes,'' Int. J. Electr. Power Energy Syst., vol. 123, Dec. 2020, Art. no. 106225.

[289] S. Chanda and A. K. Srivastava, Defining and enabling resiliency of electric distribution systems with multiple microgrids, IEEE Trans. Smart Grid, vol. 7, no. 6, pp. 2859–2868, Nov. 2016.

[290] S. Dutta, Y. Li, A. Venkataraman, L. M. Costa, T. Jiang, R. Plana, P. Tordjman, F. H. Choo, C. F. Foo, H. B. Puttgen, Load and renewable energy forecasting for a microgrid using persistence technique, Energy Procedia 143 (2017) 617–622.

[291] S. Kawano, S. Yoshizawa and Y. Hayashi, "Centralized voltage control method using voltage forecasting by JIT modeling in distribution networks," 2016 IEEE/PES Transmission and Distribution Conference and Exposition (T&D), 2016, pp. 1-5, DOI: 10.1109/TDC.2016.7520006.

[292] S. Kulkarni, K. Ashok, F. Lambert, and D. Divan, "Asset Monitoring using Smart Sensing and Advanced Analytics for the Distribution Network," 51st North Am. Power Symp. NAPS 2019, Oct. 2019.

[293] S. Luthra et al., Adoption of smart grid technologies: An analysis of interactions among barriers, Renewable and Sustainable Energy Reviews, Volume 33, 2014, Pages 554-565, ISSN 1364-0321, https://doi.org/10.1016/j.rser.2014.02.030.

[294] S. M. Mirbagheri, D. Falabretti and M. Merlo, "Voltage Control in Active Distribution Grids: A Review and a New Set-Up Procedure for Local Control Laws," 2018 International Symposium on Power Electronics, Electrical Drives, Automation and Motion (SPEEDAM), 2018, pp. 1203-1208, DOI: 10.1109/SPEEDAM.2018.8445387.

[295] S. McManus, E. Seville, D. Brunsdon, and J. Vargo, Resilience management: A framework for assessing and improving the resilience of organisations, Resilient Organ. Res. Rep., vol. 1, pp. 1–79, 2007.

[296] S. Mohanty et al., "Demand side management of electric vehicles in smart grids: A survey on strategies, challenges, modelling, and optimization," Energy Reports, vol. 8, pp. 12466–12490, Nov. 2022, doi: 10.1016/j.egyr.2022.09.023.

[297] S. S. Shapiro and M. B. Wilk, "An Analysis of Variance Test for Normality," 1965

[298] S. Sridhar, A. Hahn, and M. Govindarasu, "Cyber-physical system security for the electric power grid," Proc. IEEE, vol. 100, no. 1, pp. 210–224, Jan. 2012.

[299] S. Torres, I. Durán, A. Marulanda, A. Pavas, J. Quirós-Tortós, Electric vehicles and power quality in low voltage networks: Real data analysis and modelling, Applied Energy, Volume 305, 2022, 117718, ISSN 0306-2619, https://doi.org/10.1016/j.apenergy.2021.117718.

[300] S. Uludag, K.-S. Lui, W. Ren, and K. Nahrstedt, "Secure and Scalable Data Collection With Time Minimization in the Smart Grid," IEEE Transactions on Smart Grid, vol. 7, no. 1, 2016. Available online at: https://ieeexplore.ieee.org/document/7061965/.

[301] S. V. T. K. W. N. J. L. Nandha Kumar Kandasamy, "An electric power digital twin for cyber security testing, research and education," Computers and Electrical Engineering, vol. 101, 2022.

[302] S.F. Abdelsamad, W.G. Morsi, T.S. Sidhu, Optimal secondary distribution system design considering plug-in electric vehicles, Electric Power Systems Research, Volume 130, 2016, Pages 266-276, ISSN 0378-7796, https://doi.org/10.1016/j.epsr.2015.09.009.

[303] Saber, A.Y., Venayagamoorthy, G.K., 2010. Intelligent unit commitment with vehicle-to-grid —a cost-emission optimization. J. Power Sources 195 (3), 898–911

[304] Sai Sudharshan Ravi, Muhammad Aziz, Clean hydrogen for mobility – Quo vadis?, International Journal of Hydrogen Energy, Volume 47, Issue 47, 2022, Pages 20632-20661, ISSN 0360-3199, https://doi.org/10.1016/j.ijhydene.2022.04.158.

[305] Sanjeev Pannala, Anurag K. Srivastava, Gowtham Kandaperumal, Sajan K. Sadanandan, DINGO: Digital assistant to grid operators for resilience management of power distribution system, Electric Power Systems Research, Volume 210, 2022, 108076, ISSN 0378-7796, https://doi.org/10.1016/j.epsr.2022.108076.

[306] Satre-Meloy, Aven, & Langevin, Jared. (2019). Hourly U.S. Building Electricity Use, Cost, and Emissions Baselines to Support Time-Sensitive Analyses of Energy Efficiency and Flexibility Measures (Version 1). https://doi.org/10.5281/zenodo.3473478]

[307] Scenari della domanda elettrica in Italia (in italian, Electric demand scenarios in Italy), Terna, 2016. Available online at: https://download.terna.it/terna /0000/0925/46.PDF

[308] Scikit-learn, available online at: https://scikit-learn.org/stable/

[309] Scitkit-Learn 6. Strategies to Scale Computationally: Bigger Data. Available online: https://scikit-learn.org/0.15/modules/scaling_strategies.html#strategies-to-scale-computationally-bigger-data

[310] Sgobbi A, Nijs W, De Miglio R, Chiodi A, Gargiulo M, Thiel C. How far away is hydrogen? Its role in the medium and long-term decarbonisation of the European energy system. International Journal of Hydrogen Energy 2016;41:19–35

[311] Shuai Yuan, Jun Yan, Yongjie Yu, Chengyong Zhao, Guoyun Su, Xuan Li, Calculation method of short-circuit fault current in flexible DC grid, Energy Reports, Volume 8, Supplement 13, 2022, Pages 461-468, ISSN 2352-4847, https://doi.org/10.1016/j.egyr.2022.08.163.

[312] Siemens Electric Vehicle Charging Infrastructure Catalog. Available online at: https://new.siemens.com/global/en/products/automation/ products-for-specific-requirements/e-car-charging.html

[313] Slovenia - Country Commercial Guide, Available online at: https://www.trade.gov/country-commercial-guides/slovenia-energy

[314] Snam, Ambrosetti the European House, H2 Italy 2050, September 2020, Available online at: https://www.snam.it/export/sites/snam-rp/repository/file/Media/news_eventi/2020/H2_Italy_ 2020_ITA.pdf

[315] SOOD, Vijay K., et al. Developing a communication infrastructure for the smart grid. In: 2009 IEEE Electrical power & energy conference (EPEC). IEEE, 2009. p. 1-7.

[316] SPGLOBAL. How Hydrogen Can Fuel The Energy Transition. 2020. Comments, 19 November 2020. Available online: www.spglobal.com/ratings/en/research/articles/201119-how-hydrogen-can-fuel-the-energy-transition-11740867.

[317] Spoonamore, S., and R. L. Krutz. "Smart grid and cyber challenges–national security risks and concerns." (2009).

[318] State Grid Cooperation of China; SGCC Framework and Roadmap to Strong & Smart Grid Standards, July 2010.

[319] Strong, Derek Ryan. Impacts of diffusion policy: determinants of early smart meter diffusion in the US electric power industry. Industrial and Corporate Change, 2019, 28.5: 1343-1363.

[320] SunRiSE website, available online at: https://sunrise.rse-web.it

[321] Sutton, R. S., & Barto, A. G. (2018). Reinforcement learning: An introduction. MIT press.

[322] T. Barszcz and M. Zabaryłło, "Concept of automated malfunction detection of large turbomachinery using machine learning on transient data," Diagnostyka, vol. 20, no. 1, 2019, doi: 10.29354/diag/100399.

[323] T. Bragatto et al., "Innovative Tools for Demand Response Strategies: a Real-Life Experience", 2019 EEEIC / I&CPS Europe, Genova, Italy, 2019, pp. 1-6. DOI: 10.1109/EEEIC.2019.8783584

[324] T. Bragatto, F. Carere, M. Cresta, F.M. Gatta, A. Geri, V. Lanza, M. Maccioni, M. Paulucci, Location and sizing of hydrogen based systems in distribution network for renewable energy integration, Electric Power Systems Research, Volume 205, 2022, 107741, ISSN 0378-7796, https://doi.org/10.1016/j.epsr.2021.107741.

[325] T. Bragatto, F.M. Gatta, A. Geri, R. Lamedica, et al., "Statistical Analysis of Prosumer Behaviour in a Real Distribution Network over Two Years", 2018 IEEE EEEIC / I&CPS Europe, Palermo, Italy, 2018, pp. 1-5.

[326] T. Oxley, A. Elshkaki, L. Kwiatkowski, A. Castillo, T. Scarbrough, H. ApSimon, Pollution abatement from road transport: cross-sectoral implications, climate co-benefits and behavioural change, Environmental Science & Policy, Volumes 19–20, 2012, Pages 16-32, ISSN 1462-9011, https://doi.org/10.1016/j.envsci.2012.01.004

[327] T. Samad, E. Koch, and P. Stluka, "Automated Demand Response for Smart Buildings and Microgrids: The State of the Practice and Research Challenges," Proceedings of the IEEE, vol. 104, no. 4, 2016. Available online at: https://ieeexplore-ieee.org.ezproxy.uniroma1.it/document/7416149/.

[328] T. W. Anderson and D. A. Darling, "Asymptotic Theory of Certain "Goodness of Fit" Criteria Based on Stochastic Processes," 1952

[329] T.W. Smith, C.J. Axon, R.C. Darton, The impact on human health of car-related air pollution in the UK, 1995–2005, Atmospheric Environment, Volume 77, 2013, Pages 260-266, ISSN 1352-2310, https://doi.org/10.1016/j.atmosenv.2013.05.016

[330] Taiebat, M., Xu, M., 2019. Synergies of four emerging technologies for accelerated adoption of electric vehicles: shared mobility, wireless charging, vehicle-to-grid, and vehicle automation. J. Clean. Prod. 230, 794–797

[331] Taylor S. J., Letham B. 2017. - Forecasting to Scale. PeerJ 5 Preprints: e3190v2 https://doi.org/10.7287/peerj.preprints.3190v2.

[332] Tensorforce. Available online at: https://github.com/tensorforce/tensorforce.

[333] Terna, Italian Grid Code. Available online at: https://www.terna.it/en/electric-system/grid-codes/italian-grid-code

[334] Third UN World Conference on Disaster Risk, Reduction, United Nations Office for Disaster Risk Reduction (UNISDR), Sendai, Japan, 2015.

[335] Triviño-Cabrera, A., Aguado, J. A., & de la Torre, S. (2019). Joint routing and scheduling for electric vehicles in smart grids with V2G. Energy, 175, 113-122

[336] Tubagus Aryandi Gunawan, Ian Williamson, Diana Raine, Rory F.D. Monaghan, Decarbonising city bus networks in Ireland with renewable hydrogen, International Journal of Hydrogen Energy, Volume 46, Issue 57, 2021, Pages 28870-28886, ISSN 0360-3199

[337] Tuchnitz, Felix, et al. "Development and evaluation of a smart charging strategy for an electric vehicle fleet based on reinforcement learning." Applied Energy 285 (2021): 116382

[338] U. K. Das, K. S. Tey, M. Seyedmahmoudian, S. Mekhilef, M. Y. I. Idris, W. Van Deventer, B. Horan, A. Stojcevski, Forecasting of photovoltaic power generation and model optimisation: A review, Renewable and Sustainable Energy Reviews 81 (2018) 912–928.

[339] Ushnik Mukherjee, Azadeh Maroufmashat, Jonathan Ranisau, Mohammed Barbouti, Aaron Trainor, Nidhi Juthani, Hadi El-Shayeb, Michael Fowler, Techno-economic, environmental, and safety assessment of hydrogen powered community microgrids; case study in Canada, International Journal of Hydrogen Energy, Volume 42, Issue 20, 2017, p. 14333-14349, ISSN 0360-3199, https://doi.org/10.1016/j.ijhydene.2017.03.083.

[340] Vlad Mitrache, Ultra-Fast-Charging Stations with 500 kW Rates in Development, 0-100% in Minutes. Available online at https://www.autoevolution.com/news/ultra-fast-charging-stations-with-500-kw-rates-in-development-0-100-in-minutes-120824.html

[341] W. Ko, H. Vettikalladi, S.-H. Song, and H.-J. Choi, "Implementation of a Demand-Side Management Solution for South Korea's Demand Response Program," Applied Sciences 2020, Vol. 10, Page 1751, vol. 10, no. 5, p. 1751, Mar. 2020, doi: 10.3390/APP10051751.

[342] W. T. Li et al., "Demand response management for residential smart grid: From theory to practice," IEEE Access, vol. 3, pp. 2431–2440, Nov. 2015, doi: 10.1109/ACCESS.2015.2503379.

[343] Wang J, Li K-J, Liang Y, Javid Z. Optimization of Multi-Energy Microgrid Operation in the Presence of PV, Heterogeneous Energy Storage and Integrated Demand Response. Applied Sciences. 2021; 11(3):1005. https://doi.org/10.3390/app11031005

[344] Wei, Dong, et al. "An integrated security system of protecting smart grid against cyber attacks." 2010 Innovative Smart Grid Technologies (ISGT). IEEE, 2010.

[345] WU, Weidong, et al. Design of sound monitoring and fault diagnosis system for dry-type transformers. In: IOP Conference Series: Earth and Environmental Science. IOP Publishing, 2021. p. 012002.

[346] WU, Xiaowen, et al. Noise Characteristics of a Dry-Type Distribution Transformer Tested In a Semi-Anechoic Room. In: IOP Conference Series: Materials Science and Engineering. IOP Publishing, 2018. p. 042169.

[347] Wu, Yu, et al. "Demand side energy management of EV charging stations by approximate dynamic programming." Energy Conversion and Management 196 (2019): 878-890

[348] X. Fang, S. Misra, G. Xue, and D. Yang, "Smart Grid — The New and Improved Power Grid: A Survey," IEEE Communications Surveys & Tutorials, vol. 14, no. 4, pp. 944–980, 2012, doi: 10.1109/SURV.2011.101911.00087.

[349] Y. Guo, M. Xiao, X. Zheng, S. Wang and Z. Ullah, "Review on the Coordinated Voltage Control Methods in Distribution Networks," 2021 IEEE 4th International Electrical and Energy Conference (CIEEC), 2021, pp. 1-7, DOI: 10.1109/CIEEC50170.2021.9510940.

[350] Y. Isozaki et al., "Detection of Cyber Attacks Against Voltage Control in Distribution Power Grids With PVs," in IEEE Transactions on Smart Grid, vol. 7, no. 4, pp. 1824-1835, July 2016, DOI: 10.1109/TSG.2015.2427380.

[351] Y. Peng and H. Wang, "Application of Digital Twin Concept in Condition Monitoring for DC-DC Converter," in 2019 IEEE Energy Conversion Congress and Exposition, ECCE 2019, 2019. doi: 10.1109/ECCE.2019.8912199.

[352] Y. Xu, ''A review of cyber security risks of power systems: From static to dynamic false data attacks,'' Protection Control Mod. Power Syst., vol. 5, no. 1, pp. 1–12, Dec. 2020.

[353] Y. Zheng, S. Yang, and H. Cheng, "An application framework of digital twin and its case study," J Ambient Intell Humaniz Comput, vol. 10, no. 3, 2019, doi: 10.1007/s12652-018-0911-3.

[354] Y. Zhou, J. Wang, Z. Li, H. Lu, Short-term photovoltaic power forecasting based on signal decomposition and machine learning optimization, Energy Conversion and Management 267 (2022) 115944.

[355] Y.Yang, S.Bremner, C.Menictas, M.Kay, Battery energy storage system size determination in renewable energy systems: A review, Renewable and Sustainable Energy Reviews 91 (2018) 109–125.

[356] YALMIP package, documentation available online at: https://yalmip.github.io/.

[357] Yu Y et al. The smart grids in China -a review. Energies 2012; 5(5):1321–38

[358] Z. Bie, Y. Lin, G. Li and F. Li, Battling the Extreme: A Study on the Power System Resilience, in Proceedings of the IEEE, vol. 105, no. 7, pp. 1253-1266, July 2017, doi: 10.1109/JPROC.2017.2679040.

[359] Z. Lee, T. Li, S. H. Low. ACN-Data: Analysis and Applications of an Open EV Charging Dataset, Proc. the Tenth International Conference on Future Energy Systems (e-Energy '19), June 2019.

[360] Z. Liu, N. Meyendorf, and N. Mrad, "The role of data fusion in predictive maintenance using digital twin," in AIP Conference Proceedings, 2018, vol. 1949. doi: 10.1063/1.5031520.

[361] Z. Wang, T. Hong, M. A. Piette, Building thermal load prediction through shallow machine learning and deep learning, Applied Energy 263 (2020) 114683.